

©

1978

DONALD JAMES DEPAOLO

ALL RIGHTS RESERVED

STUDY OF MAGMA SOURCES,
MANTLE STRUCTURE AND THE
DIFFERENTIATION OF THE EARTH
FROM VARIATIONS OF $^{143}\text{Nd}/^{144}\text{Nd}$
IN IGNEOUS ROCKS

Thesis by

Donald James DePaolo

In Partial Fulfillment of the Requirements
for the Degree of
Doctor of Philosophy

California Institute of Technology

Pasadena, California

(Submitted 23 January 1978)

This thesis is dedicated to my wife, Geri,
in appreciation of her unfailing support,
encouragement and understanding.

"Drum hab ich mich der Magie ergeben,
Ob mir durch Geistes Kraft and Mund
Nicht manch Geheimnis würde kund;
Dass ich nicht mehr, mit sauerm Schweiss,
Zu sagen brauche, was ich nicht weiss;
Dass ich erkenne, was die Welt
Im Innersten zusammenhält,
Schau alle Wirkenskraft und Samen
Und tu nicht mehr in Worten kramen."

Faust, Goethe

ACKNOWLEDGEMENT

I wish to thank Jerry Wasserburg for his continued interest and enthusiasm in this work, and for invaluable advice on many topics. His passion for simplicity and clarity of thought and his ability to isolate the essence of the most ponderous problems have made strong, and I hope lasting, impressions upon me.

I am grateful to Arden Albee for suggesting this work as a possible thesis and for snickering at some other ideas.

Special thanks go to Dimitri Papanastassiou, who has taught me the ethos of careful experimental science and has unselfishly shared much of his time and considerable knowledge.

Dave Curtis was extremely patient in introducing me to rare-earth chemistry and invested much time in turning me into a Lunatic.

Fellow members of the Lunatic Asylum deserve special mention. During the past three years they have shown a remarkable propensity for making startling discoveries which have kept excitement at a high level.

I wish to thank the many persons who contributed samples for this study, especially R. J. Stern, R. W. Johnson, W. G. Melson, I. Carmichael, F. Barker, A. J. Irving and G. Goles. Many others contributed samples which were not analyzed, although not for want of desire to do so.

I wish to thank Evelyn Brown and Elizabeth Ball for their assistance and friendliness, and for generally trying hard to please all of us. Jan Scott drafted many of the figures and improved their clarity in the process. Peter Gromet gave valuable advice on the

preparation of rare-earth gravimetric standards.

I also wish to thank Rosemary Vidale, who encouraged me to go to graduate school, and the N.A.G.T.-U.S.G.S. for a summer field assistantship, the receipt of which made up my mind to pursue a career in earth sciences.

I thank my co-authors for permission to include unaltered published papers as part of this thesis.

Appendices one through three are reproduced with permission of the American Geophysical Union. Appendix four is reproduced by permission of Pergamon Press.

This work was supported by NASA Grant NGL 05-002-188 and NSF Grants PHY76-02724 and EAR 76-22494.

Abstract

The decay of ^{147}Sm to ^{143}Nd allows $^{143}\text{Nd}/^{144}\text{Nd}$ to be used to trace Sm/Nd fractionation in long time-scale geologic processes. Since Sm/Nd is a sensitive indicator of many aspects of the overall chemistry of rocks, the Sm-Nd system provides an excellent tool for the study of the chemical evolution of the earth's crust and mantle.

$^{143}\text{Nd}/^{144}\text{Nd}$ has been measured in terrestrial rock samples of different ages to establish the characteristics of Nd isotopic evolution in the crust and mantle. The evolution of $^{143}\text{Nd}/^{144}\text{Nd}$ in the mantle indicates Sm/Nd equal to that of chondrites, and implies a chondritic REE distribution for the earth. Young basalts show a significant dispersion in $^{143}\text{Nd}/^{144}\text{Nd}$ indicating the existence of distinct mantle reservoirs with characteristic $^{143}\text{Nd}/^{144}\text{Nd}$. $^{143}\text{Nd}/^{144}\text{Nd}$ in average crustal rocks today is much lower than in mantle samples and reflects their age and low Sm/Nd. Continental flood basalts and mid-ocean ridge (MOR) tholeiitic basalts have distinctly different $^{143}\text{Nd}/^{144}\text{Nd}$ which may permit a priori distinction between "continental" and "oceanic" igneous rocks. Ocean island basalts have $^{143}\text{Nd}/^{144}\text{Nd}$ intermediate between MOR and continental flood basalts. Initial $^{143}\text{Nd}/^{144}\text{Nd}$ of many continental igneous rocks through time fall on a Sm/Nd evolution curve with chondritic REE abundance ratio. Oceanic igneous rocks are derived from a different ancient reservoir which has Sm/Nd higher than chondritic. These observations indicate that many continental igneous rocks are derived from a reservoir with chondritic REE pattern which may represent primary undifferentiated material

remaining since the formation of the earth, while oceanic igneous rocks are derived from highly differentiated reservoirs. The mantle beneath the oceans appears to be more depleted in crustal components than is the mantle which is subjacent to the continental crust. In general, basalts are not derived from mantle reservoirs which have been light REE-enriched for long times.

Initial $^{143}\text{Nd}/^{144}\text{Nd}$ and $^{87}\text{Sr}/^{86}\text{Sr}$ in young basalts from both oceans and continents show a strong correlation suggesting that Sm-Nd and Rb-Sr fractionation events in the mantle may be correlative and caused by the same process. From this correlation Rb/Sr for the earth is inferred to be 0.029.

Initial $^{143}\text{Nd}/^{144}\text{Nd}$ in lunar igneous rocks show much more dispersion than in terrestrial rocks of similar age. The data suggest that the earth, unlike the moon, did not undergo an early differentiation event which greatly fractionated the rare earth elements, or if it did, a mixing process operated during the subsequent AE to erase the variation of Sm/Nd produced in this event.

Nd and Sr isotopes indicate that if the earth is made of a mixture of achondrites (low Rb/Sr) and chondrites (high Rb-Sr) that these two components must have been thoroughly mixed. The present-day isotopic heterogeneity of the earth's mantle is unrelated to accretional heterogeneity.

Transport calculations and material balance considerations for simple models of formation of the continental crust indicate that only a small portion of the earth's total budget of Sm and Nd are

found in the crust. Highly differentiated mantle reservoirs such as those from which MOR basalts are derived must represent only a small portion of the mantle, perhaps one-fourth to one-sixth or less. The data are consistent with the existence of large volumes of undifferentiated (possibly undegassed) material in the mantle. The data also suggest that the continental crust has a low Rb/Sr (less than 0.10) implying a highly layered structure for the crust, with the lower crust having a much lower Rb/Sr than the upper crust.

Island arc lavas from New Britain and the Marianas have $^{143}\text{Nd}/^{144}\text{Nd}$ similar to other oceanic basalts and distinctly different from continental flood basalts and thus appear to be derived from a high Sm/Nd, light-REE-depleted reservoir. Consideration of both Nd and Sr isotopes suggests seawater involvement in the generation of some island arc lavas and thus indicates that they may be derived from altered subducted oceanic crust. Other island arc lavas show no evidence of seawater involvement and may be derived from mantle reservoirs with affinities to the sources of ocean island basalts. Nd and Sr in some basaltic and ultrapotassic continental lavas and in some Andean volcanics indicate that some magmas in continental regions may be derived from old low-Sm/Nd reservoirs or are heavily contaminated with old continental crustal material. Fish debris from the ocean floor provides an estimate of $^{143}\text{Nd}/^{144}\text{Nd}$ in seawater and indicates that light-REE in the marine environment are derived mainly from continents.

Table of Contents

	<u>page</u>
Acknowledgement	iv
Abstract.	vi
I. Introduction.	1
Purposes of the investigation	1
Previous work	4
Original experiment design.	11
Basic principle	14
Planetary differentiation and the isotopic record.	20
The value of the Sm-Nd system--Comparison to Rb-Sr and U-Th-Pb	30
II. Data representation	34
III. REE fractionation during partial melting and variations of ϵ_{Nd}	45
IV. Sampling.	58
V. Nd results.	69
Precambrian igneous rocks	69
Young igneous rocks	78
A. Continental flood basalts and Mid-ocean ridge tholeiites.	78
B. Ocean island basalts.	83
C. Continental alkali basalts.	84
D. Island arcs	84

	<u>page</u>
E. Continental margin magmatic arcs	84
F. Lavas of extreme compositions.	86
G. Ultramafic rocks	87
H. Other samples.	88
VI. Discussion of Nd results	89
Chemical heterogeneity of the mantle	89
T_{CHUR} ages	92
Comparison of earth and moon	96
Contrast between oceanic and continental mantle.	102
Provinciality of sub-continental magma sources	105
Intraprovince variability of ϵ_{Nd}	109
REE patterns in magma sources.	116
Growth of continental crust.	119
Evidence for multi-stage evolution histories for mantle rocks.	120
VII. Sr results	123
VIII. Discussion of Sr results	132
Origin of $\epsilon_{\text{Nd}} - \epsilon_{\text{Sr}}$ correlation.	132
A. Systematics of $\epsilon_{\text{Nd}} - \epsilon_{\text{Sr}}$ variations.	133
1. Mixing relationships	133
2. Sr and Nd evolution during differentiation of a planet.	134
B. Magma contamination.	140

	<u>page</u>
C. Two-reservoir mixing	148
D. Spectrum of reservoirs	154
Further implications of $\epsilon_{\text{Nd}} - \epsilon_{\text{Sr}}$ correlation	155
The composition of the continental crust	160
IX. Mantle-crust transport models.	167
Basic problem and assumptions.	167
Discrete differentiation event	170
Continuous transport models.	175
Conclusions.	197
References	202
Appendix 1: Nd isotopic variations and petrogenetic models (co-authored by G.J. Wasserburg; published in Geophys. Res. Letters <u>3</u> , 249-252, 1976)	213
Appendix 2: Inferences about magma sources and mantle structure from variations of $^{143}\text{Nd}/^{144}\text{Nd}$ (co-authored by G.J. Wasserburg; published in Geophys. Res. Letters <u>3</u> , 743-746, 1976)	223
Appendix 3: The sources of island arcs as indicated by Nd and Sr isotopic studies (co-authored by G.J. Wasserburg; published in Geophys. Res. Letters <u>4</u> , 465-468, 1977)	233
Appendix 4: Rb-Sr and Sm-Nd chronology and genealogy of basalts from the Sea of Tranquility (co-authored by D.A. Papanastassiou and G.J. Wasserburg; published in Proc. Lunar Sci. Conf. 8th, 1639-1672, 1977)	246

	<u>page</u>
Appendix 5: Analytical procedures	280
A5.1 Chemistry.	280
A. Crushing	280
B. Dissolution.	282
C. Aliquanting and spiking.	284
D. Ion exchange elution chromatography	285
E. Blanks	298
F. Preparations of tracers and gravimetric standards.	298
A5.2 Mass spectrometry.	303
A. Loading and analysis	303
B. Oxygen isotopic abundance.	318
C. Data quality	329
D. Isotopic composition of Neodymium. . . .	331
E. Isotopic composition of Sm and λ^{147}	341
F. Selection of ^{150}Nd and ^{147}Sm tracers.	342
Appendix 6: Sample descriptions	344
Appendix 7: Major element chemistry of analyzed samples.	352
Appendix 8: Trace element concentrations.	357

I. INTRODUCTION

Purposes of the investigation

Broadly stated, the aims of this investigation are to study the chemical structure of the earth and how it has developed using the variations of $^{143}\text{Nd}/^{144}\text{Nd}$ found in igneous rocks. More specifically the aim is to identify the existence of distinct reservoirs in the earth and to try to deduce the locations and extents of these reservoirs by searching for patterns in the isotopic variations in igneous rocks which are related to geographic location, tectonic setting or rock type. Thus it is possible to deduce large scale structure in the earth and estimate its age or time of formation. This combination of information on both the existence of structure and its age is extremely powerful and is unique to the study of earth structure using radiogenic isotopes. It is hoped that ultimately this information can be combined with geophysical evidence for present-day large-scale motions in the earth to better understand the dynamics of the earth's mantle.

In addition, the data collected in this study provide new insight into long-standing problems in igneous petrogenesis. These include questions such as which chemical characteristics of magmas are inherited from parental reservoirs, which result from variations in the process of magma formation and emplacement, and which are due to contamination with wallrock. Also, the question of whether young segments of continental crust are mantle-derived or represent remelting of pre-existing crust is addressed. A question related to this last

one is whether crustal material, if derived from the mantle, is always extracted from the same limited volume of mantle, which must then change composition with time, or instead is always derived from previously untapped parts of the mantle.

A further purpose of this study, which is inseparable from the previously mentioned aims, is to determine the relative REE abundance pattern in the outer parts of the earth, and to compare this to the abundances found in chondritic meteorites. This will indicate whether any substantial REE fractionation occurred during the formation and early differentiation of the earth. Such fractionation could occur between the upper and lower mantle, between the mantle and a possible protocrust or even, perhaps, between the earth's mantle and the moon if the moon was somehow derived from the earth's mantle as has been suggested.

It has also been possible to compare Nd evolution in the earth and the moon to try to understand the possible effects of differing size and chemistry on the differentiation history of a planetary body. This has been possible by using Nd data previously measured on lunar rocks by other workers (Lugmair et al., 1975a,b; 1976) and additional measurements made as part of this thesis work (Papanastassiou et al., 1977). Sm-Nd results have shown interesting contrasts between the early histories of the two bodies.

Isotopic studies of magma sources using the Rb-Sr and U-Th-Pb systems have provided abundant information about the origin of magmas and chemical structure in the interior of the earth. Many of the Nd results are confirmatory of these earlier findings. However,

a particularly interesting result of the Nd studies, which was not foreseen at the beginning of this study, is that variations of initial Nd in young basalts are remarkably strongly correlated with variation of initial Sr in these basalts. This correlation indicates that Rb/Sr and Sm/Nd may be to a large extent covariant in the earth, and this result provides important information on the nature of the processes responsible for the formation of different reservoirs in the earth. A simple correlation between Sr and Pb isotopes in basalts did not exist. The correlation between Rb-Sr and Sm-Nd suggests that the differentiation processes at work within the earth may be simple and consistent. Therefore a portion of this study is devoted to assessing the possible origins of this correlation and its implications. As examples of the possible scope of the implications, from this correlation it has been possible to estimate Rb/Sr for undifferentiated mantle and therefore possibly also Rb/Sr of the bulk earth, to assess contamination of magmas due to assimilation of crustal material, and to evaluate the role of subducted oceanic crust in the generation of island arc lavas.

As a start towards understanding the implications of the Nd isotopic data for mantle dynamics and the origin of the continental crust, simple mathematical models of the transport of Sm and Nd between reservoirs are used to estimate the relative volumes of different reservoirs in the mantle, to illustrate possible genetic relationships between these reservoirs, and to try to assess the evidence for the existence of undifferentiated material in the earth and estimate its composition.

Previous work

The principles behind the use of the Sm-Nd radioactive system are the same as those for Rb-Sr. The first use of Rb-Sr to study the differentiation of the earth was by Gast (1955, 1960). Summaries of the relevant principles can be found in Gast (1967) and Wasserburg (1966) and in several other sources. In many respects this thesis represents a return to the problems first addressed by Gast (1955, 1960) using Rb-Sr. Similarly, the U-Th-Pb system has also been used to study the earth's differentiation (c.f. Patterson, 1964).

The Sm-Nd system was not used earlier due to the technical difficulties in making the measurements. The α decay of ^{147}Sm to ^{143}Nd has a long time constant ($\tau_{1/2} = 1.06 \times 10^{11}$ yr) and variations of Sm/Nd in nature are small, so the variations in the natural abundance of ^{143}Nd are small. The total range of measured $^{143}\text{Nd}/^{144}\text{Nd}$ is approximately 1%. At the time the first Rb-Sr studies were undertaken, the precision of isotope ratio measurements was about $\pm 0.5\%$. Thus, use of the Sm-Nd system was impossible. The development of a computer interfaced mass spectrometer with digital data acquisition by Wasserburg *et al.* (1969) allowed a factor of 100 improvement in the precision of isotope ratio measurements and made Nd isotopic studies feasible. However, before such high-precision measurements could be made, methods for the clean chemical separation of individual rare-earth elements had to be developed and adapted to the analysis of rocks. Methods for the chemical separation of rare-earths were originally developed in the 1940s to separate U fission products produced in the early reactors. These methods were not exploited by

geochemists until about two decades later. In the early 1960s simplified chemical procedures were employed to separate REE for the purpose of determining their abundances in rocks by neutron activation (cf., Haskin *et al.*, 1966a). This work required only rough separations to achieve nominal radiochemical purity of the separate elements. The methods for high-purity separation of individual rare-earths were first introduced into the field in the late 1960s by Eugster *et al.* (1970) at Caltech. They used these methods to separate Gd and Sm for isotopic analysis to measure neutron capture effects in meteorites and lunar soils. Thus by 1969 all of the necessary technical capabilities for the measurement of Nd isotopic variations were in existence. It was not until five years later that any measurements were made.

Using the chemical methods of Eugster *et al.* (1969), Lugmair (1974) and Lugmair, Scheinin, and Marti (1975a) first used the Sm-Nd method to date the meteorite Juvinas and a lunar basalt. Their work demonstrated that the system could be used to obtain precise ages of old rocks and also showed its potential usefulness in studying planetary differentiation. The thesis work described here has involved applying this method to problems of terrestrial petrogenesis.

The study of Nd isotopic variations in terrestrial rocks is unique among isotopic investigations in that it is preceded by more than a decade of intensive study of the distribution of Sm and Nd and other rare-earth elements (REE) in rocks and minerals (cf., Haskin *et al.*, 1978 for review, also Haskin *et al.*, 1966a). These studies have shown that although the REE are chemically very similar, significant

fractionation occurs in nature within the rare earth group and the relative fractionation within the group is in general a smooth function of atomic number. REE patterns in some terrestrial rocks are shown in Figure 1. In this graph the abundances measured in a rock are normalized to the abundances measured in chondritic meteorites, which are thought to represent solar system relative abundances, and plotted against atomic number from La to Lu. The upper curve is the REE abundances in a composite of North American shales. The pattern shown, with light REE enriched relative to heavy REE, is typical of the vast majority of continental crustal rocks and is thus probably representative of continental crust. The lower curve represents a sample of a peridotite intrusion at Lizard, England. Peridotite is thought to approximate in composition the earth's upper mantle and it is possible that this REE pattern may be representative of parts of the upper mantle. Figure 1b shows REE patterns in three basic volcanic rocks. It shows that Sm/Nd is highly variable even between rocks which are generally classed as "basalts." Note also that the Sm/Nd ratio is closely coupled with the overall bulk chemistry of these lavas as indicated by the rock names, and that both Sm and Nd are highly enriched in the basalts compared to chondrites. It is clear from these graphs that significant natural variation of relative REE abundances is common and can be used to characterize large lithic reservoirs in the earth. Figure 1 also shows that the Sm/Nd ratio is a sensitive indicator of the overall REE pattern, low

Figure 1: (a) Graph of rare-earth element abundances in two rock samples normalized to the abundances in ordinary chondritic meteorites. Normalized abundances are usually used in REE geochemistry in order to eliminate the odd-even effect or Otto-Harkins rule where even-numbered elements are generally more abundant than the odd-numbered elements of similar atomic number. The upper curve gives REE abundances in a composite of North American shales (cf. Haskin *et al.*, 1966a) and is probably representative of average upper crust, i.e., that part of the crust which normally becomes exposed to erosion. The lower curve is a spinel peridotite sample from the Lizard peridotite intrusion in southern Great Britain, which is regarded as a solid state intrusion of upper mantle rock into the crust (Frey *et al.*, 1971). The value of Sm/Nd for each sample is given and illustrates the range in this ratio found in nature. (b) REE patterns of three basic lavas compared to chondrites and Lizard peridotite. Note that the lavas are generally enriched in REE and that the REE patterns are smooth functions of atomic number. F values indicate the fractional enrichment or depletion of Sm/Nd in each rock relative to chondrites. Thus the leucitite, with $F = -0.61$, has Sm/Nd 61% lower than chondritic. Note also that the REE abundances and fractionation pattern are closely related to the overall rock composition. Going from top to bottom, the decreasing light REE concentrations and increasing Sm/Nd ratio correlate with a decrease in the abundances of K, Rb, Sr, U, Th, Pb, Ti, P, and many other elements. This close tie between Sm/Nd and the overall chemistry of rocks makes the Sm-Nd system a valuable tracer in geologic

processes. The data in Figure 1b for the leucitite and alkali basalt are from Kay and Gast (1973), for the tholeiite from O'Nions et al (1976), and for the peridotite from Frey (1970).

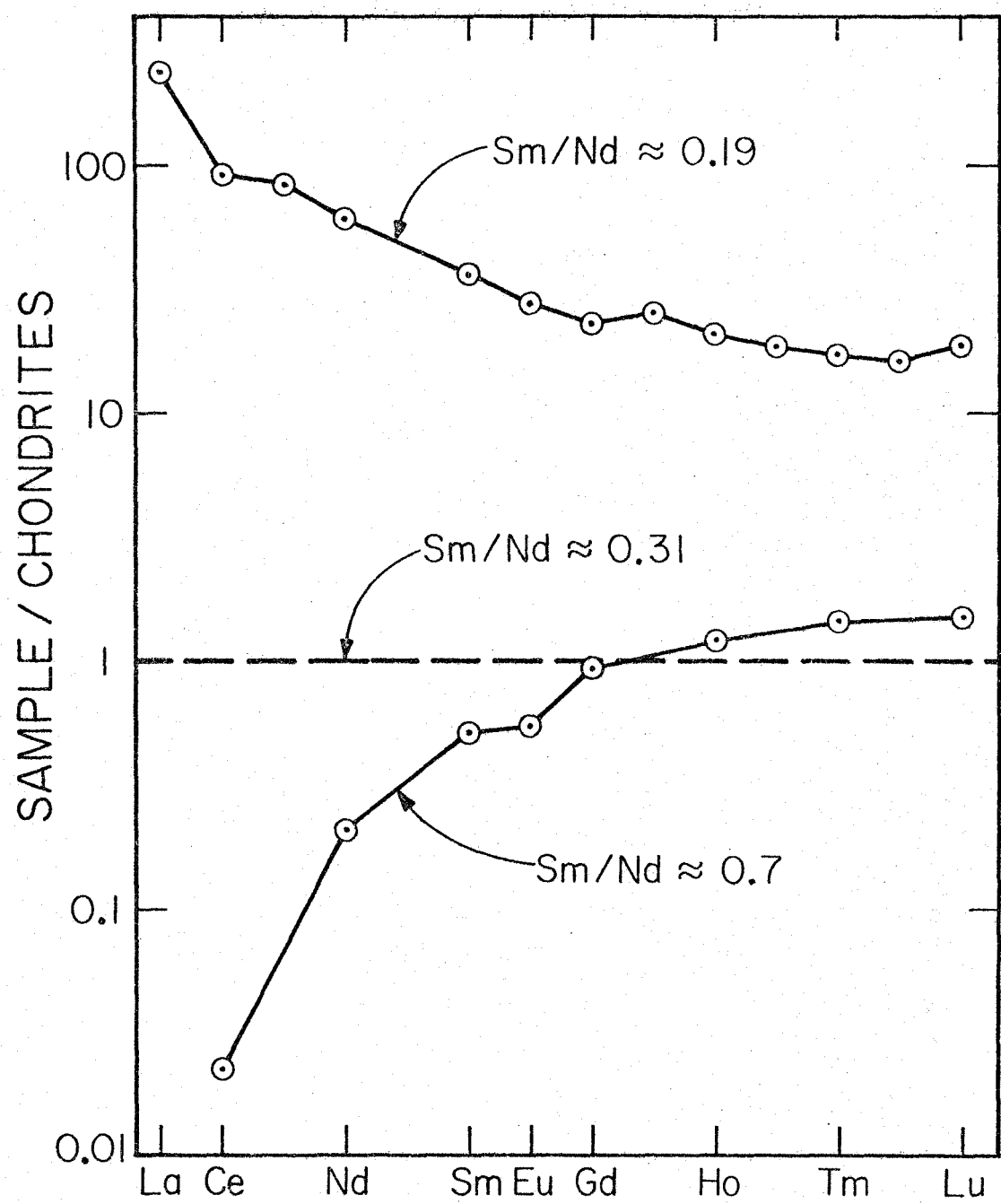


Fig. 1a

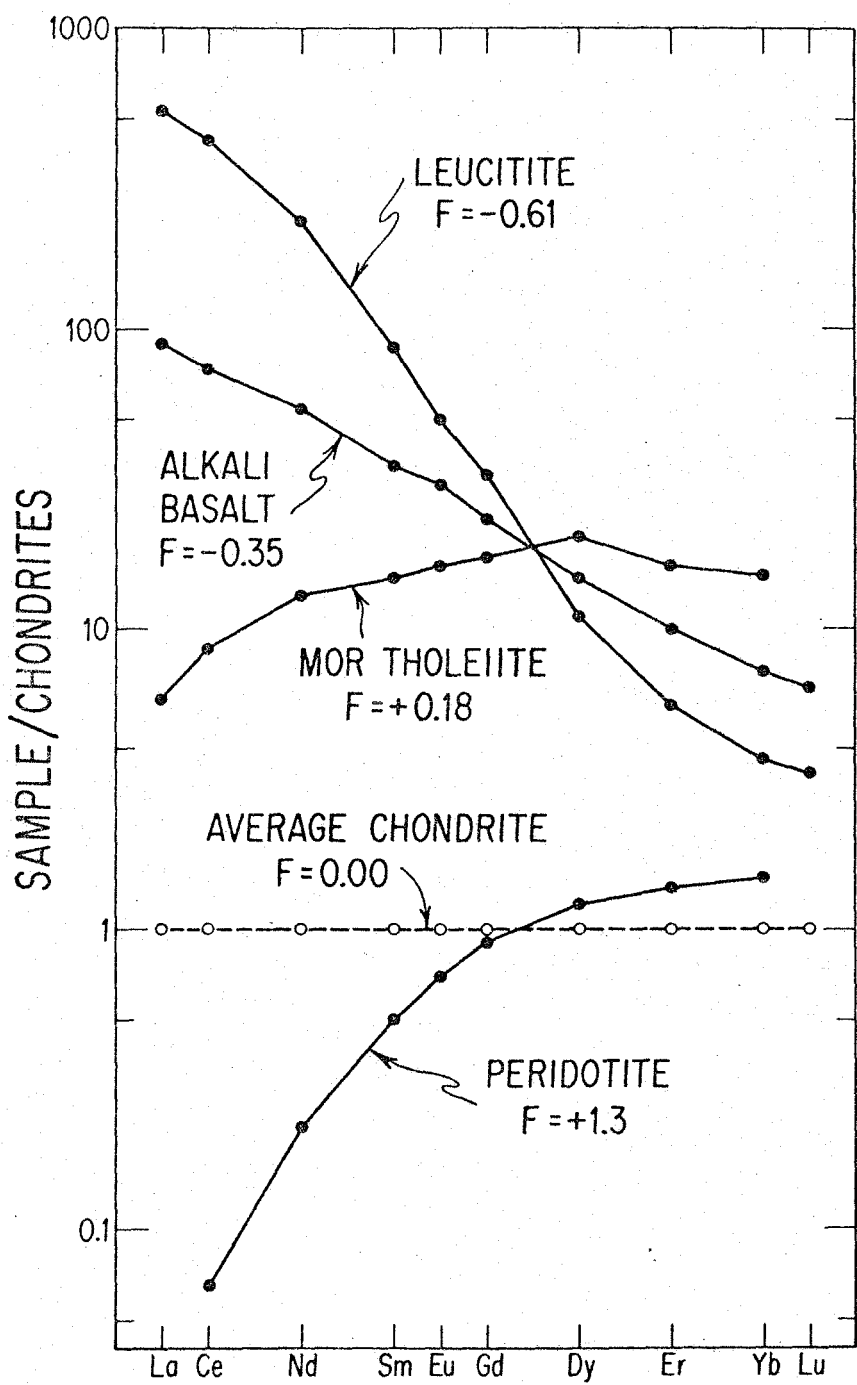


Fig. 1b

Sm/Nd is indicative of a light-REE-enriched pattern and high Sm/Nd is characteristic of a light-REE-depleted pattern. Thus information about the Sm/Nd ratio of terrestrial reservoirs derived from study of Nd isotopes also yields much broader information about the chemistry of these reservoirs. Because of the previous work on the distribution of REE, some of the Nd isotopic results could be anticipated. But important questions, such as whether the variation in REE patterns observed in rocks were inherited from parent reservoirs which formed in an early terrestrial differentiation or were merely the results of the immediate short-term magmatic processes which formed the rocks, could be answered only by the time control provided by the Sm-Nd radiometric clock.

Original experiment design

At the time of commencement of this project there existed no published Sm-Nd isotopic data on any terrestrial rocks. Therefore, the plan of the investigation was neither constrained nor guided by any previous Nd isotopic data. The abundant data on REE patterns, however, gave a rough indication of the probable magnitude and sign of effects. In particular, it was supposed that the present isotopic composition of the continental crust would be distinctly different from that of the mantle (as suggested by Figure 1a for instance), and that this contrast might be valuable as a tool for locating the sources of magmas. Another immediate aim was to try to determine when the differentiation events took place which produced the variations in REE patterns as shown in Figure 1. The age of the crust has been a

long-standing problem in geology, but the general problem of the nature of any early terrestrial differentiation was also at hand. Frey et al. (1971) had posed the question with regard to REE. They suggested that the REE patterns in the earth might be a function of depth, with perhaps the upper levels being enriched in light REE (low-Sm/Nd) and the deeper levels depleted in light REE (high Sm/Nd), or vice versa. This layering could have formed recently or near the time of formation of the earth or could have developed gradually through time. These questions seemed to have a good possibility of being answered by the Nd isotope data.

It was also known at the outset that Sr and Pb isotopic variations existed in young basalts and appeared to be useful for studying mantle structure. It was thought possible that Nd isotopes might be similarly useful. However, the probable magnitude of the Nd effects was not at all clear, and it seemed as likely as not that they would be too small to measure or else measurable but totally random. This type of application of Nd isotopes did not look to be too promising. The rather surprising regularities in the basalt data which were found during the course of this study proved this initial assessment to be far off the mark.

In addition to the problems mentioned above, it was also recognized that the Sm-Nd system could be a useful geochronological tool. From general geochemical considerations it appeared that many rocks which were not easily dateable with Rb-Sr or U-Th-Pb could be dated by Sm-Nd. In particular this applied to ancient basic and

ultrabasic rocks. However, it was decided from the outset that the main thrust of this thesis would not be the dating of rocks. Instead, samples would be used which were already well-dated by other methods, and the above-mentioned general geochemical questions would be directly addressed.

In most respects, the course taken by this thesis work has closely followed the original plans. The one exception is the extent of the investigation of Nd isotopic variations in young volcanic rocks. Several well-dated Precambrian rocks were available at Caltech from past investigations. However, an extensive library of chemically characterized young volcanic rocks was not available at Caltech. Consequently, over the past two years considerable effort has gone into obtaining such samples.

During the course of this work a significant amount of data has been published by investigators from other laboratories (Richard et al., 1976; O'Nions et al., 1977; Hawkesworth et al., 1977; Hamilton et al., 1977). These investigations mainly entailed measurements of Nd isotopes in young oceanic basalts. The appearance of these data have caused this investigation to be diverted away from study of oceanic basalts to avoid duplication of effort at a time when the overall data base is still small. The data of these other investigators is herein used freely in conjunction with data produced at Caltech. The basic patterns in the data, first set forth by DePaolo and Wasserburg (1976a,b), would be fully evident without the additional

data, but inclusion of the other data greatly strengthens the statistical significance of these patterns.

During the course of this thesis four papers were published outlining the results. These papers are included as Appendixes one through four.

Basic principle

The principle on which this investigation is based is illustrated in Figure 2. Stated in words the principle is as follows. If an original homogeneous rock reservoir, which has the same Sm/Nd and $^{143}\text{Nd}/^{144}\text{Nd}$ throughout, is differentiated by magmatic processes into two reservoirs with differing chemical and mineralogical compositions, these two reservoirs will have different Sm/Nd ratios and subsequently they will evolve different $^{143}\text{Nd}/^{144}\text{Nd}$ ratios. The Sm/Nd ratios in the two resulting reservoirs are a function of the details of the differentiation process. These reservoirs, if sampled today, contain information about the time of the differentiation event and its nature.

An example is given in Figure 2. At time T_o homogeneous rock reservoir UR is formed with $^{143}\text{Nd}/^{144}\text{Nd} = I_{UR}(T_o)$ and $\text{Sm/Nd} = \text{Sm/Nd}_{UR}(T_o)$. The $^{143}\text{Nd}/^{144}\text{Nd}$ of UR will increase with time due to the decay of ^{147}Sm to ^{143}Nd , and $^{143}\text{Nd}/^{144}\text{Nd}$ in UR as a function of time ($I_{UR}(T)$) is given by

$$(1) \quad I_{UR}(T) = I_{UR}(T_o) + \left(\frac{^{147}\text{Sm}}{^{144}\text{Nd}} \right)_{UR} (T) \left[e^{\lambda_{Sm}(T_o - T)} - 1 \right]$$

$$\approx I_{UR}(T_o) + C(\text{Sm/Nd})_{UR} \lambda_{Sm} (T_o - T)$$

Figure 2: An illustration showing how differentiation processes can be traced through time using Sm-Nd isotopes. In a through d the differentiation of an originally homogeneous volume of rock into two chemically distinct layers as a result of melting and fractional crystallization is shown. The differentiation takes place at a time T_1 years ago, and the time necessary to accomplish the differentiation (ΔT_2) is assumed to be small compared to T_1 . Figure 2e shows how $^{143}\text{Nd}/^{144}\text{Nd}$ changes with time in the uniform reservoir of rock (UR) and in the two reservoirs (A and B) formed from UR at T_1 . The slopes of the evolution lines for each reservoir are proportional to Sm/Nd in the reservoir. Therefore if $^{143}\text{Nd}/^{144}\text{Nd}$ in a reservoir can be sampled at different points in time, the Sm/Nd of the reservoir can be deduced. It is this principle which is used to study reservoirs in the earth's interior. Thus, for instance, we can determine Sm/Nd in the mantle by measuring the initial $^{143}\text{Nd}/^{144}\text{Nd}$ in basalts of different ages which provide samplings of $^{143}\text{Nd}/^{144}\text{Nd}$ in the mantle. Figure 2f is a Nd evolution diagram showing what the measured $^{143}\text{Nd}/^{144}\text{Nd}$ and $^{147}\text{Sm}/^{144}\text{Nd}$ would be like in reservoirs A and B if they could be measured today.

HOMOGENEOUS RESERVOIR
PARTIAL MELTING
DIFFERENTIATION
SOLIDIFICATION
AND COOLING

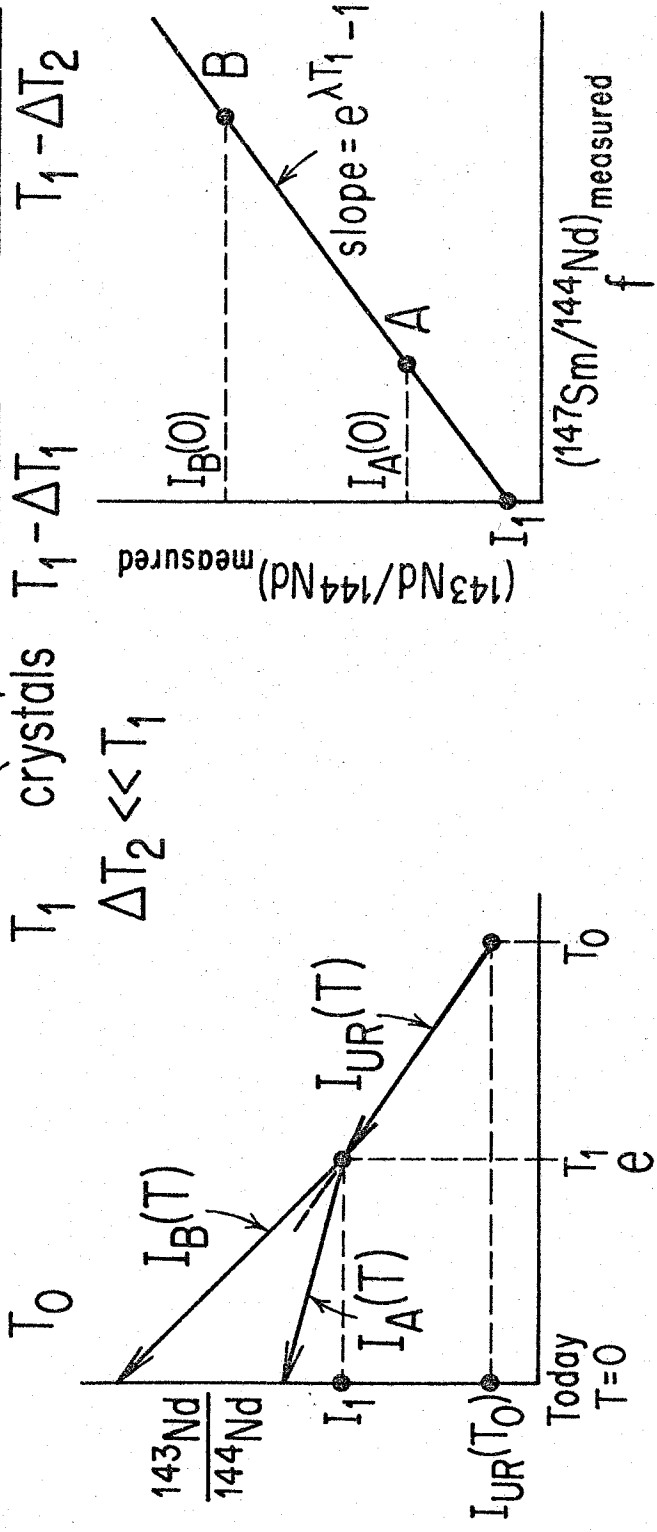
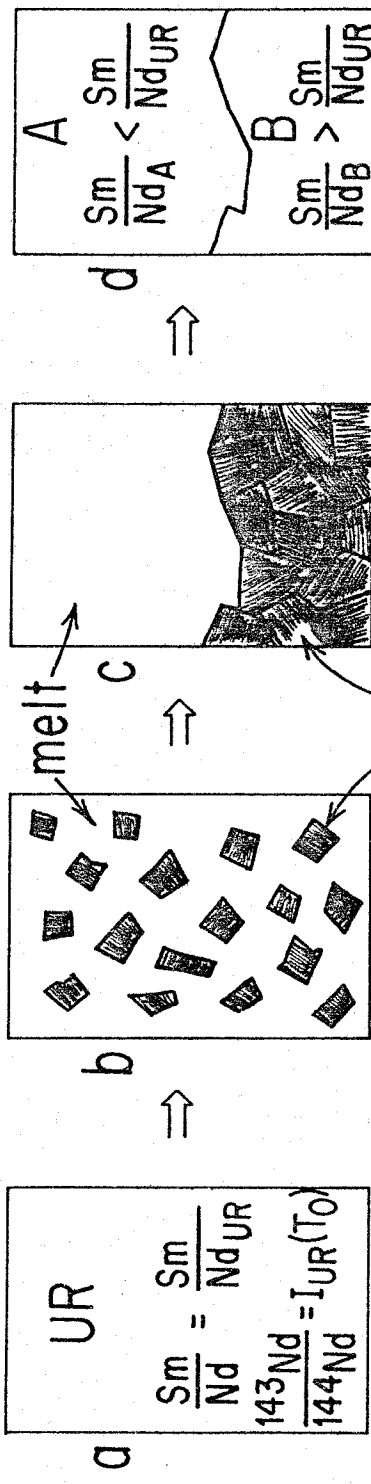


Fig. 2

where C is a constant and T is measured backward from today (i.e., $T \equiv \text{Age}$). As shown in Figure 2e, $^{143}\text{Nd}/^{144}\text{Nd}$ in UR evolves along an essentially straight line with a slope proportional to its Sm/Nd ratio. Now, at T_1 , UR is partially melted. Both the melt and the crystals have the same $^{143}\text{Nd}/^{144}\text{Nd}$, but the chemical differences between the melt and crystals are such that the crystals have a different Sm/Nd than the melt. The crystals then settle to the bottom, the melt is displaced to the top, and the whole system then solidifies and cools in a short time. Now, in place of UR, there exist two reservoirs A and B which are chemically distinct with respect to all elements and thus (incidentally) have different Sm/Nd ratios. Immediately after this differentiation event A and B still have identical $^{143}\text{Nd}/^{144}\text{Nd} = I_1$. But, as shown in Figure 5e, subsequent to T_1 $^{143}\text{Nd}/^{144}\text{Nd}$ in A, which has $\text{Sm}/\text{Nd}_A < \text{Sm}/\text{Nd}_{\text{UR}}$ (say), will evolve more slowly due to its lower Sm/Nd , and $^{143}\text{Nd}/^{144}\text{Nd}$ in B will evolve more rapidly due to its higher Sm/Nd . As shown in Figure 5f, if we sample A and B today and measure their $^{143}\text{Nd}/^{144}\text{Nd}$ and $^{147}\text{Sm}/^{144}\text{Nd}$, the slope of the line connecting the two points gives T_1 and the y intercept gives I_1 . As shown on Figure 5e and 5f, if a reservoir formed at T_1 with $\text{Sm}/\text{Nd} = 0$, then today its measured ratio would be equal to I_1 . This simple example illustrates the basic principle of geochronology. T_1 is interpreted as the "age" of reservoirs A and B. It represents the time that they could last have had the same $^{143}\text{Nd}/^{144}\text{Nd}$.

Let us consider Figure 2 as an example of an igneous intrusion which is dated using Sm-Nd. In this case the intrusion is exposed

at the earth's surface, and can be mapped and perhaps divided into two units (Reservoirs A and B) on the basis of chemical, mineralogical, and textural differences. Let us say that it is concluded that this intrusion was emplaced as a homogeneous magma, that it began to crystallize slowly, and the crystals sank to the bottom of the magma chamber. After about half the magma had crystallized the remaining melt crystallized quickly and then the entire intrusion cooled to ambient temperature. In this case the formation of Reservoirs A and B has been reconstructed by direct observation of the rocks themselves. Evidence can be drawn from various disciplines (mineralogy, geochemistry, petrology, and structure) until the processes responsible for the formation of these reservoirs are understood. When it has been concluded that A and B were formed from a single parent magma, then we can measure $^{147}\text{Sm}/^{144}\text{Nd}$ and $^{143}\text{Nd}/^{144}\text{Nd}$ in A and B and feel confident that the slope of the line they define represents the crystallization age of the intrusion as shown in Figure 2. Thus, since we can understand the formation of A and B by direct observation, the Sm-Nd isotope system would be needed only as a tool to determine the age.

Now, instead, suppose that Reservoirs A and B are large reservoirs or layers in the earth's mantle or the lower crust and are not exposed at the surface. However, suppose also that magmas are now and then produced by partial melting of parts of these reservoirs, and these magmas are erupted or emplaced into the upper crust and therefore are observable. When they are erupted the magmas will have $^{143}\text{Nd}/^{144}\text{Nd}$ which is equal to that in the reservoir from which they were

derived, but their Sm/Nd ratios may be different due to fractionation during melting or during differentiation of the magma on its way to the surface. Thus a lava derived today from A will have $^{143}\text{Nd}/^{144}\text{Nd} = I_A(0)$ and a lava from B will have $^{143}\text{Nd}/^{144}\text{Nd} = I_B(0)$. The difference in $^{143}\text{Nd}/^{144}\text{Nd}$ between these two lavas informs us of the existence of two reservoirs deep in the earth. However, unlike in the case of the intrusion we cannot directly observe the chemistry of these reservoirs. But from the measured $^{143}\text{Nd}/^{144}\text{Nd}$ in the lavas we can infer much about the chemistry, formation, and age of these reservoirs at depth. For instance, the reservoir with the higher $^{143}\text{Nd}/^{144}\text{Nd}$ must also have the higher Sm/Nd, and since, as discussed earlier, Sm/Nd is closely tied to many other chemical parameters, we can infer much about the chemical differences between the reservoirs and therefore also infer how they may have formed. Although the exact age of the reservoirs cannot be determined we can place limits on their age. If the difference in $^{143}\text{Nd}/^{144}\text{Nd}$ between the two reservoirs is ΔI , then the difference in Sm/Nd ($\Delta \text{Sm}/\text{Nd}$) and the time T_1 since they were fractionated from a common parent reservoir are related by

$$(2) \quad \Delta I \approx C(\Delta \text{Sm}/\text{Nd})T_1.$$

Thus if $\Delta \text{Sm}/\text{Nd}$ is small T_1 must be large whereas if $\Delta \text{Sm}/\text{Nd}$ is large T_1 must be small. The inferred age of the reservoirs is inversely proportional to the magnitude of the chemical contrast between them.

Thus using these principles the variations of $^{143}\text{Nd}/^{144}\text{Nd}$ in

igneous rocks can be used to study the chemical structure of the earth's interior. The igneous rocks themselves simply provide isotopic samplings of the earth's interior.

Planetary differentiation and the isotopic record

The primary aim of this study has been to use the Nd isotopic composition of igneous rocks of different ages to trace the differentiation of the outer earth through time. A somewhat detailed illustration of how the Sm-Nd system can be used in this manner is given in Figure 3 and the following discussion. Figure 3a depicts in a highly schematic way the differentiation history of a planet, while the evolution of Nd isotopic composition with time in the reservoirs within this planet are shown in Figure 3b. The ensuing discussion exhibits in a simplified manner most of the ideas which form the basis for this investigation, provides a framework for later discussion of the data, and foreshadows some of the important findings.

Following Lugmair (1974) the isotope ratio $^{143}\text{Nd}/^{144}\text{Nd}$ is used to monitor the variations in the relative abundance of ^{143}Nd due to the decay of ^{147}Sm . The growth of $^{143}\text{Nd}/^{144}\text{Nd}$ as a function of time in a reservoir where Sm/Nd is constant except for changes due to ^{147}Sm decay is given by:

$$(3) \quad \frac{^{143}\text{Nd}}{^{144}\text{Nd}}(\tau_2) = \frac{^{143}\text{Nd}}{^{144}\text{Nd}}(\tau_1) + \frac{^{147}\text{Sm}}{^{144}\text{Nd}}(\tau_2) \left[e^{\lambda(\tau_1 - \tau_2)} - 1 \right]$$

For the Sm-Nd system, generally $\lambda(\tau_1 - \tau_2) \ll 1$ so the change in $^{143}\text{Nd}/^{144}\text{Nd}$ over the time interval $\tau_2 - \tau_1$, is given approximately by:

Figure 3: (a) A schematic illustration of the differentiation of a planet. At T_c the planet condenses from the solar nebula (SN) as a uniform homogeneous sphere (UR). At time T_f the outer parts of the planet are internally differentiated into two chemically distinct layers (A and B) with different Sm/Nd as shown. The deep interior of the planet remains undifferentiated. At times T_{m1} and T_{m2} there is volcanic activity during which magmas generated by melting in the planet's interior are brought to the surface. The solid circular area in the interior of the planet represents the region of melting, the solid slabs on the surface represent lava flows and these are connected by the conduit through which the magma passed to the surface. In this illustration these magmas are thought of as simply isotopic samplings of the interior of the planet. However, in actuality the removal of magma from a certain volume within the planet can cause a change in the composition of that volume and create, in effect, a new layer. Thus, in a more general example, the magmatism would be intimately linked with the differentiation process. (b) Graph of the evolution of $^{143}\text{Nd}/^{144}\text{Nd}$ with time in the different reservoirs in the planet. The square symbols represent the initial $^{143}\text{Nd}/^{144}\text{Nd}$ and age of the lavas. Initial $^{143}\text{Nd}/^{144}\text{Nd}$ of an igneous rock is the ratio that was in the rock when it first crystallized from the liquid state.

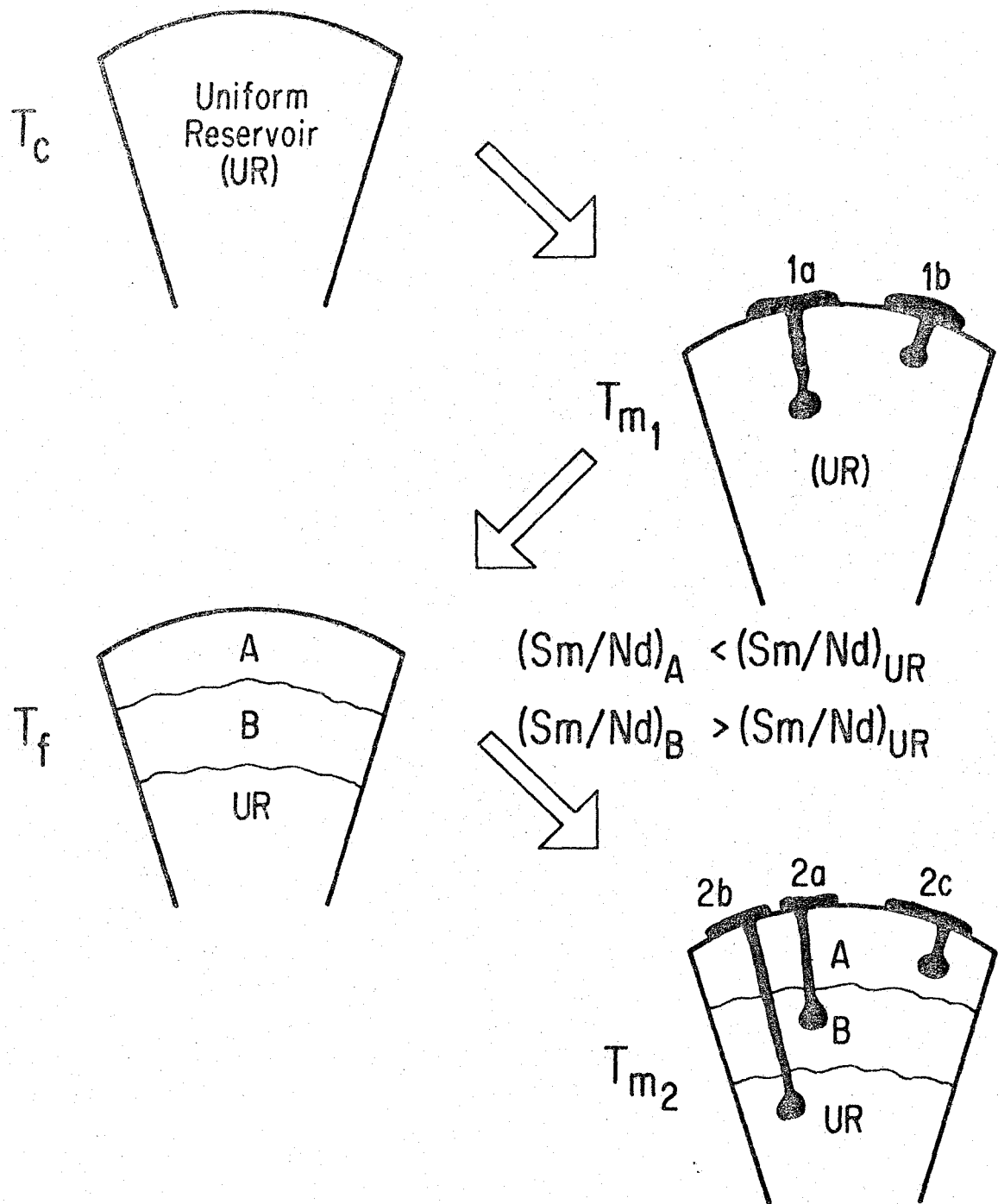


Fig. 3a

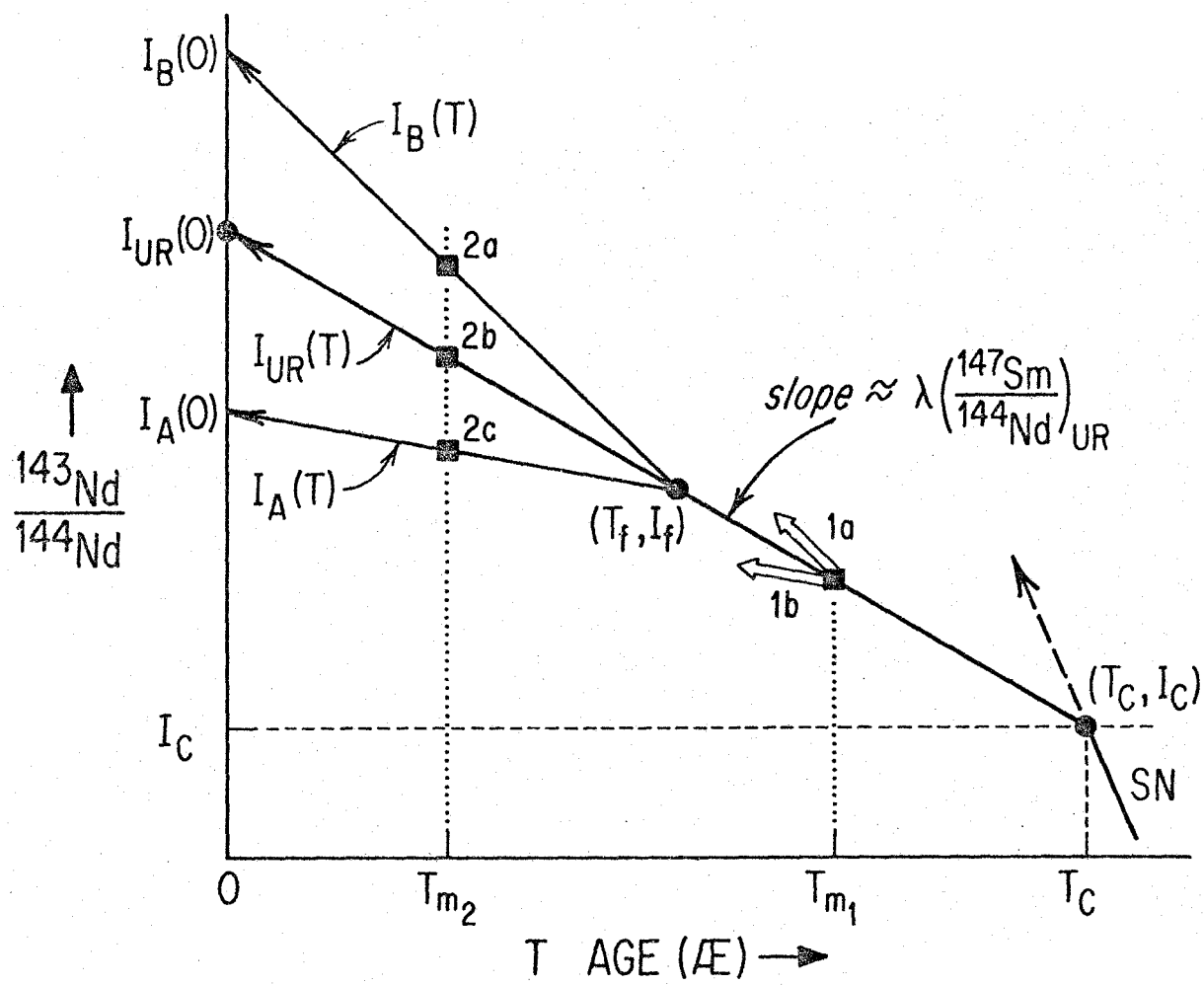


Fig. 3b

$$(4) \quad \Delta \frac{^{143}\text{Nd}}{^{144}\text{Nd}} \equiv \frac{^{143}\text{Nd}}{^{144}\text{Nd}}(\tau_2) - \frac{^{143}\text{Nd}}{^{144}\text{Nd}}(\tau_1) \approx \frac{^{147}\text{Sm}}{^{144}\text{Nd}} \lambda(\tau_1 - \tau_2)$$

which is accurate to $\sim 1.5\%$ for $\tau_1 - \tau_2 = 4.5$ AE. Thus, the rate of change of $^{143}\text{Nd}/^{144}\text{Nd}$ is directly proportional to $^{147}\text{Sm}/^{144}\text{Nd}$.

Referring to Figure 3b, consider a planet which condenses from the solar nebula at time T_C when the solar nebula has $^{143}\text{Nd}/^{144}\text{Nd} = I_C$. From T_C until the present the evolution of $^{143}\text{Nd}/^{144}\text{Nd}$ in the planet as a whole will be described by an essentially straight line such as that labelled $I_{UR}(T)$ whose slope is proportional to the Sm/Nd of the planet. A reservoir such as the bulk planet, whose Sm/Nd is constant through time and in which $^{143}\text{Nd}/^{144}\text{Nd}$ changes along a simple, essentially straight-line trajectory, is herein termed a "uniform reservoir" (UR) and its $^{143}\text{Nd}/^{144}\text{Nd}$ at any time T in the past ($I_{UR}(T)$) is given by:

$$(5) \quad I_{UR}(T) = I_{UR}(0) - \left(\frac{^{147}\text{Sm}}{^{144}\text{Nd}} \right)_{UR}^0 (e^{\lambda T} - 1)$$

where $I_{UR}(0)$ is the value of $^{143}\text{Nd}/^{144}\text{Nd}$ in UR today, $(^{147}\text{Sm}/^{144}\text{Nd})_{UR}^0$ is that in UR today and T is measured backwards from the present. As shown in Figure 3, in the general case Sm/Nd in the planet could be different from that in the solar nebula due to fractionation during condensation.

Figure 3a depicts a sequence of events in the history of a planet in the form of a series of cross-sectional views through the planet. At time T_C the planet has just condensed and accreted and is

assumed to be a compositionally uniform sphere which has the same Sm/Nd throughout. At time T_{m1} , there is an episode of magmatism where small volumes of the interior of the planet are melted and the magmas thus formed ascend to the surface of the planet and are erupted as lava flows. The shaded "plumb-bobs" in Figure 3a represent the magmas; the region of melting in the planet's interior is represented by the circular "blob"; a conduit to the surface and the lava flow on the surface are also shown. Since at time T_{m1} , the planet is still homogeneous, both lava flows 1a and 1b will have the same $^{143}\text{Nd}/^{144}\text{Nd}$ at the time of eruption and their $^{143}\text{Nd}/^{144}\text{Nd}$ will lie on the evolution curve of the bulk planet as shown in Figure 3b. However, the lavas could have Sm/Nd different from the bulk planet, so subsequent to T_{m1} , their $^{143}\text{Nd}/^{144}\text{Nd}$ could evolve away from that of the bulk planet as is shown by the two unshaded arrows on Figure 3b. If these two lava flows could be sampled today, their measured $^{143}\text{Nd}/^{144}\text{Nd}$ would be much different from the value in the bulk planet today ($I_{UR}(0)$). By measuring Sm/Nd in the lava we can correct for the ^{143}Nd produced since the lava was erupted T_{m1} years ago (determined for example by some other dating method) and calculate its initial $^{143}\text{Nd}/^{144}\text{Nd}$, which would in this case be equal to $I_{UR}(T_{m1})$ for both lava 1a and 1b. For a rock sample of age T the initial $^{143}\text{Nd}/^{144}\text{Nd}$ ($I_{sample}(T)$) is calculated from

$$(6) \quad I_{sample}(T) = \frac{^{143}\text{Nd}/^{144}\text{Nd}_{meas}}{^{147}\text{Sm}/^{144}\text{Nd}_{meas}} - \left[e^{\lambda T} - 1 \right].$$

The initial $^{143}\text{Nd}/^{144}\text{Nd}$ and the age of the sample can also be determined concurrently by determining a Sm-Nd internal isochron on the sample.

If the volume of magma extracted from the planet's interior is very small with respect to the volume of the entire planet, the removal of the magma will not affect the composition of the interior. If the planet remains a compositionally homogeneous sphere throughout its history, then all lavas derived by melting of its interior will have initial $^{143}\text{Nd}/^{144}\text{Nd}$ which lie on the UR evolution curve. In this case $I_{\text{UR}}(T)$ would be the locus of I values of all igneous rocks as a function of time, hence the notation.

At time T_f the outer part of the planet is differentiated into two layers A and B. Layer A has Sm/Nd lower than the bulk planet and layer B has higher Sm/Nd. Following the course of events on Figure 1b we see that immediately after the differentiation layers A and B and the remaining undifferentiated part of the planet still have identical $^{143}\text{Nd}/^{144}\text{Nd}$, but subsequently they evolve different $^{143}\text{Nd}/^{144}\text{Nd}$. Layer A evolves along a line of lower slope due to its lower Sm/Nd while in layer B $^{143}\text{Nd}/^{144}\text{Nd}$ evolves more rapidly due to its higher Sm/Nd.

At time T_{m2} there is a second episode of magmatism in which magmas are derived from each of layers A, B, and UR. Lava 2a, melted from layer B, will have an initial $^{143}\text{Nd}/^{144}\text{Nd}$ lying above the UR evolution curve, while the initial $^{143}\text{Nd}/^{144}\text{Nd}$ of lava 2c, melted from layer A will lie below the UR curve. Thus, unlike the rocks produced

in the melting event at T_m^1 where all lavas had identical initial $^{143}\text{Nd}/^{144}\text{Nd}$, at T_m^2 we find that different lavas have different initial $^{143}\text{Nd}/^{144}\text{Nd}$.

To trace the differentiation history of the planet we therefore attempt to determine the initial $^{143}\text{Nd}/^{144}\text{Nd}$ of igneous rocks of different ages. If these I values should fall along a single straight line such as $I_{UR}(T)$ in Figure 3b then we would conclude that the magma sources in the interior of the planet have remained essentially undifferentiated throughout its history and from the slope of the line we could infer the Sm/Nd of the planet. However, if we see dispersion in I values, then we would conclude that the planet's interior is comprised of chemically distinct reservoirs which remain isolated from each other for long periods of time.

For the simple planetary history shown in Figure 3 we would find that igneous rocks of ages greater than T_f would all fall on a single evolution curve and would thus give an indication of the Sm/Nd of the planet. Subsequent to T_f we would find that many igneous rocks would have I values which did not lie on this evolution curve. We might wish to ask the question of whether undifferentiated material still existed in the planet subsequent to T_f . This question might be important for attempting to reconstruct the thermal history of the planet. If a large number of igneous rocks with ages less than T_f also fell on the UR evolution curve, then we might conclude that undifferentiated material did still exist in the planet. However, we can see from Figure 1a that magmas derived from deep layers must pass

through the shallower layers in order to reach the surface. Thus these magmas could incorporate material from these shallower layers resulting in a change in the isotopic composition of the magmas. For example, a magma derived from layer B and having $^{143}\text{Nd}/^{144}\text{Nd}$ lower than UR could, while rising to the surface, incorporate material from layer A which has $^{143}\text{Nd}/^{144}\text{Nd}$ higher than UR so that the resulting magma erupted at the surface would have $^{143}\text{Nd}/^{144}\text{Nd}$ lying close to the UR curve. This magma would thus appear to be derived from undifferentiated UR material when in fact it had not been. It is also clear from Figure 3a that magmas derived from the deepest layers will have the greatest chance of having their isotopic compositions altered on the way to the surface. In general, the problem of magma contamination during ascent will always provide a complicating factor in the interpretation of the isotopic data. Because of this the existence of undifferentiated material in a planet which is differentiated must be argued mainly on statistical grounds, that is on the frequency of occurrence of igneous rocks with isotopic compositions lying on a simple UR evolution curve.

The determination of the evolution curve for undifferentiated material is important because, if it is known, then $^{143}\text{Nd}/^{144}\text{Nd}$ of a reservoir can provide information on what processes were involved in forming that reservoir. As noted earlier, for Sm-Nd, if a rock is partially melted, the liquid fraction will generally have a lower Sm/Nd and the crystalline residue will have a higher Sm/Nd than the starting material. Thus as in the example in Figure 2 we see that it would be

possible to identify layer A with a liquid and layer B with a residue if the bulk planet evolution curve is known. Thus layers A and B could have formed when the original UR material comprising the outer parts of the planet was partially melted and gravitationally differentiated. Such a simple interpretation may be applicable to the early differentiation of the moon. The complementary relationship between layers A and B could only be surmised if the bulk planet UR evolution curve was known. Consider, for instance, that if the UR curve actually lay below the I value of lava 2c, then it would appear that all the lavas formed at T_{m_2} were derived from material with Sm/Nd higher than the bulk planet and they could thus all be interpreted as having been derived from material which was a crystalline residue from some previous partial melting event. Thus in piecing together the differentiation history of a planet from isotopic data it is necessary to know the bulk Sm/Nd of the planet as well as possible to be able to fully interpret the variations of initial $^{143}\text{Nd}/^{144}\text{Nd}$.

Figure 3 can be interpreted in terms of a simple history of the earth. Consider UR to represent undifferentiated homogeneous mantle after formation of the earth's core early in earth history. This mantle material will have Sm/Nd equal to that of the bulk earth if the core has very low concentrations of Sm and Nd. At time T_f the outer parts of the mantle are differentiated into a low- Sm/Nd crust represented by layer A and a high- Sm/Nd complementary residue in the mantle layer B. The remaining UR material represents parts of the mantle which were not involved in the formation of the crust and are

therefore still undifferentiated. We would interpret the initial $^{143}\text{Nd}/^{144}\text{Nd}$ of lava 2c as indicating that this lava has formed by melting of crustal rocks while the I value of lava 2a would suggest it to be the product of remelting of the residual mantle material left after formation of the crust at time T_f . Lava 2b could be taken as indicating the existence of undisturbed mantle, and the isotopic difference between 2a and 2b indicates an isotopically inhomogeneous mantle. The preservation of reservoir B separate from the remaining UR material over the time interval from T_f to T_{m_2} also conveys information about mantle dynamics. If the mantle were rapidly convecting, we might expect that layer B would be rapidly remixed with the remaining UR material resulting in a homogeneous mantle. Thus the preservation of isotopic differences in the mantle over long periods of time limits the amount of mixing which can occur as a result of convection.

The value of the Sm-Nd system--Comparison to Rb-Sr and U-Th-Pb

Some questions may arise as to why it is necessary to measure Nd isotopic variations to study the differentiation of the earth when the Rb-Sr and U-Th-Pb systems can and have been used for the same purpose in the past. There are several reasons why the Sm-Nd system can be useful and may complement studies of other isotopic systems.

The Sm-Nd system differs from the other isotopic systems currently in use in that both parent and daughter element are refractory and both are lithophile elements. In contrast Rb and Pb are volatile while Sr, U, and Th are refractory, thus the parent/daughter ratios

for these systems can be drastically changed during, for instance, nebular condensation while Sm/Nd may not be affected (Boynton, 1975). Variations in Rb/Sr or U/Pb in the earth could be the result of fractionations which occurred during condensation of the material which accreted to form the earth, while variations of Sm/Nd could not. Pb also is a chalcophile element and thus formation of a core with significant (Fe, Ni)S could have drastically changed U/Pb and Th/Pb in the outer earth (Ringwood, 1966; Gancarz and Wasserburg, 1977), but would not affect Sm/Nd since neither Sm nor Nd would be expected to partition into the Fe-FeS phase. Thus while both the Rb-Sr and the U-Th-Pb systems can be affected during condensation and core formation, the Sm-Nd system is probably not affected. Therefore, the variations observed in $^{143}\text{Nd}/^{144}\text{Nd}$ in the earth are probably solely the result of variations of Sm/Nd which were caused by magmatic processes involving silicate crystal-melt equilibria. Also, large parent/daughter fractionations caused by poorly understood processes such as volatile transfer will likely not affect Sm and Nd but could affect Rb and Pb.

One of the primary ways in which the earth has differentiated is through magmatic processes. Portions of the earth's interior are continually being partially melted and the magmas thus produced ascend and are emplaced into the crust. During the partial melting process Sm and Nd may be fractionated so that the melt has Sm/Nd different from the crystalline residue (see Chapter III). The partitioning of Sm and Nd between a melt phase and a crystal assemblage depends on the composition of the melt and the particular crystal phases present and

their proportions. The partitioning of REE between coexisting minerals and between minerals and coexisting melts has been extensively studied (cf., Schnetzler and Philpotts, 1968, 1970; Weill and McKay, 1975; Drake and Weill, 1975). For this reason, the behavior of Sm and Nd during partial melting and fractional crystallization is fairly well understood. In general, if a rock of the probable composition of the earth's mantle (peridotite) is partially melted, the melt will be greatly enriched in both Sm and Nd and will have a lower Sm/Nd than the crystalline residue. As an example, an average basalt may be enriched in Nd and Sm by factors of 25 and 15 respectively over the concentrations found in the mantle.

A radioactive parent/daughter system can be useful as a tracer in magmatic processes if the parent and daughter element are fractionated by the crystalline phases. Sm and Nd will be fractionated by different residual mineral phases than are Rb-Sr or U-Pb. The U-Pb system is sensitive to sulfides and feldspar which concentrate Pb and to amphibole and several minor minerals such as zircon, apatite, and sphene which concentrate U. For Rb-Sr, plagioclase, phosphates, and clinopyroxene concentrate Sr while micas and K-feldspar are enriched in Rb. Sm and Nd are most strongly fractionated by clinopyroxene and garnet which tend to concentrate Sm more than Nd. Sm-Nd is thus particularly interesting in that they are fractionated by minerals which may be important constituents of much of the upper mantle.

Sm-Nd will also be useful for dating ancient rocks and should be complementary to the Rb-Sr and U-Th-Pb systems. It will be

especially powerful for the determination of precise ages of ancient basic and ultrabasic rocks, which have proven difficult to date by other methods. For instance, in layered mafic intrusions such as the Stillwater intrusion in Montana (cf. Hess, 1960), and the Muskox intrusion (Irvine and Smith, 1967) of the NW Territories, Canada, sufficient Sm/Nd fractionation occurs between the major mineral phases olivine, pyroxene, plagioclase, magnetite and apatite, so that a precise internal isochron could be obtained.

In general, Sm-Nd should prove to be a fruitful method for dating ancient rocks because both Sm and Nd are found mainly in the primary rock-forming mineral phases, and their lithophile geochemical character may result in their being less prone to post-crystallization redistribution than are the possibly more mobile elements Rb, Sr, U, and Pb. The success of Lugmair (1974) and Lugmair, et al. (1975a,b) in their pioneering work on basaltic achondrites and lunar basalts clearly demonstrated the potential of this method. Papanastassiou, DePaolo and Wasserburg (1977) also showed that the Sm-Nd method could be used to obtain precise crystallization ages of lunar basalts which are very poor in Rb and thus difficult to date by Rb-Sr. Due to the limited variation of Sm/Nd in minerals the Sm-Nd method will be restricted to the dating of Precambrian rocks unless substantial improvements in analytical precision are made.

III. DATA REPRESENTATION

$^{143}\text{Nd}/^{144}\text{Nd}$ data are expressed in this work using a notation which differs significantly from that which has been used for Sr and Pb isotopic data. This notation grew out of discussions of the data as it became clear that a concise vehicle for communication was lacking. The following is an explanation of this notation, and following it is a discussion of why this type of notation was selected. Although, it was originally tailor-made for the Sm-Nd system, an analogous notation may be found to be quite useful in other isotopic systems, and we have ventured to introduce such notation for Rb-Sr also (DePaolo and Wasserburg, 1977).

Figure 4 is a graphical illustration of the notation. $^{143}\text{Nd}/^{144}\text{Nd}$ are always normalized to $^{143}\text{Nd}/^{144}\text{Nd}$ in a "uniform reservoir", as defined previously. For our purposes we have chosen this reservoir to have the average chondritic Sm/Nd for all time. The evolution of $^{143}\text{Nd}/^{144}\text{Nd}$ in this CHondritic Uniform Reservoir (CHUR) is tentatively assumed to be identical to that in the Juvinas achondrite. Juvinas has a crystallization age of 4.56 AE (Lugmair, *et al.*, 1976) and has a present-day Sm/Nd (0.307 atomic) which is almost identical to the average value of Sm/Nd measured in chondritic meteorites (0.309 ± 0.005 lo) (Masuda, *et al.*, 1973, Nakamura, 1974). Thus $^{143}\text{Nd}/^{144}\text{Nd}$ in CHUR as a function of time T_1 measured backward from today, is given by:

$$(7) \quad I_{\text{CHUR}}(T) = I_{\text{CHUR}}(0) - \left(\frac{^{147}\text{Sm}}{^{144}\text{Nd}} \right)_{\text{CHUR}}^0 \left[e^{\lambda_{\text{Sm}} T} - 1 \right]$$

Figure 4: (a) Graph of $^{143}\text{Nd}/^{144}\text{Nd}$ versus time (age) illustrating the notation used to present Nd isotope data. Meas \equiv measured, $T_c \equiv$ time of condensation or original formation of the earth, CHUR \equiv Chondritic Uniform Reservoir, S \equiv sample, $T_x \equiv$ crystallization age. $I_{\text{CHUR}}(T)$ and $I_s(T)$ are defined in the text. (b) Graph of ϵ_{Nd} versus time. The line $\epsilon_{\text{Nd}} = 0$ corresponds to the line $I_{\text{CHUR}}(T)$ in Figure 4a. This diagram simply presents a magnified view of the data so that the deviations of the data from the $I_{\text{CHUR}}(T)$ line can be more closely examined.

$$\epsilon_{Nd}(0) \equiv \left[\frac{(^{143}\text{Nd}/^{144}\text{Nd})_{\text{meas}}}{I_{\text{CHUR}}(0)} - 1 \right] \times 10^4$$

$$\epsilon_{Nd}(T_X) \equiv \left[\frac{I_S(T_X)}{I_{\text{CHUR}}(T_X)} - 1 \right] \times 10^4$$

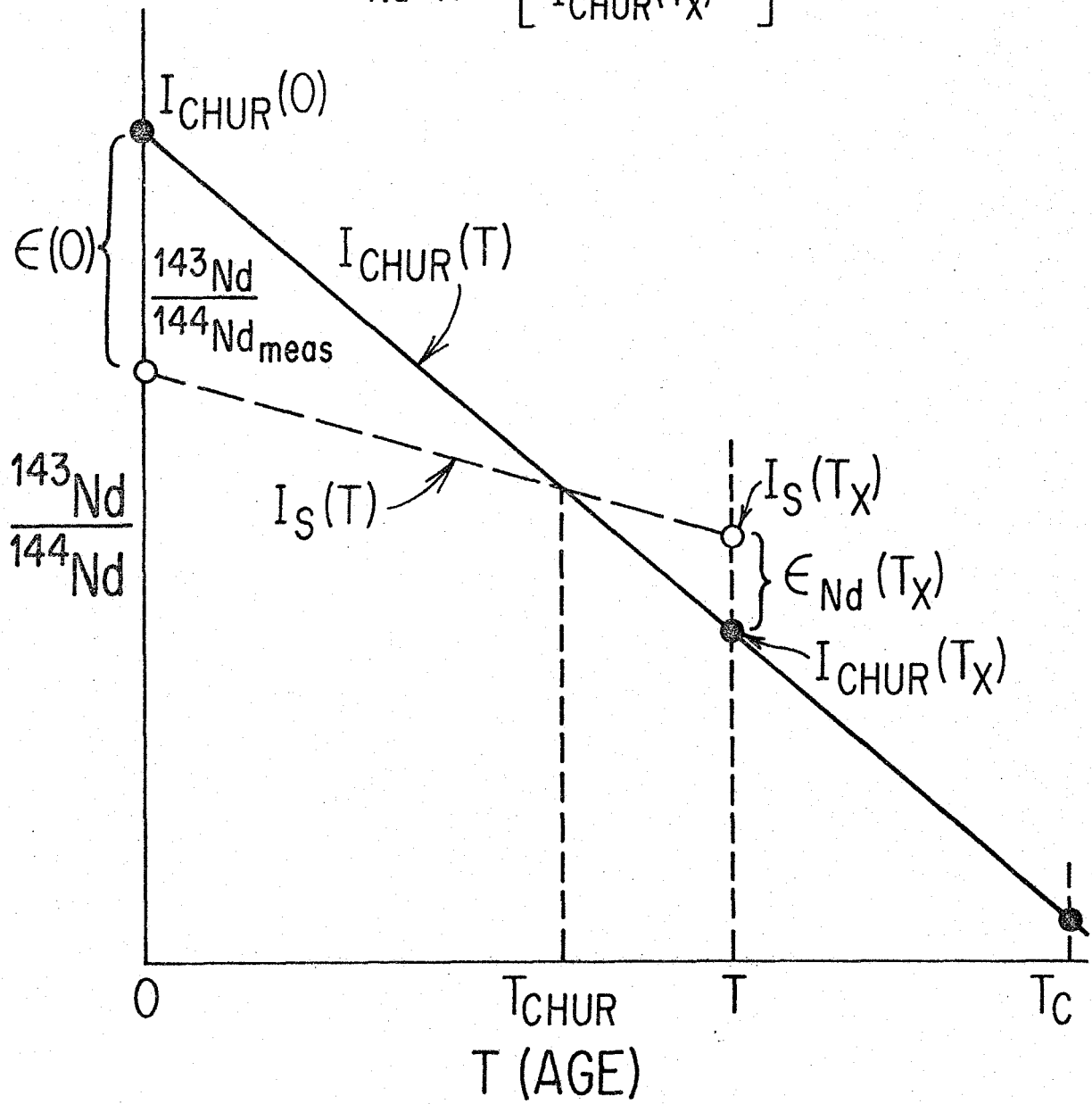


Fig. 4a

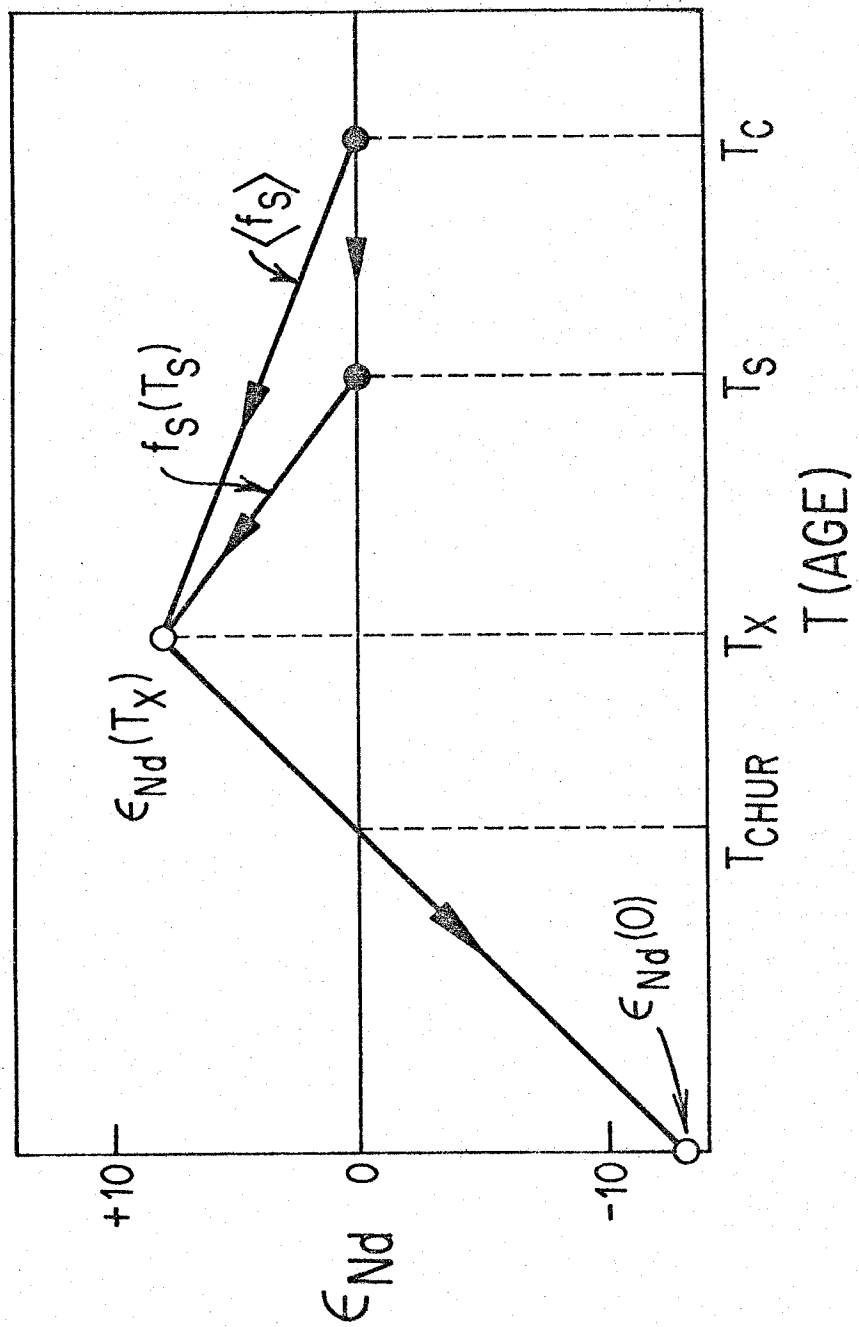


Fig. 4b

$^{143}\text{Nd}/^{144}\text{Nd}$ in CHUR today is $I_{\text{CHUR}}(0) = 0.511836$ (Lugmair, pers. comm.; normalized to $^{150}\text{Nd}/^{142}\text{Nd} = 0.2096$, see Appendix 5) and $(^{147}\text{Sm}/^{144}\text{Nd})_{\text{CHUR}}^0 = 0.1936$. The evolution curve is calculated backward in time from measured values since the measured values are well-defined observable quantities. Initial $^{143}\text{Nd}/^{144}\text{Nd}$ for Juvinas, or a "best" initial for Nd which would be similar to BABI in the Rb-Sr system (Papanastassiou and Wasserburg, 1969), are presently poorly defined due to the fact that no mineral phases exist which have near-zero Sm/Nd. As shown in Figure 4, $^{143}\text{Nd}/^{144}\text{Nd}$ measured in a sample is expressed as the fractional deviation in parts in 10^4 from the present value in CHUR. This fractional difference is termed $\varepsilon_{\text{Nd}}(0)$ and defined:

$$(8) \quad \varepsilon_{\text{Nd}}(0) \equiv \left[\frac{(^{143}\text{Nd}/^{144}\text{Nd})_{\text{meas}}}{I_{\text{CHUR}}(0)} - 1 \right] \times 10^4$$

Generally, we are interested in the initial $^{143}\text{Nd}/^{144}\text{Nd}$ of igneous rocks, which is the value in the rock at the time it first crystallized. For a rock of age T_x , its initial $^{143}\text{Nd}/^{144}\text{Nd}$ ($\equiv I_s(T_x)$) can be calculated from the measured values of $^{143}\text{Nd}/^{144}\text{Nd}$ and $^{147}\text{Sm}/^{144}\text{Nd}$ by the relation:

$$(9) \quad I_s(T_x) = (^{143}\text{Nd}/^{144}\text{Nd})_{\text{meas}} - (^{147}\text{Sm}/^{144}\text{Nd})_{\text{meas}} \left[e^{\lambda_{\text{Sm}} T_x} - 1 \right].$$

The initial $^{143}\text{Nd}/^{144}\text{Nd}$ is expressed as the fractional deviation from the value in CHUR at T_x and termed $\varepsilon_{\text{Nd}}(T_x)$. This is defined as:

$$(10) \quad \epsilon_{\text{Nd}}(T_x) \equiv \left[\frac{I_s(T_x)}{I_{\text{CHUR}}(T_x)} - 1 \right] \times 10^4$$

In normal usage we drop the time designation, and ϵ_{Nd} is taken always to refer to the initial $^{143}\text{Nd}/^{144}\text{Nd}$. Measured values are referred to as $\epsilon_{\text{Nd}}(0)$. The Sm/Nd ratios are also normalized to the value in CHUR. The Sm/Nd of a rock is expressed in terms of an enrichment factor $f_{\text{ROCK}}^{\text{Sm/Nd}}$ which is defined:

$$(11) \quad f_{\text{ROCK}}^{\text{Sm/Nd}} \equiv f_R = \frac{(\text{Sm/Nd})_{\text{ROCK}}}{(\text{Sm/Nd})_{\text{CHUR}}} - 1$$

A similar enrichment factor $f_{\text{SOURCE}}^{\text{Sm/Nd}} (\equiv f_s)$ can be defined for a source reservoir. With this parameter in hand a simple expression can be written for $\epsilon_{\text{Nd}}(T_x)$:

$$(12) \quad \epsilon_{\text{Nd}}(T_x) \approx \epsilon_{\text{Nd}}(0) + f_R Q_{\text{Nd}} T_x$$

$$\text{where } Q_{\text{Nd}} = \frac{\lambda_{\text{Sm}} (^{147}\text{Sm}/^{144}\text{Nd})_{\text{CHUR}}^0}{I_{\text{CHUR}}(0)} \cdot 10^4 \quad \text{is a constant.}$$

The deviations ϵ_{Nd} from the CHUR growth curve are presented in a diagram as shown in Figure 4b. This diagram shows the evolution of the sample shown in Figure 4a on a plot of ϵ_{Nd} vs. T .

ϵ_{Nd} gives information on the Sm/Nd in the magma source or "parent reservoir". Thus, a rock with $\epsilon_{\text{Nd}}(T_x) = 0$ was derived from

a reservoir which had chondritic Sm/Nd during the time period from the condensation of the earth T_c until T_x . A rock with $\epsilon_{Nd}(T_x) > 0$ (as illustrated in Figure 4) was derived from a reservoir which must have had a higher than chondritic Sm/Nd during some part of the interval from T_c to T_x . Similarly, $\epsilon_{Nd} < 0$ indicates the rock was derived from a reservoir which had Sm/Nd less than chondritic for some time. The average value of f_s over the time interval $T_c - T_x$ is given by:

$$(13) \quad \langle f_s \rangle \equiv Q \frac{\epsilon_{Nd}}{(T_c - T_x)} \equiv \frac{f^*T^*}{T_c - T_x}$$

f^*T^* ($\equiv \epsilon_{Nd}/Q$) is a generalized quantity which expresses the fact that the deviation ϵ_{Nd} is proportional to the product of the enrichment factor in the reservoir and the time over which the reservoir has had this enrichment factor. Thus, as shown in Figure 4b if the source reservoir evolved in two discrete stages, i.e. from T_c until T_s it had $f_s = 0$, and from T_s until T_x it had f_s , then for any assumed T_s we can calculate f_s to be:

$$(14) \quad f_s(T_s) = \frac{f^*T^*}{T_s - T_x}$$

T_s is a "model age" of the source reservoir of a rock. Taken literally it implies that the reservoir began with a chondritic Sm/Nd at T_c , at time T_s it acquired an Sm/Nd enrichment factor of f_x and was melted at T_x to form the rock. From $f_s(T_s)$ and the measured Sm/Nd

enrichment factor in the rock (f_R) one can calculate a model Sm/Nd enrichment factor for the sample relative to the source reservoir g :

$$(15) \quad g = \left[\frac{1 + f_R}{1 + f_s (T_s)} \right]^{-1}$$

In general the evolution of the source can occur in multiple stages and the ϵ_{Nd} of the source at any time is the sum of the growth of ϵ_{Nd} over all the stages:

$$(16) \quad \epsilon_{Nd} (T_x) = \sum_{i=1}^n (f_s)_i Q_{Nd} \Delta T_i \equiv \langle f_s \rangle Q_{Nd} (T_c - T_x)$$

where $\sum_{i=1}^n \Delta T_i = T_c - T_x$. The simplest model g is calculated from

$$(17) \quad g = \left[\frac{1 + f_R}{1 + \langle f_s \rangle} \right]^{-1}$$

The true fractionation factor for the rock relative to the source for an n -stage source history is

$$(18) \quad g = \left[\frac{1 + f_R}{1 + (f_s)_n} \right]^{-1}$$

As shown in Figure 4, the time corresponding to the point where the evolution of $^{143}\text{Nd}/^{144}\text{Nd}$ in the rock sample $I_s (T)$ intersects $I_{CHUR} (T)$ is termed T_{CHUR} . T_{CHUR} is a "model age" of the rock which is equal to the crystallization age if the rock was derived directly from a

CHUR reservoir, i.e., if $\varepsilon_{\text{Nd}}(T_x) = 0$. T_{CHUR} is given approximately by:

$$(19) \quad T_{\text{CHUR}} \cong \frac{\varepsilon_{\text{Nd}}(0)}{f_R Q}$$

The notation outlined above was initially adopted because the variations of $^{143}\text{Nd}/^{144}\text{Nd}$ are small. The total change of $^{143}\text{Nd}/^{144}\text{Nd}$ in 4.5 AE in a reservoir with a chondritic Sm/Nd is only 1.13%. It was thus thought necessary to express the measured values of the numbers as deviations from a standard value. This has been used quite successfully for oxygen and deuterium isotopic variations (c.f. Epstein and Mayeda, 1953). The standard reference material was chosen to be a hypothetical reservoir with chondritic Sm/Nd because chondritic abundances have been traditionally used as a standard for rare-earth element abundances. The CHUR reference also has the added advantage of being a good a priori first estimate of the evolution of $^{143}\text{Nd}/^{144}\text{Nd}$ in the bulk earth. As discussed previously, knowledge of the bulk earth evolution curve is necessary to fully interpret the isotopic data. Thus this notation tends to emphasize the divergence of secondary growth curves from a primary reference curve, as shown in Figure 3. As was immediately shown by the first data collected (DePaolo and Wasserburg, 1976a), the initial $^{143}\text{Nd}/^{144}\text{Nd}$ of terrestrial rocks cluster tightly about the CHUR evolution curve and this data representation scheme allows the variations about that curve, which are small compared to the overall growth of $^{143}\text{Nd}/^{144}\text{Nd}$, to be brought out more clearly.

Besides being an aid in data presentation, the ϵ_{Nd} values are closely tied to the interpretation of data. Through the f^*T^* values information about the fractionation history of reservoirs is readily available and this is true in like manner for samples of any age. The fractionation factor g between the sample and the source reservoir also is easily calculated from these parameters. g is an extremely useful petrogenetic indicator since it can be modelled with Sm and Nd mineral/melt distribution coefficients with assumptions about the mineralogy of the magma source, the degree of melting and the fractional crystallization history of the sample as discussed in the next section.

In theory this approach could also be used for Rb-Sr. However, the evolution curve of a meaningful reference reservoir which might approximate the bulk earth is not defined for Rb-Sr. The Rb/Sr of the earth appears to be much different from chondritic (Gast, 1960) and initial $^{87}\text{Sr}/^{86}\text{Sr}$ ratios of igneous rocks through time have so far not been found to cluster about a single evolution curve. However, during the course of this work it has been possible to obtain an estimate of the earth's Rb/Sr and so this approach has been intrepidly extended to the Rb-Sr system.

Initial $^{87}\text{Sr}/^{86}\text{Sr}$ are expressed in terms of a parameter ϵ_{Sr} defined in a manner analogous to ϵ_{Nd} for $^{143}\text{Nd}/^{144}\text{Nd}$. We therefore define

$$(20) \quad \epsilon_{\text{Sr}}(T) \equiv \epsilon_{\text{I Sr}}^{\text{UR}}(T) \equiv \left[\frac{I_{\text{S}}(T)}{I_{\text{UR}}(T)} - 1 \right] \times 10^4$$

$\epsilon_{\text{Sr}}(T)$ is the deviation of initial $^{87}\text{Sr}/^{86}\text{Sr}$ in a sample from the value in a standard uniform reservoir UR at time T. The standard reservoir used here for reference is defined by $I_{\text{UR}}(0) = 0.7045$ and $(^{87}\text{Rb}/^{86}\text{Sr})_{\text{UR}}^0 = 0.0839$. Our choice of this standard reservoir for Rb-Sr is based upon the correlation of initial Nd and Sr in young basalts (DePaolo and Wasserburg, 1976b). $I_{\text{S}}(T)$ is the initial $^{87}\text{Sr}/^{86}\text{Sr}$ of the sample, T is the sample's age, $I_{\text{UR}}(T) = I_{\text{UR}}(0) - (^{87}\text{Rb}/^{86}\text{Sr})_{\text{UR}}^0 [e^{\lambda_{\text{Rb}} T} - 1]$, and $\lambda_{\text{Rb}} = 1.39 \times 10^{-11} \text{ yr}^{-1}$. In this notation a zero age rock with $^{87}\text{Sr}/^{86}\text{Sr} = 0.7045$ has $\epsilon_{\text{Sr}} = 0$ while a zero age MOR basalt with $^{87}\text{Sr}/^{86}\text{Sr} = 0.70239$ has $\epsilon_{\text{Sr}} = -30$. This notation allows comparison of Nd and Sr in a similar manner for rocks of arbitrary age, and makes it much easier to compare initial $^{87}\text{Sr}/^{86}\text{Sr}$ in rocks of greatly different ages by subtracting the effects of "normal" growth of $^{87}\text{Sr}/^{86}\text{Sr}$ with time.

The most useful reference reservoirs for Sr and Nd would be those representative of the bulk earth, since then variations of the ϵ_{Sr} and ϵ_{Nd} values could be directly related to the processes involved in differentiation of the planet into various different reservoirs. The standard reference reservoirs proposed here for both Nd and Sr are presently thought to be close approximations to bulk earth values (DePaolo and Wasserburg, 1976b). However, incorporation of this inference into the notation has been purposely avoided because it is based on limited data and understanding and the values in the bulk earth should therefore be considered as important parameters which are still to be firmly established.

III. REE FRACTIONATION DURING PARTIAL MELTING AND VARIATIONS OF ϵ_{Nd}

The rare-earth elements can be strongly fractionated during magmatic processes such as partial melting or fractional crystallization. Nd isotopic variations can be used to study the chemical layering in the earth which results from the operation of these processes. The following illustrates the magnitude of REE fractionation during partial melting and shows how the fractionations are related to variations of ϵ_{Nd} .

The mathematical development of the behavior of trace elements during partial melting was presented by Gast (1966) and Shaw (1970). For this example we will assume that when a rock is partially melted, the ratio of the concentration of a trace element i in the melt to the concentration in the solid residue is a constant, D_i . Figure 5a shows the REE patterns which will result from partial melting of a rock which originally has a chondritic REE pattern. To make the example concrete, the D_i 's for the REE have been calculated from measured melt/mineral D_i 's taken from the literature (Kay and Gast, 1973) for a rock with the mineralogy given in Figure 5b. This mineralogy was chosen because it may approximate that of the upper mantle. Figure 5a gives the REE patterns in the melt and the crystalline residue after 1%, 10%, and 30% of the rock is melted. The Sm/Nd enrichment factor ($f_{Sm/Nd}$) for each melt and residue are also given.

Consider first a single melting event, shown in Figure 5a. The light REE are more strongly partitioned into the melt phase than are the heavy REE. After only one weight percent of the rock is melted, the melt contains 60% of the Ce in the system. After 10% is melted, 90% of

Figure 5: Calculated REE patterns for melts and crystalline residues formed by different degrees of partial melting of a rock with the mineralogy given in Figure 5b. All REE patterns are normalized to the abundances in the original source rock as shown in Figure 5a which are assumed to be chondritic for simplicity.

These patterns were calculated assuming 1) a bulk liquid/solid distribution coefficient $D_i = \text{constant}$ describes the behavior of each rare-earth element, and 2) the melt is extracted from the residue in infinitesimal increments and collected in an isolated reservoir (Shaw, 1970; equation 10). The D_i 's were calculated using data given by Kay and Gast (1973).

Referring to Figure 5a, if the rock is 1% melted, the melt will have the REE pattern labelled "1% melt" and the remaining crystalline residue will have the pattern labelled "residue 1% melt." The f values shown are the Sm/Nd enrichment factors. Note that for this model the heavy REE are strongly retained in the crystalline residue in preference to the light REE. This effect is due to the presence of garnet in the crystalline residue, which concentrates heavy REE. The patterns labelled "melts" represent what one would expect to find in mantle-derived melts such as basalts perhaps. Figure 5b shows the patterns which would result in magmas formed by a second melting of the "residue 1% melt" from Figure 5a. In this case the starting material is slightly depleted in light REE relative to heavy REE. Figure 5c shows the patterns resulting from melting of a source rock which is even more highly depleted in light REE. Figures 5a, b, and c, taken together,

show how REE patterns in a volume of mantle rock will change as this rock is melted 1% three successive times with the melt being totally removed from the crystalline residue in each case.

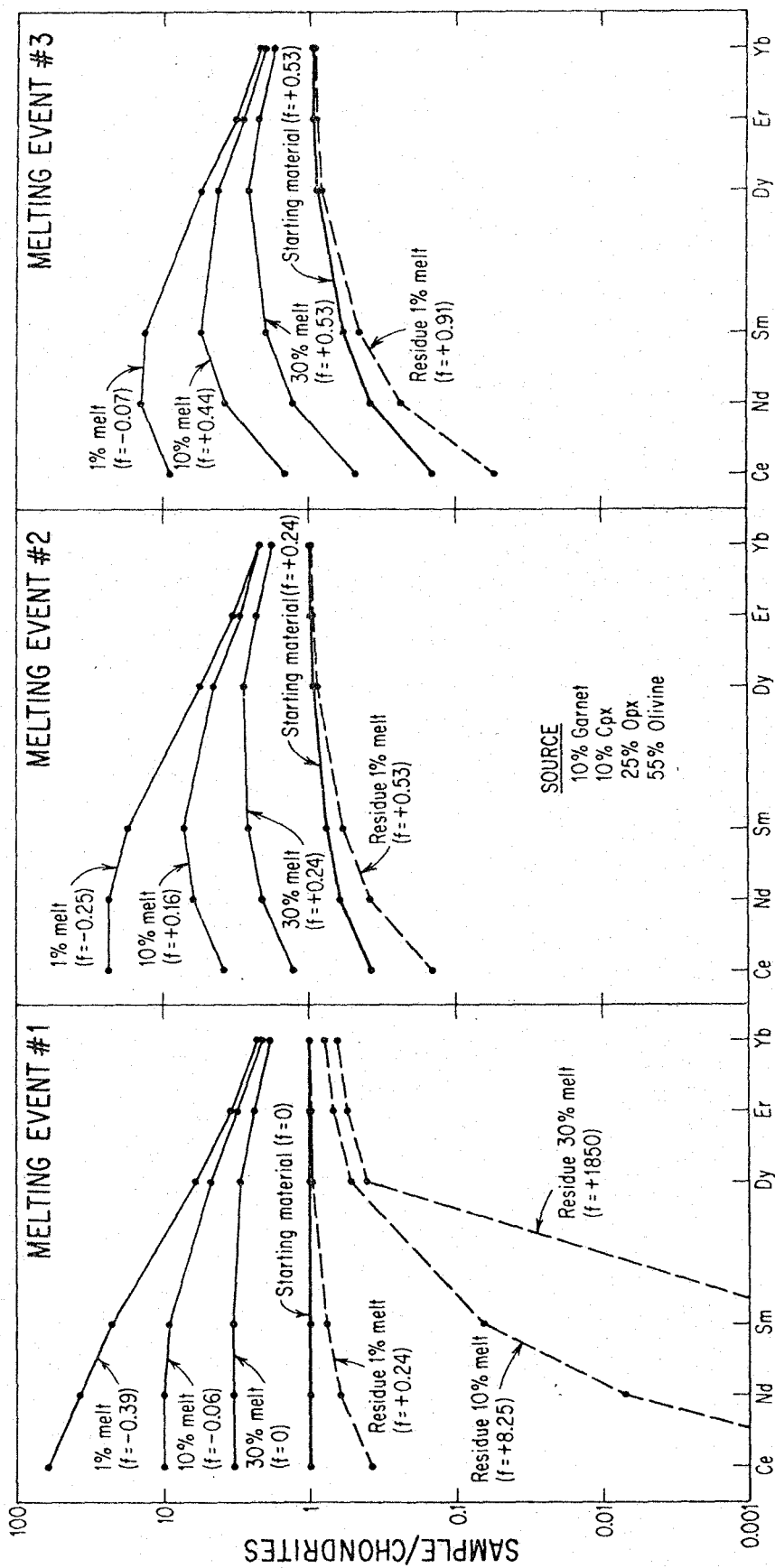


Fig. 5

the Ce, Nd, and Sm are in the melt. With regard to the fractionation of Sm and Nd the following points should be noted:

- (1) The $f_{\text{Sm}/\text{Nd}}$ of the melt is always less than or equal to the $f_{\text{Sm}/\text{Nd}}$ of the source rock or starting material.
- (2) The greatest Sm-Nd fractionation between the melt and the starting material occurs for the first increment of melt and is given by $g_{\text{max}} = D_{\text{Sm}}/D_{\text{Nd}} - 1$. The $f_{\text{Sm}/\text{Nd}}$ of this first increment is given by:

$$\frac{D_{\text{Sm}}}{D_{\text{Nd}}} (1 + f_s) - 1$$

where f_s is the Sm/Nd enrichment factor of the starting material. As the percentage of melting increases $f_{\text{Sm}/\text{Nd}}$ of the melt approaches $f_{\text{Sm}/\text{Nd}}$ of the starting material, i.e., $g \rightarrow 0$.

- (3) As the percentage of melting increases $f_{\text{Sm}/\text{Nd}}$ of the crystalline residue becomes very large, reaching absolute values much greater than $f_{\text{Sm}/\text{Nd}}$ of the melt.

Now suppose that a volume of rock which originally had a chondritic REE pattern is melted 1% and the melt is removed. The remaining solid material has a REE pattern given in Figure 5a and labelled "Residue 1% melt." Suppose that this residual material is now partially melted at some later time. This situation is shown in Figure 5b. For the same fraction of partial melting, the REE patterns of the melts look significantly different from those in Figure 5a, especially for the light REE. The $f_{\text{Sm}/\text{Nd}}$'s of the melts are drastically different from those in Figure 5a, and for larger percentages of melting the melts have

positive values of $f_{\text{Sm}/\text{Nd}}$ in contrast to the negative values shown in Figure 5a for the melts.

If 1% melt is again extracted, the crystalline residue will have a REE pattern like that labelled "Residue 1% melt" in Figure 5b. If this residue is then partially melted, the REE patterns shown in Figure 5c result. Note that for this case, only small percentage melts will have $f_{\text{Sm}/\text{Nd}}$ less than zero. In general, the $f_{\text{Sm}/\text{Nd}}$ of a melt can be positive only if the $f_{\text{Sm}/\text{Nd}}$ of the source is positive. The $f_{\text{Sm}/\text{Nd}}$ of a melt can be negative even if $f_{\text{Sm}/\text{Nd}}$ of the source is positive if the percentage melting is small. But if $f_{\text{Sm}/\text{Nd}}$ of the source is greater than $D_{\text{Nd}}/D_{\text{Sm}} - 1$, then no partial melt can have $f_{\text{Sm}/\text{Nd}} < 0$.

These examples illustrate the magnitude of Sm-Nd fractionation during partial melting and how it relates to the distribution coefficients (D_{Sm} and D_{Na}) and the percentage of melting.

It should be kept in mind that a very simple melting model is being considered here, and some of the above rules may not hold in more complicated models (cf., Langmuir et al., 1977).

Now we will consider how ϵ_{Nd} will change as a result of the REE fractionations shown in Figure 5, by relating those REE patterns to a model of the growth of the continental crust. In this model the crust grows by addition of magmas formed by repeated partial melting of a segment of the mantle. We assume that this segment of mantle began 4.5 AE ago with a chondritic REE pattern. At 4.0 AE ago a 1% partial melt is removed and goes to form the first layer of continental crust. This crustal layer has the REE pattern labelled "1% melt" in Figure 5a and the mantle segment then has the pattern labelled "Residue 1% melt." At 2.5 AE another 1% melt is removed to form a second layer of crust (Figure 5b). At 1.0 AE ago a third 1% melt is removed to form a third layer of crust (Figure 5c). The mantle segment becomes more depleted in the light REE and acquires a higher $f_{\text{Sm}/\text{Nd}}$ after each melting event. Each successive crustal layer has lower abundances of light REE and higher $f_{\text{Sm}/\text{Nd}}$ than the preceding layer. The evolution of $\epsilon_{\text{Nd}}(T)$ in the mantle segment and the crustal layers is shown in Figure 6. The solid arrows represent $\epsilon_{\text{Nd}}(T)$ in the mantle segment and the open arrows represent $\epsilon_{\text{Nd}}(T)$ in the crustal layers. Thus from 4.5 AE to 4.0 AE ϵ_{Nd} in the mantle segment remains equal to zero since $f_{\text{Sm}/\text{Nd}} = 0$. At 4.0 AE $f_{\text{Sm}/\text{Nd}}$ becomes +0.24 due to the removal of the 1% melt. Thenceforth ϵ_{Nd} of the mantle segment begins to evolve away from the line $\epsilon_{\text{Nd}}(T) = 0$. At 2.5 AE, the second melting event causes $f_{\text{Sm}/\text{Nd}}$ to increase to +0.53 and ϵ_{Nd} then begins to evolve along a line of appropriately steeper slope. Finally, at 1.0 AE the third melting event

Figure 6: The evolution of $\epsilon_{\text{Nd}}(T)$ in a rock reservoir from which partial melts are repeatedly extracted to form continental crust. The REE composition (Sm/Nd) of the source rock and the partial melts are taken from Figure 5. Before time T_{m_1} the source rock has a chondritic Sm/Nd ($f_{\text{Sm}/\text{Nd}} = 0$) and its evolution curve follows the CHUR curve as shown by the heavy arrow labelled ΔT_1 . At T_{m_1} a 1% partial melt is extracted leaving the source rock with increased $f_{\text{Sm}/\text{Nd}}$ (Figure 5a). During the time period ΔT_2 the rock gradually evolves a positive ϵ_{Nd} (heavy arrow). At T_{m_2} it is melted again, a 1% partial melt is again extracted, and $f_{\text{Sm}/\text{Nd}}$ is increased again. At T_{m_3} another melting event further increases $f_{\text{Sm}/\text{Nd}}$ (cf. Figure 5b, c). As shown by the succession of heavy arrows, as the low melting fraction is removed through time, the ϵ_{Nd} of the rock reservoir diverges from the CHUR evolution curve. The evolution of ϵ_{Nd} in the crustal layers formed from the extracted magmas are shown by the open arrows. The range of ϵ_{Nd} in young basalts is much smaller than might be expected (Chapter V).

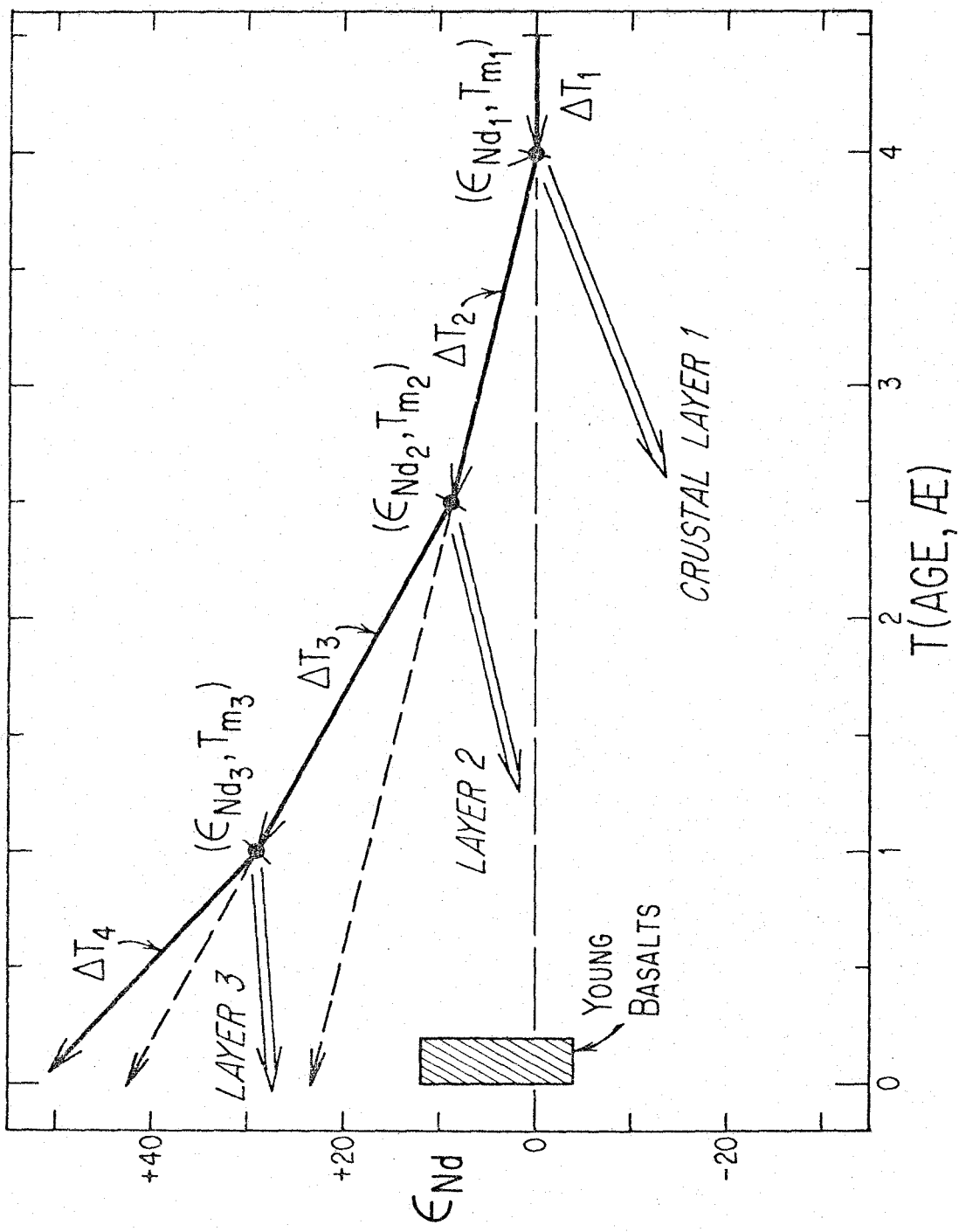


Fig. 6

causes ϵ_{Nd} to increase to +0.91 and ϵ_{Nd} then evolves at a very rapid rate until the present. The present value of ϵ_{Nd} in this reservoir is given by:

$$(21) \quad \epsilon_{Nd}(0) \approx (f_{Sm/Nd})_2 Q(T_{m_1} - T_{m_2}) + (f_{Sm/Nd})_3 Q(T_{m_2} - T_{m_3}) + (f_{Sm/Nd})_4 Q(T_{m_3}) \cong Q \sum_{i=1}^4 (f_{Sm/Nd})_i \Delta T_i$$

where the ΔT_i are defined in Figure 6 and Q is a constant defined in equation 12.

As is shown in this example, if the earth's mantle originally had a chondritic REE pattern, then the segments of the mantle from which magmas have been extracted during the course of earth history should have $\epsilon_{Nd}(0) > 0$. Unmelted mantle segments will have $\epsilon_{Nd}(0) = 0$. For the crustal layers the possibilities are more numerous. A layer such as Layer 1 derived by partial melting of a previously unmelted mantle segment must have $\epsilon_{Nd}(0) \leq 0$ today. However, layers formed by melting of residues from previous partial melting events can have $\epsilon_{Nd}(0)$ either greater than or less than zero depending on their $f_{Sm/Nd}$, age, and ϵ_{Nd} , as exemplified by Layers 2 and 3 in Figure 6. Thus Layer 2 has $\epsilon_{Nd} > 0$ but will have $\epsilon_{Nd}(0)$ less than zero, while Layer 3 has both ϵ_{Nd} and $\epsilon_{Nd}(0)$ greater than zero.

Thus, in a model such as this, where continental crust is built by repeatedly tapping the same volume of mantle, we would expect to see a continuous increase in the ϵ_{Nd} values in crustal rocks of younger and younger age. In contrast, if crustal layers were always

formed from melting of mantle segments which were previously unmelted, we would expect crustal rocks of all ages to have $\epsilon_{Nd} = 0$. As shown in Figure 6 these two possibilities should be distinguishable.

Figure 6 gives an indication of the magnitude of the ϵ_{Nd} variations which might be expected. As shown by the dashed line, the residue from the 1% melting at 4.0 AE will have $\epsilon_{Nd}(0) = +23$, a sizable deviation from $\epsilon_{Nd}(0) = 0$. If a 5% partial melt rather than a 1% partial melt had been extracted at 4.0 AE, the residue would have $\epsilon_{Nd}(0) = +153$. Since it is generally believed that basalt magmas represent 1-20% melting of mantle rock, it is clear that very large variations of ϵ_{Nd} should be expected in the mantle.

Figure 7 shows the proportions of Nd and Sm which are in the crust and the mantle after each melting event shown in Figures 5 and 6. After the first event at T_{m1} nearly 40% of the Nd in the system is already in the crust, even though the crust comprises only one percent of the system by weight. After the third melting event at T_{m3} 76% of the Nd and 45% of the Sm are in the crust.

Figure 7: Proportions of Sm and Nd in "mantle" and "crust" as the crust is gradually built from partial melts of the mantle. The crust is composed of the 1% melts shown in Figures 5a, b, and c. After the first crust is formed at T_{m_1} , almost 40% of the Nd is in the crust. After the third crust-forming event (T_{m_3}), about 75% of the Nd is in the crust. This diagram shows that the crust may hold a significant amount of the earth's Nd and Sm.

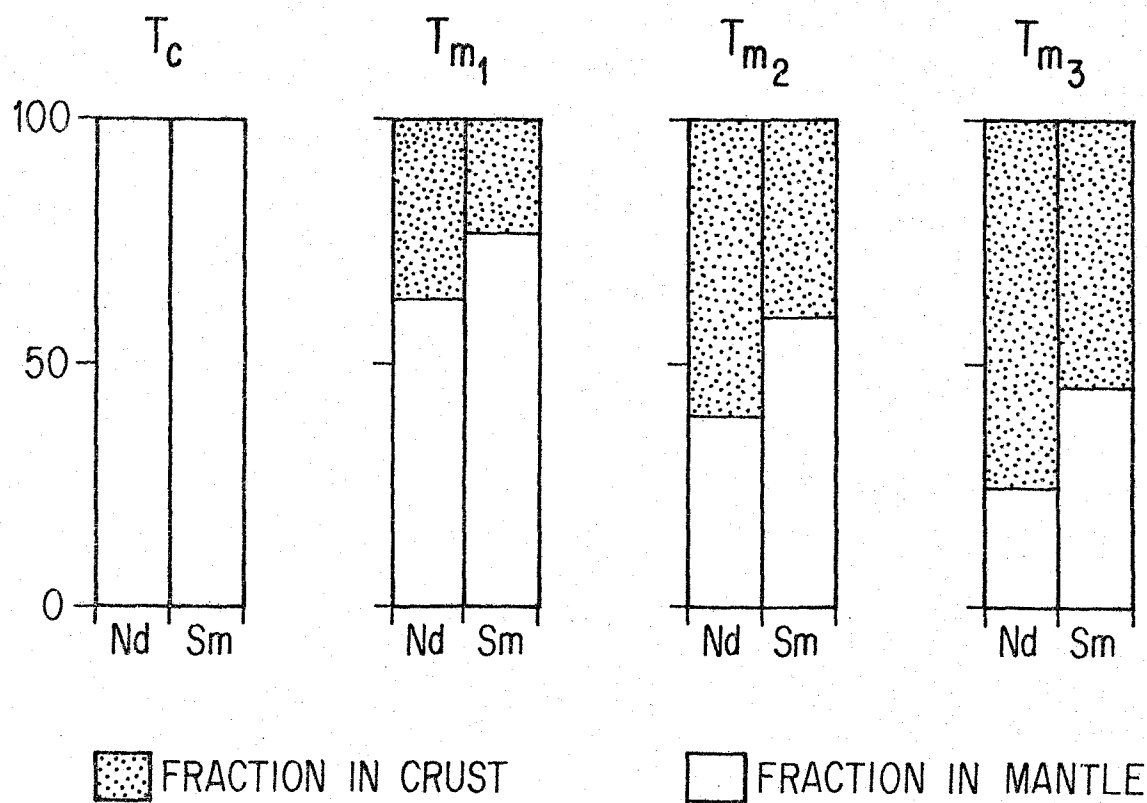


Fig. 7

IV. SAMPLING

The samples can be separated into two groups: essentially zero-age samples (<200 million years), and more ancient samples. This grouping on the basis of age represents a first-order difference in the type of information which can be gained. The zero-age samples represent an extensive sampling in a narrow interval of time. Furthermore, the data on these samples can be related to the tectonic position of the sample. Thus, for instance, young basalt samples can be divided into such categories as mid-ocean ridge basalts, continental flood basalts, oceanic island basalts, island arcs, etc. The magmatism in these areas can be related to observed tectonic environments such as spreading ridges or subducting plates, and the isotopic evidence for mantle structure can be integrated with known seismic structure, heat flow and other characteristics of the underlying mantle from which the magmas must have been derived. Thus for young rocks this additional information can be used together with the isotopic data to deduce something about mantle structure. Old rocks are found only on continents. At times greater than the age of the ocean floor, it then becomes impossible to a priori determine if a lava is a continental or oceanic basalt, and extremely difficult to specify with certainty anything about the tectonic setting in which the magmatism occurred. With these older rocks one must work primarily with the chemical classification of the rock as the parameter upon which interpretations of the isotopic data can be made.

The zero age samples which have been measured have been chosen on the basis of geographic position, petrologic province, and chemistry. To test for possible differences in magma sources in continental and oceanic regions measurements have been made on basalts from continental tholeiitic flood basalt provinces and on mid-ocean ridge tholeiitic basalts. These represent the most voluminous lavas erupted in each environment. Samples of basalts from intraplate oceanic islands were selected because they represent a class of oceanic magmas which are significantly different in chemistry and Pb and Sr isotopes from the MOR basalts. Similarly alkaline basalts from some continental areas have been measured to determine if they indicate sub-continental magma sources which are different from the sources of the flood basalts. Also, measurements have been made on some basalts from the Afar region, a province which may be transitional between continental and oceanic. An additional province which has been investigated is the continental margin-island arc. These rocks were chosen because of their transitional oceanic-continental location and their location above inclined seismic zones, which may be a unique environment for magma generation. There is additional interest in these rocks because they have been identified with major new additions to the continental crust and therefore may be indicative of the composition of material now being added to the continents. In addition to the sampling by province, several samples have been measured which represent extreme chemical types, such as carbonatites and leucitites and lavas other than basalts such as rhyolite. These were measured to determine if

their chemical compositions, in particular their highly fractionated REE patterns may be the result of their being derived from special mantle reservoirs, or in the case of rhyolites, remelting of continental crust.

Measurements on ancient rocks have been mostly restricted to samples for which precise crystallization ages already existed. This enables initial $^{143}\text{Nd}/^{144}\text{Nd}$ to be calculated from measured whole-rock values without having to determine a Sm-Nd internal isochron. Samples of basaltic rocks were measured to try to trace the growth of $^{143}\text{Nd}/^{144}\text{Nd}$ in the mantle through time. This was done both as an attempt to determine the Sm/Nd of the earth and to try to determine if the Sm/Nd of the mantle has been constant or has changed with time. As was illustrated in the discussion in the introduction changes in Sm/Nd in the mantle can occur due to removal of material such as basalt magma or crustal material. Ancient granitic rocks were measured to compare their initial $^{143}\text{Nd}/^{144}\text{Nd}$ to those of the mafic rocks to determine whether they were derived from the same reservoir, presumably the mantle, or if they represent the products of melting of an earlier-formed crust.

Brief descriptions of the samples analyzed in this study are given in Appendix 6. All Nd and Sr data are given in Table 1. Major and trace element compositions are given in Appendixes 7 and 8.

TABLE 1 : Nd AND Sr EVOLUTIONARY PARAMETERS

Sample	Age (AE)	$f_{\text{Sm/Nd}}$	$\epsilon_{\text{Nd}}(0)$	$\epsilon_{\text{Nd}}(\text{T}_x)$	$f_{\text{Rb/Sr}}$	$\epsilon_{\text{Sr}}(0)$	$\epsilon_{\text{Sr}}(\text{T}_x)$	$f^{*T*}_{\text{Sm/Nd}}$	$f^{*T*}_{\text{Rb/Sr}}$
Old Mafic Rocks									
DUL-4	1.13 ^a	-0.4649	-14.5±0.6	-1.7±0.7	-0.790	+33.1±0.9	+48.0±1.2	-0.7	+28.4
AR	1.12 ^b	-0.194	-2.0±0.4	+3.4±0.5	-0.741	-18.6±1.6	-4.8±2.0	+1.4	-2.8
RHO-1	2.51 ^c	-0.251	-16.5±1.0	-0.8±1.4	-	-	+12.7	-0.3	+7.5
WGA210	2.8 ^d	-0.4081	-29.9±0.8	-1.1±1.7	-	-	-	-0.4	-
MP22D	1.4-1.7 ^e	-0.4561	-19.9±0.4	-3-0	-	-	-	-1.2-0	-
Old Granitic Rocks									
ZL-3D	1.01 ^f	-0.2665	-4.4±0.7	+2.3±0.8	-	-	-	-	+0.9
WYWR-4D	2.65 ^g	-0.4344	-29.6±0.6	-0.9±1.0	-	-	-	-	-0.4
RN-3	2.65 ^h	-0.4855	-31.2±0.6	+0.9±1.4	-	-	-	+0.4	-
OGG128,10	3.59 ⁱ	-0.390	-35.4±0.6	-0.3±1.7	-	-	-	-0.1	-

TABLE 1 : Nd AND Sr EVOLUTIONARY PARAMETERS (CONTINUED)

Sample	Age (AE)	$f_{\text{Sm/Nd}}$	$\epsilon_{\text{Nd}}(0)$	$\epsilon_{\text{Nd}}(\text{T}_x)$	$f_{\text{Rb/Sr}}$	$\epsilon_{\text{Sr}}(0)$	$\epsilon_{\text{Sr}}(\text{T}_x)$	$f^*_{\text{Sm/Nd}}$	$f^*_{\text{Rb/Sr}}$
Mid-Ocean Ridge Basalts									
111240	0.01	+0.054	+10.3±0.4	+10.3±0.4	-0.459	-30.4±1.6	-30.4±1.6	+4.1	-17.8
1113152	0	+0.0894	+8.7±0.7	+8.7±0.7	-	-	-	+3.5	-
VG295	0	-	+10.6±0.9	+10.6±0.9	-	-31.8±0.9	-31.8±0.9	+4.2	-18.8
BD37-2	0	-0.003	11.0±3.0	+11.0±3.0	-	-	-	+4.4	-
BD17-1	0.15 ^j	+0.027	+8.0±0.6	+8.0±0.6	-	-14.5±3.4	-	+3.2	-
1113031	0	-0.399	+5.4±0.8	5.4±0.8	+0.752	-23.1±2.1	-23.1±2.1	+2.2	-13.7
Oceanic Island Basalts									
HN-1	0	-0.365	+7.3±0.6	+7.3±0.6	-0.124	-18.5±1.1	-18.5±1.1	+2.9	-11.0
HT-1	0	-0.179	+0.8±0.6	+0.8±0.6	-0.348	-6.7±0.9	-6.7±0.9	+0.3	-2.7
GT-2	0	-0.403	+6.2±0.8	+6.2±0.8	-	-	-	+2.5	-
Continental Flood Basalts									
BCR-1	0.01	-0.27	+0.1±0.4	+0.2±0.4	+3.92	+5.1±0.9	+4.4±0.9	+0.1	+2.6
PG16D	0.01	-	+6.6±0.5	+6.6±0.5	-0.479	-15.5±0.9	-15.5±0.9	+2.6	-9.2

TABLE 1 : Nd AND Sr EVOLUTIONARY PARAMETERS (CONTINUED)

Sample	Age (AE)	$f_{\text{Sm/Nd}}$	$\epsilon_{\text{Nd}}(0)$	$\epsilon_{\text{Nd}}(T_x)$	$f_{\text{Rb/Sr}}$	$\epsilon_{\text{Sr}}(0)$	$\epsilon_{\text{Sr}}(T_x)$	f^*T^* (Sm/Nd)	f^*T^* (Rb/Sr)
Continental Flood Basalts (Continued)									
DTB-1	0.05	-0.150	+1.5±0.7	+1.7±0.7	+0.686	-3.0±1.7	-3.6±1.7	+0.7	-2.1
SK-38	0.05	-0.314	-4.3±0.6	-3.9±0.6	-0.348	+12.8±1.7	+13.1±1.7	-1.6	+7.8
SWB-1D	0.15 ^k	-0.127	-1.2±0.5	-0.7±0.5	-0.403	+26.8±0.9	+27.8±0.9	-0.3	+16.5
KAS-2	0.15 ^m	-0.127	-0.7±0.4	-0.2±0.4	-0.400	+6.0±0.7	+7.0±0.7	-0.1	+4.1
PEA-3	0.10	-0.396	-20.1±1.6	-18.6±1.6	+17.59	+341.7±0.7	+312±4	-7.4	+185
PD-1	0.20 ⁿ	-0.205	-1.2±0.7	-0.2±0.7	+2.397	+32.9±1.4	+25.3±1.5	-0.1	+15.0
PAR-1	0.12 ^o	-0.470	-2.9±0.4	-1.5±0.4	+0.849	+8.2±1.6	+6.6±2.0	-0.6	+3.9
PAR-2	0.12 ^o	-0.308	-5.1±0.5	-4.2±0.5	+1.276	+18.3±0.7	+15.7±0.7	-1.7	+9.3
ADT-2	0.165 ^p	-	-5.7±0.4	-	+6.09	+115±5	+98±10	+58	
AF-133	0	-	+4.9±0.5	+4.9±0.5	-	-	-	+2.0	-
Island Arcs									
BMR-1	0	+0.147	+7.7±0.4	+7.7±0.4	-0.45	-18.6±1.6	-18.6±1.6	+3.1	-11.0
BMR-2	0	-0.12	+8.3±0.4	+8.3±0.4	+1.83	-15.2±0.6	-15.2±0.6	+3.3	-9.0

TABLE 1 : Nd AND Sr EVOLUTIONARY PARAMETERS (CONTINUED)

Sample	Age (AE)	$f_{\text{Sm/Nd}}$	$\epsilon_{\text{Nd}}(0)$	$\epsilon_{\text{Nd}}(\text{T}_x)$	$f_{\text{Rb/Sr}}$	$\epsilon_{\text{Sr}}(0)$	$\epsilon_{\text{Sr}}(\text{T}_x)$	$f^*\text{T}^*$ (Sm/Nd)	$f^*\text{T}^*$ (Rb/Sr)
Island Arcs (Continued)									
BMR-3	0	-0.34	+7.8±0.5	+7.8±0.5	+2.48	-13.5±1.3	-13.5±1.3	+3.1	-8.0
BMR-4	0	-0.16	+7.9±0.5	+7.9±0.5	-0.59	-15.9±0.9	-15.9±0.9	+3.2	-9.4
BMR-5	0	-0.16	+8.3±0.5	+8.3±0.5	+2.00	-15.0±0.7	-15.0±0.7	+3.3	-8.9
BMR-6	0	-0.16	+7.3±0.5	+7.3±0.5	-0.55	-18.6±0.9	-18.6±0.9	+2.9	-11.0
BMR-7	0	-0.44	+7.1±0.3	+7.1±0.3	+8.14	-14.9±0.6	-14.9±0.6	+2.8	-8.8
MAR-1	0	-0.349	+7.9±0.6	+7.9±0.6	+0.168	-18.6±0.9	-18.6±0.9	+3.2	-11.0
MAR-2	0	-0.143	+6.8±0.5	+6.8±0.5	+0.442	-19.0±1.0	-19.0±1.0	+2.7	-11.2
MAR-4	0	-0.189	+7.2±0.5	+7.2±0.5	+0.812	-18.9±0.5	-18.9±0.5	+2.9	-11.2
MAR-6	-0.05	-0.339	+8.7±0.5	+9.1±0.5	+0.180	+0.3±0.7	+0.1±0.7	+3.6	+0.1
GU-4	0.05	-0.091	+9.2±0.6	+9.4±0.6	+2.099	-12.2±1.1	-13.1±1.1	+3.8	-7.8
GU-7	0.05	0.000	+8.2±0.4	+8.2±0.4	-0.479	-20.9±1.1	-21.3±1.1	+3.3	-12.6

TABLE 1 : Nd AND Sr EVOLUTIONARY PARAMETERS (CONTINUED)

Sample	Age (AE)	$f_{\text{Sm/Nd}}$	$\epsilon_{\text{Nd}}(0)$	$\epsilon_{\text{Nd}}(\text{T}_x)$	$f_{\text{Rb/Sr}}$	$\epsilon_{\text{Sr}}(0)$	$\epsilon_{\text{Sr}}(\text{T}_x)$	f^*_{Nd} (Sm/Nd)	f^*_{Sr} (Rb/Sr)
Continental Margin Magmatic Arcs									
PER-1									
PER-1	0	-0.494	-8.9±0.5	-8.9±0.5	+0.514	+42.0±1.4	+42.0±1.4	-3.6	+24.9
PER-2	0	-0.530	-12.7±0.1	-12.7±0.1	+4.51	+64.3±1.3	+64.3±1.3	-5.1	+38.0
CAS-1	0	-	+4.6±0.3	+4.6±0.3	-0.38	-11.9±0.9	-11.9±0.9	+1.8	-7.0
MEX-1	0	-	+7.4±0.4	+7.4±0.4	-	-10.4±1.4	-10.4±1.4	+3.0	-6.2
WMG-1	0.12 ^q	-0.261	+2.8±0.5	+3.6±0.5	+13.39	+13.1±0.7	-13.4±2.0	+1.4	-7.9
SMG-1	0.12 ^q	-0.211	+4.1±0.6	+4.7±0.6	-0.687	-15.9±0.7	-14.7±0.7	+1.9	-8.7
RL-1	0.12 ^q	-0.228	+0.6±0.5	+1.3±0.5	+73.2	+128.2±0.9	-18 ±5	+0.5	-10.5
LAK-8D	0	-0.422	+1.3±0.8	+1.3±0.8	-	-	-	+0.5	-
Continental Alkali Basalts									
CSQ-3	0	-	+6.7±0.5	+6.7±0.5	-	-21.1±0.7	-21.1±0.7	+2.7	-12.5
PCB-1	0	-0.366	+6.2±0.8	+6.2±0.8	-	-14.8±0.9	-14.8±0.9	+2.5	-11.1
ANB2128	0	-	+4.0±0.2	+4.0±0.2	-	-	-	+1.6	-

TABLE 1 : Nd AND Sr EVOLUTIONARY PARAMETERS (CONTINUED)

Sample	Age (AE)	$f_{\text{Sm/Nd}}$	$\epsilon_{\text{Nd}}(0)$	$\epsilon_{\text{Nd}}(\text{T}_x)$	$f_{\text{Rb/Sr}}$	$\epsilon_{\text{Sr}}(0)$	$\epsilon_{\text{Sr}}(\text{T}_x)$	$f^*\epsilon_{\text{T}}$ (Sm/Nd)	$f^*\epsilon_{\text{T}}$ (Rb/Sr)
Continental Alkali Basalts (Continued)									
ANB2102Q	0	-	+4.5±0.3	+4.5±0.3	-	-	-	+1.8	-
RGB-1	0	-	+0.2±0.7	+0.2±0.7	+0.286	-2.0±1.7	-2.0±1.7	+0.1	-1.2
WBK-1	0.01	-	+5.0±0.4	+5.1±0.4	-	-11.6±0.6	-	+2.0	-
CHA-2	0	-	+3.9±0.3	+3.9±0.3	+2.176	-4.1±0.9	-4.1±0.9	+1.6	-2.4
V-9	0	-	+2.3±0.3	+2.3±0.3	+0.517	-5.1±0.7	-5.1±0.7	+0.9	-3.0
Khibina	0.29	-0.5093	+0.5±0.3	+3.7±0.3	-	-	-	+1.5	-
Lavas of extreme Composition									
OLC-1	0	-	+0.1±0.9	+0.1±0.9	-	-4.8±1.0	-4.8±1.0	0.0	-2.8
LH-1	0.05	-0.607	-14.0±1.0	-13.2±1.0	+4.84	+16.7±0.6	+12.6±0.8	-5.3	+7.5
DUL11	0	-	-2.3±0.4	-2.3±0.4	-	+13.1±1.6	+13.1±1.6	-0.9	+7.8

TABLE 1 : Nd AND Sr EVOLUTIONARY PARAMETERS (CONTINUED)

Sample	Age (AE)	$f_{\text{Sm/Nd}}$	$\epsilon_{\text{Nd}}(0)$	$\epsilon_{\text{Nd}}(T_x)$	$f_{\text{Rb/Sr}}$	$\epsilon_{\text{Sr}}(0)$	$\epsilon_{\text{Sr}}(T_x)$	f^*T^* (Sm/Nd)	f^*T^* (Rb/Sr)
Ultramafic Rocks									
SPP-1	0 (?)	-0.76	+5.9±0.5	+5.9±0.5	-	-12.9±0.6	-12.9±0.6	+2.4	-7.6
Other Samples									
NAS216D	"0"	-0.38	-14.4±0.5	-	-	-	-	-	-
DOS-1	0	-	-9.2±0.9	-	-	-	-	-	-

References for Table 1:

^aSilver and Green (1972)

^bSmith and Silver (1975)

^cHamilton et al. (1977)

^dBlack et al. (1973)

^eLanphere (1964)

^fZartman (1964)

^gNaylor et al. (1970)

^hSteiger and Wasserburg (1969)

ⁱBaadsgaard (1973)

^jDSDP Inventory of Igneous Rock Recovery (1973)

^kMcDougall (1963)

^lMcDougall (1963)

^mEriksen and Kulp (1961)

ⁿAmaral et al. (1966)

^oMcDougall (1961)

^pHeier et al. (1965)

^qSilver (1975)

V. Nd RESULTSPrecambrian Igneous Rocks

All of the Precambrian samples analyzed, with the exception of the Mountain Pass shonkinite, have been well-dated by other methods.

Initial $^{143}\text{Nd}/^{144}\text{Nd}$ for each sample has been calculated from the measured $^{143}\text{Nd}/^{144}\text{Nd}$ and $^{147}\text{Sm}/^{144}\text{Nd}$ and the known ages. For sample RN3 a two-point internal Sm-Nd isochron was obtained on a total rock sample and an apatite separate and provides an internal check on the calculated ϵ_{Nd} . The isochron is shown on Figure 8. The Sm-Nd age of 2.64 ± 0.08 AE agrees impressively with the U-Pb age of 2.65 AE (Steiger and Wasserburg, 1969; recalculated with revised U decay constants) and the ϵ_{Nd} determined from the internal isochron is essentially identical to that calculated using the U-Pb age. Figure 9 is a histogram showing the measured $\epsilon_{\text{Nd}}(0)$ and calculated ϵ_{Nd} for each of the samples. The magnitudes of the corrections for in situ ^{147}Sm decay are readily apparent from this graph. Note also that all of these crustal rocks have negative $\epsilon_{\text{Nd}}(0)$ and the absolute value of the $\epsilon_{\text{Nd}}(0)$ values generally increases with increasing sample age. A graph of initial $^{143}\text{Nd}/^{144}\text{Nd}$ versus age is given in Figure 10 and the ϵ_{Nd} values of the samples as a function of age are also given in Figure 10.

Samples DUL-4 and RHO-1 are gabbroic or diabasic intrusions which are taken to be representative of old continental tholeiitic basalts similar to more modern continental flood basalts (cf., Carmichael, et al., 1974). WGA210 may also represent a basaltic magma since the Fiskenaeset anorthosite may be part of a layered basic intrusion of original near-basaltic composition (Windley, 1969). AR

Figure 8: Two point internal isochron for sample RN3. Note that the difference in $^{143}\text{Nd}/^{144}\text{Nd}$ between the two samples is only 0.2%. The lack of a sample with $^{147}\text{Sm}/^{144}\text{Nd}$ near zero results in a poorly defined initial ratio. Since near-zero Sm/Nd ratios are almost non-existent in nature, this will be an omnipresent characteristic of Sm-Nd isochrons.

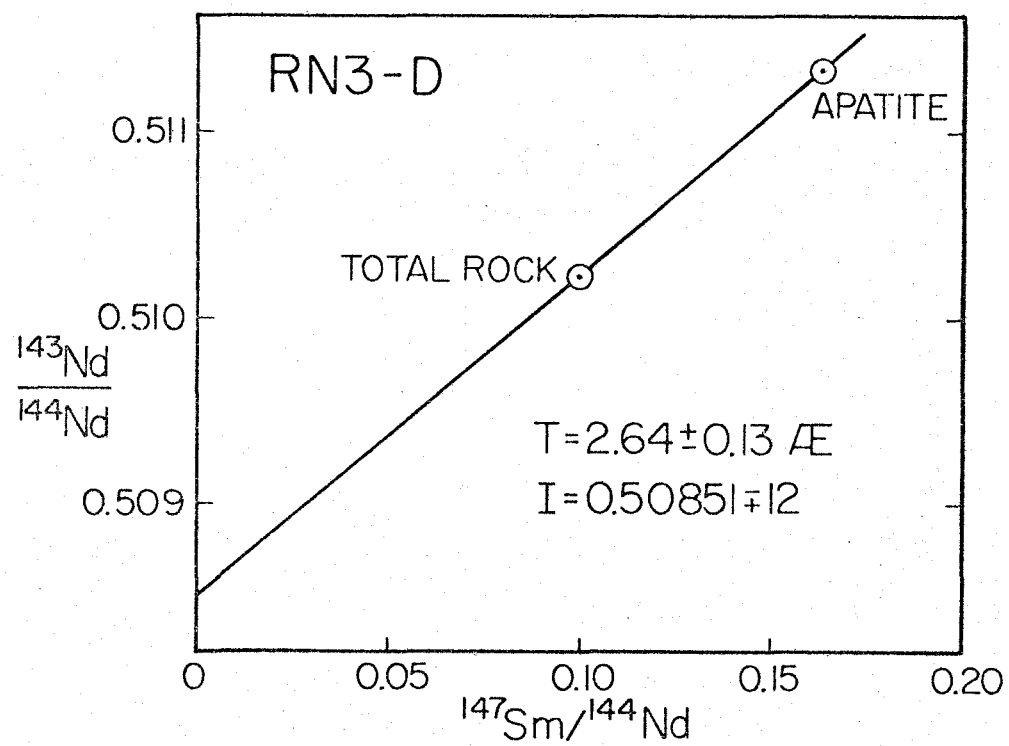


Fig. 8

Figure 9: Histogram of measured $\epsilon_{Nd}(0)$ values and calculated $\epsilon_{Nd} (\equiv \epsilon_{Nd}(T_x))$ values for the Precambrian rocks analyzed in this study.

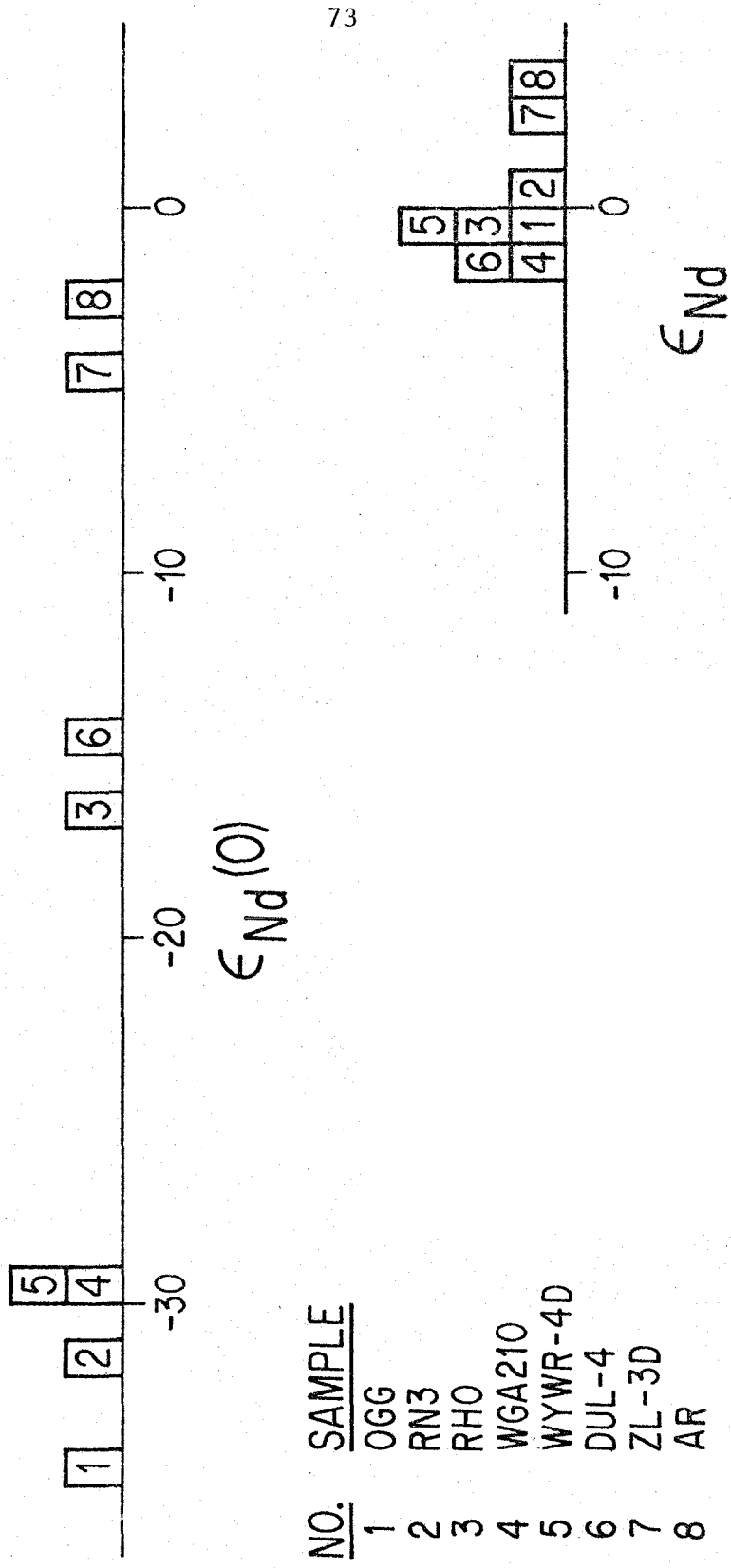


Fig. 9

Figure 10: Graph of initial $^{143}\text{Nd}/^{144}\text{Nd}$ versus age for all samples with ages greater than about 0.2 AE. Stippled area is the field of most young basalts. Note that the total evolution of $^{143}\text{Nd}/^{144}\text{Nd}$ in terrestrial magma sources over 4.5 AE is only a little more than 1%. Inset shows ϵ_{Nd} versus age for the same samples, excluding the Khibina sample. The initial ratio for Archean greenstones measured by Hamilton et al. (1977) would almost coincide with that of WYWR.

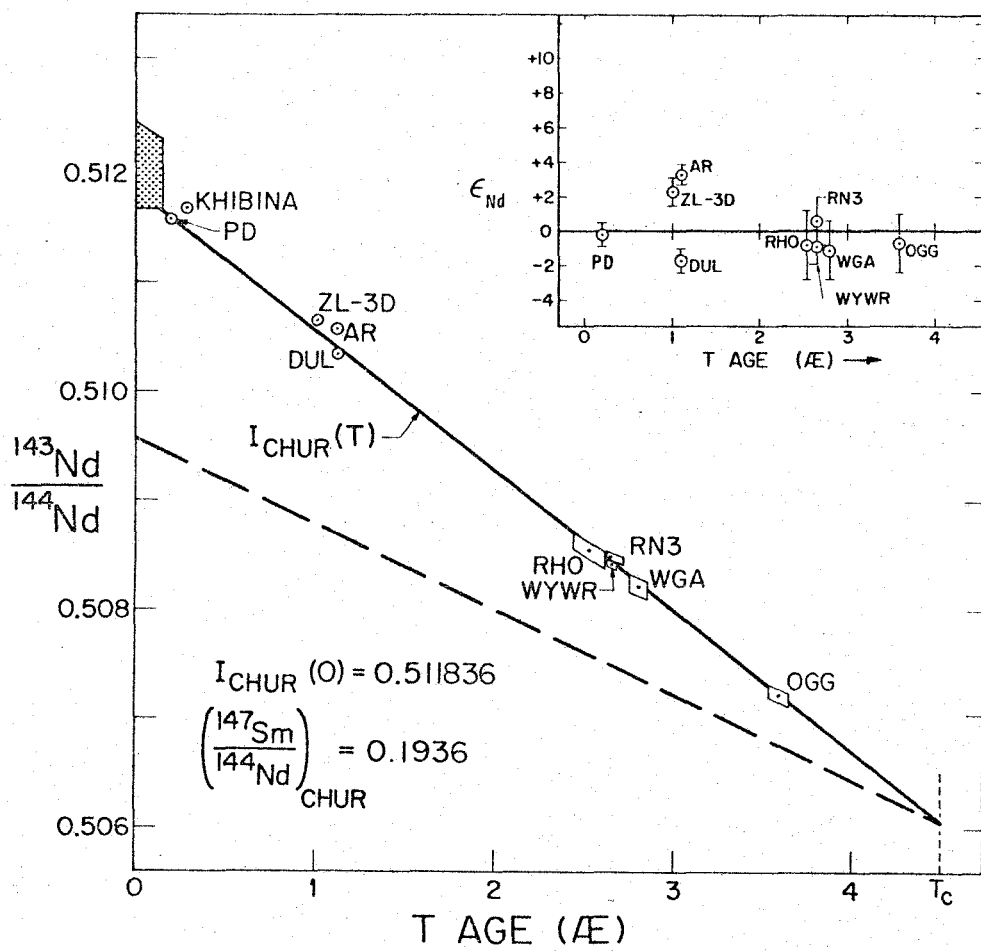


Fig. 10

is a moderate-sized diabasic intrusion and may not be associated with large-scale basaltic magmatism as is the case with DUL-4 and RHO-1. The mafic igneous rocks probably represent magmas derived from the mantle and thus their initial $^{143}\text{Nd}/^{144}\text{Nd}$ may be taken to be indicative of the evolution of $^{143}\text{Nd}/^{144}\text{Nd}$ in the upper mantle. As shown in Figure 10 the mafic samples all fall on or very close to the CHUR evolution curve. This can be seen more clearly in the insert in Figure 10. Samples RHO-1 and WGA-210 fall within error on the curve at 2.5 and 2.8 AE respectively. DUL-4 falls slightly below the curve at 1.1 AE and AR falls substantially above the curve at 1.1 AE. MP22D is not plotted due to the uncertainty in its age (Lanphere, 1964). However, MP22D is probably no younger than the Rb-Sr biotite age obtained by Lanphere (1964) of ~ 1.4 AE and must be younger than the rocks which it intrudes which are ~ 1.7 AE old. Thus since the age is bracketed between 1.4 and 1.7 AE, its ϵ_{Nd} must lie between -3 and 0, and thus it also lies close to the CHUR curve.

The clustering of these samples about the CHUR evolution curve strongly suggests that the upper mantle has had an approximately chondritic Sm/Nd over much of the history of the earth. The difference in ϵ_{Nd} of 5 units between DUL-4 and Ar, however, indicates that the mantle had attained some substantial degree of heterogeneity by 1.1 AE ago. DUL-4 may have been affected to some degree by crustal contamination (see Chapter VII), which may partially account for its lower ϵ_{Nd} .

The initial $^{143}\text{Nd}/^{144}\text{Nd}$ and the ϵ_{Nd} values of the Precambrian granitic rocks are also shown in Figure 10. These samples also lie on

or very near the CHUR curve. Figure 10 insert shows that the Archean samples OGG128, RN3, and WYWR-4D, all of which are typical calc-alkaline granodiorites, all fall within error on the CHUR evolution curve. ZL-3D is a true granite and falls slightly above the curve at 1.0 AE. A long-standing controversy in geology has centered around the question of whether the silicic rocks which make up a large portion of the continental crust were derived from the mantle at various times during the history of the earth or represent the products of episodic remelting of an ancient silicic crust which has existed since near the time of formation of the earth. Typical silicic crustal material has $f_{\text{Sm}/\text{Nd}} \approx -0.4$. The evolution of $^{143}\text{Nd}/^{144}\text{Nd}$ in a hypothetical ancient silicic crust formed 4.5 AE ago is shown by the dashed line in Figure 10. The evolution curve for such material is clearly distinct from the CHUR curve and the initial $^{143}\text{Nd}/^{144}\text{Nd}$ for the granitic samples lie far off such an evolution curve. Insofar as the granitic samples strongly cluster about the same evolution curve as the basaltic rocks, the data strongly suggest that they are derived from the same reservoir as the basalts, inferred to be the upper mantle. There is no evidence in this data that the granitic rocks are formed by remelting of much older silicic crustal material.

The granitic rocks could not be derived by remelting of typical silicic crustal material which had existed for more than about 10^8 years or at most 2×10^8 years prior to their crystallization ages. The crystallization ages of these granodiorites therefore date the time at which they were differentiated from mantle material which had a chondritic REE pattern. If these granodiorites represent significant

segments of the continental crust, then the fractionated REE patterns of crustal rocks have not been inherited from a protocrust or upper mantle which formed with a fractionated REE pattern near the time of formation of earth, but rather result from fractionation occurring during differentiation of the crust from an unfractionated mantle reservoir at various times corresponding to the crystallization ages of the rocks. This conclusion is in agreement with conclusions reached by Moorbat (1975) based on Rb-Sr isotopic studies of Archean rocks.

Thus all of the Precambrian igneous rocks appear to be derived from a reservoir with approximately chondritic REE relative abundances. In particular, the four samples with ages between 2.5 and 2.8 AE, plus the results of the study of Hamilton *et al.* (1977) on some South African greenstones (Age = 2.64 AE, $\epsilon_{\text{Nd}} = 1.5 \pm 0.6$), represent rocks from geographically widely separate localities all of which lie within error of the CHUR curve and thus closely limit the position of the growth curve at ~ 2.6 AE. These data strongly suggest that the CHUR curve describes Nd evolution in an important and widespread reservoir, most probably the mantle, and as such can be taken as a representation of the bulk earth's evolution curve. Thus the earth appears to have Sm/Nd and presumably REE relative abundances which are essentially identical to those of chondrites.

Young Igneous Rocks

A. Continental Flood Basalts and Mid-Ocean Ridge Tholeiites

Nd isotopic data for these samples are shown in a histogram in Figure 11a. The continental flood basalts include samples from major flood basalt provinces including the Karroo (Southern Africa),

Figure 11: Histogram of ϵ_{Nd} values in young volcanic rocks. Some of the data shown were taken from Richard et al (1976), O'Nions et al (1977), Hawkesworth et al (1977), and McDougall et al (1977).

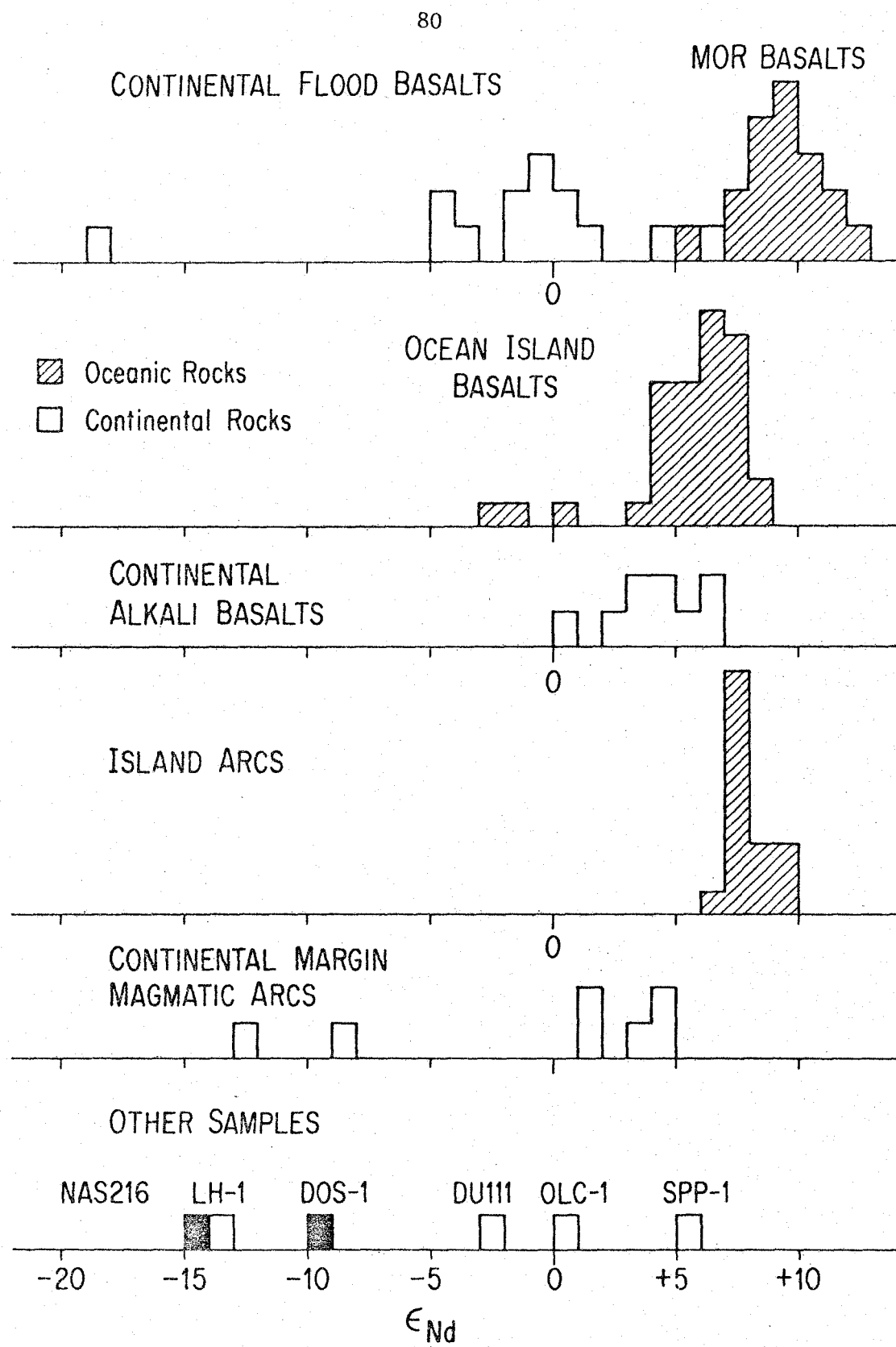


Fig. 11

Columbia River (NW United States), Deccan (India), Parana (Brazil), and East Greenland as well as samples of the Palisades Diabase, which is considered as a representative of the Triassic basalt-diabase province of Eastern North America, a sample of the Red Hill diabase, Tasmania, and a sample of flood basalt from the Afar depression, Ethiopia. The mid-ocean ridge (MOR) basalts include samples from on or near ridges in each of the Atlantic, Pacific, and Indian Oceans.

Before interpreting these data it is necessary to discuss the individual samples which appear to be special cases. As shown in Figure 9, old continental crustal rocks typically have $\epsilon_{\text{Nd}}(0)$ values ranging from about -10 to -35. Thus in general contamination of mantle-derived basaltic magmas with crustal Nd will tend to drag the ϵ_{Nd} of the basalts down to more negative values. Samples PEA-3 ($\epsilon_{\text{Nd}} = -18.4$) and sample ADT-2 ($\epsilon_{\text{Nd}} = -4.7$) may be examples of basalts which are contaminated with crustal Nd. Sr isotope data on these two samples supports this and will be discussed in more detail in a later section. A K-Ar age of 103 m.y. on PEA-3 was generously provided by S.P. Smith confirming that it was a Karroo basalt. Sample PG16D ($\epsilon_{\text{Nd}} = +6.6$) is a Picture Gorge basalt from the Columbia River basalt province while BCR-1 ($\epsilon_{\text{Nd}} = +0.2$) is a Yakima basalt. The Picture Gorge basalts have been recognized as being distinct from the much more voluminous Yakima basalts of the Columbia River province in both major element chemistry (Waters, 1961) and trace-element and Sr isotopic composition (Nathan and Fruchter, 1974; McDougall, 1976). Since the Picture Gorge basalts comprise only ~10% by volume of the Columbia Plateau lavas, whereas the Yakima basalts comprise 85 to 90% (D. Swanson, pers. comm.) of the

lavas and are fairly uniform in chemical composition and Sr isotope ratios (McDougall, 1976), the ϵ_{Nd} of BCR-1 is taken to be representative of the Columbia Plateau province. The Picture Gorge lavas appear to be isotopically distinct from most other continental flood basalts. Sample 113031 ($\epsilon_{\text{Nd}} = +5.4$) is one of very few true alkali basalt samples dredged from a mid-ocean ridge and has a somewhat lower ϵ_{Nd} than the other MOR basalts which are tholeiitic basalts.

The continental flood basalts cluster about a value of $\epsilon_{\text{Nd}} = 0$ but show a range of ϵ_{Nd} from about -5 to +6. The MOR basalts have ϵ_{Nd} averaging about +10 and ranging from +7 to +12. The bimodality of the data in Figure 11a implies the existence of two distinctly different, widespread mantle magma sources. From the difference of f^*T^* values of $\sim 4 \times 10^8$ yr for the two groups of samples (Table 1), and assuming a difference of f_s of less than 0.4, we calculate that these two reservoirs must have been separate for at least 10^9 years. Thus MOR tholeiites and continental flood tholeiites appear to be derived from two ancient, profoundly different reservoirs in the earth's mantle. Differences in concentrations of certain minor and trace elements between these two lithologic types (Schilling, 1971; Haskin *et al.*, 1966) thus are most likely a reflection of ancient differences rather than a result of differentiation processes occurring at the time of magma generation as has been suggested (Schilling, 1971). The nominal value of $\epsilon_{\text{Nd}} \approx 0$ for the continental flood basalts indicates they are derived from a reservoir which has maintained an unfractionated, chondritic Sm/Nd throughout the history of the earth. The MOR basalts, however, are derived from a reservoir which has had Sm/Nd at least 10% greater than chondritic.

The lower ϵ_{Nd} of continental flood basalts could possibly be caused by crustal contamination, but other evidence, discussed in Chapter VII, and the pronounced bimodality of the data are inconsistent with crustal contamination.

B. Ocean Island Basalts

The Nd data shown on the histogram in Figure 11b include the data from Table 1 plus data from O'Nion's et al. (1977) and Richard et al. (1976). These data represent samples from the Hawaiian Islands, Galapagos Islands, Iceland, the Azores, Canary Islands, Ascension Island, Tristan da Cunha and Bouvet but more than half the samples are from either Iceland or the Hawaiian Islands. The samples include both tholeiitic and alkali basalts. As shown in Figure 7b most of the ocean island lavas have $\epsilon_{\text{Nd}} = +4$ to $+8$ averaging about $+6$. These values are somewhat lower than those of the MOR basalts but still clearly higher than the continental flood basalts. The ocean island basalts may be derived from a third mantle reservoir, distinct from those of the flood basalts and MOR basalts or they may be derived from a blend of the other two reservoirs or by mixing of magmas derived from those reservoirs. However, the rather narrow range of ϵ_{Nd} values found for the ocean island rocks argues against their being a mixture, since for a mixture, we might expect ϵ_{Nd} values ranging from -2 to $+12$ with no strong clustering. However, the clustering could be a result of the fact that the sample population is primarily comprised of rocks from only two islands.

C. Continental Alkali Basalts

The ϵ_{Nd} values of these lavas are given in Figure 11c. With the exception of sample RGB-1 from the Rio Grande Rift, these lavas were all erupted in regions close to continental margins and generally characterized by some amount of regional extensional faulting. Their ϵ_{Nd} values show a range from 0 to +6.7. They overlap the range of ocean island basalts and tend to be somewhat higher than the flood basalts but distinctly lower than the MOR basalts. Many of the continental alkalic basalts have ϵ_{Nd} identical to many ocean island alkali basalts. Thus continental and oceanic alkalic lavas, which have similar major and trace element compositions may also be derived from mantle reservoirs which are chemically similar.

D. Island Arcs

The ϵ_{Nd} values of basalts, andesites and rhyolite from the Marianas and Bismarck Island arcs (Table 1) and the South Sandwich Islands (Hawkesworth *et al.*, 1977) are shown in Figure 11d. The island arc lavas display a narrow range of ϵ_{Nd} from +6.8 to +9.8, averaging about +8. They fall within the range of MOR basalts and overlap the upper range of ocean island basalts. The ϵ_{Nd} values of the island arc samples are distinctly higher than those of the continental flood basalts and are in fact higher than any of the continental rocks. A more extensive discussion of the island arc data is given in Appendix 3.

E. Continental Margin Magmatic Arcs

These samples include gabbro, granodiorite and granite from the Cretaceous Peninsular Ranges batholith, a basalt from Mt. Shasta, a

rhyolite from Northern California, a basaltic andesite from Arenal volcano in Costa Rica, and an andesite and rhyolite from El Misti, an active volcano in the Andes of Peru. These rocks may be the continental-margin equivalents of island arc rocks (Dickinson, 1970). The Arenal sample has ϵ_{Nd} identical to the island arc rocks. The other samples have ϵ_{Nd} substantially lower than the island arc rocks. The North American samples have ϵ_{Nd} greater than zero, but generally lower than the ocean island basalts. The Andean samples, however, have large negative ϵ_{Nd} , strikingly different from the island arc and other continental margin lavas. The lower ϵ_{Nd} values for these rocks relative to the island arcs suggests that at continental margins, the pre-existing continental crust, which would have negative ϵ_{Nd} , may play a role in the generation of magmas, perhaps as a contaminant to magmas coming from the mantle. Alternatively, it could be an indication of differences between suboceanic and subcontinental magma sources in the mantle. The Andean samples appear to be products of remelting of old silicic crustal materials or else must be heavily contaminated with old crustal Nd. Since the crust beneath the central Andes may be up to 70 km thick, it is perhaps not surprising that it has been involved in the generation of these magmas. However, Brooks et al. (1976) and James et al. (1976) measured Sr isotopes in lavas from the same volcano and although the $^{87}\text{Sr}/^{86}\text{Sr}$ ratios were high, they concluded that the lavas were melted from the mantle beneath the crust and had not been significantly affected by their passage through the crust. By virtue of the contrast between the ϵ_{Nd} of these Peruvian lavas

and the ϵ_{Nd} values of most other young igneous rocks, and the general rarity of large negative ϵ_{Nd} values, it appears that the Nd data contradict the conclusions of Brooks *et al.* and James *et al.*

F. Lavas of Extreme Compositions

The ϵ_{Nd} values of these samples are shown in Figure 11f. OLC-1, a carbonate lava from within the East African rift system, has $\epsilon_{\text{Nd}} = 0$, identical to the average for the continental flood basalts. This lava, which represents an extreme rock type with high REE concentrations and a fractionated REE pattern, thus does not appear to be derived from a special reservoir. Rather, it appears to be derived from a typical mantle reservoir similar to the source of continental flood basalts. Therefore, its strange composition must be entirely the result of fractionation during short-time-scale magmatic processes.

Similarly DULL1 is a mafic ultrapotassic lava ($\sim 5\% \text{K}_2\text{O}$) also from the East African rift and represents another extreme rock type. It too has ϵ_{Nd} within the range of the flood basalts and thus also does not appear to be derived from a special reservoir. It is hypothesized that lavas of the composition of DULL1 are derived by melting very deep in the mantle (~ 200 km down) (Carmichael, pers. comm.). This sample therefore may be an indication that deeper parts of the upper mantle may have $\epsilon_{\text{Nd}}(0)$ near 0 and thus may have a nearly chondritic REE pattern.

LH-1 is another ultrapotassic lava ($\sim 10.5\% \text{K}_2\text{O}$), but in contrast to DULL1, it has a large negative ϵ_{Nd} . This lava thus appears to be

derived from an ancient (~ 1 AE), low-Sm/Nd reservoir. This reservoir could be ancient continental crust or possibly a rare, peculiar mantle reservoir. Kay and Gast (1973) have calculated the percentage melting and residual phase mineralogy necessary to derive various alkalic lavas from a mantle with a chondritic relative REE pattern. Sample LH-1 is one of the samples they considered. They calculated that to account for the extreme light REE enrichment this lava would have to form by extremely small degrees of melting ($\sim 0.5\%$). The Nd data now make this calculation meaningless because it appears that this lava was derived by melting of a rock which was already enriched in light REE and which therefore may not have had a composition anything like that presumed for the average mantle.

G. Ultramafic Rocks

One sample of spinel peridotite mylonite from St. Paul's rocks was analyzed in this study. St. Paul's Islands are a group of small islands in the equatorial Atlantic on the Mid-Atlantic Ridge which are comprised almost entirely of mylonitized spinel peridotite (Melson *et al.*, 1967a, 1972). The peridotite is thought to be an intrusion of material brought up directly from the mantle largely in the solid state. This locality might be one where the upper mantle can be directly sampled. The ϵ_{Nd} of this sample is shown in Figure 11f. It is similar to the average of the ocean island basalts and is within error of the alkali basalt sample 113031 which was dredged from near St. Paul's rocks. Melson *et al.* (1972) suggested that St. Paul's rocks could be representative of the type of mantle material which can be

melted to form alkali basalts such as those found on oceanic islands.

The Nd data are in agreement with this conclusion, but are also in agreement with the suggestion made by Frey (1970) on the basis of REE studies, that the St. Paul's peridotite may be a cumulate of minerals which gravitationally settled out of an alkali basalt magma.

H. Other Samples

$\epsilon_{\text{Nd}}(0)$ for the North American shale composite NAS216 is shown in Figure 11f. The shale represents a sample of material which has been eroded from the crystalline igneous and metamorphic rocks which make up the North American continent. As such it is a sample of "average crust" or "average upper crust." Its large negative ϵ_{Nd} undoubtedly reflects the age and low Sm/Nd of this crustal material.

Sample DOS-1 has $\epsilon_{\text{Nd}} = -9.2$ and thus also lies far below the CHUR evolution curve (Figure 11f). Fish debris is a scavenger of heavy metals in seawater during slow dissolution on the deep ocean floor (Arrhenius, Bramlette and Piccioto, 1957) and gives an estimate of ϵ_{Nd} of seawater. The ϵ_{Nd} of this sample is close to that of average North American shale (DePaolo and Wasserburg, 1976a) which may be representative of REE in the continental crust (Haskin *et al.*, 1966) and is far displaced from the values found in oceanic volcanic rocks. Thus if average crustal material has $\epsilon_{\text{Nd}} \approx -14$ and average oceanic volcanics have $\epsilon_{\text{Nd}} \approx +8$, then from the ϵ_{Nd} of the fish debris it can be calculated that about 75% of the Nd in authigenic phases on the ocean floors is derived from continental sources and 25% is from oceanic regions.

VI. DISCUSSION OF Nd RESULTSChemical heterogeneity of the mantle

Figure 12 shows the data from Figure 10 plotted together with some of the data on the young continental rocks. The data shown in this figure clearly suggest that the source of magmas during the first 2 AE of earth history was a uniform chondritic-Sm/Nd reservoir (CHUR) since there are no samples with ages $\gtrsim 2.5$ AE which have ϵ_{Nd} significantly different from zero. The young rocks, in contrast, show marked differences in ϵ_{Nd} and indicate that today the earth's mantle cannot be considered to be a single homogeneous reservoir, but must instead be highly stratified with respect to Sm/Nd and REE relative abundances. This conclusion is in accord with conclusions drawn from studies of variations of Sr and Pb isotopes (Gast *et al.*, 1964; Tatsumoto, 1966; Gast, 1968; and many others). The apparent contrast between the young samples and the old rocks may be an indication that the present-day mantle is chemically much more inhomogeneous than was the Archean mantle. However, it should be cautioned that for the old samples the smaller amount of time available for the growth of isotopic heterogeneity, when coupled with the larger uncertainties in ϵ_{Nd} , make heterogeneity more difficult to discern. The mean Sm/Nd enrichment factor $\langle f_s \rangle$ for a magma source, which at time T_x yields a rock with $\epsilon_{\text{Nd}}(T_x)$ was defined as

$$(22) \quad \langle f_s \rangle = \epsilon_{\text{Nd}}(T_x) / Q_{\text{Nd}}(T_c - T_x).$$

The variability of this quantity among the sources for the majority of the young rocks can be calculated from the range of ϵ_{Nd} ($\Delta\epsilon_{\text{Nd}} \approx 16$).

Figure 12: Graph of ϵ_{Nd} versus age. Individual data points are continental rocks. Ruled area is the field of mid-ocean ridge basalts. Dashed line shows $\epsilon_{\text{Nd}}(T)$ of a reservoir diverging from CHUR at 4.5 AE which has $\epsilon_{\text{Nd}}(0)$ equal to the average of MOR basalts.

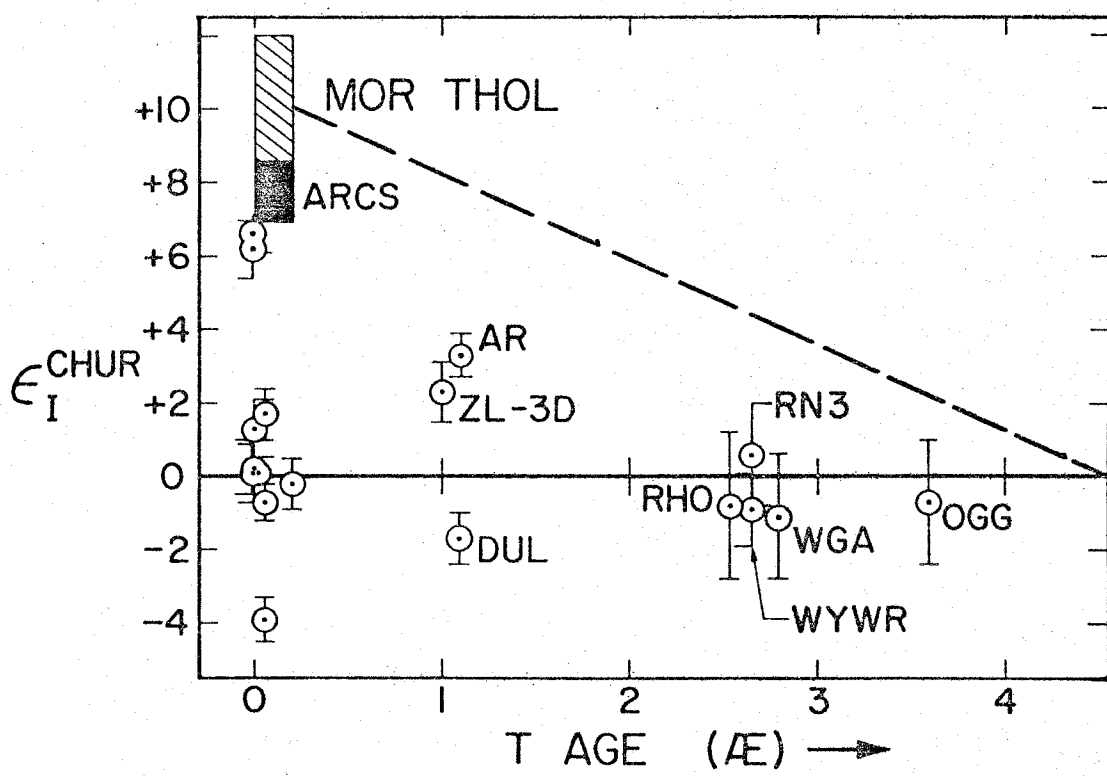


Fig. 12

Setting $T_x = 0$, $T_c = 4.5$ AE gives:

$$(23) \quad \Delta \langle f_s \rangle = \frac{16}{(25)(4.5)} = 0.14$$

Therefore, the ϵ_{Nd} values of young basalts indicate a range in $\langle f_s \rangle$ of 14%. In comparison, the error bar on the ϵ_{Nd} of sample OGG ($T_x = 3.59$ AE) spans a range of ϵ_{Nd} of ± 1.7 or 3.4 units. This uncertainty alone allows a range of $\langle f_s \rangle$ 3.59 AE ago given by:

$$(24) \quad \Delta \langle f_s \rangle = \frac{3.4}{(25)(4.5-3.59)} = 0.15$$

or about the same range as the young samples. However, the range of ϵ_{Nd} for 2.6 AE old samples (neglecting error bars) limits $\langle f_s \rangle$ to 0.04, substantially less than the variability indicated by the young samples. Thus a contrast in the degree of heterogeneity in the mantle today versus Archean times is suggested by the data, but could only be quantified with more precise determinations of ϵ_{Nd} for more ancient rocks.

Nevertheless, it should be noted that initial $^{87}\text{Sr}/^{86}\text{Sr}$ on Archean igneous rocks do not seem to cluster tightly about a single evolution curve. Thus, the Nd data provide the first suggestion of a growth in the heterogeneity of the mantle with time.

T_{CHUR} Ages

The observation that the CHUR evolution curve is the locus of initial ratios of many continental igneous rocks attaches age significance to the measured $^{143}\text{Nd}/^{144}\text{Nd}$ of rocks. As defined previously

the measured $\varepsilon_{\text{Nd}}(0)$ of a rock is given by

$$(25) \quad \varepsilon_{\text{Nd}}(0) \approx \varepsilon_{\text{Nd}}(T_x) + f_R Q T_x$$

where T_x is the crystallization age and f_R is the measured Sm/Nd enrichment factor in the rock. Thus, if we know that $\varepsilon_{\text{Nd}}(T_x) = 0$, then the crystallization age is given by:

$$(26) \quad T_x \approx \frac{\varepsilon_{\text{Nd}}(0)}{f_R Q} \cong T_{\text{CHUR}}$$

This "model age" is termed T_{CHUR} . It is given exactly by the following expression which is shown graphically in Figure 13.

$$(27) \quad T_{\text{CHUR}} = \frac{1}{\lambda} \ln \left[1 + \frac{\frac{143}{144} \text{Nd} / \frac{144}{144} \text{Nd}_{\text{meas}} - I_{\text{CHUR}}(0)}{\frac{147}{144} \text{Sm} / \frac{144}{144} \text{Nd}_{\text{meas}} - (\frac{147}{144} \text{Sm} / \frac{144}{144} \text{Nd})_{\text{CHUR}}} \right]$$

For the Archean rocks analyzed, the T_{CHUR} age is equal to the crystallization age within the limits of uncertainty. It appears from Figure 10 that, especially for rocks of age > 1.5 AE, T_{CHUR} ages may be a way of obtaining quite accurate ages. This method could be used to determine the ages of crustal rocks in a reconnaissance fashion to estimate the volume of the crust as a function of time. Since one only needs to measure $\varepsilon_{\text{Nd}}(0)$ and f_R on whole rocks the age of large portions of shield areas could be determined on a fairly fine scale with a minimum of analytical effort. It is valuable because it can be used to date not only granitic rocks, which could be dated in a similar fashion with Rb-Sr, but also mafic or ultramafic rocks, which

Figure 13: Illustration of T_{CHUR} model age calculation. The approximate expression given for T_{CHUR} is accurate to 1.5% for $T_{\text{CHUR}} = 4.5 \text{ AE}$. For all Archean rocks which have been analyzed, the T_{CHUR} ages are identical to the crystallization ages within experimental uncertainty.

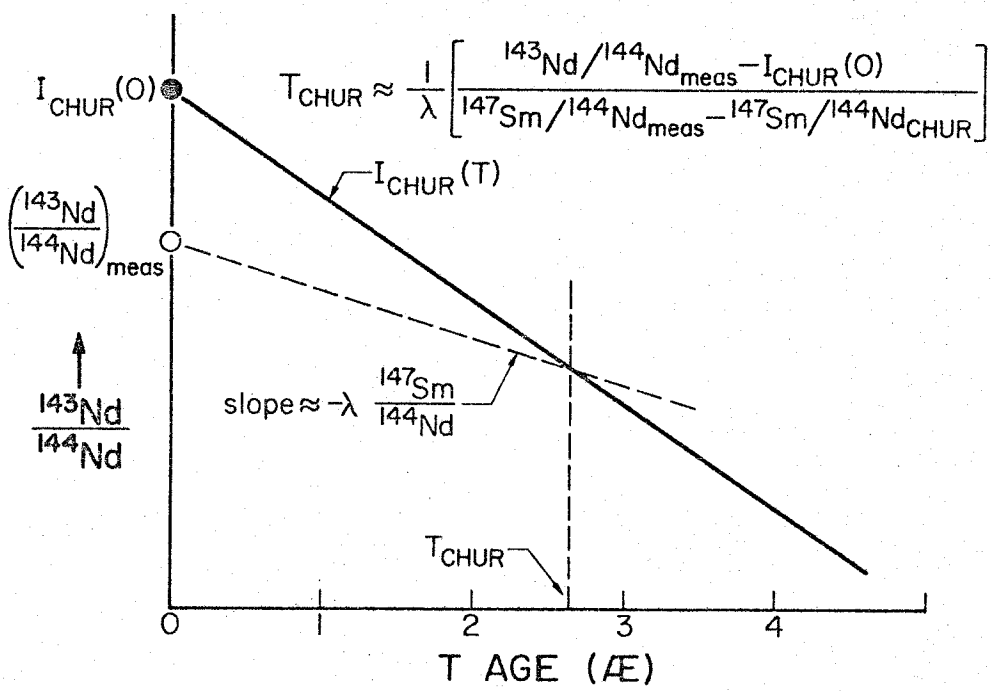


Fig. 13

cannot be dated by Rb/Sr, but could yield precise T_{CHUR} ages. The determination of the time of formation of continental crust has been hampered by the possibility that profound metamorphic events may obscure the true age of a crustal segment due to redistribution of parent and daughter isotopes. However, the evidence to date (Haskin *et al.*, 1968) suggests that REE patterns of rocks are not significantly changed even during high grade metamorphism. If this is the case, then T_{CHUR} ages could provide real "crust-formation ages" for a wide variety of rocks, including metamorphic rocks, since the T_{CHUR} age of the original igneous rock would be unaffected by the later metamorphism. Thus T_{CHUR} ages may be a way to see past metamorphic events to the time when the sialic material differentiated from its source region. These ideas are discussed more fully by McCulloch and Wasserburg (1978) who used T_{CHUR} ages to determine the average age of large segments of the North American shield.

Comparison of Earth and Moon

The ϵ_{Nd} values of all Lunar rocks which have been measured are shown in Figure 14. Mare basalts ranging in age from 3.3 to 3.9 AE exhibit a range in ϵ_{Nd} from -2 to +7. This range in ϵ_{Nd} is similar in magnitude to that shown by the young terrestrial basalt samples, and is much larger than the range shown by terrestrial Archean rocks. This range in ϵ_{Nd} in the lunar rocks exists despite the fact that the lunar samples are very old. Thus, large variations of ϵ_{Nd} were able to evolve in the moon over a time interval of only 1 AE, whereas similar variations on the earth took 4.5 AE

Figure 14: Graph of ϵ_{Nd} versus age for lunar igneous rocks showing large variations in ϵ_{Nd} of lunar rocks. Filled points are samples for which Sm-Nd internal isochrons have been determined. H indicates highland samples, the remaining samples being mare basalts. Lines diverging from CHUR at 4.4 AE represent Nd evolution in reservoirs fractionated from CHUR with Sm/Nd equal to 1.4 and 0.85 times chondritic. Note that only one sample lies within error on the $\epsilon_{\text{Nd}} = 0$ line in contrast to the terrestrial igneous rocks. This figure is taken from Papanastassiou *et al* (1977; Appendix 4).

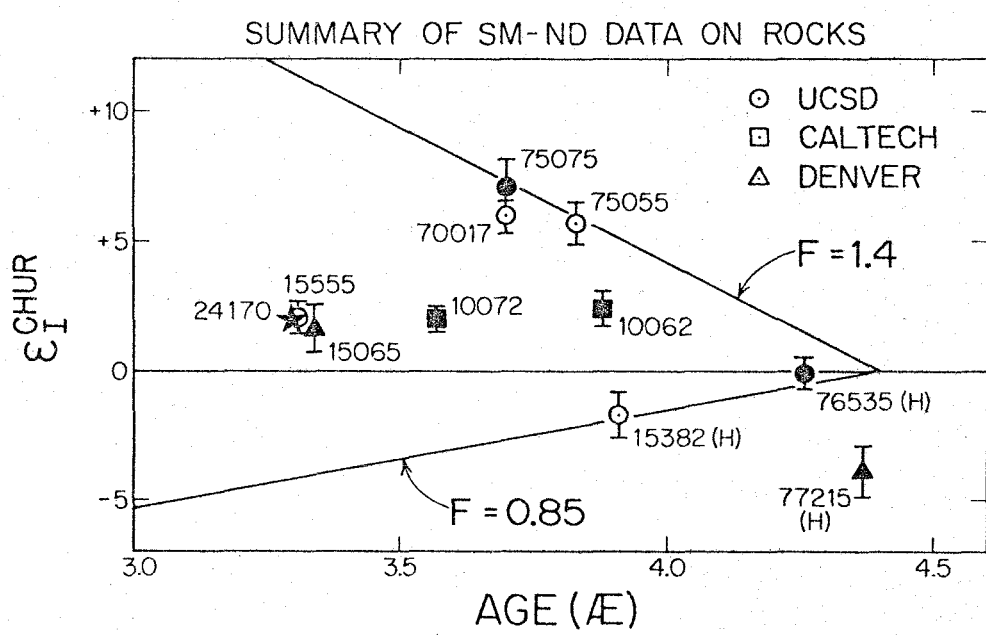


Fig. 14

to develop (Figure 15). The lunar data indicate a range of Sm/Nd of some 40% to 50% in magma sources on the moon compared to ~10% on the earth. Of the ten data points shown in Figure 14, only one has $\epsilon_{Nd} = 0$. Lugmair and Marti (1977) have interpreted their data on green glass balls as indicating that some magmas were differentiated from a deep nearly-chondritic lunar source. However, there is a general lack of evidence for the existence of a long-lived chondritic Sm/Nd reservoir in the moon as found in the earth. Thus unlike in the case of the earth the variability of Sm/Nd in the moon makes it impossible to deduce with confidence the bulk lunar Sm/Nd.

The contrast between the lunar and terrestrial Nd isotope data may imply a grossly different early differentiation history for these two planets. The lunar data indicate that reservoirs with greatly different Sm/Nd were formed very early in lunar history and preserved over at least 1.5 AE until the end of mare volcanism. Rare earth element abundance and Rb-Sr data also suggest early lunar differentiation in order to account for the Eu anomaly in lunar basalts. In contrast, the earth seems to have remained a fairly uniform Sm/Nd reservoir over most of its early history. A possible explanation for this difference between the earth and the moon is that a profound early differentiation event, such as affected the moon, never occurred in the earth. However, this would be surprising since the gravitational energy possibly available for the moon is much smaller than for the earth. Alternatively, the differentiation began in both planets early but it was "frozen in" on the moon at an early stage due to the limited energy available. In this case, the lunar reservoirs

Figure 15: Comparison of ϵ_{Nd} versus age for terrestrial and lunar rocks. Data points represent selected lunar rocks (see Figure 14) and stippled areas enclose most terrestrial data. This figure shows that large variations of ϵ_{Nd} evolved early in the moon, but apparently did not evolve until much later on the earth. Lines diverging from CHUR represent $\epsilon_{\text{Nd}}(T)$ in reservoirs fractionated from CHUR at about 4.5 AE. Reservoirs with these evolution curves could have been the parent reservoirs of some of the mare basalts. If early formed, highly-fractionated reservoirs such as these had formed in the earth and were still present today, we would expect a much wider range of ϵ_{Nd} for terrestrial rocks of all ages.

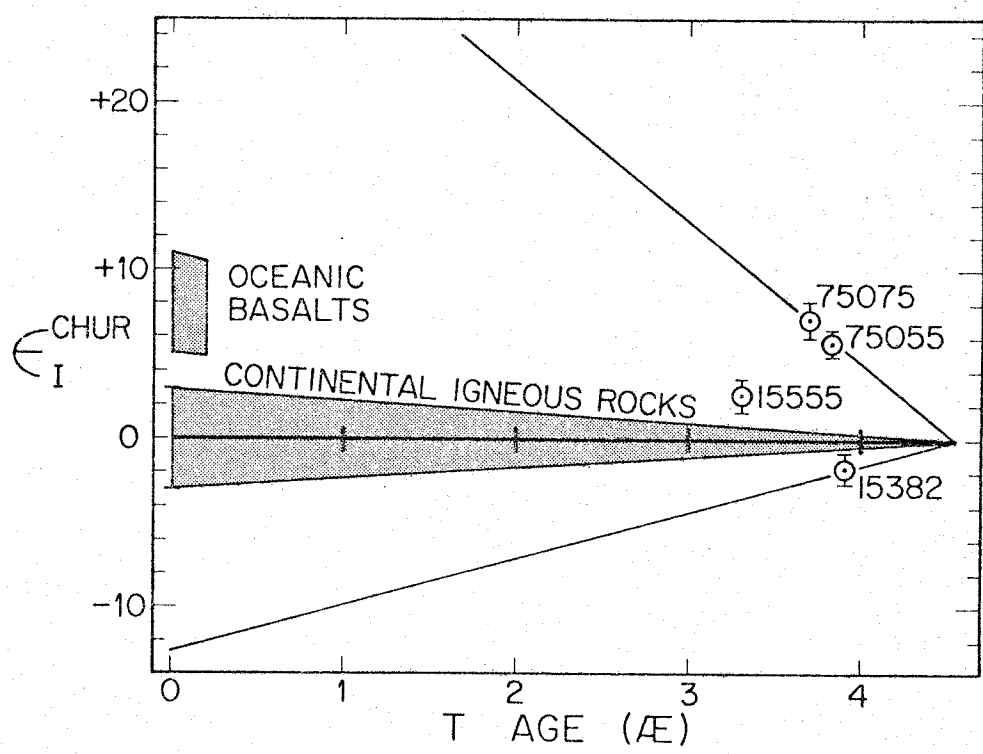


Fig. 15

which formed early with variable Sm/Nd remained subsequently largely undisturbed and were able to evolve their widely varying $^{143}\text{Nd}/^{144}\text{Nd}$. On the earth, however, sufficient energy may have been available so that mixing processes, e.g., convection, competed with differentiation and prevented reservoirs from being isolated long enough to evolve isotopic differences. In any case, this contrast appears to represent a first-order difference in planetary evolution and must be closely related to the early thermal histories of the two planets.

Contrast between oceanic and continental mantle

Inspection of Figure 11 reveals that no young continental rocks have ϵ_{Nd} greater than +7. In contrast, essentially all of the MOR basalts and many island arc rocks have $\epsilon_{\text{Nd}} > +7$ as do a substantial number of ocean island basalts. These data therefore indicate a profound difference between the suboceanic and subcontinental mantle magma sources which has persisted for a time period probably on the order of 1 AE.

The possibility of a chemical difference between suboceanic and subcontinental mantle is one that has interested petrologists for some time. Gast (1966) presented a compilation of Sr isotope data on young volcanic rocks. His figure 6 is reproduced here as Figure 16. This figure shows that the Sr isotope data available in 1966 showed no difference between continental and oceanic rocks. Although the oceanic distribution tended to be skewed to somewhat lower values than the continental, the fact that the lowest values of $^{87}\text{Sr}/^{86}\text{Sr}$ in both areas were the same (0.702), while the conti-

Figure 16: Histogram of $^{87}\text{Sr}/^{86}\text{Sr}$ in young volcanic rocks. Data represent measurements made prior to 1966. Figure taken from Gast (1966).

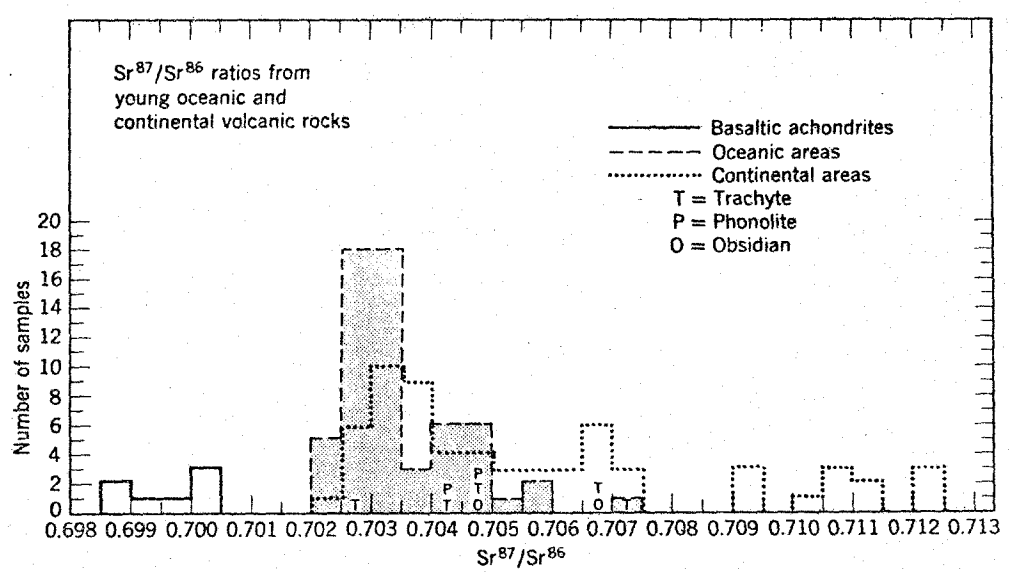


Fig. 16

nental samples extended to higher values, suggested that crustal contamination of the continental lavas could be solely responsible for any observed difference. Leeman and Manton (1971) summarized Sr isotope data on continental tholeiites and suggested that they indicated a difference between the sources of continental and oceanic tholeiites. However, large uncertainties in many of the data points and the restriction of the discussion to only continental tholeiites make the conclusion difficult to evaluate. Pb isotope studies have not shown any consistent difference between oceanic and continental basalts.

Thus the Nd data appear to indicate for the first time a clear chemical difference between suboceanic and subcontinental mantle. Such a difference may also be indicated by Sr isotopes when more precise data are available.

Provinciality of Sub-Continental Magma Sources

Although the Nd isotopic composition of young continental igneous rocks is generally different from that of oceanic basalts, there is considerable variation in ϵ_{Nd} of the continental rocks. These variations appear to display patterns indicative of large-scale structure in the sub-continental mantle. The ϵ_{Nd} of eleven Mesozoic and Cenozoic igneous rocks from western North America are plotted on a sketch map in Figure 17. Also shown on Figure 17 are the boundaries of Pb isotopic provinces as outlined by Zartman (1974). These provinces are based on measurements of Pb in Mesozoic and Cenozoic rocks and ore minerals. Area I leads are least radiogenic (lowest $^{206}\text{Pb}/^{204}\text{Pb}$)

Figure 17: ϵ_{Nd} values in young igneous rocks from western North America. Zones Ia, b, II, and III are lead isotopic provinces defined by Zartman (1974). Samples represented by the ϵ_{Nd} values are : +0.1 - BCR-1, Yakima basalt; +6.6 - PG16D, Picture Gorge basalt; +4.6 - CAS-1, Mt. Shasta basalt; +0.2 - RGB-1, Rio Grande Rift alkali olivine basalt; +6.2 - PCB-1, Pisgah crater trachybasalt; +1.9 - RL-1, Rubideaux leucogranite; +4.4 - SMG-1, San Marcos gabbro; +3.6 - WMG-1, Woodson Mtn. granodiorite; +6.7 - CSQ-3, San Quintin basanite. Sample BCR-1 is actually from farther west than shown. It is placed as is on the figure because most of the Yakima basalts are thought to have originated from vents near the Washington-Idaho-Oregon border (D. Swanson, personal communication).

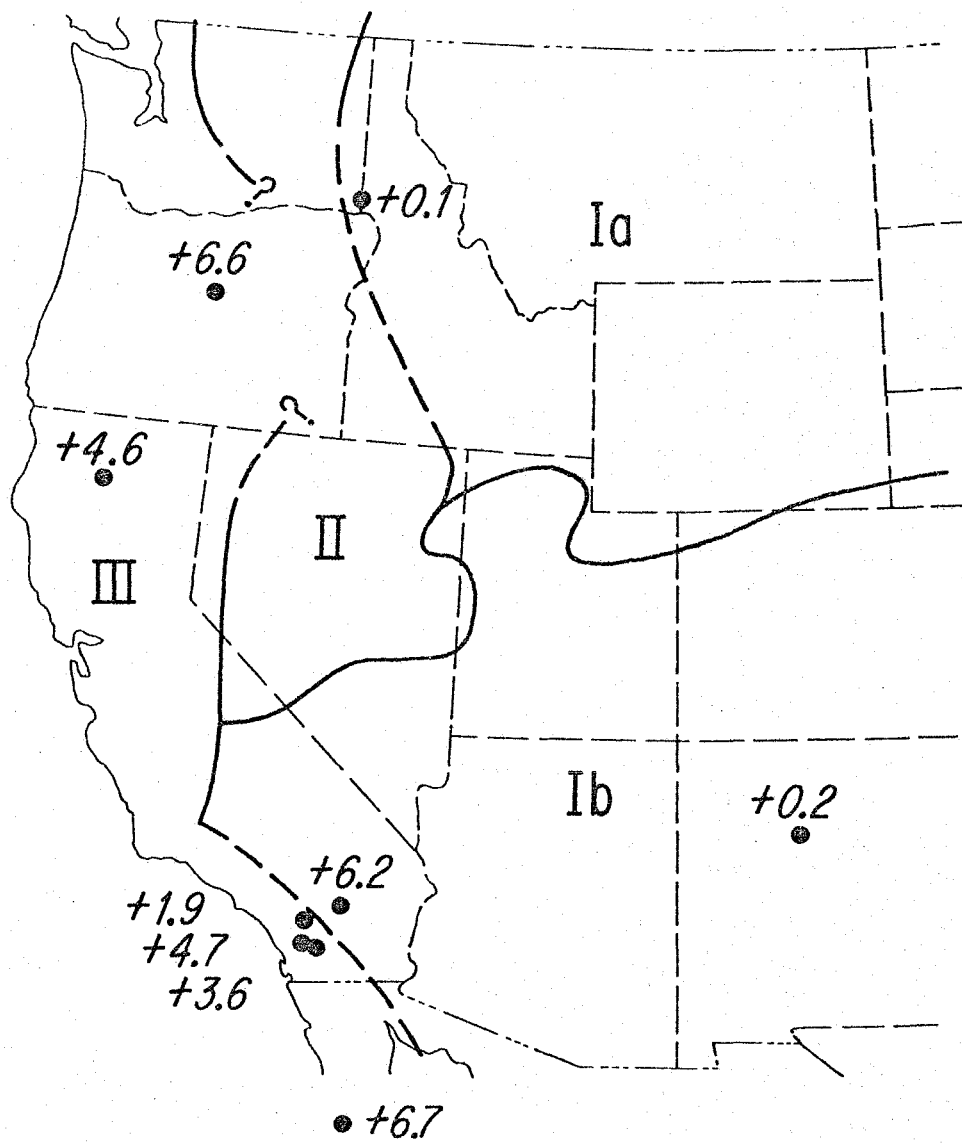


Fig. 17

but highly variable, Area III leads are more radiogenic and not variable and Area II leads are most radiogenic. Zartman (1974) noted that the boundary between Area I and Areas II and III roughly follows the western limit of known Precambrian basement and suggested that the isotopic variations in the igneous rocks could be related to fundamental differences in the lower crust or mantle under the two areas. The Nd data shown in this figure also give a suggestion of some regularity. The samples erupted in the more interior parts of the continent have ϵ_{Nd} near zero while those near the continental margin have $\epsilon_{Nd} > 0$ and within the range of ϵ_{Nd} found in oceanic island basalts. Area II and III Pb compositions are also similar to ocean island Pb. Thus lower ϵ_{Nd} values appear to correspond to lower $^{206}\text{Pb}/^{204}\text{Pb}$ values in a general way. The meager Nd data appear so far to be consistent with Pb data. The Pisgah basalt ($\epsilon_{Nd} = +6.2$) appears to belong to Area III rather than I, but the western boundary of Area I at this latitude is poorly defined by Zartman's data and additional more recent data have considerably altered the probable location of this province boundary (Everson and Silver, 1976).

In general the Nd data indicate that the mantle underlying the western borderlands of North America may be more "oceanic" in character than that underlying the continental interior. This conclusion agrees in general with Sr isotope data also (Leeman, 1974). This transition may be related to recent subduction along the coast of North America and the apparent termination of the East Pacific Rise in the Gulf of California. However, the ϵ_{Nd} of the

1.1 AE old Sierra Ancha diabase ($\epsilon_{\text{Nd}} = +3.4$) suggests that the "oceanic" character of the mantle in this region may date from Precambrian times.

Intraprovince variability of ϵ_{Nd}

The discussions of variations of ϵ_{Nd} in young igneous rocks have thus far been concerned with differences between rocks falling in rather broad geographic or petrologic categories. In order to evaluate the meaning and significance of these variations it is helpful to have some idea of the variability of ϵ_{Nd} within a single petrologic province, within lavas erupted from a single volcano, and within a single lava flow. No investigation has yet been made on variations within a single flow, but Figure 18 presents data from provinces where multiple analyses are available. Figure 18 shows that intraprovince variability ranges from no measurable variation, as in the case of Bouvet Island, to variations of the same magnitude as those found between the major groupings discussed earlier, as seen in the Hawaiian data.

The eight samples from the island of Hawaii show a total spread in ϵ_{Nd} of 3 units; there is no apparent relationship between ϵ_{Nd} and rock type (O'Nions *et al.*, 1977). The three samples from Oahu show a marked contrast. Two nephelinites have identical ϵ_{Nd} while a tholeiite has a drastically different ϵ_{Nd} which is similar to many continental flood basalts. The tholeiite and nephelinites appear to be derived from totally different reservoirs despite their coincident location. The nephelinites on Oahu are

Figure 18: Histogram of ϵ_{Nd} values in young igneous rocks grouped by petrologic province. Data from Iceland, Tristan da Cunha, Bouvet, Ascension, and most of the Hawaiian data are from O'Nions et al (1977).

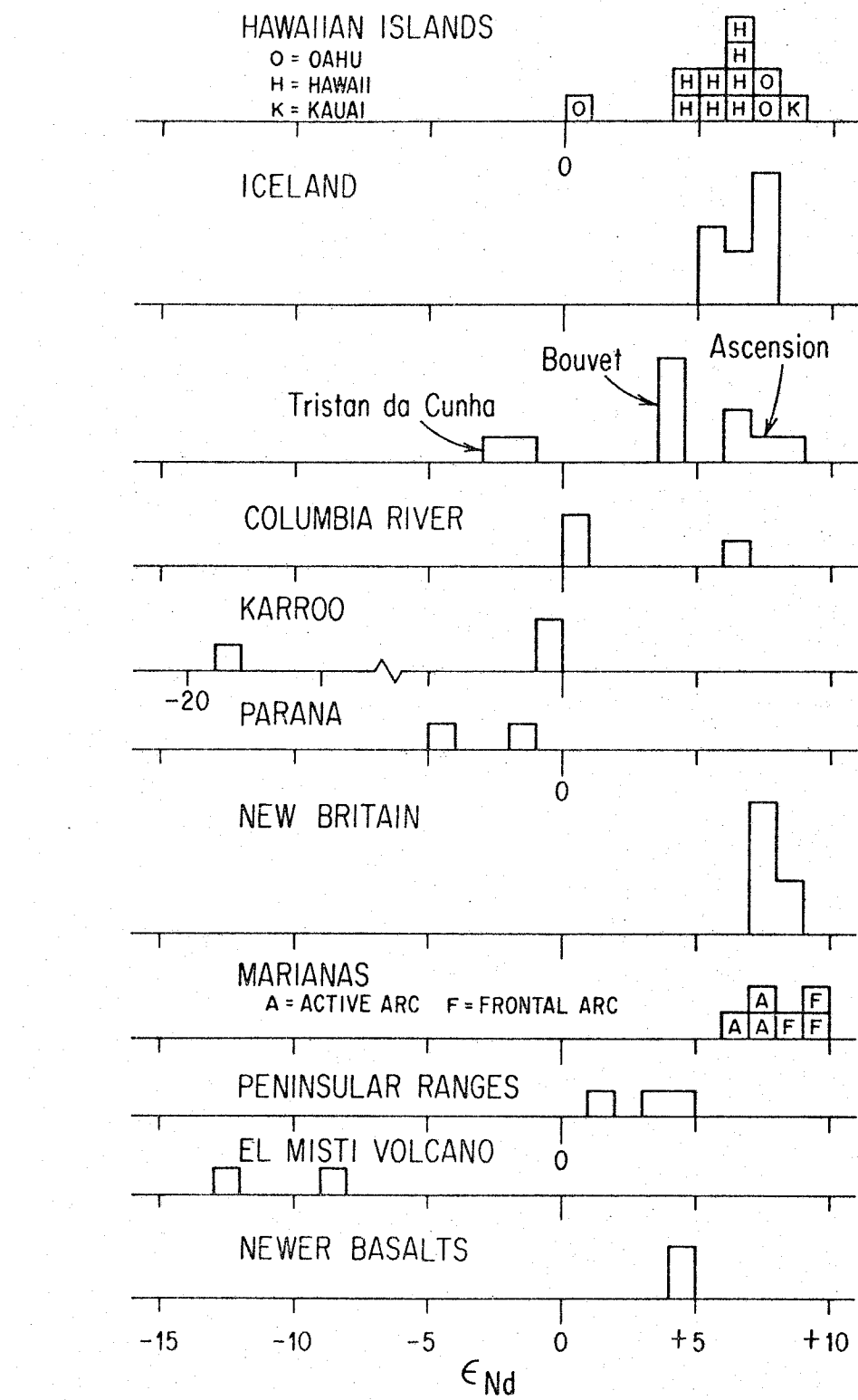


Fig. 18

younger than the tholeiites, being erupted after an eruptive hiatus of a few million years (Doell and Dalrymple, 1973). In this case it appears that resumption of magmatic activity may have resulted in melting of a mantle reservoir different from that which yielded the magmas during the main phase of volcanism. These data show that a single volcanic conduit system can access a variety of mantle reservoirs of distinctive chemistry and age. The only Hawaiian samples with $\epsilon_{\text{Nd}} > +7$ are nephelinites, which suggests some relation between magma chemistry and isotopic properties. However, these nephelinites are also from different islands than are the bulk of the other samples which complicates the interpretation. In the past Hawaii has been considered based on Sr isotope data, to be an example of a province where lavas of diverse chemistry have a uniform isotope composition. The data given here and newer Sr data (O'Nions et al., 1976) clearly show that this is not the case. The older Sr data were of too low a precision relative to the overall variations in oceanic lavas to detect it (Hedge, 1966).

Ten samples from Iceland show a total variation in ϵ_{Nd} of three units, with no discernible relationship between ϵ_{Nd} and rock type. Four samples from Ascension Island exhibit a range of three units while two samples from Tristan da Cunha are nearly identical. The Tristan da Cunha samples have ϵ_{Nd} much different than the average for the other oceanic islands and are the only island lavas which appear to be derived from a "continental-type" source.

As discussed earlier, the sample of Yakima basalt from the Columbia River province has ϵ_{Nd} much different from the Picture Gorge

sample. The Picture Gorge lavas were erupted from a different fissure system than were the Yakima basalts (Waters, 1961), and the isotopic difference may be a reflection of the isotopic provinces which appear to exist in western North America. The Columbia River data suggest that during a single large magmatic event, the region of melting may transgress fundamental large-scale chemical boundaries in the mantle.

Two samples of Karroo basalt from the Stormberg Series in South Africa have identical ϵ_{Nd} . These two samples were collected over 100 km from each other and suggest that the southern Karroo province may be isotopically homogeneous. The third Karroo sample is from several hundred kilometers farther north in Mozambique. The Karroo basalts of Mozambique have been only cursorily described in the literature and little information on their chemistry and their relationship to other parts of the Karroo province is available. The Nd data suggest that their genesis or emplacement history may have been drastically different from that of the better-known lavas farther south.

The two Parana basalts come from a single drill core at stratigraphic levels separated by 450 meters and both have K-Ar ages of about 120 million years. The difference of 3 units in ϵ_{Nd} could again reflect derivation from different reservoirs although the possible effects of crustal contamination cannot yet be assessed.

Seven samples from the New Britain region in the Bismarck Island Arc, including samples of basalt, andesite, and rhyolite,

show a remarkably narrow range of ϵ_{Nd} . These lavas also were erupted at different distances from the submarine trench. In contrast to Hawaii, it appears that the source of these New Britain magmas is a well-homogenized reservoir. The data suggest that fractional crystallization may be responsible for much of the chemical variation between the lava types.

The samples from the Marianas arc show substantially more variation than the New Britain samples. However, the three samples from the presently active arc have identical ϵ_{Nd} while the three samples from the now dormant Eocene-Miocene frontal arc also have identical ϵ_{Nd} , but uniformly higher than the active arc lavas. It appears that when the locus of volcanism moved to the north between Miocene time and the present, a different reservoir began to be tapped.

The three samples from the Peninsular Ranges batholith show a significant variation in ϵ_{Nd} . The variations seem to be correlated with rock type with the gabbro having $\epsilon_{\text{Nd}} = +4.7$, the granodiorite having $\epsilon_{\text{Nd}} = +3.6$ and the leucogranite having $\epsilon_{\text{Nd}} = +1.9$. The fact that the more silicic rocks have lower ϵ_{Nd} suggests that old silicic crust may be involved in their genesis to some degree. However, variations in other trace elements and $^{87}\text{Sr}/^{86}\text{Sr}$ (Silver, 1975) generally do not correlate with rock type, but show more complex variations indicating that the generation of these batholithic rocks cannot be described in terms of one simple process. The ϵ_{Nd} of the San Marcos gabbro sample is identical to that of a basalt from Mt. Shasta in the Cascade Range,

and supports the notion that the batholith may have been formed in continental margin volcanic arc environment. However, these ϵ_{Nd} values are substantially lower than those found in the true island arcs.

Two samples (andesite and rhyolite) erupted from El Misti volcano in the Peruvian Andes give an indication of the possible variability of ϵ_{Nd} in lavas from the same volcano erupted at closely spaced points in time. The difference of four units in ϵ_{Nd} is quite large. However, these lavas may be derived by remelting of old continental crust. Since continental crust may be isotopically grossly heterogeneous on a fine scale, it may be more common to find large isotopic differences in lavas derived from melting of crust than in lavas derived from the mantle.

In conclusion, the variations of ϵ_{Nd} found within a single

magmatic province or within lavas from a single eruptive center may be quite significant compared to the variations found on a global scale between broad petrologic categories or geographic regions.

In the continental rocks, some of the dispersion may be due to crustal contamination rather than being a true reflection of heterogeneities in the magma sources. However, the ocean island data, especially those from Hawaii, strongly suggest that a substantial amount of variation must be attributable to the mantle magma sources. This variation, exhibited at a single location, clearly indicates the existence of substantial vertical differentiation in the upper mantle and that such layered structure must be preserved for at least several hundred million years. On the other

hand, the narrow range of ϵ_{Nd} values shown by the Bismarck Island arc samples indicates how homogeneous a large-scale magma source can be. The total variation of 1.2 ϵ_{Nd} units is just larger than twice the 2σ uncertainty in a single analysis and thus barely detectable. These data provide a working definition of a "homogeneous reservoir."

REE patterns in magma sources

With the simple models discussed in Chapter III we can evaluate the implications of the ϵ_{Nd} values measured in young rocks for the REE patterns in their respective parental mantle regions. By inspection of Figures 9 and 11 it can be seen that in general $\epsilon_{\text{Nd}}(0)$ of continental rocks of a wide range of ages are less than zero while ϵ_{Nd} of the vast majority of young basalts, which represent $\epsilon_{\text{Nd}}(0)$ in the mantle, are greater than zero. These data are thus consistent with a simple model of evolution of the outer earth, whereby it had originally a chondritic REE pattern, and through time a low-melting fraction (the continental crust) with $f_{\text{Sm}/\text{Nd}} < 0$ was extracted from the mantle and stored near the surface of the earth leaving the upper mantle with $f_{\text{Sm}/\text{Nd}} \geq 0$. This is just the same type of model as was discussed in Chapter III. The continental crust is here identified with the low-melting fraction because the crust is the only reservoir known where low-Sm/Nd material is stored for geologically long times without being remixed with the mantle.

For purposes of discussion mantle material which has lost a low melting fraction will be termed "depleted mantle," and it will be assumed that such mantle material has $f_{\text{Sm}/\text{Nd}} > 0$ with the "most

depleted" material having the highest $f_{\text{Sm}/\text{Nd}}$ as can be deduced from Figure 5. Thus most zero age basalts which have $\epsilon_{\text{Nd}} > 0$ can be presumed to be derived by melting of depleted mantle material, which was left as a residue from a previous partial melting event. The MOR basalts, since they have the highest ϵ_{Nd} , are derived from mantle reservoirs which are most depleted. Only the continental flood basalts, which tend to cluster about a value of $\epsilon_{\text{Nd}} = 0$, may be derived from undepleted mantle which, prior to the generation of the flood basalts, had existed since the formation of the earth without being partially melted. Continental flood basalts may represent a special type of magmatic event in which primordial mantle material is melted for the first time. Study of these basalts may yield more veracious information on the composition of the earth than does study of oceanic basalts which are derived from material which has been previously differentiated. Finally, if the inference is correct that undifferentiated mantle material is still present in the earth, then it may imply that the earth is still heating up due to heat generated by radioactive decay rather than cooling off due to loss of original heat from accretion or core formation.

Prior to this study, it had been concluded from trace element studies that MOR basalts were derived from depleted mantle reservoirs (Gast, 1968). This had been deduced from the observation that many MOR basalts have light-REE depleted patterns ($f_{\text{Sm}/\text{Nd}} > 0$) which as discussed in Chapter III implies that their parental reservoirs have this property. Thus the Nd evidence confirmed this earlier hypothesis.

However, the Nd data add knowledge about the length of time that these reservoirs have been depleted. If they are very old ($T_s \approx 4.5$ AE), then from the f^*T^* values of 4×10^8 yr and equation 14 we calculate $f_s \approx +0.09$. By comparison with Figure 5 it can be seen that this would imply very mildly light-REE depleted patterns in the sources of MOR basalts. However, if these reservoirs became depleted only 0.5 AE ago (i.e., $T_s = 0.5$ AE), then they must have $f_{Sm/Nd} \approx +0.80$, indicative of a highly fractionated, light-REE-depleted pattern. Obviously, partial melting models of the generation of MOR basalts based on rare-earth elements will depend heavily upon the T_s age of the MOR basalt source reservoirs. For example, f_R for a typical MOR basalt is about +0.10. For $T_s = 4.5$ and equation 15 we calculate $g \approx 0$. In contrast, for $T_s = 0.5$ AE, $g = -0.39$. By reference to Figure 5, we see that the latter would indicate that MOR basalts form by small degrees of partial melting while the former would imply large degrees of melting.

Unlike the case of the MOR basalts, the Nd isotopic data have to some degree contradicted previous ideas about the REE patterns in the parental reservoirs of ocean island basalts and island arc volcanics. Ocean island basalts have light REE enriched patterns ($f_{Sm/Nd} < 0$) and thus give no evidence to suggest that $f_{Sm/Nd}$ of their source reservoir is > 0 . Furthermore, ocean island basalts have $^{87}Sr/^{86}Sr$ which is somewhat higher than those of MOR basalts. This was taken as an indication that their source reservoirs were indeed chemically different than those of MOR basalts. Thus it was hypothesized (cf., Kay and Gast, 1973) that the ocean island lavas were derived from

primitive undepleted mantle. Since island arc rocks have $^{87}\text{Sr}/^{86}\text{Sr}$ similar to ocean island lavas, it was further hypothesized that they too might be derived from undepleted mantle reservoirs. The Nd data, however, suggest that the source reservoirs of ocean island basalts as well as island arc lavas are depleted.

Sun and Hanson (1975) suggested more recently that there was evidence from the trace element patterns of alkali basalts similar to those found on ocean islands, that indicated that their source reservoirs were not primitive and unfractionated. They concluded that these reservoirs had become enriched in light REE at some time during the past. They suggested that this light-REE enrichment may have occurred in Precambrian times although they noted that it could have occurred very recently. The Nd data clearly indicate that such light-REE enrichment could not have occurred in Precambrian times, since then the ϵ_{Nd} of ocean island lavas would be expected to be somewhere in the range -10 to -30 in contrast to the observed range of +4 to +8. If the source reservoirs of these lavas are light-REE enriched ($f_{\text{Sm/Nd}} = -0.4$ as suggested by Sun and Hanson, 1975) then they must have become enriched within the last $\sim 4 \times 10^8$ years.

Growth of Continental Crust

The bulk composition and REE abundances of island arcs and continental margin volcanics arcs closely approximate the composition of average continental crust (Taylor and White, 1965). This observation together with the fact that island arcs are usually found at or near continental margins has led to the hypothesis that

they are the site of production of new continental crust. Continents thus may grow through time by accreting at their margins material produced in island arcs. If this is the case, then the measurements made in this study indicate that new continental material has a Nd isotopic composition similar to oceanic basalts and should not lie on the CHUR curve.

The ancient partial melting events which depleted the source reservoirs of the island arc rocks could have contributed to building of the continental crust. Thus if island arcs represent the typical materials being added to form new continental crust, then it must be concluded that continental crust is now being derived from depleted mantle reservoirs which were previously tapped to form continental crust in earlier epochs of crust-building. Since these reservoirs may be more depleted in "crustal components" today than in the past, new continental material derived from them may have a significantly different average composition than Archean crust.

Evidence for multi-state evolution histories for mantle rocks

The notion that mantle reservoirs may have complicated fractionation histories, which is implicit in the suggestions of Sun and Hanson (1975), finds some degree of support from the Nd data on the St. Paul's spinel peridotite (sample SPP-1) which may be a direct sampling of an upper mantle segment. This rock has a highly fractionated REE pattern with a very low $f_{\text{Sm}/\text{Nd}} (= -0.76)$ (Frey, 1970). Despite its negative $f_{\text{Sm}/\text{Nd}}$, this rock has a positive $\epsilon_{\text{Nd}} = +5.9$. This is similar to the example shown in Figure 4b. Thus,

in order to explain this, this rock must have had at least a three-stage history. Presumably it began with a chondritic REE pattern ($f_{\text{Sm}/\text{Nd}} = 0$). In order to have evolved an $\epsilon_{\text{Nd}} > 0$, at some time in the past it must have acquired an $f_{\text{Sm}/\text{Nd}} > 0$, perhaps after being partially melted and losing a light-REE enriched melt fraction. More recently it has acquired its present-day negative $f_{\text{Sm}/\text{Nd}}$, perhaps by being injected with a light-REE enriched magma which was generated in the mantle at deeper levels as suggested by Green (1971) and Frey and Green (1974). Whether or not the models of generation are correct, it is clear that mantle segments may indeed have complicated histories. Regarding the suggestion by Sun and Hanson (1975) that oceanic alkali basalts are derived from light-REE-enriched mantle material of peridotite composition, the St. Paul's sample at least demonstrates that such material, with ϵ_{Nd} similar to those of the alkali basalts, does exist.

In Figure 6 was given examples of the magnitude of ϵ_{Nd} variations which might be expected to be found in the mantle due to fractionation from partial melting events. Values of ϵ_{Nd} of from +20 to +150 or more might be expected to be found in the mantle today. However, young basalts have ϵ_{Nd} mostly in the range -4 to +12, much closer to zero than expected, and spanning a much smaller range than could plausibly be present in the mantle.

Thus, if basalts are produced by about 5% partial melting of the mantle, and if the ϵ_{Nd} values of young basalts are an unbiased sampling of all mantle reservoirs, then the data suggest that a mantle

segment affected by a specific large melting event, such as one producing about 10^5 km^3 of flood basalt, must be remixed with the remaining undepleted mantle within about 0.5 AE after the melting event. The amount of mantle material which would be affected by such an event ($\sim 10^{22} \text{ g}$) represents only about $2 \times 10^{-4}\%$ of the total mantle.

A second possibility is that the small range of ϵ_{Nd} in the mantle could mean that all igneous rocks represent only very small degrees of melting of the mantle (<0.5%) so that no part of the mantle ever acquires an $f_{\text{Sm/Nd}} > 0.10$. However, this alternative seems unlikely since orogenic lherzolites, which are probably segments of uplifted mantle, have been found with $f_{\text{Sm/Nd}}$ in the range +0.5 to +1.5 (Frey *et al.*, 1971). Thus the fact that almost all rocks have ϵ_{Nd} not far from 0 ($\lesssim +10$) indicates that mantle reservoirs with $f_{\text{Sm/Nd}} \geq 1.0$ are rarely, if ever, preserved for times longer than 0.5 AE.

An alternative explanation is that the basalts do not give an unbiased sampling of ϵ_{Nd} in the mantle. Instead, they may be melted only from those reservoirs which are relatively undepleted. Mantle segments which become severely depleted may never be subsequently remelted to produce basalts.

VII. Sr RESULTS

Most of the samples analyzed for $^{143}\text{Nd}/^{144}\text{Nd}$ were also analyzed for $^{87}\text{Sr}/^{86}\text{Sr}$. The results of these analyses are given in Table 1. The $^{87}\text{Sr}/^{86}\text{Sr}$ ratios are expressed as ϵ_{Sr} as explained in Chapter II. Figure 19 shows the Sr isotope data on a graph of ϵ_{Sr} versus ϵ_{Nd} . Included in this figure are only those basalt samples with $\epsilon_{\text{Sr}} < +15$; island arc samples are not shown. Figure 19 shows that ϵ_{Sr} and ϵ_{Nd} are strongly correlated in basalts from a wide variety of tectonic settings on both continents and oceans. MOR basalts have the highest ϵ_{Nd} and lowest ϵ_{Sr} and lie at one extreme of the trend. Continental basalts generally tend to have highest ϵ_{Sr} and lowest ϵ_{Nd} , while the ocean island basalts are intermediate in both ϵ_{Nd} and ϵ_{Sr} . This remarkable correlation is the first such correlation ever discovered between two radioactive isotope systems in nature. Although Pb and Sr isotopes had been intensively studied for more than two decades no such simple correlation was ever found between Pb and Sr isotope variations in young basalts.

The slope of the trend indicates that reservoirs with low Rb/Sr have high Sm/Nd and those with high Rb/Sr have low Sm/Nd. Generally when a rock is partially melted, the liquid will have higher Rb/Sr and lower Sm/Nd than the original rock, and the solid residue will have lower Rb/Sr and higher Sm/Nd. Thus, if reservoirs in the earth are formed by such processes (as shown in Figure 2) the reservoirs with highest ϵ_{Nd} will have lowest ϵ_{Sr} and vice versa. The slope of the correlation trend is thus consistent with the hypothesis

that Nd and Sr isotopic variations in the earth today are the result of Sm/Nd and Rb/Sr fractionations which were caused by magmatic processes in the past.

This correlation between Nd and Sr isotope variations was first discovered and noted by DePaolo and Wasserburg (1976c) and the first substantial data documenting the correlation were given by DePaolo and Wasserburg (1976b) along with a short statement of its possible origin. From this work it was clear that a strong correlation existed and that it appeared to apply to both oceanic and continental volcanics. These authors found rocks with ϵ_{Nd} ranging from +11 down to -4 which lay on the same trend. Richard et al. (1976) also found that there was a suggestion of some correlation between $^{143}\text{Nd}/^{144}\text{Nd}$ and $^{87}\text{Sr}/^{86}\text{Sr}$ in some young basalts they measured, but the precision of their $^{143}\text{Nd}/^{144}\text{Nd}$ measurements was too poor to show this conclusively. O'Nions et al. (1977), in a study restricted to oceanic rocks, presented more evidence for a correlation. They noted a fine-scale correlation in lavas from Iceland and the Reykjanes Ridge and also noted that a broad correlation existed in all their data, although most of their data was in the more restricted interval of $\epsilon_{\text{Nd}} = +12$ to $\epsilon_{\text{Nd}} = +4$ and because of the substantial dispersion did not appear to suggest such a strong correlation.

The solid line in Figure 19 was drawn through the data as an approximation to the trend. As is shown, $\epsilon_{\text{Nd}} = 0$ on this trend corresponds to $^{87}\text{Sr}/^{86}\text{Sr} = 0.7045 \pm 5$. Since $\epsilon_{\text{Nd}} = 0$ should represent an unfractionated reservoir, this implies that a value of $^{87}\text{Sr}/^{86}\text{Sr} =$

Figure 19: Graph of ε_{Nd} versus ε_{Sr} in young basalts which have ε_{Sr} less than +15. The ε_{Sr} scale has been arbitrarily set so that the line drawn through the data passes through the point $\varepsilon_{\text{Nd}} = 0$, $\varepsilon_{\text{Sr}} = 0$. The corresponding initial $^{87}\text{Sr}/^{86}\text{Sr}$ are given on the scale at the top. This figure includes data from O'Nions et al. (1977) and Richard et al. (1976).

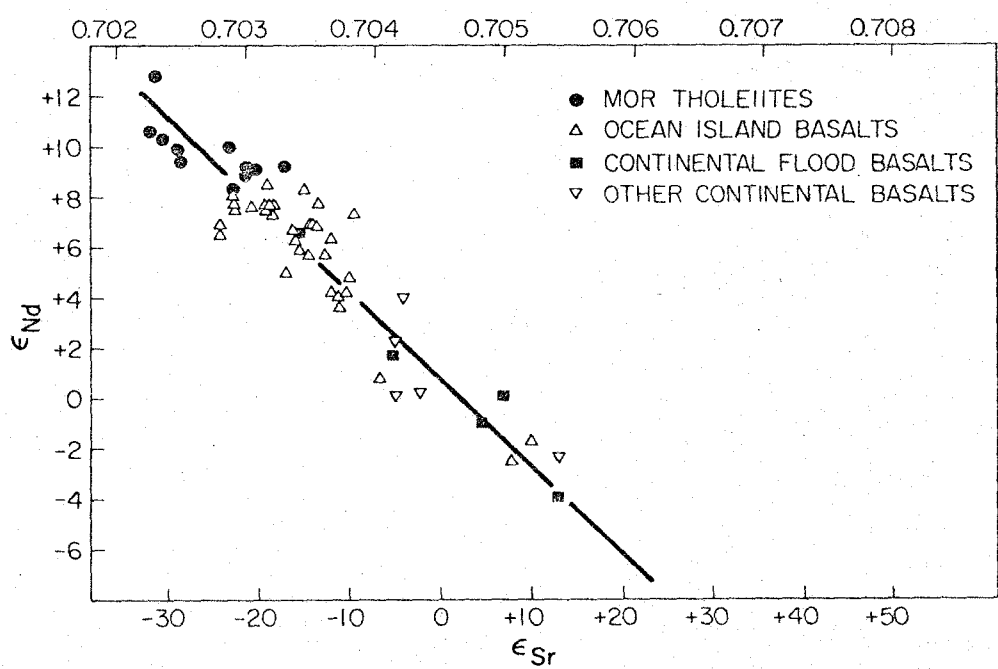


Fig. 19

0.7045 should be associated with unfractionated mantle reservoirs today.

From this number and BABI ($=0.69898$; Papanastassiou and Wasserburg, 1969) it can be calculated that the Rb/Sr of undifferentiated mantle material is 0.029 ± 0.003 . This correlation trend thus gives the first clear indication of Rb/Sr for unfractionated mantle.

As discussed in Chapter II, the values of Rb/Sr and Sm/Nd calculated for a reservoir with $\epsilon_{\text{Nd}}(0) = 0$ and $\epsilon_{\text{Sr}}(0) = 0$ may be those of the bulk earth. However, this inference is directly tied to the interpretation of the correlation trend. Although the interpretation favored at the present time suggests that these may be bulk earth values, there exist plausible interpretations of the trend which would suggest that they are not. At present the origin of the correlation is not sufficiently well understood to conclude that the Rb/Sr and Sm/Nd values are those of the bulk earth. They are, however, the present best estimates of bulk earth values and may be useful for assessing simple models of terrestrial differentiation.

The samples with $\epsilon_{\text{Sr}} > +15$ or $\epsilon_{\text{Nd}} < -6$ are shown on an expanded diagram in Figure 20. In general, for samples with $\epsilon_{\text{Nd}} < 0$, ϵ_{Nd} and ϵ_{Sr} appear still to be correlated, but in a much more diffuse way. However, a striking regularity is shown by several continental flood basalt samples. These samples form a regular array extending from $\epsilon_{\text{Nd}} = 0$, $\epsilon_{\text{Sr}} = 0$, to $\epsilon_{\text{Nd}} = -18$, $\epsilon_{\text{Sr}} = +312$. This trend has a slope which is much different from that of the trend defined by samples with $\epsilon_{\text{Nd}} > 0$. The trend is almost exactly that which would be expected in basalts which originally had $\epsilon_{\text{Nd}} = \epsilon_{\text{Sr}} = 0$, but were contaminated to varying degrees with average old Rb-rich upper crustal material. This explanation of

Figure 20: Graph of ϵ_{Nd} versus ϵ_{Sr} showing data on continental flood basalts including some samples not shown on Figure 19. Also shown are other samples not shown on Figure 19, the correlation line from Figure 19, and the approximate fields of MOR and ocean island basalts. The dashed line indicates a trend suggested by some of the flood basalt data which may result from crustal contamination of the basalt magmas.

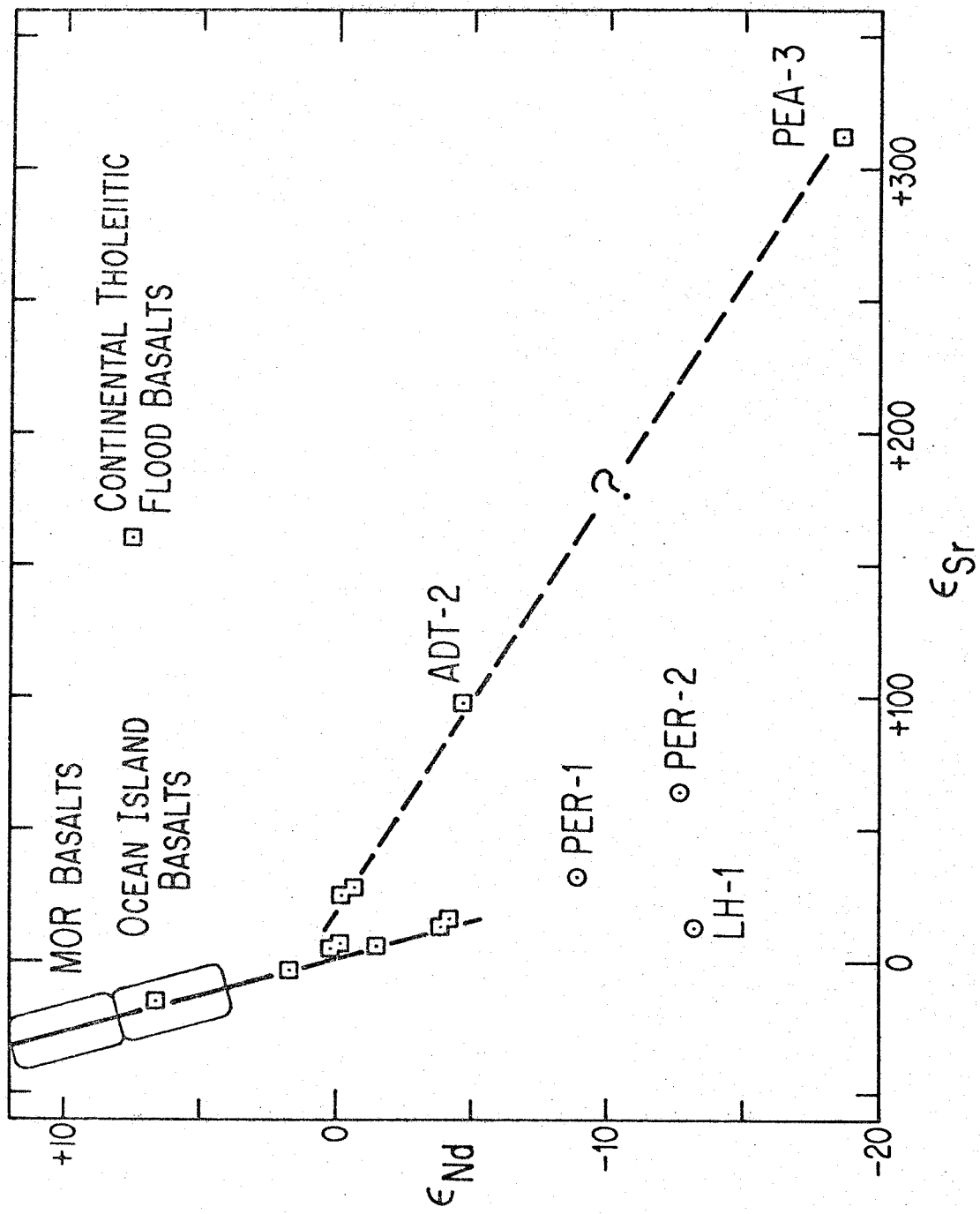


Fig. 20

the trend is plausible, since many of these continental basalts appear to be highly differentiated and thus may have spent relatively long times in magma chambers within the crust where contamination would have had opportunity to occur. There are arguments against contamination as an explanation. For instance, sample PEA-3 would have to be enormously highly contaminated in order to be displaced by +300 in ϵ_{Sr} . If the contaminant were average 2.5 AE old crust, then this magma would have to contain 80% contaminant. It is possible, however, that the contamination is not bulk dissolution of wallrock in the magma, but rather contamination from some phase such as a fluid which is enriched in crustal Nd and Sr or which acts as an exchange medium between the magma and the wallrock. If this trend is not caused by crustal contamination, then it may be indicative of a special history for some parts of the subcontinental mantle. If the trend is caused by contamination, then it shows that Nd is much less sensitive than Sr to contamination, suggesting that Nd isotopes may provide a better tool for the study of subcontinental magma sources than does Sr. The fact that the trend extrapolates back to the correlation line at $\epsilon_{\text{Nd}} = 0$ indicates that after subtraction of the effects of crustal contamination continental flood basalts still have a markedly different isotopic composition from MOR basalts and thus must be derived from a distinct reservoir.

Three samples (PER-1, 2; LH-1) lie in a much different region of this diagram than do the flood basalts. These data are as yet poorly understood. It was suggested earlier from the Nd data that these

samples may be the product of melting of the lower crust. If so, the lower ϵ_{Sr} values of these lavas and the low ϵ_{Nd} 's would suggest a lower crust which is depleted in Rb (and U, Th) relative to the upper crust, as suggested by Heier (1965) and Zartman and Wasserburg (1969), but which has a REE pattern which is similar to that of the upper crust. However, this explanation is still highly speculative.

In summary, the data fall into three broad categories:

- (1) Those samples with $\epsilon_{\text{Sr}} < +15$ which fall along the trend shown in Figure 19;
- (2) Continental flood basalt samples which fall along a mixing line between a magma with $\epsilon_{\text{Nd}} = \epsilon_{\text{Sr}} = 0$ and average upper crust;
- (3) Some other continental volcanics which fit neither trend and whose ϵ_{Nd} and ϵ_{Sr} values are not understood.

In addition, some island arc rocks and some oceanic basalts also diverge from the trend shown in Figure 19. The island arc rocks are discussed in Appendix 3. Both the island arc rocks (DePaolo and Wasserburg, 1977) and the oceanic basalts (O'Nions *et al.*, 1977) are believed to diverge from the trend due to contamination with seawater.

VIII. DISCUSSION OF Sr RESULTSOrigin of $\epsilon_{\text{Nd}} - \epsilon_{\text{Sr}}$ correlation

The data presented in Chapter VII show that initial $^{143}\text{Nd}/^{144}\text{Nd}$ and $^{87}\text{Sr}/^{86}\text{Sr}$ in young basalts are strongly correlated for rocks with initial $^{87}\text{Sr}/^{86}\text{Sr}$ less than ~ 0.705 (DePaolo and Wasserburg, 1976b,c,1977; O'Nions *et al.*, 1977). The relationship suggests that Rb/Sr and Sm/Nd may be covariant in the lithic reservoirs in the earth's interior, a somewhat surprising result considering the geochemical dissimilarity of the elements involved. The correlation thus suggests that the processes which have operated to differentiate the earth's interior into chemically distinct domains may be extremely uniform. In this section, we will consider possible origins of this isotopic correlation and its implications for the differentiation history of the earth's mantle and crust. It should be kept in mind that two phenomena require explanation: (1) the correlation trend itself, and (2) the dispersion in the data about the correlation line.

Three possible origins of the correlation shown in Figure 19 will be considered. First, the possibility is entertained that the variations of ϵ_{Nd} and ϵ_{Sr} do not reflect differences in the parent reservoirs of the magmas but rather result from different amounts of crustal contamination of magmas which are melted from a single mantle reservoir with ϵ_{Nd} and ϵ_{Sr} similar to MOR basalts. The second possibility is that only two distinct reservoirs exist from which basalts are derived; one has ϵ_{Nd} and ϵ_{Sr} similar to MOR basalts and the other has $\epsilon_{\text{Nd}} = \epsilon_{\text{Sr}} = 0$ or perhaps lies along the extension of the

trend but with $\varepsilon_{\text{Nd}} < 0$ and $\varepsilon_{\text{Sr}} > 0$. A third possibility is that the ε_{Sr} and ε_{Nd} values of the basalts represent the present day compositions of a spectrum of reservoirs in the earth, each of which has formed independently in a separate fractionation event.

Given below is a brief explanation of the systematics of the $\varepsilon_{\text{Nd}}-\varepsilon_{\text{Sr}}$ diagram. Following that, each of the above-mentioned possible origins for the correlation will be evaluated and the implications of each will be discussed.

A. Systematics of $\varepsilon_{\text{Nd}}-\varepsilon_{\text{Sr}}$ variations

1. Mixing relationships

Mixing of two reservoirs can produce linear or near-linear trends on an $\varepsilon_{\text{Nd}}-\varepsilon_{\text{Sr}}$ diagram. If a mixture of two reservoirs A and B contains a weight fraction X_B of reservoir B, the difference between ε_{Nd} in the mixture and ε_{Nd} of A ($\Delta\varepsilon_{\text{Nd}}$) is given by:

$$(28) \quad \Delta\varepsilon_{\text{Nd}} = \frac{[\text{Nd}]_B (\varepsilon_{\text{Nd}}^B - \varepsilon_{\text{Nd}}^A) X_B}{[\text{Nd}]_A + ([\text{Nd}]_B + [\text{Nd}]_A) X_B}$$

$$\approx \frac{[\text{Nd}]_B}{[\text{Nd}]_A} (\varepsilon_{\text{Nd}}^B - \varepsilon_{\text{Nd}}^A) X_B \quad \text{for } X_B \ll 1$$

An exactly analogous equation holds for ε_{Sr} . The relative effects on ε_{Sr} and ε_{Nd} for small X_B are thus:

$$(29) \quad \frac{\Delta\varepsilon_{\text{Nd}}}{\Delta\varepsilon_{\text{Sr}}} = \frac{(\text{Nd/Sr})_B}{(\text{Nd/Sr})_A} \left(\frac{\frac{\varepsilon_{\text{Nd}}^B - \varepsilon_{\text{Nd}}^A}{\varepsilon_{\text{Sr}}^B - \varepsilon_{\text{Sr}}^A}}{\frac{\varepsilon_{\text{Nd}}^B - \varepsilon_{\text{Nd}}^A}{\varepsilon_{\text{Sr}}^B - \varepsilon_{\text{Sr}}^A}} \right)$$

Thus the shape of the mixing curve between two reservoirs depends on the ratio of Nd/Sr in the two reservoirs.

Figure 21 shows mixing lines for mixtures of two reservoirs for different ratios of Sr/Nd in the reservoirs. A straight line results only if Sr/Nd is the same in both reservoirs. If the Sr/Nd of the two reservoirs are greatly different, the mixing line becomes strongly curved. Thus a linear array on an $\epsilon_{\text{Nd}} - \epsilon_{\text{Sr}}$ diagram can be caused by two-component mixing only if the components have similar Nd/Sr.

2. Sr and Nd evolution during differentiation of a planet

In this section, the characteristics of the isotopic evolution of Nd and Sr in reservoirs in a planet which undergoes a simple differentiation history are presented. This development may clarify the possible implications of the data shown in Figures 19 and 20 and will aid in the assessment of the models presented below. It will be analogous to the discussion presented in the introduction but considers the Rb-Sr and Sm-Nd systems concurrently.

Consider a planet which forms 4.5 AE ago as a compositionally uniform sphere and has the parent/daughter ratios Sm/Nd_{UR} and Rb/Sr_{UR} . The evolution of $^{143}\text{Nd}/^{144}\text{Nd}$ and $^{87}\text{Sr}/^{86}\text{Sr}$ in the planet is shown as the curves $I_{\text{UR}}^{\text{Nd}}(T)$ and $I_{\text{UR}}^{\text{Sr}}(T)$ in Figure 22a. At time T_f a portion of the planet differentiates into two reservoirs A and B. Suppose that reservoir A has $f_{\text{Sm/Nd}} > 0$ and $f_{\text{Rb/Sr}} < 0$. Reservoir B must then have $f_{\text{Sm/Nd}} < 0$ and $f_{\text{Rb/Sr}} > 0$. This would be the case if reservoir B were formed from a partial melt of the UR reservoir and A were the solid residue left after melting (as in Figure 2). The evolution of

Figure 21: ε_{Nd} and ε_{Sr} for mixtures of two components, A and B. The shape of the mixing line depends on the parameter $K = (\text{Sr/Nd})_A / (\text{Sr/Nd})_B$. The mixing line is a straight line only if $K = 1$.

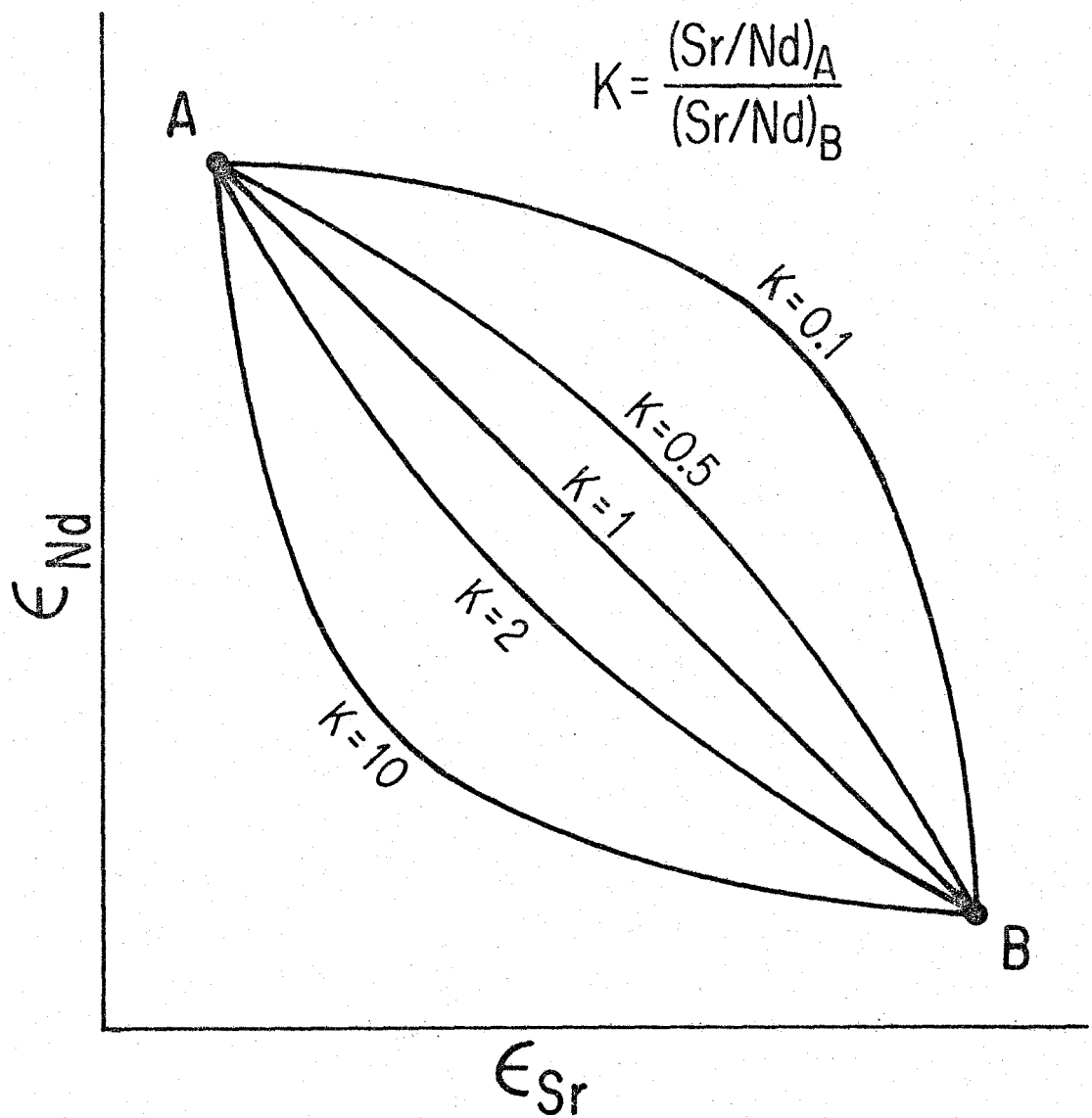


Fig. 21

Figure 22: Series of graphs displaying the evolution of the isotopic composition of Nd and Sr in two reservoirs A and B fractionated from an UR reservoir at time T_f . Relative to UR reservoir A has higher Sm/Nd and lower Rb/Sr and vice versa for reservoir B. Figure 22a shows the evolution of $^{143}\text{Nd}/^{144}\text{Nd}$ and $^{87}\text{Sr}/^{86}\text{Sr}$. Figure 22b shows $\epsilon_{\text{Nd}}(T)$ and $\epsilon_{\text{Sr}}(T)$. Figure 22c shows the present-day isotopic composition of the three reservoirs on a plot of $\epsilon_{\text{Nd}}(0)$ versus $\epsilon_{\text{Sr}}(0)$. The dotted line shows the isotopic composition of mixtures of reservoirs A and B. The relationships between the locations of the points on Figure 22c and the Sm/Nd and Rb/Sr enrichment factors are also given. Note that if mixing of reservoirs such as A and UR were responsible for the $\epsilon_{\text{Nd}}-\epsilon_{\text{Sr}}$ correlation in young basalts (Figure 19), then the slope of the correlation trend would provide information about the chemistry of the complementary reservoir (B), which might, for instance, be the continental crust.

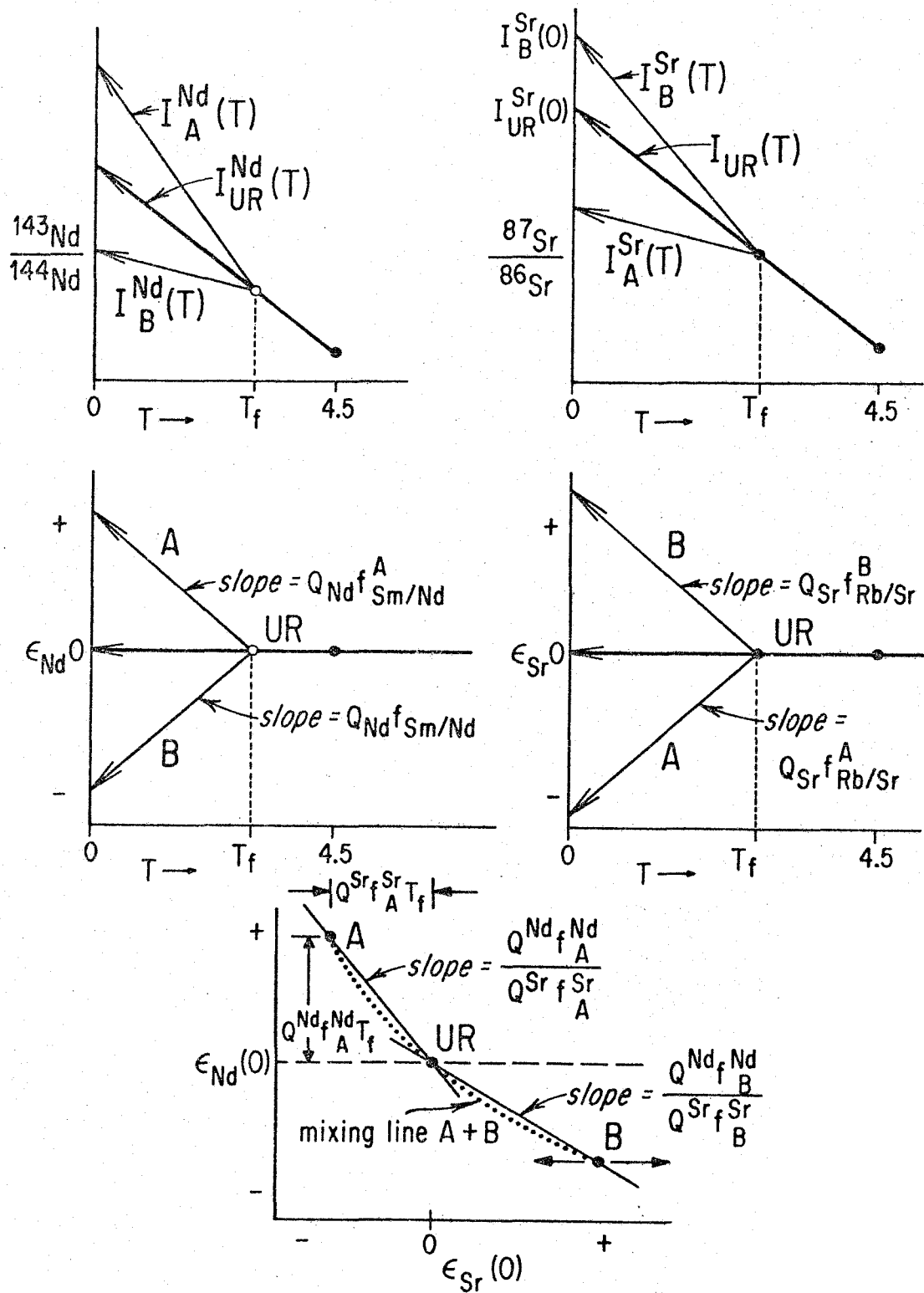


Fig. 22

$^{143}\text{Nd}/^{144}\text{Nd}$ and $^{87}\text{Sr}/^{86}\text{Sr}$ in reservoirs A and B is shown in Figure 22a.

The information shown in Figure 22a is shown in Figure 22b on graphs of ϵ_{Nd} versus time and ϵ_{Sr} versus time. Subsequent to T_f reservoir A evolves a positive ϵ_{Nd} but a negative ϵ_{Sr} and vice versa for reservoir B. As indicated on these diagrams, the slopes of the ϵ_{Nd} and ϵ_{Sr} evolution lines are proportional to $f_{\text{Sm/Nd}}$ and $f_{\text{Rb/Sr}}$ respectively. Finally, Figure 22c shows the present-day $\epsilon_{\text{Nd}}(0)$ and $\epsilon_{\text{Sr}}(0)$ of reservoirs A, B, and UR plotted on the $\epsilon_{\text{Nd}}-\epsilon_{\text{Sr}}$ diagram. As shown in this figure, for Reservoir A: $\epsilon_{\text{Nd}}(0) = Q_{\text{Nd}} f_{\text{Sm/Nd}}^A T_f$ and $\epsilon_{\text{Sr}}(0) = Q_{\text{Sr}} f_{\text{Rb/Sr}}^A T_f$. These relationships are also obvious from Figure 22b. Analogous equations hold for Reservoir B. The slope of the line segment A-UR is therefore equal to $Q_{\text{Nd}} f_{\text{Sm/Nd}}^A / Q_{\text{Sr}} f_{\text{Rb/Sr}}^A$ and is independent of time. As time progresses the slope remains constant and the point A will move farther away from UR. Any reservoir which forms from UR with $f_{\text{Sm/Nd}}/f_{\text{Rb/Sr}}$ equal to that in A will lie along the line A-UR for all time. Its distance from the point UR today will depend on the magnitude of the product $f_{\text{Sm/Nd}} T_f$. Similarly, any reservoir which forms from UR with $f_{\text{Sm/Nd}}/f_{\text{Rb/Sr}}$ equal to that of B will lie on the line UR-B for all time. The slopes of the two line segments are related by:

$$(30) \quad \frac{\text{slope UR-B}}{\text{slope A-UR}} = \frac{(\text{Sr/Nd})_B}{(\text{Sr/Nd})_A}$$

Thus the slopes of the lines connecting the compositions of the complementary reservoirs A and B to UR on the $\epsilon_{\text{Nd}}-\epsilon_{\text{Sr}}$ plot are dependent upon the relative partitioning of Nd and Sr between the reservoirs. The distances A-UR and B-UR are dependent upon the

$f_{\text{Rb/Sr}}$ and $f_{\text{Sm/Nd}}$ in the reservoirs and T_f . The equation given above expresses the additional constraint which comes from the simultaneous consideration of two isotopic systems and may prove to be quite powerful as shown below.

The reservoirs A, UR, and B will be colinear on Figure 20c only if Nd/Sr is equal in all three reservoirs. The dotted line shows the compositions which result if today parts of reservoirs A and B are mixed together. This mixing line must pass through UR. However, if there is mixing of magmas derived from A and B, the resulting mixing line will depend on Nd/Sr in the two magmas and is not required to pass through the UR point.

Thus we see from these considerations that the Nd and Sr isotopic compositions of a population of reservoirs will line on a single straight line on an $\epsilon_{\text{Nd}} - \epsilon_{\text{Sr}}$ diagram if (1) all the reservoirs were derived from a single homogeneous reservoir (such as UR, and (2) all the reservoirs have identical $f_{\text{Sm/Nd}}/f_{\text{Rb/Sr}}$.

Magma contamination:

To evaluate an origin for the correlation trend by magma contamination the isotopic changes have been calculated which would result from contamination of typical magmas with possible contaminating materials using the mixing relations given in equation 28. These are then compared to the observed correlation trend. Of course, in any particular rock contamination can also be assessed by considering other aspects of the chemistry but for this discussion only the effect on the isotopic compositions of Nd and Sr will be considered.

Before proceeding it is necessary to assess the present day isotopic composition of possible contaminants. Figure 23 shows the present $\epsilon_{\text{Nd}}(0)$ and $\epsilon_{\text{Sr}}(0)$ found in young basalts, in several crustal samples measured in this study, and calculated for some composite samples. The $f_{\text{Rb/Sr}}$ and $f_{\text{Sm/Nd}}$ of average upper crust are from Taylor (1976). Its $\epsilon_{\text{Nd}}(0)$ and $\epsilon_{\text{Sr}}(0)$ were calculated from the given $f_{\text{Rb/Sr}}$ and $f_{\text{Sm/Nd}}$ assuming an average age of 1.5 AE and $\epsilon_{\text{Nd}}(1.5 \text{ AE}) = \epsilon_{\text{Sr}}(1.5 \text{ AE}) = 0$. GL represents a composite of granulite facies gneisses taken from Heier and Thoresen (1971). $f_{\text{Sm/Nd}}$ for these gneisses was estimated from the data of T.H. Green *et al.* (1972), and they also were assumed to be 1.5 AE old. These granulites may be representative of lower crustal rocks. In contrast to the upper crustal average, they are richer in Sr and have lower Rb/Sr. The only other samples shown which were not discussed previously are the Vermilion Granite (VG; 2.6 AE), whose Sm/Nd was taken from Arth and Hanson (1975) and Seawater, whose $\epsilon_{\text{Nd}}(0)$ is taken as that of the fish debris, sample DOS-1, Table 1.

This diagram shows the wide diversity of compositions found in the continental crust. It is immediately obvious that relative to the variations found in the young basalts, the variations in ϵ_{Sr} in crustal rocks are a factor of 10 to 100 greater than the variations of ϵ_{Nd} , illustrating why Sr is expected to be more susceptible to contamination. In general, the $\epsilon_{\text{Nd}}(0)$ of the rocks increases with increasing rock age because $f_{\text{Sm/Nd}}$ of crustal rocks is fairly constant. $\epsilon_{\text{Sr}}(0)$ is more dependent on chemistry than on age. Thus 0.12 AE old Rb-rich Rubidoux Leucogranite (RL-1) has $\epsilon_{\text{Sr}}(0)$ similar to the 2.6 AE old

Figure 23: $\epsilon_d(0)$ and $\epsilon_{Sr}(0)$ in several crustal rocks, composite samples of crustal rocks, and seawater, showing their relationship to the data on young basalts. Note that the points represent the values which would be measured in these rocks today. Unlike in the basalt magma sources, $\epsilon_{Nd}(0)$ and $\epsilon_{Sr}(0)$ are not strongly correlated in crustal rocks.

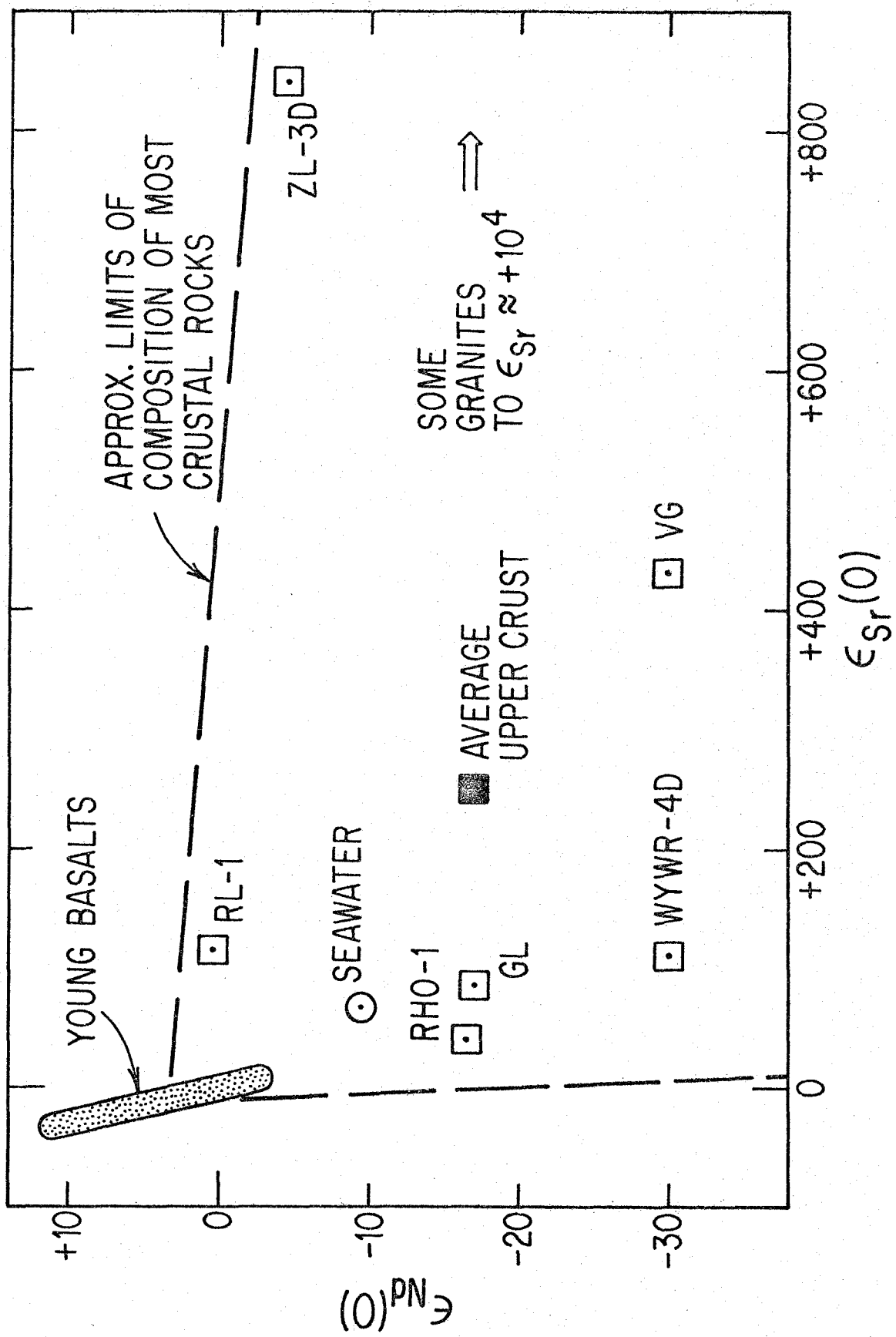


Fig. 23

granodiorite WYWR-4D, while the 1.0 AE Town Mountain Granite has ϵ_{Sr} much higher than the 2.5 AE basaltic Great Dyke.

The concentrations of Nd and Sr, $\epsilon_{\text{Nd}}(0)$ and $\epsilon_{\text{Sr}}(0)$ and Sr/Nd for average MOR basalt, average continental flood basalt and three examples of contaminating material are given in Table 2. The mixing lines for MOR basalt and continental flood basalt and the contaminants listed in Table 2 are shown in Figure 24. The values of the weight fraction of contaminant in the magma (X_c) are indicated along the curves. For seawater, instead of X_c the numbers given are water/rock mass ratios, so 10 indicates the resulting composition if 10g of water equilibrates isotopically with 1g of MOR basalt. Figure 24 shows that contamination of MOR basalt with any of the materials considered results in a trend much different from the $\epsilon_{\text{Sr}} - \epsilon_{\text{Nd}}$ trend defined by the young basalts (shown by the dashed line). The trend could be caused by contamination only if the contaminating material had much higher (Nd/Sr) and/or lower $|\epsilon_{\text{Sr}}(0)/\epsilon_{\text{Nd}}(0)|$. Low values of $|\epsilon_{\text{Sr}}(0)/\epsilon_{\text{Nd}}(0)|$ could be found in plagioclase rich crustal rocks, but plagioclase-rich rocks tend to have low rather than high Nd/Sr ratios. These calculations therefore lend no support to a magma contamination origin for the correlation line. However, some of the dispersion about the correlation line could be the result of small amounts of contamination of the magmas with crustal rocks, seawater, or oceanic sediments which are similar in composition to the upper crust.

Note in Figure 24 that because of the extremely low Nd/Sr of seawater, its interaction with oceanic basalt will not alter ϵ_{Nd} of

Table 2: Compositions of Basalt Magmas and Possible Contaminants

<u>Material</u>	<u>Nd (ppm)</u>	<u>Sr (ppm)</u>	<u>$\epsilon_{Nd}(0)$</u>	<u>$\epsilon_{Sr}(0)$</u>	<u>Sr/Nd</u>
MOR Basalt	10	136 ^d	+10	-30	13.6
Cont. Flood Basalt	25	250	0	0	10
Ave. Upper Crust ^a	32	350	-17 ^c	+250 ^c	11
Granulite (GL) ^b	25	572	-17 ^c	+85 ^c	23
Seawater	3×10^{-5} ^e	8 ^f	-9 ^g	+64 ^h	2.7×10^5

^aTaylor (1977) ^bHeier and Thoresen (1971); Green, Brunfelt and

Heier (1972) ^cAverage age assumed = 1.5 AE

^dSun and Hanson (1975) ^eHøgdahl et al. (1968) ^fMason (1966)

^gBased on analysis of fish debris (sample DOS-1)

^hPapanastassiou and Wasserburg (1970)

Figure 24: Effects of contamination on the isotopic composition of magmas of average mid-ocean ridge (MOR) basalt and continental flood basalt composition. Arrows represent simple mixing lines between the magmas and possible contaminants. Labelled tick marks on the arrows give the weight fraction of contaminant in the mixture necessary to displace the isotopic composition of the basalt to that point along the mixing line. For seawater the tick marks give the water/rock mass ratio. The dashed line represents the correlation trend from Figure 19; it is distinct from all of the mixing lines shown. The compositions of the magmas and contaminating rocks used for the calculations are given in Table 2.

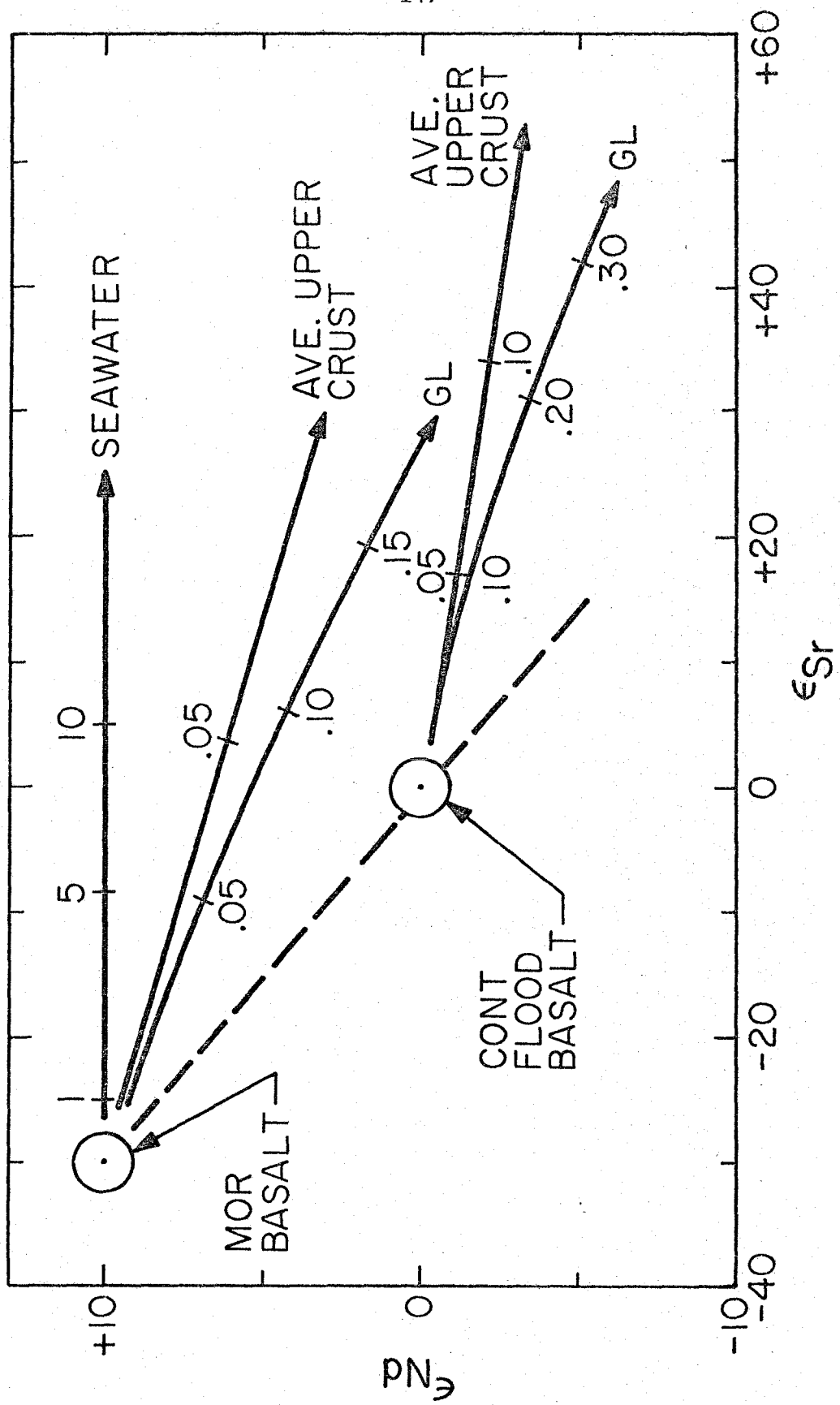


Fig. 24

the basalt. Thus, exchange between seawater and submarine basalts, which has complicated the interpretation of $^{87}\text{Sr}/^{86}\text{Sr}$ measured in the basalts, will not be a factor for evaluating $^{143}\text{Nd}/^{144}\text{Nd}$ in these basalts. This has been shown experimentally by O'Nions *et al.* (1977). This property of seawater has been used to investigate the origin of island arc magmas (Appendix 3).

The contamination of continental flood basalt ($\epsilon_{\text{Nd}} = \epsilon_{\text{Sr}} = 0$) with materials typical of both the upper and possibly the lower crust produces a trend on Figure 23 which very closely mimics the trend shown by some of the continental flood basalts on Figure 20. This strongly suggests that this trend may indeed result from crustal contamination of magmas which originally lay on the correlation trend with $\epsilon_{\text{Nd}} \approx 0$. In general, the fact that these contamination trends all have slopes significantly different from the correlation trend indicates that concurrent use of Nd and Sr isotopes will be a powerful petrogenetic tool which, using the correlation line as a base line, may enable the effects of contamination on the isotopic composition of magmas to be evaluated.

Two-Reservoir Mixing

The correlation trend could be explained by mixing of two reservoirs which are fairly homogeneous and have isotopic compositions lying at the extremes of the correlation trend or beyond. In order for a linear trend to result the two reservoirs must have similar Sr/Nd. Two such reservoirs could be formed in a variety of ways. Two possible models for their creation are as follows.

In Model I the two reservoirs are formed near the time of formation of the earth and have existed as separate entities ever since. In this case an original homogeneous earth was differentiated into one reservoir which was relatively enriched in Rb and Nd (EUR) and another reservoir relatively depleted in Rb and Nd (DUR). These reservoirs then evolved through time as independent uniform reservoirs. It is implicit in this model that neither of these reservoirs has the same composition as the original bulk earth, and thus that no unfractionated reservoir is now present in the earth. If unfractionated material is present in the earth, then three reservoirs instead of two are required. This situation could have arisen if for instance only part of the earth differentiated into EUR and DUR reservoirs leaving the remainder of the earth as a primitive CHUR reservoir. These two possibilities are depicted in Figure 25. Also shown in Figure 25 are possible present day compositions of these reservoirs on a graph of $\epsilon_{\text{Nd}}(0)$ versus $\epsilon_{\text{Sr}}(0)$.

Model II is depicted in Figure 26. In this model the mantle starts out as a uniform reservoir UR and through time magmas derived from the upper mantle contribute to building the continental crust. These magmas are enriched in Rb relative to Sr and in Nd relative to Sm so as the crust is gradually built the upper mantle becomes more and more depleted in Rb and Nd relative to Sr and Sm. The upper mantle in this case is fluid and rapidly convecting so that it is always well-mixed. However, it is isolated from the undifferentiated

Figure 25: Illustration of one model of the formation of two reservoirs in a single event early in earth history. In a the entire earth (mantle?) is differentiated into two compositionally distinct layers. In b only the outer part of the earth is differentiated into two layers leaving the deeper regions unmodified. The possible present-day $\epsilon_{\text{Nd}}(0)$ and $\epsilon_{\text{Sr}}(0)$ of the reservoirs is shown in the graphs at the bottom of the figure. Mixing of two reservoirs formed in this manner could explain the $\epsilon_{\text{Nd}}-\epsilon_{\text{Sr}}$ correlation in young basalts. Note that the "enriched" (EUR) and "depleted" (DUR) reservoirs need not be colinear with the UR reservoir.

MODEL I

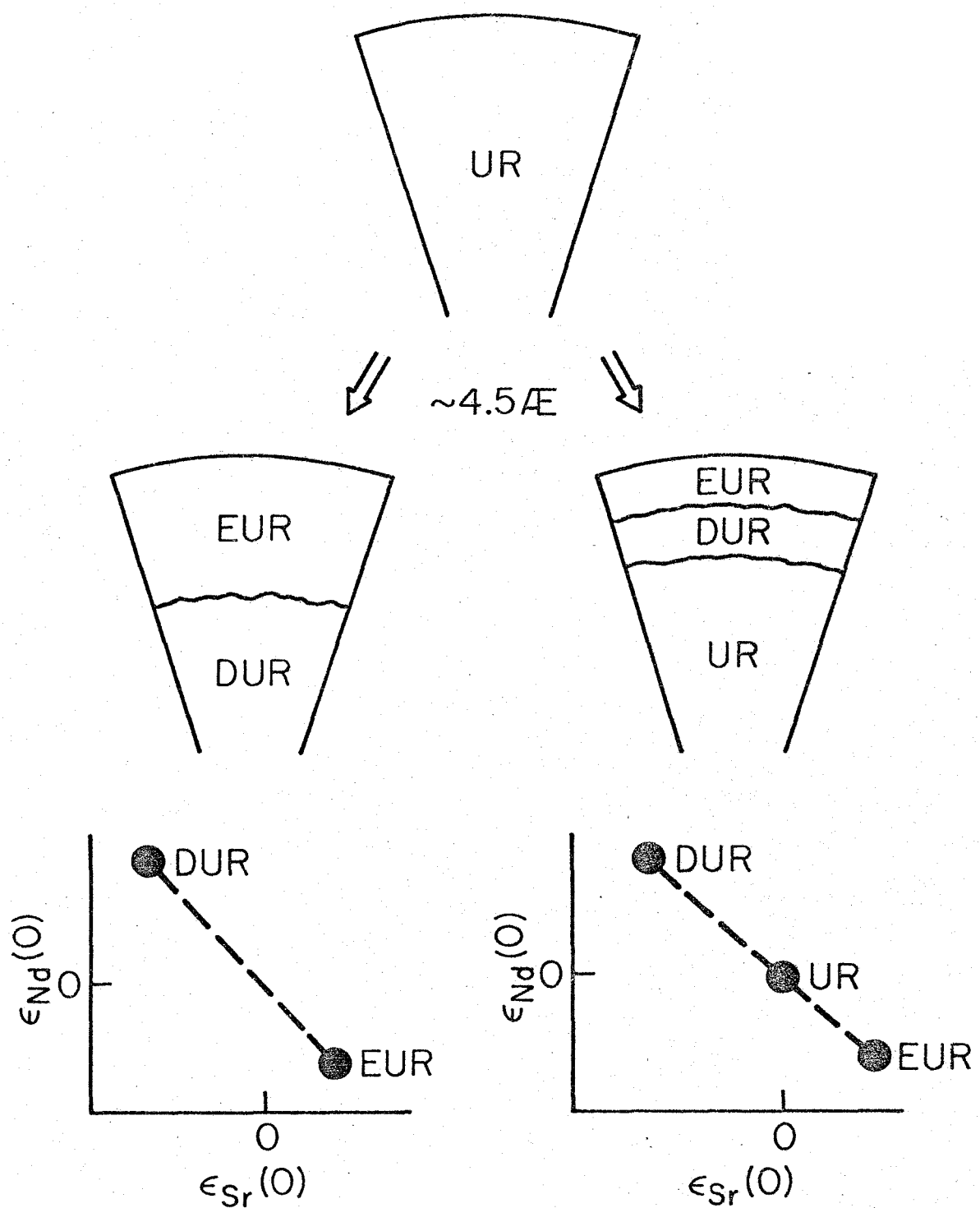


Fig. 25

Figure 26: Second model showing how a two layer mantle can form.

In this model the continental crust is built gradually through time from material which is partially melted from the upper mantle. The upper mantle convects vigorously and always remains well mixed.

Since the crust is enriched in Rb and Nd with respect to Sr and Sm the upper mantle gradually evolves a low Rb/Sr and a high Sm/Nd.

The lower mantle remains totally inert. The possible isotopic compositions found today in the lower mantle (UR), the depleted upper mantle (DR), and in the continental crust are shown in the graph.

If young basalts were derived from a mix of DR and UR reservoirs it could explain the $\epsilon_{\text{Nd}} - \epsilon_{\text{Sr}}$ correlation trend.

MODEL II

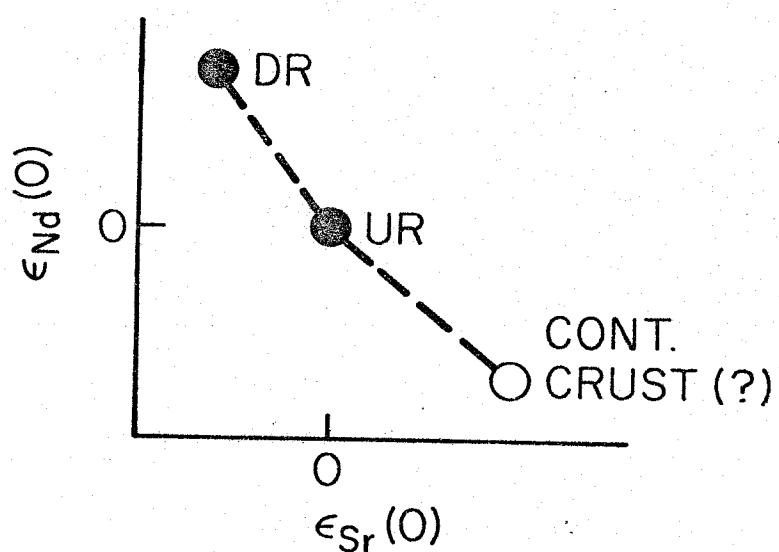
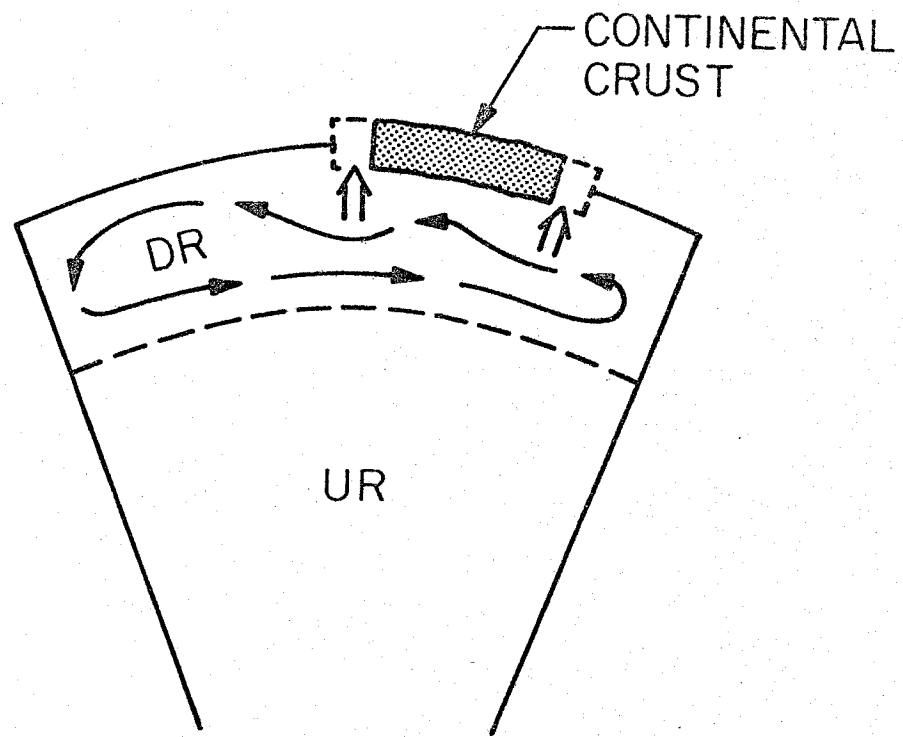


Fig. 26

lower mantle. The present-day composition of the depleted upper mantle (DR) and the unfractionated lower mantle (UR) are also shown in Figure 26. Note that in this model there is no mantle reservoir with $\epsilon_{\text{Nd}}(0) < 0$. Therefore, in this model, all rocks with $\epsilon_{\text{Nd}} < 0$ and $\epsilon_{\text{Sr}} > 0$ must result from crustal contamination.

Further implications of these two reservoir models will be discussed after the following section.

Spectrum of Reservoirs

The third possibility is that the correlation trend indicates the existence of not just two reservoirs but a continuous spectrum of reservoirs which have $\epsilon_{\text{Nd}}(0)$ and $\epsilon_{\text{Sr}}(0)$ lying all along the extent of the trend. The origin of such an array of reservoirs was discussed in an earlier section (cf., Figure 22).

Note that this model requires that each time a differentiation event takes place, the elements must be partitioned in a rigidly defined manner so that $f_{\text{Sm/Nd}}/f_{\text{Rb/Sr}}$ in every reservoir is the same. This implies a high degree of uniformity in the processes involved. If for instance partial melting and magma removal is the process responsible for these differentiation events, then a uniform percentage of melting and a specific residual mineralogy in all melting events is required. However, since there is considerable scatter about the correlation trend some variability in these parameters would be allowed. The requirement of constant ratios of enrichment factors in every differentiation event makes this model significantly different from Model II discussed previously for the

two-reservoir models. Model II does not require a specific fractionation of elements in every event, because the depleted reservoir is well mixed and its composition is just a function of the average fractionation factors.

If this correlation trend does describe the compositions of a spectrum of reservoirs which have arisen in the manner described here, then it implies that Rb/Sr and Sm/Nd are strictly covariant in the various reservoirs in the mantle. This would be somewhat surprising considering that Rb and Sr are geochemically much different from Sm and Nd. Rb is volatile and singly charged while Sr is refractory and occurs as a doubly-charged ion. In contrast Sm and Nd are both refractory and tri-positive and differ only in ionic radius. Thus since the relative distribution of Sm and Nd is almost entirely due to difference in ionic radius, the correlation suggests that the relative distribution of Rb and Sr in mantle reservoirs is also primarily due to difference in ionic radius. Volatility effects and minerals which strongly discriminate between Rb and Sr on the basis of charge must not be important in the formation of mantle reservoirs.

Further implications of $\epsilon_{\text{Nd}} - \epsilon_{\text{Sr}}$ correlation

From the preceding discussion it can be concluded that the $\epsilon_{\text{Sr}} - \epsilon_{\text{Nd}}$ correlation in young basalts does not result from crustal contamination and thus must be a fundamental property of the mantle reservoirs from which basaltic magmas are derived. The correlation trend thus provides information about when and how these reservoirs

formed.

The existence of the correlation leads to some interesting conclusions about the distribution of Rb in the earth. It has been suggested that relative to chondrites Rb is depleted in the earth's mantle due to its incorporation into the core (Lewis, 1971).

Variations of $^{87}\text{Sr}/^{86}\text{Sr}$ in the mantle today therefore could have resulted from variations of Rb/Sr which were produced as a result of incorporation of Rb in the core. Low Rb/Sr would be characteristic of those parts of the mantle which had lost the most Rb and high Rb/Sr would be found in parts of the mantle which had retained much of their Rb due to variability in the efficiency of the process.

However, such variations of Rb/Sr would not be accompanied by variations of Sm/Nd because neither Sm nor Nd would be expected to enter the core. This process, therefore, would not lead to a correlation between Nd and Sr isotopic variations. Thus the correlation indicates that the currently-existing variations of Rb/Sr in the mantle are not related to the core-formation process. This does not mean that Rb could not have entered the core. Rather it indicates that if it did enter the core, that after the process was complete the mantle was rehomogenized with a new, lower Rb/Sr and was subsequently affected only by differentiation events which changed both Rb/Sr and Sm/Nd.

Models for the accretion of the earth have been proposed in which the deepest parts of the earth are made up of refractory materials which condensed out of the solar nebula early at high temperatures

while the outer parts of the earth accreted from low-temperature volatile-rich material which condensed later (cf., Turekian and Clark, 1969). In this model one would expect low Rb/Sr in the early condensates and high Rb/Sr in the late additions. This model cannot produce significant differences in Sm/Nd since these elements are both refractory and will therefore enter all condensates in about the same proportions. Figure 27 shows the possible present-day compositions of early and late condensates on a graph of $\epsilon_{Nd}(0)$ versus $\epsilon_{Sr}(0)$. The early condensates are modelled after the basaltic achondrites (or their parent bodies) which are volatile-depleted and enriched in refractories while the late condensates are modelled after carbonaceous chondrites. Also shown is the field of ϵ_{Nd} and ϵ_{Sr} for the basalts making up the correlation trend as well as some individual samples with $\epsilon_{Nd} < 0$ and average continental crust. It is clear from this diagram that the $\epsilon_{Nd} - \epsilon_{Sr}$ patterns found in the earth's mantle today (represented by the basalts) are nothing like that expected from a mixture of early and late condensates shown by the solid line. This demonstrates that the present variations of Rb/Sr in the earth are not related to accretional heterogeneity. The rather narrow range of ϵ_{Sr} found in the young basalts at $\epsilon_{Nd} = 0$ also clearly shows that if the earth is a mixture of condensates with such disparate ϵ_{Sr} , a very thorough mixing of these components must have occurred. The relative proportions of early and late condensates necessary to make an earth with $\epsilon_{Sr} = 0$ can be readily calculated from the information in Figure 27 if the concentration of Sr in each component is known.

Figure 27: Graph of $\epsilon_{\text{Nd}}(0)$ and $\epsilon_{\text{Sr}}(0)$ in young basalts, average upper crust and in meteorites which may represent early and late condensates from the solar nebula. Fields for early and late condensates are approximate and are calculated from measured Rb/Sr and Sm/Nd ratios in achondrites and chondrites respectively. Isotopic variations in the earth's mantle, given by the young basalt trend, could not result from accretional heterogeneity if the earth is made of the two end members shown.

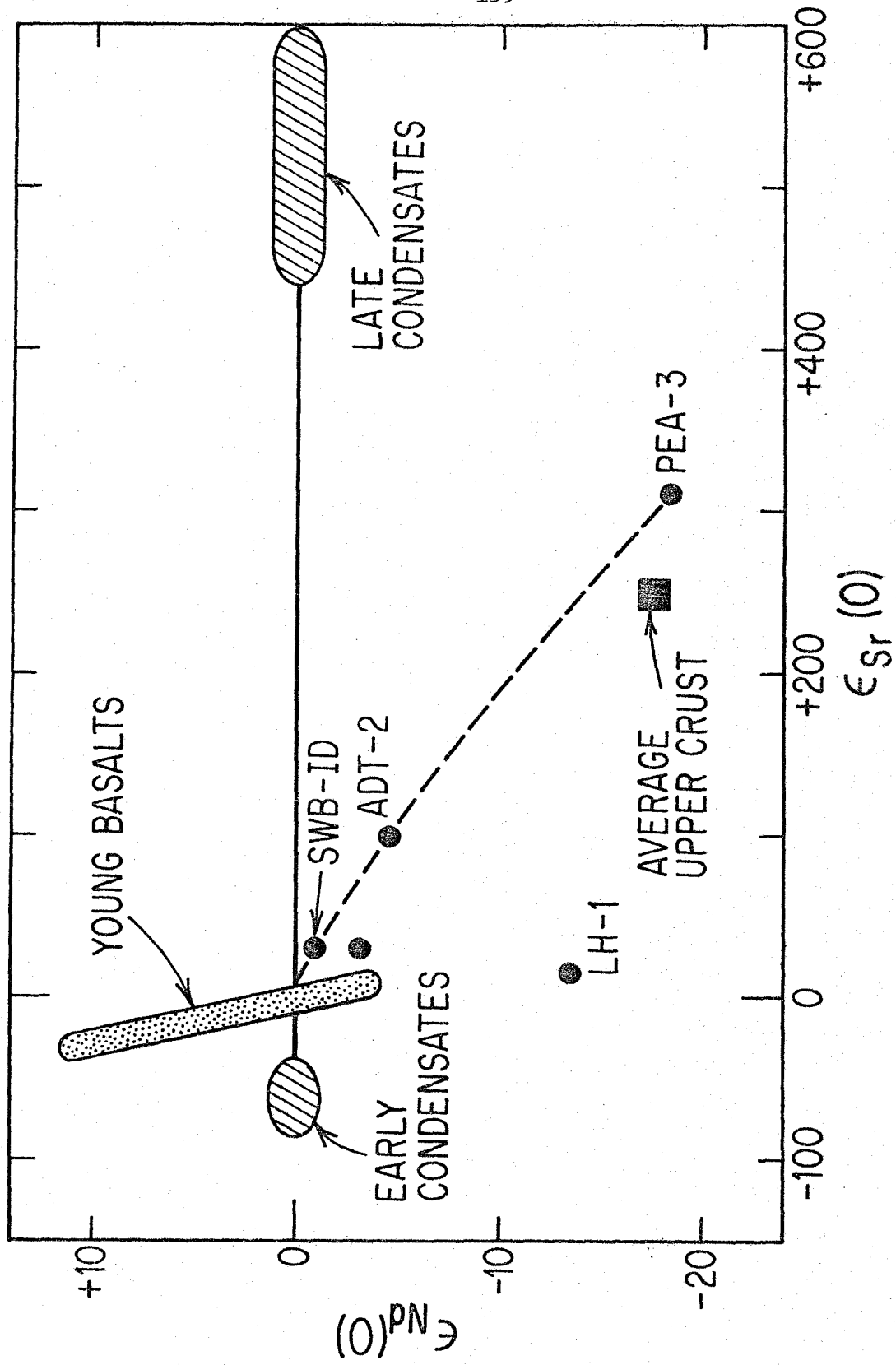


Fig. 27

The composition of the continental crust

The Rb/Sr ratio of the continental crust is an extremely important geochemical parameter which has been subject to considerable uncertainty due to lack of sufficient knowledge of the Rb content of the lower crust. The Rb content of the crust is important because it is an indicator of the amount of the heat-producing elements K, U, and Th which are in the crust. Knowledge of the concentrations of these elements in the crust is necessary to understand heat flow on the continents and for assessing how much of the earth's budget of these elements is still buried in the mantle and whether they contribute significantly to global heat flow or can drive convection cells in the mantle. The $\epsilon_{\text{Nd}} - \epsilon_{\text{Sr}}$ correlation may provide information on the Rb/Sr of the crust.

Consider a simple model of differentiation of the earth where an initially homogeneous reservoir differentiates into a series of complementary reservoirs A_i , B_i such as shown in Figure 22c. Today, the isotopic compositions of the reservoirs A_i lie along the line A-UR in Figure 22c and the reservoirs B_i lie along the line UR-B. Suppose that the reservoirs A_i are the mantle reservoirs from which young basalts are derived, and define the $\epsilon_{\text{Nd}} - \epsilon_{\text{Sr}}$ trend shown in Figure 19. The reservoirs B_i are segments of the continental crust. This would be a plausible explanation of the $\epsilon_{\text{Nd}} - \epsilon_{\text{Sr}}$ correlation since the continental crust is the only known high-Rb/Sr, low-Sm/Nd reservoir which could be the complement of the low-Rb/Sr, high-Sm/Nd reservoirs represented by the basalt data. If this model were

correct, the slope of the $\epsilon_{\text{Nd}} - \epsilon_{\text{Sr}}$ correlation trend would provide information on Rb/Sr, Sm/Nd, and Sr/Nd in the continental crust.

Model II (Figure 26) would lead to a similar conclusion.

The reservoirs A_i we will call depleted mantle (DM). From equation 28 and the relationships given in Figure 22c, the following relation can be derived:

$$(31) \quad \left(\frac{f_{\text{Sm/Nd}}}{f_{\text{Rb/Sr}}} \right)_{\text{crust}} = K \left(\frac{f_{\text{Sm/Nd}}}{f_{\text{Rb/Sr}}} \right)_{\text{DM}}$$

where $K = (\text{Sr/Nd})_{\text{crust}} / (\text{Sr/Nd})_{\text{DM}}$. From Figure 19, $(f_{\text{Sm/Nd}} / f_{\text{Rb/Sr}})_{\text{DM}} = 0.25$. The relationship between $(f_{\text{Sm/Nd}})_{\text{crust}}$ and $(f_{\text{Rb/Sr}})_{\text{crust}}$ derived for this model for different values of K is graphed in Figure 28. Since $f_{\text{Sm/Nd}}$ in most crustal rocks is fairly constant, the average $f_{\text{Sm/Nd}}$ of the crust can be estimated with some confidence. This is shown by the shaded region in Figure 28. Thus if we can set limits on K the $f_{\text{Rb/Sr}}$ of the crust can be inferred.

Table 5 gives the concentrations of Rb, Sr, Sm, and Nd in several recent estimates of the overall continental crust and the upper crust. Also given are the concentrations of these elements in an average chondrite. These estimates show a range of Sr/Nd in the crust from about 0.5 of the chondritic value up to about 1.5 times the chondritic value. Over the past fifteen years estimates of Rb and Nd in the crust have gradually decreased while estimates of the concentration of Sr have increased. The earlier estimates for the total crust are similar to the latest estimates for the upper crust. The upper crust estimates are based on considerable data. The total

Table 3: Recent estimates of the composition of continental crust

Author	Rb	Sr	Sm	Nd	$f_{Rb/Sr}$	$f_{Sm/Nd}$	Sr/Nd
Total Crust							
Vinogradov (1962)	150	340		37	+15.2		9.2
Taylor (1964)	90	375	6	28	+8.3	-0.33	13.4
Hurley (1968)	70	461			+5.2		
Ronov <u>et al.</u> (1972)			4	17		-0.27	
Taylor (1977)	50	400	3.7	16	+4.3	-0.28	26.6
Upper Crust							
Shaw <u>et al.</u> (1976)	110	316	4.5	26	+12.0	-0.46	12.2
Taylor (1977)	110	350	5.6	32	+10.8	-0.45	10.9
Chondrites	2.5	10	0.19	0.60	+7.6	0.000	16.7

crust estimates reflect different models for the composition of the lower crust, which is at present largely unknown. The latest total crust models have incorporated the hypotheses that (1) the granitic upper crust, which is rich in U, Th, and K, cannot extend to depths of more than about 10km and (2) the lower crust must be plagioclase-rich to offset the negative europium anomaly found in upper crustal rocks (cf., Taylor, 1977). Since plagioclase is rich in Sr but poor in Nd and Rb, the estimates of Rb/Sr and Nd/Sr in the crust have gradually decreased.

We do not know a priori what the ratio Sr/Nd is in the depleted mantle; however, since Sr and Nd are both refractory elements we can assume that Sr/Nd of undepleted mantle is the same as that of chondrites. Thus if Sr/Nd of the crust is greater than chondritic, then by material balance Sr/Nd of depleted mantle must be less than chondritic. Thus, for a given $(Sr/Nd)_{crust}$, K will depend on the relative amount of Nd now contained in the crust and the depleted mantle. As is discussed more in Chapter IX the crust probably contains no more than half the Nd in the system. Thus, for example, if the crust has Sr/Nd of 1.5 times chondritic then the depleted mantle must have Sr/Nd greater than 0.5 chondritic and vice versa. Therefore, the data in Table 5 imply that K must be between about 0.3 and 3. However, the model of Vinogradov (1962) can probably be ruled out, since recent estimates based on sediment abundances (Balashov and Tugarinov, 1976) indicate a crustal Nd abundance substantially less than 30ppm, and thus a higher Sr/Nd for the crust than he estimated. Thus it is most likely that K is greater than 0.5.

As shown in Figure 28, these estimates for K indicate that $f_{Rb/Sr}$ in the crust is less than three. This is considerably lower than any of the estimates in Table 5. The model of Taylor (1977) which has a high Sr/Nd in the crust implies a very low $f_{Rb/Sr}$ in crust (less than 1.0).

Thus the slope of the $\epsilon_{Nd} - \epsilon_{Sr}$ correlation is consistent with removal from the mantle of material with low $f_{Rb/Sr}$ in relation to $|f_{Sm/Nd}|$. If this removed material is the continental crust, then the crust must have a lower $f_{Rb/Sr}$ than estimated in crustal models in the literature. This would require that the crust have a highly layered structure, with elements such as K, Rb, U, Th, and Pb highly concentrated in the upper crust but depleted in the lower crust. The low $f_{Rb/Sr}$ calculated for the crust would be more consistent with a basaltic composition for the total crust than with a more silicic composition such as granodiorite. A basaltic major element composition for the crust has also been suggested by McGetchin and Silver (1972).

If it is assumed that the concentration of Sr in the earth is chondritic (~10ppm) and the earth has $Rb/Sr = 0.029$, an $f_{Rb/Sr}$ for the crust of 1.5 to 2.0 would imply that about 30 to 35% of the earth's Rb is in the crust. This estimate is at least a factor of two lower than previous estimates. The prohibitively high concentrations of Rb, U, and Ba calculated for the crust from previous crustal models (greater than 70% of earth's Rb in the crust) prompted suggestions that the earth might be enriched in Sr and other refractories relative to chondrites (cf., Ringwood, 1975). Thus the decrease in the proportion of Rb in the crust suggested here would remove the necessity for a terrestrial enrichment of refractory elements. Furthermore, if the concentrations of K, U, and Th in the crust were also proportionately less than previously estimated, it would mean that a substantially larger proportion of these heat-producing elements are still buried in the mantle than was previously thought.

Figure 28: Relationship between $f_{\text{Sm}/\text{Nd}}$ and $f_{\text{Rb}/\text{Sr}}$ of the continental crust implied by the assumption that the mantle reservoirs with correlated $\epsilon_{\text{Nd}}(0)$ and $\epsilon_{\text{Sr}}(0)$ (Figure 19) were depleted in Rb and Nd in the past due to loss of a melt fraction that went to form a segment of the continental crust. A low-Rb/Sr crust is implied by this model.

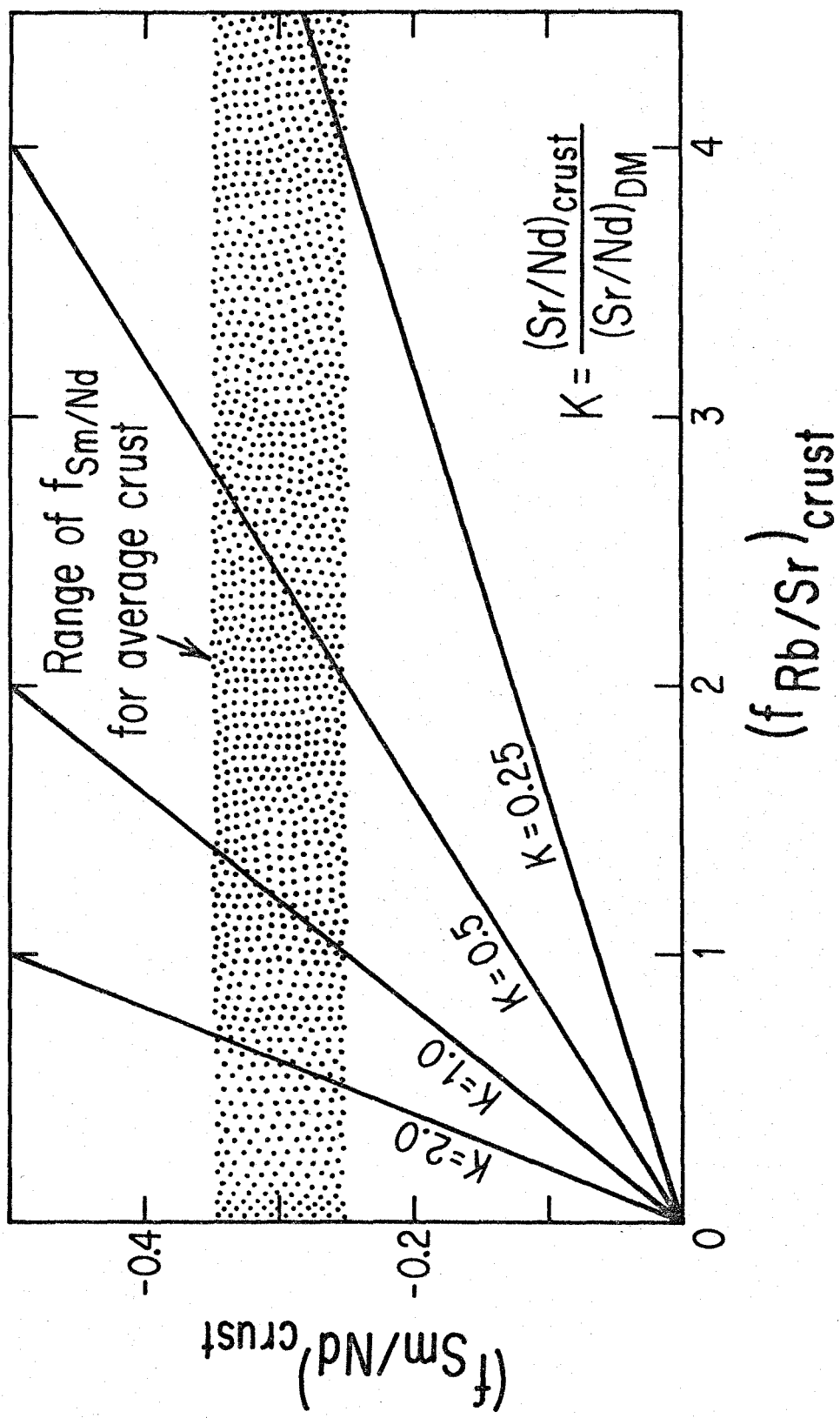


Fig. 28

IX. MANTLE-CRUST TRANSPORT MODELSBasic problems and assumptions

A basic question about the earth which has been difficult to answer is whether the earth as a whole is thoroughly differentiated and outgassed, or instead is only slightly differentiated and contains primitive material which is still representative of the bulk composition of the earth. This question is intimately related to the question of whether the earth is presently heating up due to the buildup of heat generated by the decay of radioactive isotopes or is cooling off due to loss of initial heat from accretional energy or rapid core formation. If the earth is heating up, much of the earth may never have been melted and thus much of the earth's volatiles and radioactive elements may still be buried deep in the mantle. On the other hand, if the earth is cooling off, then it must have been much hotter in the past and could have been at least partially molten throughout at one time. Such a fluid early earth might have been rapidly convecting and thus may have been thoroughly degassed and scavenged of its heat-producing elements, which became highly concentrated in the crust.

This discussion will be concerned with assessing (1) what proportion of the earth's budget of certain elements are presently residing in the crust, (2) whether these elements were extracted from the interior of the earth early in earth history or recently, and (3) whether they were extracted uniformly from the entire mantle or preferentially from some parts of the mantle (e.g., the upper

mantle) leaving other parts of the mantle undifferentiated. In theory, every radioactive parent-daughter pair provides a tool for assessing these problems. The parameters which need to be known in order to interpret the isotopic data are the masses of the earth's crust, mantle and core, the concentration of the daughter element in each, and the parent/daughter ratio for the bulk earth and each of the three reservoirs. If these parameters were known it would be possible to model the evolution of the crust, mantle and core and compare the resulting isotopic patterns with those which can be observed in the crust and upper mantle.

The Sm-Nd isotopic system is particularly valuable for studying the differentiation of the silicate portion of the earth. This is because 1) we can make a good estimate of Sm/Nd in the bulk earth based on meteorite abundances and the data presented earlier and 2) we expect these lithophile elements to be totally excluded from the core so that the silicate portion of the earth contains the total earth budget of Sm and Nd. In contrast, similar estimates of the bulk earth Rb/Sr and U/Pb ratios have been nearly impossible to make due to the possibility that Rb and Pb were lost through volatilization during accretion. Estimates of Rb/Sr and U/Pb in the silicate portion of the earth, i.e., the mantle-crust system, have also been hampered by the possible loss of Pb (and possibly Rb) to the core. Thus these other systems may be useful for studying accretion and core formation (cf., Gancarz and Wasserburg, 1977), but the Sm-Nd system provides the first opportunity to model the evolution of the crust-mantle system independent of complications introduced by parent-

daughter fractionation during accretion and core-formation.

Thus, in the following discussion the core will be essentially ignored. The silicate portion of the earth will be considered to have evolved independently of core formation as far as the rare-earth elements are concerned. It is therefore assumed that the initial state of the earth is a core containing no REE surrounded by a homogeneous mantle which has chondritic REE relative abundances. The final state is a crust and mantle of known present-day masses. The abundances of Sm and Nd in the crust can be estimated (cf., Table 3). The absolute abundances of Sm and Nd in the silicate portion of the earth are subject to considerable uncertainty. A lower limit would probably be the chondritic abundances adjusted for the fractional mass of the earth contained in the core, or $\sim 1.5 \times$ chondritic concentrations. An upper limit for refractories is provided by the concentrations of U and Th calculated from present heat flow ($\sim 3.75 \times$ chondritic, Wasserburg *et al.*, 1964) which gives $\sim 5 \times$ chondritic in the silicate portion. For the models considered here the lowest concentrations (1.5x chondritic) will be assumed for the silicate portion.

Table 6 gives the masses of the silicate reservoirs in the earth which will be used in the modelling. The concentrations of Sm, Nd, Rb, Sr in each reservoir are also given. The Rb and Sr abundances for the crust are taken from Taylor (1977). These are not directly used in any calculations but rather are left as adjustable parameters which

may be evaluated in a manner similar to that discussed in Chapter VIII. The Sm and Nd concentrations in the crust are compromises from Table 5. Note that even assuming the lower limit Nd concentration in the mantle, the crust contains only about 11% of the total earth budget of Nd and a similar fraction of the Sr. Only Rb appears highly depleted in the mantle (50% in the crust), but as discussed in Chapter VIII, this could be due to overestimation of the concentration of Rb in the crust. Comparison of columns 1 and 2 in Table 6 shows that the amount of Nd and Sr in the crust is large compared to that originally held in the upper 400 km of the mantle. Therefore, if the continental crust were extracted entirely from the upper mantle, the upper mantle would now be depleted of about 70% of its Sr and Nd. According to the Taylor (1977) model, the upper mantle did not contain enough Rb to make the crust. It is the purpose of this chapter to evaluate what magnitude variations of $\epsilon_{Nd}(0)$ would be expected in the crust and mantle today due to the extraction of the crust from the mantle and compare them to the observed variations. The $\epsilon_{Nd}(0)$ variations will depend on when the crust was formed and whether the crust was extracted uniformly from the entire mantle or from only a small part of the mantle.

Discrete differentiation event

Assume first that the crust was formed during a single differentiation event T_f years ago. Using the concentrations of Sm and Nd and the reservoir masses given in Table 4 we can calculate the evolution of ϵ_{Nd} in the crust and the mantle after the

Table 4: Crust and Mantle compositions

	Continental Crust	Upper Mantle ^a to 400 km depth	Total ^a Mantle	Chondrite
Mass (10^{25} g)	1.8	62	407	
Sm (ppm)	4.7	.288	.288	.192
Nd (ppm)	22.5	.900	.900	.600
Rb (ppm)	b	.44	.44	2.5
Sr (ppm)	b	15	15	10
$f_{\text{Sm}/\text{Nd}}$	-0.35	0.0	0.0	0.0
$f_{\text{Rb}/\text{Sr}}$	b	0.0	0.0	+7.62

^a Compositions prior to formation of crust.

^b These parameters are evaluated in the discussion in the text.

differentiation. Suppose first that the material in the crust was extracted uniformly from the entire mantle. The evolution of ϵ_{Nd} in the crust and mantle for this case is shown in Figure 29 for $T_f = 4.5$ and 1.5 AE. This figure shows that if the entire mantle was scavenged for the creation of continental crust, then $\epsilon_{\text{Nd}}(0)$ of the mantle would be about +5 if the crust formed 4.5 AE ago. If the crust formed later, then the $\epsilon_{\text{Nd}}(0)$ of the mantle would be closer to zero. For $T_f = 1.5$ AE, which may approximate the mean age of the continents, the $\epsilon_{\text{Nd}}(0)$ of the mantle would be essentially indistinguishable from zero. The $\epsilon_{\text{Nd}}(0)$ values for the total mantle would be even closer to zero if the earth has refractory element abundances which are greater than chondritic.

The dashed lines in Figure 29 show the evolution of ϵ_{Nd} in the upper mantle if the crust were extracted only from the upper mantle leaving the remainder of the mantle undifferentiated. Extraction of the crust from the upper 400 km of the mantle would deplete the upper mantle of 70% of its Nd and 45% of its Sm. As shown in Figure 29 this would result in large positive values of $\epsilon_{\text{Nd}}(0)$ in the upper mantle. Again, higher concentrations of Sm and Nd in the earth would result in smaller values of $\epsilon_{\text{Nd}}(0)$ in the upper mantle.

These simple calculations show that the amount of Sm and Nd removed from the mantle during formation of the continental crust could not significantly affect the $\epsilon_{\text{Nd}}(0)$ of the mantle as a whole unless the crust is very old. If the crust is about 1.5 AE old then the $\epsilon_{\text{Nd}}(0)$ of the bulk mantle must be between 0 and +2 depending on its initial concentration of refractory elements.

Figure 29: The evolution of $\varepsilon_{\text{Nd}}(T)$ in the crust and mantle if the crust were differentiated from the mantle in a single event at (a) 4.5 AE ago and (b) 1.5 AE. The dashed lines give $\varepsilon_{\text{Nd}}(T)$ in the upper mantle (to 400km depth) for the case that the crust is derived wholly from the upper mantle leaving the lower mantle undifferentiated.

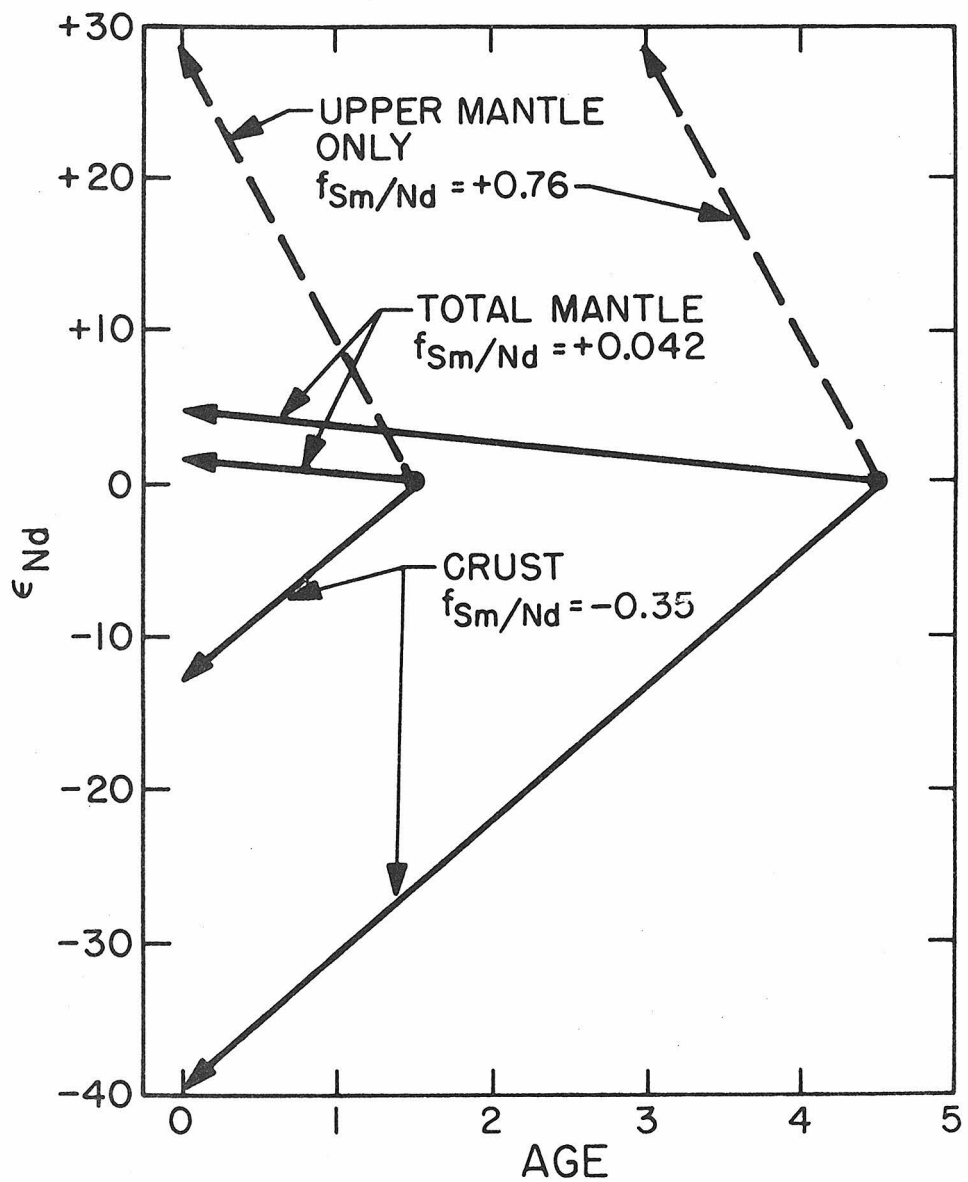


Fig. 29

These calculations can help estimate the relative masses of reservoirs which have been identified to exist in the mantle on the basis of the variations of ϵ_{Nd} in young basalts.

If the mantle is composed of a series of reservoirs with masses M_i and $\epsilon_{Nd}(0)_i = \epsilon_{Nd}(0)_m$ we have that:

$$(32) \quad \frac{1}{[Nd]_m M_m} \sum_i M_i [Nd]_i \epsilon_{Nd}(0)_i = \epsilon_{Nd}(0)_m$$

where $[Nd]_i$ is the concentration of Nd in i , $\epsilon_{Nd}(0)_m$ is that of the bulk mantle, and M_m is the mass of the mantle. From the above calculation we have $\epsilon_{Nd}(0)_m = +5.0$ for $T_f = 4.5$ AE and $\epsilon_{Nd}(0)_m = +1.7$ for $T_f = 1.5$ AE.

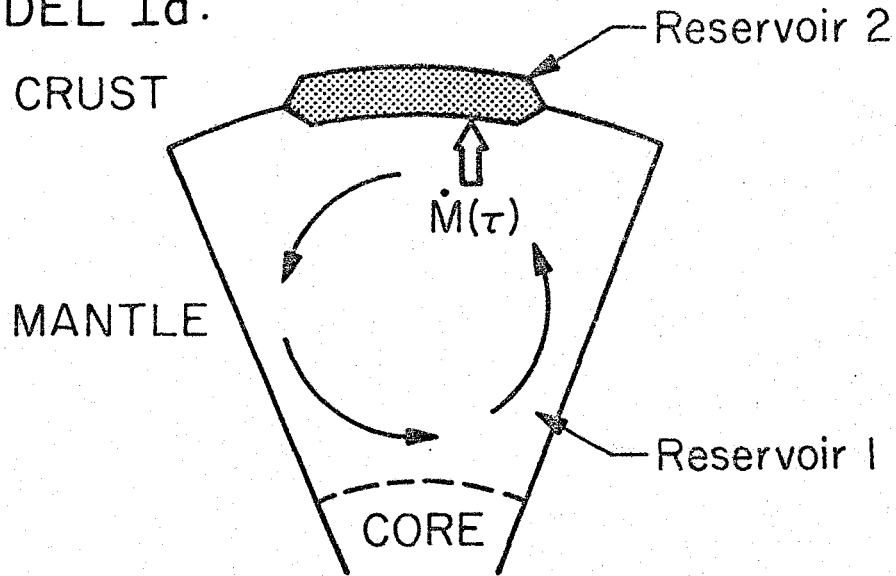
Let us assume that there are only three reservoirs: (1) that of the MOR basalts (MORR, $\epsilon_{Nd} = +10$), (2) that of the ocean island basalts OIR ($\epsilon_{Nd} = +6$), and (3) CHUR ($\epsilon_{Nd} = 0$) and that the concentration of Nd in each is roughly equal. Thus for $T_f = 4.5$ AE we find that the maximum mass of MORR (obtained when $M_{OIR} \approx 0$) is $0.5M_m$ and the maximum mass of OIR is $0.83M_m$. For $T_f = 1.5$ AE, the maximum mass of MORR is $0.17M_m$ and the maximum mass of OIR is $0.28M_m$. Thus we find that CHUR and OIR could comprise most of the mantle but MORR could not. If the earth contained Nd in abundance higher than chondritic, the $\epsilon_{Nd}(0)_m$ would be lowered and the estimates for the masses of MORR and OIR would be decreased.

Continuous transport models

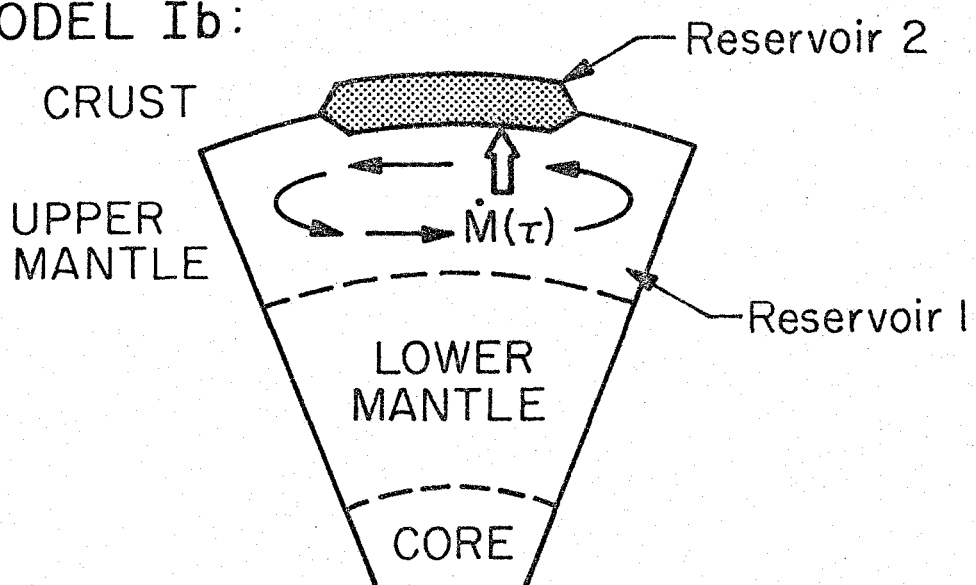
Models in which the crust is built gradually throughout the 4.5 AE history of the earth are considered next. These models are illustrated in Figure 30. In Model Ia, the crust is extracted from the entire mantle, which always remains well-mixed and homogeneous as indicated by the arrows. In Model Ib the crust is

Figure 30: Model for continuous growth of continental crust by differentiation from the mantle. The accretion rate of the continent is $\dot{M}(\tau)$. In Model Ia the entire mantle remains a well-mixed homogeneous reservoir. In Model Ib crustal material is taken only from the upper mantle, which remains well-mixed but totally isolated from the lower mantle.

MODEL Ia:



MODEL Ib:



mass of reservoir 2:

$$M_2(\tau) = \int_0^\tau \dot{M}(t) dt$$

Fig. 30

extracted from only the upper mantle, which is well mixed but completely isolated from the lower mantle. In each model, mass is added to the crust at a rate $\dot{M}(\tau)$. An increment of matter dM which is added to the crust at time τ is enriched in Sm and Nd by factors of D_{Sm}^* and D_{Nd}^* respectively over the concentrations in the mantle at time τ . The reservoir which is being depleted to form the crust will be called Reservoir 1 and the crust will be called Reservoir 2. If $M_1(\tau)$ is the mass of Reservoir 1, then the change of concentration of a stable nuclide i in Reservoir 1 ($C_i^1(\tau)$) is given by:

$$(33) \quad \frac{dC_i^1(\tau)}{d\tau} = - \frac{\dot{M}(\tau)}{M_1(\tau)} C_i^1(\tau) (D_i^* - 1)$$

where D_i^* is the enrichment factor for element i . The equation describing the concentration of a radioactive nuclide j is:

$$(34) \quad \frac{dC_j^1(\tau)}{d\tau} = - \left[\frac{\dot{M}(\tau)}{M_1(\tau)} (D_j^* - 1) + \lambda_j \right] C_j^1(\tau)$$

The concentration of a radiogenic nuclide i^* (daughter of j) is given by:

$$(35) \quad \frac{dC_{i^*}^1(\tau)}{d\tau} = - \frac{\dot{M}(\tau)}{M_1(\tau)} (D_i^* - 1) C_{i^*}^1(\tau) + \lambda_j C_j^1(\tau)$$

The concentrations of the elements in Reservoir 2 can be found by difference.

The rate of production of crust $\dot{M}(\tau)$ could have a variety of forms. Three plausible forms of $\dot{M}(\tau)$ could be:

$$1) \dot{M}(\tau) = \dot{M}_0 e^{-\lambda\tau}$$

$$2) \dot{M}(\tau) = \frac{\dot{M}}{2} (1 + \sin \omega\tau)$$

$$3) \dot{M}(\tau) = \dot{M}$$

Form 1 would reflect the decrease in the earth's heat productivity with time. Form 2 would reflect episodicity in crust formation as is suggested by some geochronological data. Form 3 would be a constant rate of crust production with time. For the calculations done here the simplifying assumption was made that $\dot{M}(\tau)/M_1(\tau)$ is a constant. Since M_1 changes little for the examples here, this is essentially the same as $\dot{M}(\tau) = \text{constant}$. Thus each element has an effective transport coefficient K_i given by:

$$(36) \quad K_i = \frac{\dot{M}}{M_1} (D_i^* - 1).$$

The resulting equations for $f_{\text{Sm}/\text{Nd}}(\tau)$ and $\varepsilon_{\text{Nd}}(\tau)$ in Reservoirs 1 and 2 are given in Table 5. Inspection of this table shows that $f_{\text{Sm}/\text{Nd}}^1(\tau)$ and $\varepsilon_{\text{Nd}}^1(\tau)$ are functions only of τ and the parameter $(K_{\text{Sm}} - K_{\text{Nd}})$. This model is identical to that discussed by Wasserburg (1966) for U-Pb.

The evolution of $f_{\text{Sm}/\text{Nd}}$ and ε_{Nd} in the mantle and average crust is shown in Figure 31 for Model Ia and in Figure 32 for Model Ib.

Also given on these figures are the values used for D_{Sm}^* , D_{Nd}^* and

\dot{M}/M_1 . \dot{M}/M_1 is a function of the masses of Reservoirs 1 and 2 as shown in Equation 5 in Table 5. D_{Sm}^* and D_{Nd}^* were chosen so as to produce the concentrations in the crust given in Table 4 from those assumed for the mantle, also given in Table 4. As shown in Figure 31, if the entire mantle is involved in the production of the crust, the evolution of ϵ_{Nd} in the mantle will be essentially indistinguishable from that of CHUR. Figure 31 also shows that $f_{Sm/Nd}$ of material added to the crust will be essentially constant with time. Figure 32 shows that, as deduced earlier from the simpler model, if the crust is extracted from a limited volume of mantle, in this case a volume of about 1/7 of the total mantle, the $f_{Sm/Nd}$ of that limited volume will be strongly affected by the removal of the crustal material and that part of the mantle will evolve a substantial positive ϵ_{Nd} .

As a result of this change in $f_{Sm/Nd}$ in the mantle through time, $f_{Sm/Nd}$ of new crustal additions will change quite drastically with time. Thus in this model, modern additions to the crust would have $f_{Sm/Nd} = -0.20$ compared to $f_{Sm/Nd} = -0.36$ in 3.6 AE old crust.

For this model we get $\epsilon_{Nd}(0)_m \approx +2$. From equation 32 the maximum mass of MORR is calculated to be $0.2M_m$ and that of OIR is $0.33M_m$.

For Model 1 we can also calculate the evolution of ϵ_{Sr} in the crust and mantle. We assume again that undepleted mantle material has $\epsilon_{Sr}(0) = 0$ ($^{87}Sr/^{86}Sr = 0.7045$). If we constrain the depleted mantle to have $\epsilon_{Sr}(0)$ and $\epsilon_{Nd}(0)$ lying on the correlation line (Figure 19) then we have the condition that:

Table 5: Summary of equations for Model I

$$1) f_{Sm/Nd}^1(\tau)^* = e^{(K_{Nd} - K_{Sm})\tau} - 1$$

$$2) f_{Sm/Nd}^2(\tau) = \left(\frac{\frac{\dot{M}}{M_1} D_{Sm} \tau}{1 - e^{-\frac{\dot{M}}{M_1} D_{Nd} \tau}} \right) - 1$$

$$3) \epsilon_{Nd}^1(\tau) = Q_{Nd} \left[\frac{e^{-\lambda_{Sm} \tau} - 1}{\lambda_{Sm}} - \frac{e^{-(K_{Sm} - K_{Nd} + \lambda_{Sm})\tau} - 1}{K_{Sm} - K_{Nd} + \lambda_{Sm}} \right]$$

$$4) \epsilon_{Nd}^2(\tau) = \frac{\epsilon_{Nd}^1(\tau)}{\frac{\dot{M}}{M_1} D_{Nd} \tau}$$

$$5) \frac{\dot{M}}{M_1} = \frac{-\ln \left(\frac{1 - M_2(\tau)}{M_1(0)} \right)}{\tau}$$

* $\tau = 0$ at 4.5 AE ago and increases to 4.5 AE today.

Figure 31: ϵ_{Nd} and $f_{Sm/Nd}$ as functions of time for the mantle and overall crust for Model Ia.

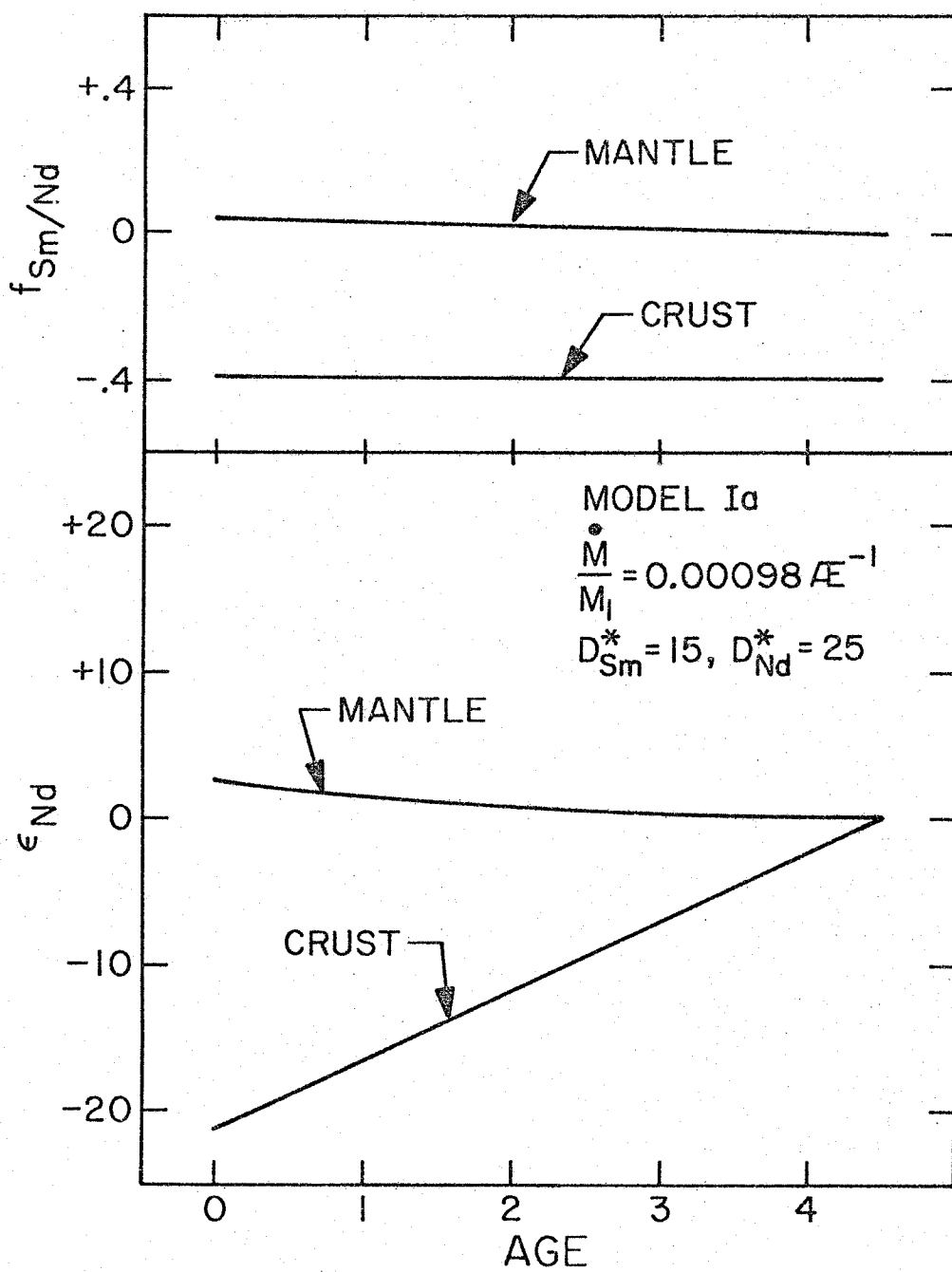


Fig. 31

Figure 32: ϵ_{Nd} and $f_{\text{Sm/Nd}}$ as functions of time for the overall crust, the upper mantle, and the lower mantle for Model Ib.

$f_{\text{Sm/Nd}}$ of new additions to the continental crust is also shown. ϵ_{Nd} of a new addition to the crust will be the same as that of the upper mantle. For example, ϵ_{Nd} of 3.6AE old crust would be +1 while ϵ_{Nd} of zero age crust would be +17.

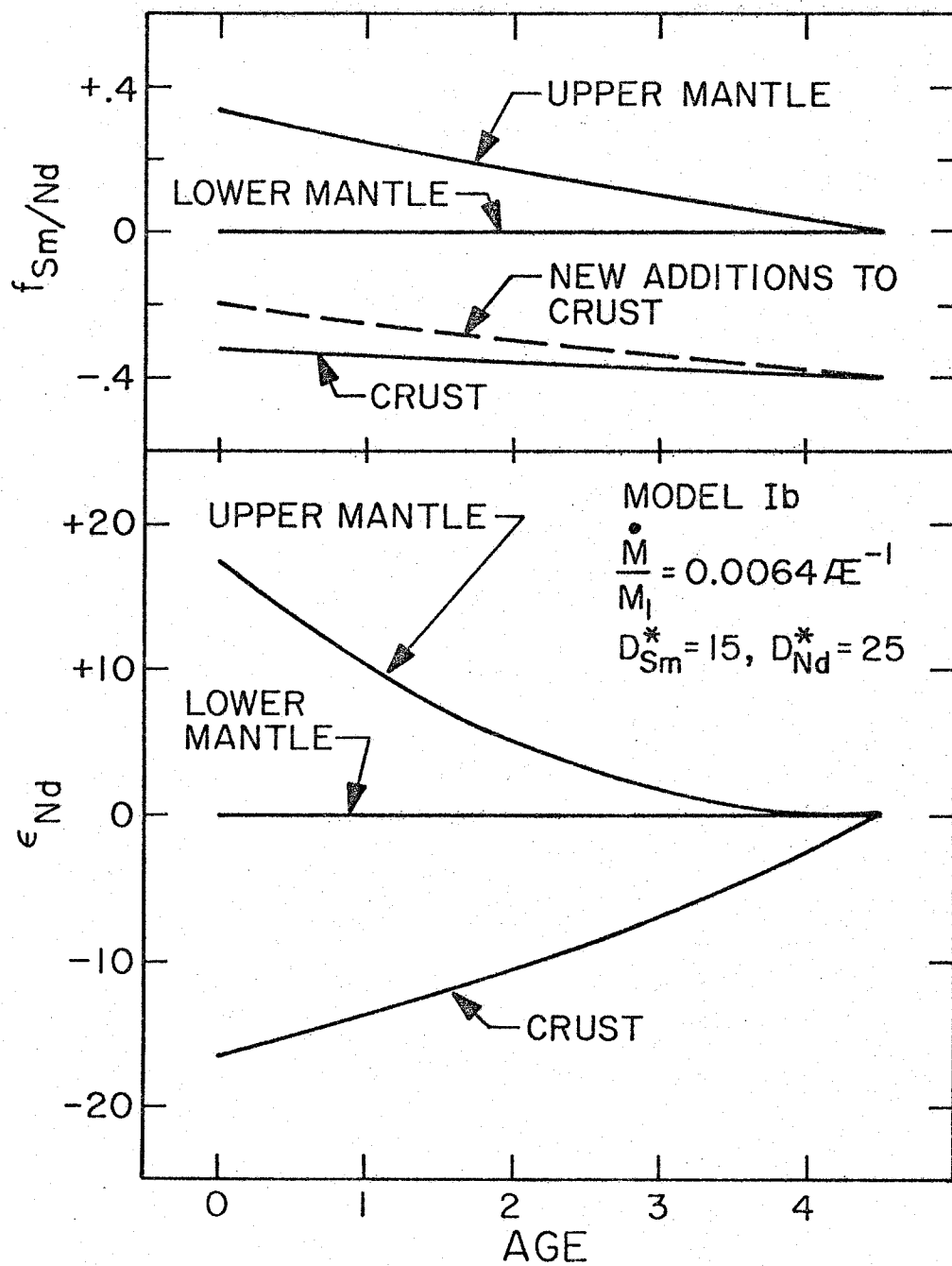


Fig. 32

$$(37) \quad - \frac{D_{Sm}^* - D_{Nd}^*}{D_{Rb}^* - D_{Sr}^*} = 0.16$$

For Model Ib we had $D_{Sm}^* - D_{Nd}^* = -10$ which gives $D_{Rb}^* - D_{Sr}^* = 62.5$.

The only parameter which remains to be specified is D_{Sr}^* . We will

consider three possible cases which are analogous to the three cases

shown in Figure 26. These are 1) $D_{Sr}^* = D_{Nd}^*$, 2) $D_{Sr}^* = 0.5 D_{Nd}^*$

and 3) $D_{Sr}^* = 2D_{Nd}^*$. These are equivalent to $K = 1$, $K = 0.5$ and

$K = 2.0$ respectively (cf., Figure 28).

The evolution of $f_{Rb/Sr}$ and ϵ_{Sr} in the mantle and average crust is shown in Figure 33 for Model Ia and in Figure 34 for Model Ib. For each model three curves are given for the crust, which corresponds to the three choices for D_{Sr}^* given above, and one curve is shown for the mantle since its $f_{Rb/Sr}(\tau)$ and $\epsilon_{Sr}(\tau)$ are functions of $\frac{M}{M_0} (D_{Rb}^* - D_{Sr}^*)$ only. For Model Ia we see that extraction of the crust causes modest changes in $f_{Rb/Sr}$ and ϵ_{Sr} in the mantle. We also see that $f_{Rb/Sr}$ of the crust depends on D_{Sr}^* and therefore on (Sr/Nd) in the crust as discussed earlier. For Model Ia $f_{Rb/Sr}$ in the crust is essentially constant through time. For Model Ib Figure 32 shows that $f_{Rb/Sr}$ and ϵ_{Nd} in the upper mantle are drastically affected by removal of crustal material. In this model the upper mantle would be depleted of over 90% of its Rb and its present-day Rb/Sr would be about 0.005. For Model Ib the present-day $f_{Rb/Sr}$ of the crust is fairly low for all three values of D_{Sr}^* and will not be greater than 1.0 unless $D_{Sr}^* < 25$, i.e., unless Sr/Nd in crust is substantially lower than chondritic. The reason for the low $f_{Rb/Sr}$ of the crust is

Figure 33: ϵ_{Sr} and $f_{\text{Rb/Sr}}$ for the overall continental crust and the mantle as functions of time for Model 1a. Three curves are shown for the crust, corresponding to different values of D_{Sr}^* .

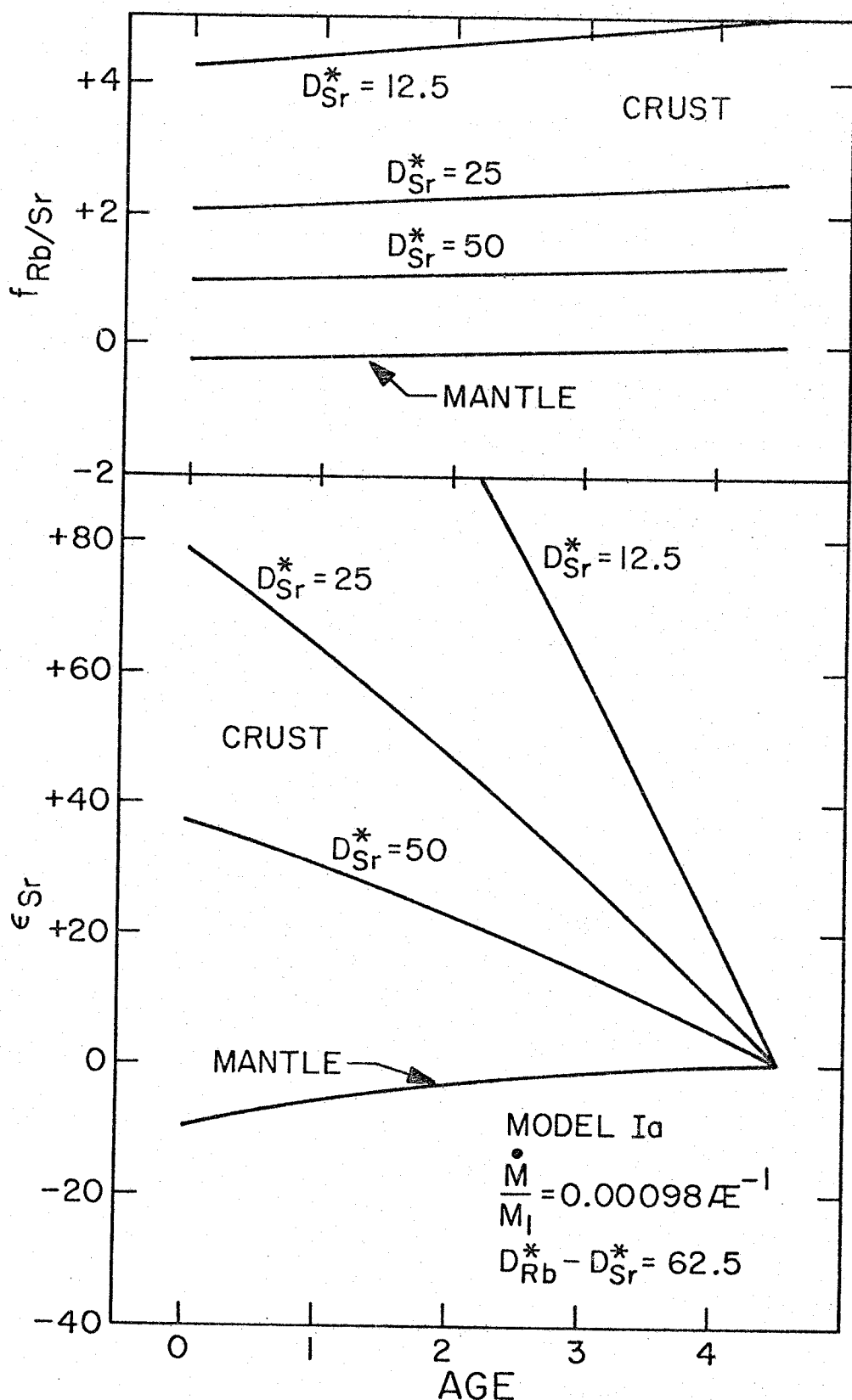


Fig. 33

Figure 34: ϵ_{Sr} and $f_{\text{Rb/Sr}}$ for the overall continental crust, the upper mantle, and the lower mantle as functions of time for Model Ib. Again, three curves are shown for the crust corresponding to different values of D_{Sr}^* . The dashed line shows $f_{\text{Rb/Sr}}$ of new additions to the continental crust for $D_{\text{Sr}}^* = 25$. Note that in this model the upper mantle loses most of its Rb so that its present Rb/Sr is close to zero.

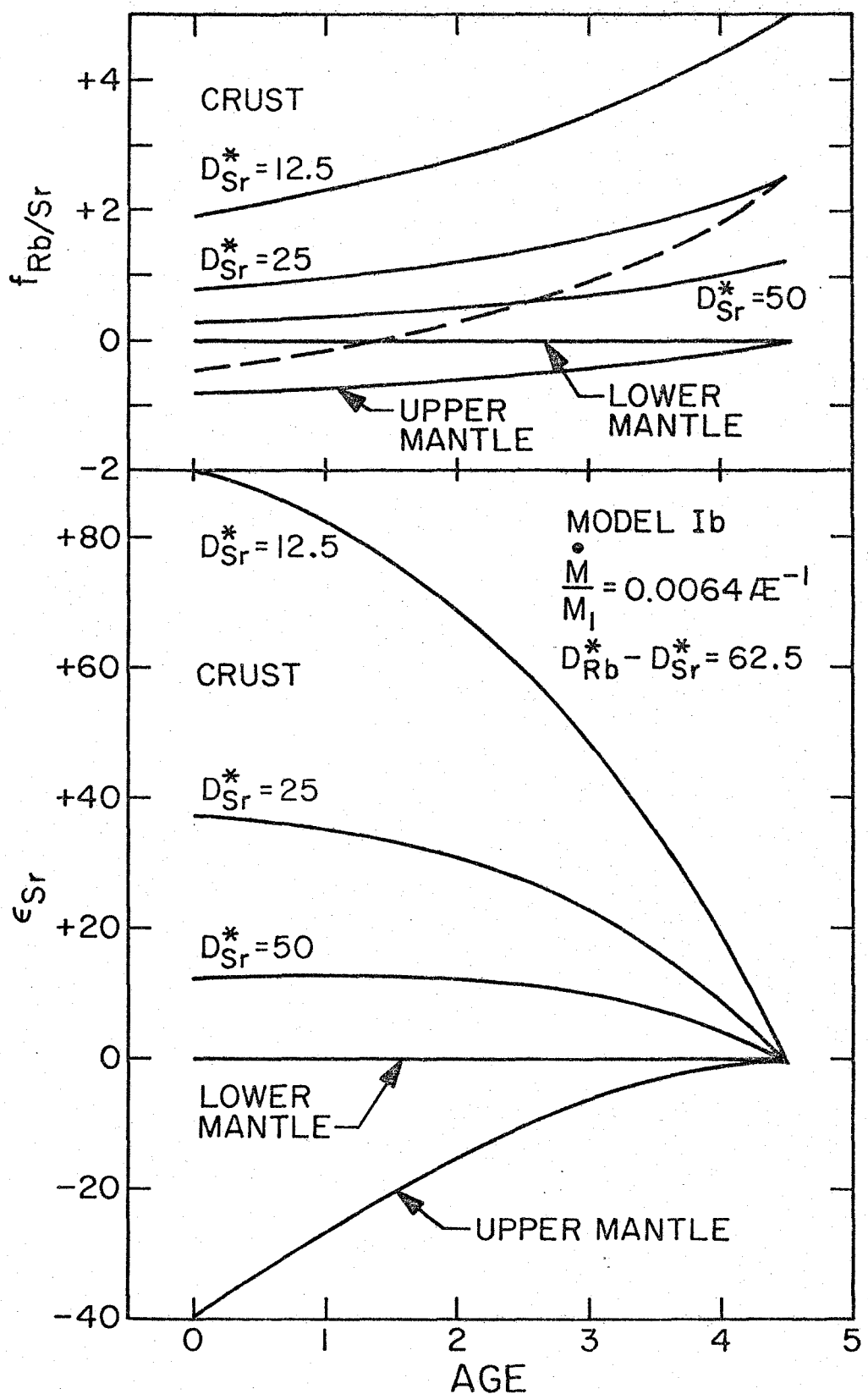


Fig. 34

that the mantle rapidly becomes depleted in Rb so that the later additions to the crust have low $f_{\text{Rb/Sr}}$. The $f_{\text{Rb/Sr}}$ of new additions to the crust as a function of time is shown by the dashed line in Figure 34. Young additions to the crust actually have $f_{\text{Rb/Sr}} < 0$.

The models discussed so far consider the mantle as being a homogeneous unit, implying that the mantle as a whole remains well-mixed. Other models could also be constructed which consider what would result if there were no mixing in the mantle. It could be assumed that after a given mass of mantle has been depleted in its crustal components it thereafter remains isolated from the remainder of the mantle. Such a model is depicted in Figure 35. In this model there is transport of matter from the mantle to the crust at a rate $\dot{M}(\tau)$ as in the previous model. The first increment of mass dM_1 extracted from the mantle to form the crust is extracted from a layer of mantle extending from a depth of zero to a depth Z_1 . The next increment of mass added to the crust is extracted from a mantle layer between depths Z_1 and $Z_1 + dZ$. In this model the crustal material is always derived from primitive undepleted mantle. Thus, as the crust grows by an increment of mass dM the thickness of the "depleted" outer part of the mantle is extended downward by a distance dZ . We will assume further that the material transported upward to form the crust is partially melted from the mantle and that each increment of matter dM added to the crust is an m weight percent partial melt of the mantle. The thickness ($Z(\tau)$) of the

Figure 35: Alternative model for continuous generation of continental crust by differentiation of the mantle. In this model the mantle is stagnant, and no mixing occurs in the mantle on any scale. The accretion rate of the crust is $\dot{M}(\tau)$. Each time material is added to the crust, it is derived from a layer of previously undifferentiated mantle (MANTLE_a), just below the lower boundary of the previously depleted mantle (MANTLE_b). Thus the addition of an increment of mass dM to the crust results in a thickening of the depleted mantle layer by an amount dz .

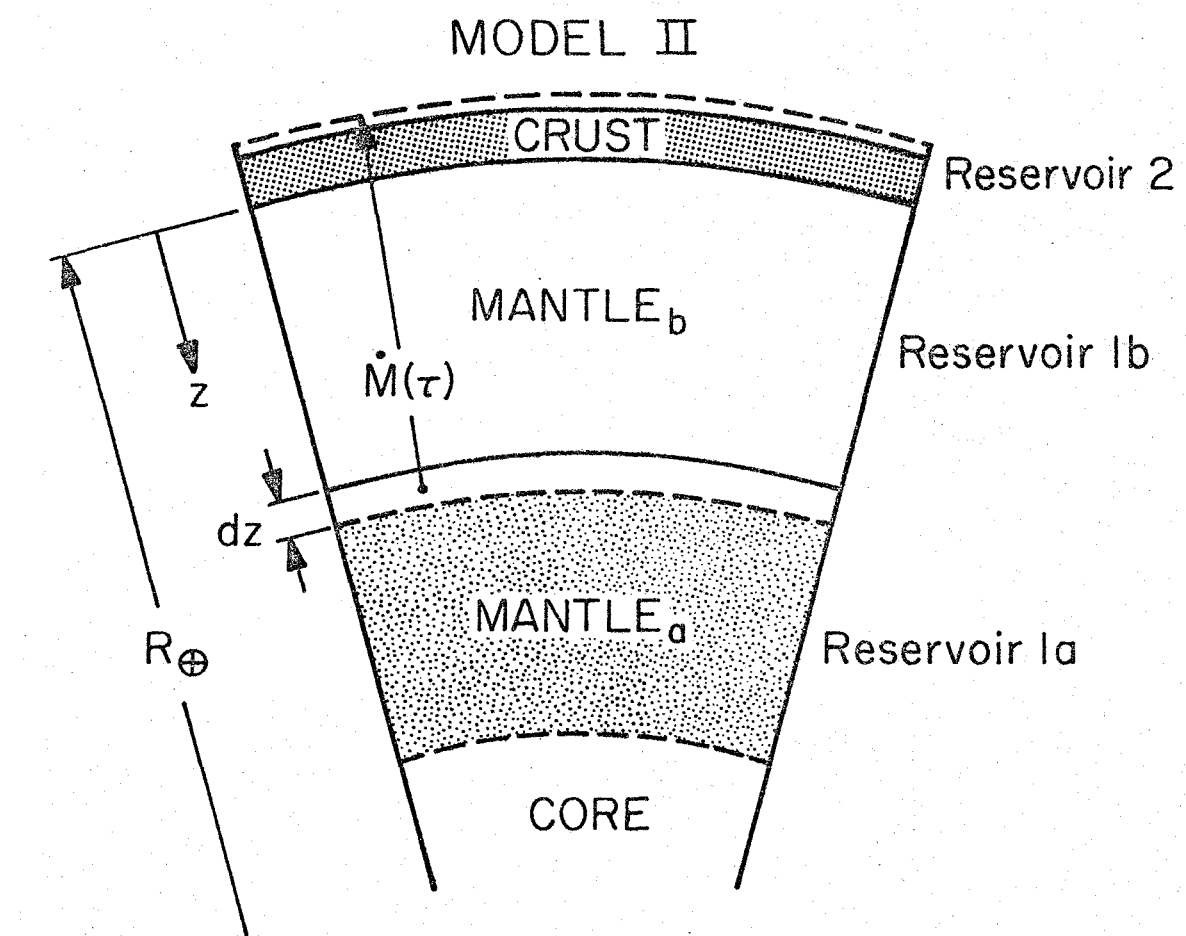


Fig. 35

depleted mantle (Reservoir 1b) is related to the mass $M_2(\tau)$ of the crust (Reservoir 2) by the relation:

$$(38) \quad Z(\tau) = R_\oplus - \left[R_\oplus^3 - \frac{(3(100-m) M_2(\tau))}{4\pi\rho_M m} \right]^{1/3}$$

where R_\oplus is the radius of the earth and ρ_M is the density of the mantle. The concentration of an element i in the crust is given by:

$$(39) \quad c_i^2 = c_i^{1a} / \left[\frac{1}{D_i} + \frac{m}{100} \left(1 - \frac{1}{D_i} \right) \right] .$$

where c_i^{1a} is the concentration of i in the undepleted mantle (Reservoir 1a) and D_i is the liquid/solid distribution coefficient.

The concentration of element i in the depleted mantle is:

$$(40) \quad c_i^{1b} = c_i^{1a} / \left[1 + \frac{m}{100} (D_i - 1) \right] .$$

Figure 34 shows $Z(\tau)$ and profiles of present-day $f_{\text{Sm}/\text{Nd}}$ and $\epsilon_{\text{Nd}}(0)$ in the mantle as a function of depth for two cases where $\dot{M}(\tau) =$ constant. The first case is $m = 0.015$ with $D_{\text{Sm}} = 25$ and $D_{\text{Nd}} = 50$ and the second case is $m = 0.005$ with $D_{\text{Sm}} = 18$ and $D_{\text{Nd}} = 30$. The values of m are arbitrary. D_{Sm} and D_{Nd} were chosen so as to give reasonable concentrations of Sm and Nd in the crust (Table 4). This model is much different from the models considered earlier in that while the mantle contains only two chemically distinct domains, $\epsilon_{\text{Nd}}(0)$ of the mantle is a continuous function of depth. Since $f_{\text{Sm}/\text{Nd}}$ is the same in all layers of depleted mantle, the $\epsilon_{\text{Nd}}(0)$ of a layer is just proportional to the time elapsed since it became

Figure 36: Thickness of depleted layer as a function of time, and the present-day $f_{\text{Sm}/\text{Nd}}$ and ε_{Nd} of the mantle as a function of depth for Model II (Figure 33). Two cases are shown, one for the fraction of partial melting $m = 1.5\%$ and one for $m = 0.5\%$.

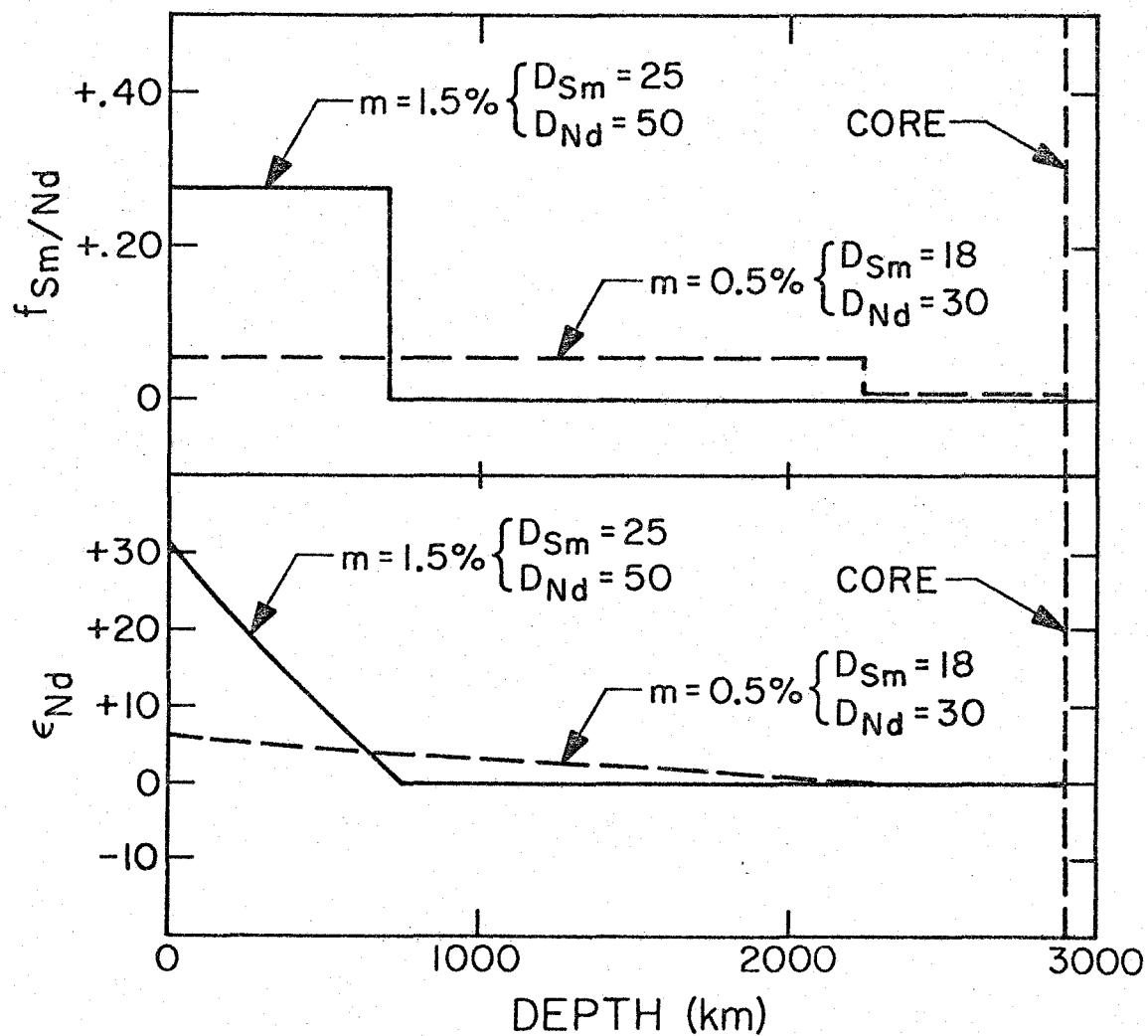
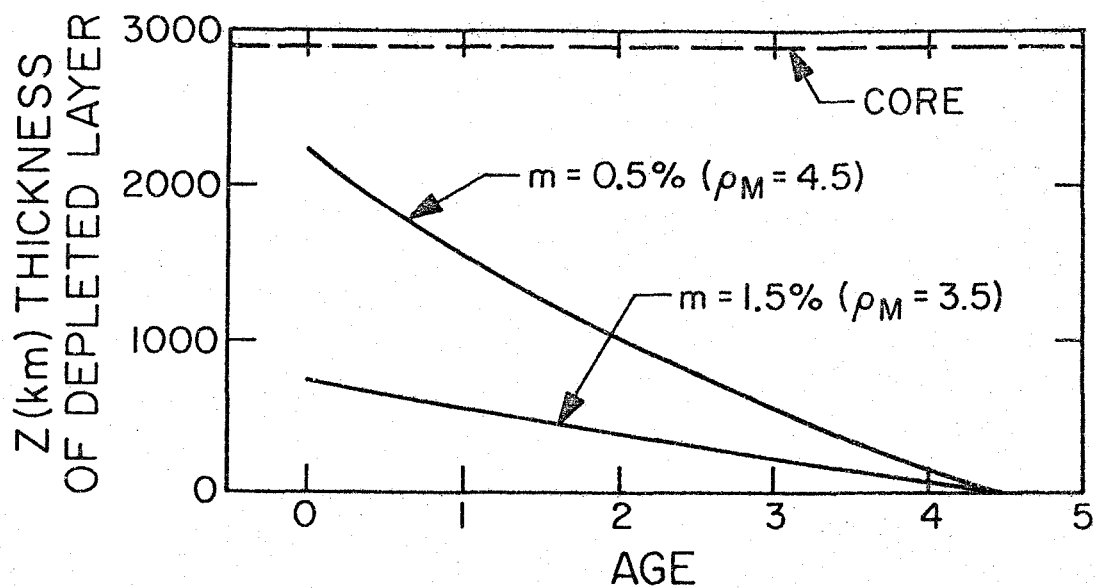


Fig. 36

depleted. Note that unless m is very small $\epsilon_{Nd}(0)$ values much greater than the maximum in young basalts (+12) are expected to be found in the mantle. In this type of model, a difference in $\epsilon_{Nd}(0)$ between two reservoirs does not necessarily imply a difference in the chemistry of the reservoir, but rather implies a difference in age.

Conclusions

All of the models described above indicate that the partitioning of Sm and Nd between crust and mantle is such that the Sm/Nd and ϵ_{Nd} of the bulk mantle have been little affected by the formation of the crust. Thus mantle reservoirs with $\epsilon_{Nd}(0)$ greatly different from zero, such as the mantle source of MOR basalts, must comprise only small fractions of the mantle. The existence of these reservoirs which are much more highly differentiated than average mantle implies the existence of other reservoirs which are less differentiated than average mantle. Thus these calculations suggest that it is possible that undifferentiated, and possibly undegassed, reservoirs may still exist within the earth. This conclusion is in harmony with the presence of excess 3He in some young basalts (Clark *et al.*, 1969). The hypothesis of Ringwood (1966, 1975), that basalts erupted at mid-ocean ridges or in other parts of the ocean basins give information on the composition of the total earth, must be considered highly suspect. The reservoirs which those basalts represent must be highly differentiated and limited in extent.

Consideration of the transport of Rb and Sr from the mantle to the crust, when combined with consideration of Sm-Nd transport, suggest that if the crust is the sole storage reservoir in the earth

for high-Rb/Sr, low-Sm/Nd material, then the crust must have a fairly low Rb/Sr in the range 0.05-0.10. This would be consistent with a highly stratified continental crust in which the lower crust has lower Rb/Sr, but Sm/Nd similar to, the upper crust and an overall crust which has a basaltic composition. Such a model crust would be similar in Rb-Sr characteristics to that discussed by Zartman and Wasserburg (1969). This conclusion would be invalidated if the hypothesis is wrong that the $\epsilon_{\text{Sr}} - \epsilon_{\text{Nd}}$ correlation trend passes through the coordinates of undifferentiated mantle.

These transport calculations raise the question of whether any such simple models are close to a description of the actual transport of these elements in the earth. A further question is whether existing or future data could help discriminate between models.

Consider for example Figure 37. This figure shows much of the existing data on ϵ_{Nd} in igneous rocks through time. Superimposed on these data are trajectories of ϵ_{Nd} for three types of reservoirs. A is a reservoir formed at 4.5 AE ago which retains a constant Sm/Nd through time. Such a reservoir might be the undifferentiated mantle if the silicate portion of the earth had Sm/Nd \approx 10% higher than chondritic, or it could be a reservoir formed in an early terrestrial differentiation prior to the beginning of formation of continental crust. B is a reservoir such as the "upper mantle" of Model Ib (Figure 30) which is gradually depleted in Nd relative to Sm through time due to extraction of material to build the crust. C is the evolution of a CHUR reservoir, and would describe the ϵ_{Sr} of crustal material for Model II, where

Figure 37: Comparison of ϵ_{Nd} of continental rocks with that predicated for the crust for different models. A represents the case of a reservoir formed in a discrete event 4.5AE ago with Sm/Nd about 10% higher than chondritic. B represents a reservoir such as the "upper mantle" of Model Ib which is gradually depleted in Nd relative to Sm. C represents the CHUR reservoir and might describe ϵ_{Nd} of crust material for models like Model II (Figure 35) and Model Ia (approximately) (Figure 30). Note that the three curves can best be distinguished in the time interval from about 1 to 2 AE ago.

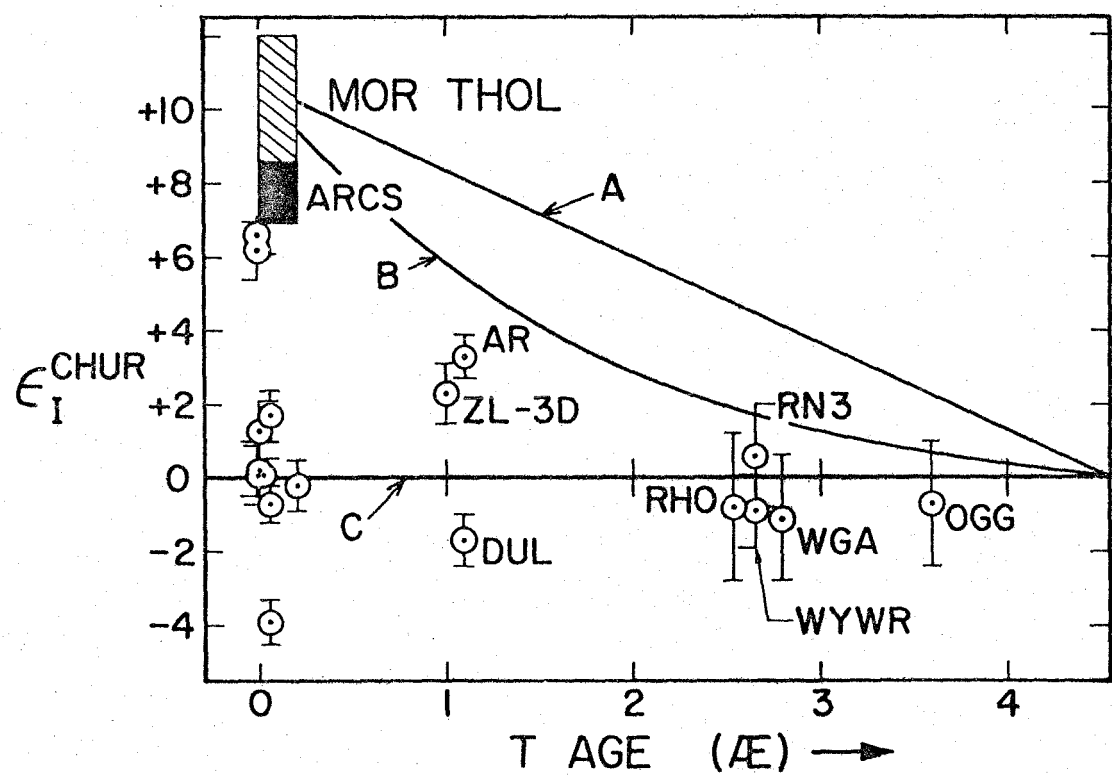


Fig. 37

crust is always derived from unfractionated material or for Model Ia, where the crust is derived from the entire mantle, which is not affected due to its large mass. The question is whether any of these curves describes ϵ_{Sr} of crustal material as a function of time. The data needed to answer this question are ϵ_{Sr} values for rocks representing large additions to the continental crust at different points in time. The existing data are divided mostly into two groups, samples 2.5 AE or older and zero-age samples. The ancient samples are not sensitive discriminators since curves B and C are essentially indistinguishable and curve A is only barely distinguishable from B and C during early earth history. Curves A and B can be distinguished from curve C with zero age samples. But here the question arises as to what rocks are representative of major new additions to the crust. It has been suggested that island arcs represent new or future additions to the continental crust. If this is true, the island arc data could be interpreted as supporting models such as A or B over Model C. However, the samples from the Peninsular Ranges batholith, which may also represent a major new addition to the North American crust, have ϵ_{Nd} values much closer to zero than the island arc samples. Thus the existing data do not give a clear indication of the average ϵ_{Nd} of new additions to the crust, although there is a suggestion that it is greater than zero. It appears from Figure 37 that samples of ages 1 to 2 AE may help to distinguish between these models, since the three curves are distinct in this time interval.

REFERENCES

Amaral, G., U.G. Cordani, K. Kawashita and J.H. Reynolds, Potassium-argon dates of basaltic rocks from southern Brazil, Geochim. Cosmochim. Acta 30, 159-189, 1966.

Arrhenius, G., M.N. Bramlette and E. Piccioto, Localization of radioactive and stable heavy nuclides in ocean sediments, Nature 180, 85-86, 1957.

Arth, J.G. and G.N. Hanson, Geochemistry and origin of early Precambrian crust of northeastern Minnesota, Geochim. Cosmochim. Acta 39, 325-362, 1975.

Baadsgaard, H., U-Th-Pb dates on zircons from the early Precambrian Amitsoq Gneisses, Godthaab District, West Greenland, Earth Plan. Sci. Letters, 19, 22-28, 1973.

Bacon, C.R. and I.S.E. Carmichael, Stages in the P-T path of ascending basalt magma: An example from San Quintin, Baja California, Contr. Mineral Petrol. 41, 1-22, 1973.

Balashov, Y.A. and A.I. Tugarinov, Abundance of rare-earth elements in the earth's crust: Evidence for origin of granites and recent sedimentary rocks, Geochem. Jour. 10, 103-106, 1976.

Bence, A.E. and S.R. Taylor, Petrogenesis of mid-Atlantic ridge basalts at DSDP Leg 37 Sites 332A and B from major and trace element geochemistry, in Initial Reports of the Deep Sea Drilling Project, 37, 1976.

Black, L.P., S. Moorbat, R.J. Pankhurst, B.F. Windley, $^{207}\text{Pb}/^{206}\text{Pb}$ whole rock age of the Archaean granulite facies metamorphic event in West Greenland, Nature, 244, 50-53, 1973.

Bowman, H.R., F. Asaro and I. Perlman. On the uniformity of composition in obsidians and evidence for magmatic mixing. J. Geol., 81, 312-327, 1973.

Boynton, W.V., Fractionation in the solar nebula: condensation of yttrium and the rare earth elements, Geochim. Cosmochim. Acta, 39, 569-584, 1975.

Brooks, C., D.E. James and S.R. Hart, Ancient lithosphere: Its role in young continental volcanism, Science 193, 1086-1094, 1976.

Carmichael, I., The mineralogy and petrology of the volcanic rocks from the Leucite Hills, Wyoming, Contr. Mineral. and Petrol. 15,

24-66, 1967.

Carmichael, I.S.E., F.J. Turner and J. Verhoogen, Igneous Petrology, McGraw-Hill Book Co., San Francisco, 739p., 1974.

Clark, W.B., M.A. Beg and H. Craig, Excess ${}^3\text{He}$ in the sea: Evidence for terrestrial primordial helium, Earth Plan. Sci. Letters 6, 213-220, 1969.

Cordani, U.G. and P. Vandoros, Basaltic rocks of the Parana Basin, in Problems in Brasilian Gondwana Geology.

Cross, W., Lavas of Hawaii and their relations, U.S. Geol. Survey, Prof. Paper 88, 1-97, 1915.

Dawson, J.B., The geology of Oldoinyo Lengai, Bull. Volcanologique 24, 349-388, 1962.

_____, Reactivity of the cations in carbonate magmas, Proc. Geol. Assoc. Canada 15, 103-113, 1964.

Dawson, K.R. and E.H.T. Whitten, The quantitative mineralogical composition and variation of the Lacorne, Lamotte and Preissac granitic complex, Quebec, Canada. J. Petrol. 3, 1-37, 1962.

DePaolo, D.J. and G.J. Wasserburg, Nd isotopic variations and petrogenetic models, Geophys. Res. Letters 3, 249-252, 1976a.

_____, and _____, Inferences about magma sources and mantle structure from variations of ${}^{143}\text{Nd}/{}^{144}\text{Nd}$, Geophys. Res. Letters 3, 743-746, 1976b.

_____, and _____, Variation of ${}^{143}\text{Nd}/{}^{144}\text{Nd}$ in continental and oceanic igneous rocks and chemical zonation of the mantle (abs.), Geol. Soc. Am. Abs. 8, 835, 1976c.

_____, and _____, The sources of island arcs as indicated by Nd and Sr isotopic studies, Geophys. Res. Letters 4, 465-468, 1977.

Dickinson, W.R., Relations of andesites, granites and derivative sandstones to arc-trench tectonics, Rev. Geophys. Space Phys. 8, 813-860, 1970.

Doell, R.R. and G.B. Dalrymple, Potassium-argon ages and paleomagnetism of the Waianae and Koolau volcanic series, Oahu, Hawaii, Bull. Geol. Ser. Am. 84, 1217-1243, 1973.

Donhoffer, D., Determination of the half-lives of radioactive nuclides ${}^{147}\text{Sm}$ and ${}^{176}\text{Lu}$ occurring in nature by means of liquid scintillators, Nucl. Phys. 50, 489-496, 1963.

Drake, M.J. and D.F. Weill, Partition of Sr, Ba, Ca, Y, Eu^{2+} , Eu^{3+} and other REE between plagioclase feldspar and magmatic liquid: An experimental study, Geochim. Cosmochim. Acta 39, 689-712, 1975.

Epstein, S. and T. Mayeda, The variations in O^{18} content of water from natural sources, Geochim. Cosmochim. Acta 4, 213, 1953.

Eriksen, G.P. and J.L. Kulp, Potassium-argon measurements on the Palisades Sill, New Jersey, Bull. Geol. Soc. Am. 72, 649-652, 1961.

Eugster, O., F. Tera, D.S. Burnett, and G.J. Wasserburg, The isotopic composition of gadolinium and neutron capture effects in some meteorites, J. Geophys. Res. 75, 2753-2768, 1970.

Everson, J.E. and L.T. Silver, Contrasting lead isotopic characteristics of late Cenozoic basalts from the southwestern Colorado Plateau and the nearby Basin and Range Province (abs), Geol. Soc. Am. Abs. 8, 857-858, 1976.

Flanagan, F.J., 1972 values for international geochemical reference samples, Geochim. Cosmochim. Acta 37, 1189-1200, 1973.

Frey, F.A., Rare earth and potassium abundances in St. Paul's Rocks, Earth. Plan. Sci. Letters 7, 351-360, 1970.

_____, L.A. Haskin and M.A. Haskin, Rare earth abundances in some ultramafic rocks, J. Geophys. Res. 76, 2057-2070, 1971.

_____, and D.H. Green, The mineralogy, geochemistry and origin of Iherzolite inclusions in Victorian basanites, Geochim. Cosmochim. Acta 38, 1023-1059, 1974.

Gancarz, A.J. and G.J. Wasserburg, Initial Pb of the Amitsoq Gneiss, West Greenland and implications for the age of the earth, Geochim. Cosmochim. Acta 41, 1283-1301, 1977.

Gast, P.W., Abundance of Sr^{87} during geologic time, Bull. Geol. Soc. Am. 69, 1369-1410, 1955.

_____, Limitations on the composition of the upper mantle, J. Geophys. Res. 65, 1287-1297, 1960.

_____, Isotope geochemistry of volcanic rocks, in Basalts, vol. 1, 325-358, John Wiley and Sons, Inc., New York, 1967.

_____, Trace element fractionation and the origin of tholeiitic and alkaline magma types, Geochim. Cosmochim. Acta 32, 1057-1086, 1968.

Gast, P.W., G.R. Tilton, and C. Hedge, Isotopic composition of lead and strontium from Ascension and Gough Islands, Science 145, 1181-1185, 1964.

Gerasimovsky, V.I., V.P. Volkov, L.N. Kogarko, and A.I. Polyakov, Kola Peninsula, 206-21, in Sorenson, Ed., The Alkaline Rocks, John Wiley and Sons, New York, 62p., 1974.

Green, D.H., Composition of basaltic magmas as indicators of conditions of origin: application to oceanic volcanism, Phil. Trans. Roy. Soc. London A 268, 707-725, 1971.

Green, T.H., A.O. Brunfelt and K.S. Heier, Rare earth element distribution in anorthosites and associated high grade metamorphic rocks, Lofoten-Vesteraalen, Norway, Earth Plan. Sci. Letters 7, 93-98, 1969.

_____, Rare-earth element distribution and K/Rb ratios in granulites, mangerites and anorthosites, Lofoten-Vesteraalen, Norway, Geochim. Cosmochim. Acta 36, 241-257, 1972.

Gupta, M.C. and R.D. McFarlane, The natural alpha radioactivity of samarium, J. Inorg. Nucl. Chem. 32, 3425-3432, 1970.

Hamilton, P.J., R.K. O'Nions and N.M. Evensen, Sm-Nd dating of Archaean basic and ultrabasic volcanics, Earth and Plan. Sci. Letters 36, 263-268, 1977.

Haskin, L.A., F.A. Frey, R.A. Schmitt, and R.H. Smith, Meteoritic, solar, and terrestrial rare-earth distributions, Physics and Chemistry of the Earth 7, 167-321, 1966a.

_____, T.R. Wildeman, F.A. Frey, K.A. Collins, C.R. Keedy, and M.A. Haskin. Rare earths in sediments, J. of Geophys. Res. 71, 6091-6105, 1966b.

_____, M.A. Haskin, F.A. Frey, T.R. Wildeman. Relative and absolute terrestrial abundances of the rare earths, in Origin and Distribution of the Elements, Ahrens, ed., Pergamon, 1178pp., 1968.

_____, and T.P. Paster, Geochemistry and mineralogy of the rare earths, in Eyring, L. and K. Gschneidner, eds. Handbook of the Rare Earths (in press) 1978.

Hawkesworth, C.J., R.K. O'Nions, R.J. Pankhurst, P.J. Hamilton and N.M. Evensen, A geochemical study of island-arc and back-arc tholeiites from the Scotia Sea, Earth Plan. Sci. Letters 36, 253-262 (1977).

Hedge, C.E., Variations in radiogenic strontium found in volcanic rocks, J. Geophys. Res. 71, 6119-6126, 1966.

Heier, K.S., Metamorphism and the chemical differentiation of the crust, Geol. Fören. Stockh. Förh. 87, 249-256, 1965.

_____, W. Compston, and I. McDougall, Thorium and uranium concentration, and the isotopic composition of strontium in the differentiated Tasmanian dolerites, Geochim. Cosmochim. Acta 29, 643-659, 1965.

_____, and K. Thoresen, Geochemistry of high grade metamorphic rocks, Lofoten-Vesterålen, North Norway, Geochim. Cosmochim. Acta 35, 89-99, 1971.

Hess, H.H., Stillwater igneous complex, Montana. A quantitative study. Geol. Soc. America Mem. 80, 230p., 1960.

Høgdahl, Ø.T., S. Melson, and V. Bowen (1968) Neutron activation analysis of lanthanide elements in seawater, Adv. Chem. Ser. 73, 308-325, 1968.

Hurley, P.M., Absolute abundance and distribution of Rb, K and Sr in the earth, Geochim. Cosmochim. Acta 32, 273-283, 1968.

Irvine, T.H. and C.H. Smith, The ultramafic rocks of the Muskox intrusion, Northwest Territories, Canada, in Ultramafic and Related Rocks, P.J. Wyllie, ed., John Wiley and Sons, Inc., New York, 464p., 1967.

Irving, A.J. and D.H. Green, Geochemistry and petrogenesis of the Newer Basalts of Victoria and south Australia, J. Geol. Soc. Australia 23, 45-66, 1976.

James, D.E., C. Brooks and A. Cuyubomba, Andean Cenozoic volcanism: Magma genesis in the light of strontium isotopic composition and trace-element geochemistry, Bull. Geol. Soc. Am. 87, 592-600, 1976.

Kay, R.W. and P.W. Gast (1973), The Rare-earth content and origin of alkali-rich basalts, J. Geol. 81, 653-682, 1973.

Kuno, H., K. Yamasaki, C. Iida, and K. Nagashima, Differentiation of Hawaiian magmas, Japan. J. Geol. Geography. Trans. 28 (4), 179-218, 1957.

Langmuir, C.H., J.F. Bender, A.E. Bence and G.N. Hanson, Petrogenesis of basalts from the FAMOUS area: Mid-Atlantic Ridge, Earth. Plan. Sci. Letters 36, 133-156, 1977.

Lanphere, M.A., Geochronologic studies in the eastern Mojave Desert, California, J. Geol. 72, 381-399, 1964.

Larsen, E.S., Batholith and associated rocks of Corona, Elsinore, and San Luis Rey quadrangles southern California, Geol. Soc. America Mem. 29, 182p., 1948.

Lederer, C.M., J.M. Hollander, and I. Perlman, Table of Isotopes, John Wiley and Sons, Inc., New York, 594p., 1967.

Leeman, W.P., Late Cenozoic alkali-rich basalt from the western Grand Canyon area, Utah and Arizona: Isotopic composition of strontium, Bull. Geol. Soc. Am. 85, 1691-1696, 1974.

____ and W.I. Manton, Strontium isotopic composition of basaltic lavas from the Snake River plain, Southern Idaho, Earth, Plan. Sci. Letters 11, 420-434, 1971.

Lewis, J.S., Consequences of the presence of sulfur in the core of the earth. Earth. Plan. Sci. Letters 11, 130-134, 1971.

Lugmair, G.W., Sm-Nd ages: a new dating method (abs.) Meteoritics, 9, 369, 1974.

____, Sm-Nd systematics of some Apollo 17 basalts, in Origins of Mare Basalts, LSI, 205p., 1975.

____, N.B. Scheinin, Sm-Nd Systematics of the Stannern Meteorite, Meteoritics 10, 447-448, 1975.

____, N.B. Scheinin, and K. Marti, Sm-Nd age of Apollo 17 basalt 75075: Evidence for early differentiation of the lunar exterior, Proc. Lunar Sci. Conf. 6th, 1419-1429, 1975a.

____, N.B. Scheinin, and K. Marti, Search for Extinct ^{146}Sm , 1. The isotopic abundance of ^{142}Nd in the Juvinas meteorite, Earth. Plan. Sci. Letters 27, 79-84, 1975b.

____, K. Marti, J.P. Kurtz, N.B. Scheinin, History and genesis of lunar troctolite 76535 or: How old is old? Proc. Lunar Sci. Conf. 7th, 2009-2033, 1976.

____ and K. Marti, Evolution of the Lunar Interior: Sm-Nd systematics of Al5 green glass and the question of the lunar initial $^{143}\text{Nd}/^{144}\text{Nd}$ (abs.), in Lunar Science VIII, the Lunar Sci. Inst., Houston, 597-599, 1977.

Mason, B., Principles of Geochemistry, John Wiley and Sons, Inc., New York, 329p., 1966.

Masuda, A., N. Nakamura, T. Tenaka, Fine structures of mutually normalized rare-earth patterns of chondrites, Geochim. Cosmochim. Acta 37, 239-248, 1973.

McCulloch, M.T. and G.J. Wasserburg, Sm-Nd and Rb-Sr chronology of continental crust formation, Science (in press) 1978.

McDougall, I., Determination of the age of a basic igneous intrusion by the potassium-argon method, Nature 190, 1184-1186, 1961.

_____, Differentiation of the Tasmanian dolerites: Red Hill dolerite-granophyre Association, Bull. Geol. Soc. Am. 73, 279-316, 1962.

_____, Potassium-argon age measurements on dolerites from Antarctica and South Africa, J. Geophys. Res. 68, 1535-1545, 1963.

_____, Geochemistry and origin of basalt of the Columbia River Group, Oregon and Washington, Bull. Geol. Soc. Am. 87, 777-792, 1976.

McGetchin, T.R. and L.T. Silver, A crustal-upper-mantle model for the Colorado plateau based on observations of crystalline rock fragments in the Moses Rock dike, J. Geophys. Res. 77, 7022-7037, 1972.

Melson, W.G., E. Jarosewich, V.T. Bowen, and G. Thompson, St. Peter and St. Paul Rocks: A high-temperature mantle-derived intrusion, Science 155, 1532-1535, 1967a.

_____, E. Jarosewich, R. Cifelli, G. Thompson, Alkali Olivine Basalt dredged near St. Paul's Rock, Mid-Atlantic Ridge, Nature 215, 381-382, 1967b.

_____, S.R. Hart and G. Thompson, St. Paul's Rocks, Equatorial Atlantic: Petrogenesis, radiometric ages, and implications on sea-floor spreading, Geol. Soc. of Am. Mem. 132, 1972.

Mennell, F.P., The northward and eastward extension of the Karroo lavas, Geol. Mag. 59, 166-170, 1922.

_____, Some Mesozoic and Tertiary igneous rocks from Portuguese East Africa, Geol. Mag. 66, 529-540, 1929.

Moorbath, S., The geological significance of early Precambrian rocks, Proc. Geol. Assoc. London 86, 259-279, 1975.

Nakamura, N., Determination of REE, Ba, Fe, Mg, Na and K in carbonaceous and ordinary chondrites, Geochim. Cosmochim. Acta, 38, 757-775, 1974.

_____, M. Tatsumoto, P.D. Nunes, D.M. Unruh, A.P. Schwab and T.R. Wildeman, 4.4b.y.-old clast in Boulder 7, Apollo 17: A comprehensive chronological study by U-Pb, Rb-Sr and Sm-Nd methods, Proc. Lunar Sci. Conf. 7th, 2309-2333, 1976.

Nathan, S. and J.S. Fruchter, Geochemical and paleomagnetic stratigraphy of the Picture Gorge and Yakima basalts (Columbia River Group) in Central Oregon, Bull. Geol. Soc. America 85, 63-76, 1974.

Naylor, R.S., R.H. Steiger, and G.J. Wasserburg, U-Th-Pb and Rb-Sr systematics in 2700×10^6 -year old plutons from the southern Wind River Range, Wyoming, Geochim. Cosmochim. Acta 34, 1133-1159, 1970.

Nier, A.O., A redetermination of the relative abundances of the isotopes of carbon, nitrogen, oxygen, argon, and potassium, Phys. Rev., 77, 789-793, 1950.

O'Nions, R.K., R.J. Pankhurst and K. Grönvold, Nature and development of basalt magma sources beneath Iceland and the Reykjanes Ridge, J. Petrology, 17, 1976.

_____, P.J. Hamilton and N.M. Evensen, Variations in $^{143}\text{Nd}/^{144}\text{Nd}$ and $^{87}\text{Sr}/^{86}\text{Sr}$ ratios in oceanic basalts, Earth Planet. Sci. Letters 34, 13-22, 1977.

Osawa, M. and G.G. Gales, Trace element abundances in Columbia River basalts, Proc. Second Columbia River Basalt Symposium, 1969.

Papanastassiou, D.A. and G.J. Wasserburg, Initial Strontium isotopic abundances and the resolution of small time differences in the formation of planetary objects, Earth. Plan. Sci. Letters 5, 361-376, 1969.

_____, D.J. DePaolo and G.J. Wasserburg, Rb-Sr and Sm-Nd chronology and genealogy of basalts from the Sea of Tranquility, Proc. Lunar Sci. Conf. 8th, 1639-1672, 1977.

Patterson, C., Characteristics of lead isotope evolution on a continental scale in the earth, 244-268, in Craig, H., ed., Isotopic and Cosmic Chemistry, North Holland, 553p., 1964.

Peterman, Z.E., I.S.E. Carmichael and A.L. Smith, $^{87}\text{Sr}/^{86}\text{Sr}$ ratios of Quaternary lavas of the Cascade Range, northern California, Bull. Geol. Soc. Am. 81, 311-318, 1970.

Richard, P., N. Shimizu, and C.J. Allegre, $^{143}\text{Nd}/^{146}\text{Nd}$, a natural tracer, An application to oceanic basalts, Earth Plan. Sci. Letters 31, 269-278, 1976.

Ringwood, A.E., The chemical composition and origin of the earth, in Advances in Earth Science, P.M. Hurley, ed., 287-356, M.I.T. Press, Cambridge, Mass., 1966.

, Composition and Petrology of the Earth's Mantle, McGraw-Hill, Inc., 618p., 1975.

Ronov, A.B., Yu.A. Balashov, Yu.P. Girin, R.Kh. Bratishko, and G.A. Kazakov, Trends in rare-earth distribution in the sedimentary shell and in the earth's crust, Geochem. International 12, 987-1016, 1972.

Russ, G.P. III, Neutron stratigraphy in the lunar regolith, Ph.D. Thesis, California Institute of Technology, 1974.

Schilling, J-G. and J.W. Winchester, Rare earth contribution to the origin of Hawaiian lavas, Contr. Mineral. and Petrol. 23, 27-37, 1969.

Schilling, J.G., Sea-floor evolution: rare-earth evidence, Phil. Trans. Roy. Soc. London A. 268, 663-706, 1971.

Schnetzler, C.C. and J.A. Philpotts, Partition coefficients of rare-earth elements between igneous matrix material and rock-forming mineral phenocrysts, pt. II, Geochim. Cosmochim. Acta 34, 331-340, 1970.

Shaw, D.M., Trace element fractionation during anatexis, Geochim. Cosmochim. Acta 34, 237-243, 1970.

, J. Dostal, R.R. Keays, Additional estimates of continental surface Precambrian shield composition in Canada, Geochim. Cosmochim. Acta 40, 73-83, 1976.

Silver, L.T. and J.C. Green, Time constants for Keweenawan igneous activity, Geol. Soc. Am. Abs. 4, 665, 1972.

, Petrological, geochemical and geochronological asymmetries of the Peninsular Ranges batholith (abs.), Geol. Soc. Am. Abs. 7, 375-376, 1975.

Smith, A.L. and I.S.E. Carmichael, Quaternary lavas from the southern Cascades, western U.S.A., Contr. Mineral Petrol. 19, 212-238, 1968.

and _____, Quaternary trachybasalts from southeastern California, Am. Mineral. 54, 909-923, 1969.

Smith, D. and L.T. Silver, Potassic granophyre associated with Precambrian diabase, Sierra Ancha, Arizona, Bull. Geol. Soc. Am. 86, 503-513, 1975.

Steiger, R.H. and G.J. Wasserburg, Comparative U-Th-Pb systematics in 2.7×10^9 yr plutons of different geologic histories, Geochim. Cosmochim. Acta 33, 1213-1232, 1969.

Stuckless, J.S. and A.J. Irving, Strontium isotope geochemistry of megacrysts and host basalts from southeastern Australia, Geochim. Cosmochim. Acta 40, 209-213, 1976.

Sun, S.S. and G.N. Hanson, Origin of Ross Island basanitoids and limitations upon the heterogeneity of mantle sources for alkali basalts and nephelinites. Contr. Mineral. Petrol. 52, 77-106, 1975.

Tatsumoto, M., Isotopic composition of lead in volcanic rocks from Hawaii, Iwo Jima, and Japan, J. Geophys. Res. 71, 1721-1723, 1966.

Taylor, S.R., Abundances of chemical elements in the continental crust: a new table. Geochim. Cosmochim. Acta 28, 1273-1285, 1964.

and A.J.R. White, Geochemistry of andesites and the growth of continents, Nature 205, 271-273, 1965.

(1977) Island arc models and the composition of the continental crust, 325-336, in T. and W.C. Pitman III, eds., Island Arcs, Deep Sea Trenches and Back-Arc Basins, Am. Geophys. Union, Washington, 1977.

Turekian, K. and S.P. Clark, Inhomogeneous accumulation of the earth from the primitive solar nebula, Earth Plan. Sci. Letters 6, 346-348, 1969.

Vinogradov, A.P., Average contents of chemical elements in the principal types of igneous rocks of the earth's crust, Geochemistry 7, 641-664, 1962.

Walker, F., Differentiation of the Palisade Diabase, New Jersey, Bull. Geol. Soc. Am. 51, 1059-1106, 1940.

Wasserburg, G.J., G.J.F. MacDonald, F. Hoyle and W.A. Fowler,
 Relative contributions of uranium, thorium and potassium to
 heat production in the earth, Science 143, 465-467, 1964.

, Geochronology and isotopic data bearing on the
 development of the continental crust, in Advances in Earth
 Sciences, M.I.T. Press, 1966.

, D.A. Papanastassiou, E.V. Nenow, and C.A. Bauman, A
 programmable magnetic field mass spectrometer with on-line
 data processing, Rev. Sci. Instr. 40, 288-295, 1969.

Waters, A.C., Stratigraphic and lithologic variations in the Columbia
 River basalt, Am. Jour. Sci. 259, 283-311, 1961.

Weill, D.F. and G.A. McKay, The partitioning of Mg, Fe, Sr, Ce, Sm,
 Eu and Yb in lunar igneous systems and a possible origin of
 KREEP by equilibrium partial melting, Proc. Lunar Sci. Conf.
6th, 1143-1158, 1975.

Windley, B.F., Anorthosites of southern West Greenland, Am. Assoc.
 Petrol. Geol. Mem. 12, 899-915, 1969.

Wright, P.M., E.P. Steinberg and L.E. Glendenin, Half-life of
 samarium-147, Phys. Rev. 123, 205-208, 1961.

Wright, T.L., M.J. Grolier, and D.A. Swanson, Chemical variation
 related to the stratigraphy of the Columbia River basalt,
Bull. Geol. Soc. Am. 84, 371-386, 1973.

Zartman, R.E. A geochronologic study of the Lone Grove Pluton from
 the Llano Uplift, Texas, J. Petrol. 5, 359-408, 1964.

and G.J. Wasserburg, the isotopic composition of lead in
 potassium feldspars from some 1.0 b.y. old North American
 igneous rocks, Geochim. Cosmochim. Acta 33, 901-942, 1969.

, Lead isotopic provinces in the Cordillera of the western
 United States and their geologic significance, Econ. Geol. 69,
 792-805, 1974.

APPENDIX 1

Nd ISOTOPIC VARIATIONS and PETROGENETIC MODELS

D. J. DePaolo and G. J. Wasserburg

Lunatic Asylum, Div. Geological and Planetary Sciences,

California Institute of Technology, Pasadena, California 91125

Abstract: The decay of ^{147}Sm to ^{143}Nd allows $^{143}\text{Nd}/^{144}\text{Nd}$ to be used to trace Sm/Nd fractionation in long time-scale geologic processes. $^{143}\text{Nd}/^{144}\text{Nd}$ has been measured in terrestrial rock samples of different ages to establish the characteristics of Nd isotopic evolution in the crust and mantle. The evolution of $^{143}\text{Nd}/^{144}\text{Nd}$ in the mantle indicates Sm/Nd essentially equal to that of chondrites, and implies a chondritic REE distribution for the earth. Variations in $^{143}\text{Nd}/^{144}\text{Nd}$ do exist in the mantle, however, indicating Sm/Nd heterogeneity and the existence of distinct mantle reservoirs with characteristic $^{143}\text{Nd}/^{144}\text{Nd}$. $^{143}\text{Nd}/^{144}\text{Nd}$ in average crustal rocks today is much lower than found in recent mantle samples and reflects their age and low Sm/Nd. Oceanic tholeiites and alkali basalt are derived from sources with Sm/Nd which has been 5-10% greater than chondritic over the age of the earth. Alkali basalt can not be derived from mantle reservoirs which have been light REE-enriched for long times.

Long-lived, naturally-occurring radioisotopes are important not only in the measurement of absolute time, but also as indicators of chemical processes involved in rock formation. ^{147}Sm decays to ^{143}Nd with a half-life of 1.06×10^{11} years. Sm and Nd are even-numbered light lanthanide elements, so their cosmic abundances and chemical properties are similar. But, Sm/Nd fractionation is commonly observed in rocks and minerals, and is a sensitive indicator of fractionation in the light rare-earth elements (REE). The use of Sm-Nd as a dating method was pioneered by *Lugmair* (1974) and *Lugmair et al.* (1975 a,b,c,d) who determined ages of the Juvinas and Stannern achondrites and one lunar basalt. The purpose of this study is to investigate the isotopic composition of Nd in selected *terrestrial* rocks to gain information about its implications for petrogenesis and the history of the earth's crust and mantle. The potential usefulness of the Sm-Nd system for the dating of terrestrial rocks is also made manifest. A symbolism is introduced which may be useful in presentation and interpretation of the data.

As discussed by *Lugmair* (1974) the ratio $^{143}\text{Nd}/^{144}\text{Nd}$ is an indicator of changes in the relative abundance of ^{143}Nd due to ^{147}Sm decay. For formation and chemical evolution of a planet, the growth of $^{143}\text{Nd}/^{144}\text{Nd}$ with time in various reservoirs may be shown schematically (Figure 1). At T_c a planet condenses from the solar nebula (SN). The rate of $^{143}\text{Nd}/^{144}\text{Nd}$ growth in the bulk planet may be different from the growth rate in the solar nebula due to a change in Sm/Nd occurring during condensation (*Boynton*, 1975). If a reservoir with Sm/Nd = 0 were isolated at T_c , I_c would record $^{143}\text{Nd}/^{144}\text{Nd}$ at the time of condensation. If the planet remains a closed system with respect to Sm and Nd subsequent to T_c , the evolution of its average $^{143}\text{Nd}/^{144}\text{Nd}$ will be described by a line whose slope is proportional to its average Sm/Nd. The bulk planet is herein termed a "uniform reservoir" (UR) and the growth of $^{143}\text{Nd}/^{144}\text{Nd}$ in UR as a function of time is the curve $I_{UR}(T)$. The value of $^{143}\text{Nd}/^{144}\text{Nd}$ in UR today is defined as $I_{UR}(0)$. $^{143}\text{Nd}/^{144}\text{Nd}$ in UR at any time T in the past is given by

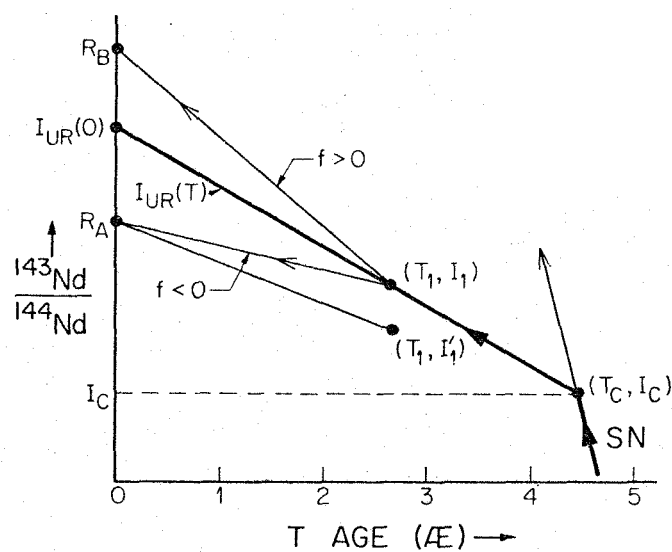


Fig. 1: Schematic representation of the evolution of $^{143}\text{Nd}/^{144}\text{Nd}$ with time in the solar nebula (SN) and in a hypothetical planetary object condensed at T_c . The growth rate of $^{143}\text{Nd}/^{144}\text{Nd}$ is proportional to Sm/Nd, f is the Sm/Nd enrichment factor relative to UR.

Table 1: Normalized Nd isotope ratios^a

Sample	142/144	143/144	145/144	146/144	148/144
113031	1.13821	0.512115	0.348952	0.724082	0.243066
	± 8	± 40	± 30	± 35	± 30
111240	1.13828	0.512361	0.348975	0.724113	0.243091
	± 5	± 22	± 18	± 26	± 26
113152	1.13823	0.512280	0.348950		b 0.243112
	± 7	± 35	± 42		± 43
BCR-1	1.13827	0.511839	0.348977	0.724088	0.243070
	± 4	± 22	± 19	± 36	± 19
Khibina Ap.	1.13827	0.511862	0.348970	0.724116	0.243082
	± 4	± 17	± 19	± 30	± 20
NAS-216D	1.13823	0.511101	0.348968	0.724086	0.243110
	± 4	± 27	± 38	± 54	± 29
RHO-1D	1.13819	0.510994	0.348943	0.724079	0.243089
	± 15	± 48	± 48	± 113	± 34
RN3-D(TR)	1.13830	0.510245	0.348977	0.724139	0.243072
	± 8	± 31	± 42	± 58	± 38
RN3-D(TR)	1.13821	0.510234	0.348913		b 0.243065
	± 9	± 37	± 46		± 65
RN3 Ap.	1.13825	0.511343	0.348965	0.724122	0.243084
	± 5	± 23	± 27	± 31	± 28
OGG128,10D	1.13826	0.510026	0.348965	0.724103	0.243089
	± 6	± 30	± 17	± 44	± 22
NN1	1.13829	0.510306	0.348952	0.724091	0.243080
	± 6	± 19	± 28	± 43	± 30
NN1	1.13829	0.510329	0.348978		b 0.243091
	± 5	± 21	± 15		± 17
NN2	1.13826	0.511132	0.348946	0.724115	0.243061
	± 3	± 16	± 13	± 20	± 14
NN2	1.13827	0.511148	0.349009	0.724156	0.243092
	± 6	± 31	± 17	± 45	± 31
NN2	1.13824	0.511124	0.348993		b 0.243074
	± 9	± 18	± 26		± 33

^aNormalized to $^{150}\text{Nd}/^{142}\text{Nd} = 0.2096$, errors are 2σ mean. ^bSpiked with ^{150}Nd and normalized to $^{146}\text{Nd}/^{142}\text{Nd} = 0.636155$

$$I_{UR}(T) = I_{UR}(0) - \left(\frac{^{147}Sm}{^{144}Nd} \right)_{UR}^0 (e^{\lambda T} - 1), \quad (1a)$$

where $(^{147}Sm/^{144}Nd)_{UR}^0$ is that in UR today and $\lambda = 6.54 \times 10^{-12} \text{ yr}^{-1}$. If a rock is derived from this average reservoir at time T, its initial $^{143}Nd/^{144}Nd$ would be $I_{UR}(T)$.

Chemical differentiation in the planet subsequent to T_c will result in reservoirs with different Sm/Nd. The Sm/Nd of a reservoir can be expressed relative to UR in terms of a Sm/Nd

$$\text{enrichment factor } f, \text{ where } f = \left\{ \frac{(Sm/Nd)_{Res}}{(Sm/Nd)_{UR}} - 1 \right\}. \text{ If at a time } T_1 \leq T_c$$

$T_1 \leq T_c$ a secondary reservoir A is isolated from UR with initial value I_1 and $f < 0$, $^{143}Nd/^{144}Nd$ in this reservoir would evolve from (T_1, I_1) along a line of lower-slope to the value R_A observed today. Similarly $^{143}Nd/^{144}Nd$ in a reservoir B, isolated from UR at T_1 with $f > 0$ would evolve along a steeper trajectory to R_B today. For rocks of zero age the Nd isotopic composition of the source region is identical to that measured in the rock. $^{143}Nd/^{144}Nd$ in source regions of old rocks is found by determination of the initial $^{143}Nd/^{144}Nd$ (I). This can be obtained from an internal isochron or, if the age is known, from the measured $^{143}Nd/^{144}Nd$, $^{147}Sm/^{144}Nd$, and the age T:

$$I = \left(\frac{^{143}Nd}{^{144}Nd} \right)_{meas} - \left(\frac{^{147}Sm}{^{144}Nd} \right)_{meas} (e^{\lambda T} - 1). \quad (1b)$$

As shown in Figure 1, two rocks of the same age T_1 , but different initial I_1 and I'_1 , must have been derived from distinct parent reservoirs.

In a reservoir whose Sm/Nd is equal to that in chondritic meteorites (0.31) (Masuda *et al.*, 1973), $^{143}Nd/^{144}Nd$ will increase by 1.13% in 4.5 AE. REE abundance patterns in various rocks indicate that sufficient variation in Sm/Nd exists so that initial $^{143}Nd/^{144}Nd$ may be used to distinguish different source regions. Some of the isotopic patterns can be anticipated from the extensive experimental and theoretical studies of REE abundances and fractionation patterns. (cf. Haskin *et al.*, 1966a.)

Analytical Procedure and Data. In general, the chemical and mass spectrometric procedures used closely follow those which have been used here for the past eight years for Gd and Sm. Separation of Sm and Nd was accomplished using the procedure described for Gd separation by Eugster *et al.* (1970), with slight modifications. Sm and Nd were eluted from Dowex AG 50W-X4 cation exchange resin using 0.2M 2-Methylalactic

acid with pH adjusted to 4.60. Total procedural blank for Nd was 10^{-10} gm. Nd was loaded in 1.0 N HCl onto a single flat Re ribbon and oxidized. Nd isotopic ratios were measured on the Lunatic I mass spectrometer (Wasserburg *et al.*, 1969), as NdO^+ . The ion beam intensity at mass 160 ($^{144}\text{Nd}^{16}\text{O}$) was 10^{-11} A at filament temperatures between 1220° and 1280°C. Ion beam intensity ratios were calculated relative to mass 160. At each mass the high zero, peak and low zero are measured with an integration time of 1 sec at each position. Data is taken in sets of 10 mass scans, averaged; corrected for oxygen and then discrimination. The effect of peak tails on zeros was assessed by measuring the zeros with beam on and beam off. The background offset is less than 0.005% of the peak intensity for all isotopes. Oxygen corrections were made using the composition by Nier (1950). Mass discrimination corrections were made by normalizing to $^{150}\text{Nd}/^{142}\text{Nd} = 0.2096$, the average measured value in several mass spectrometer runs. In a typical run of 200 ratios, 1σ is 0.01% and 2σ mean is 0.005%. Possible spectral interferences were monitored by scanning at high sensitivity from mass 125 to mass 200. Peaks could be detected representing LaO^+ and GdO^+ at intensities $< 1.5 \times 10^{-6}$ A and SmO^+ at 10^{-5} A. Occasionally Ba^+ was detected ($< 10^{-5}$ A). No other peaks were observed at a detection limit of 2.5×10^{-7} A. Interference from SmO^+ ions is corrected by monitoring the signal at mass 170 ($^{154}\text{Sm}^{16}\text{O}$). The net correction to $^{143}\text{Nd}/^{144}\text{Nd}$ when the signal at mass 170 is 0.01% of the 160 signal is only 4×10^{-4} %. Isotopic measurements were made on spiked and unspiked aliquants which were passed through chemistry. Sm and Nd concentrations were determined on the same aliquant. Internal consistency of isotopic measurements is shown by agreement of *all* isotope ratios from different samples and from spiked and unspiked runs on the same sample. Reproducibility is demonstrated by repeat runs on normals. Nd isotopic data are given in Table 1, and are the first high precision Nd abundances obtained using modern techniques.

Data representation. Because of the variations in $^{143}\text{Nd}/^{144}\text{Nd}$ are small, data will be presented normalized to a uniform reservoir (UR) as described above. This is a somewhat different approach than has been used for Rb-Sr, where there are large variations of $^{87}\text{Sr}/^{86}\text{Sr}$ and there is no clearly defined, meaningful reference reservoir representative of the earth. $^{143}\text{Nd}/^{144}\text{Nd}$ measured in a sample today is given as fractional deviations from $I_{\text{UR}}(0)$ in parts in 10^4 (ϵ_0^{UR}):

$$\epsilon_0^{\text{UR}} = \left[\frac{(^{143}\text{Nd}/^{144}\text{Nd})_{\text{meas}}}{I_{\text{UR}}(0)} - 1 \right] \times 10^4. \quad (2a)$$

Similarly, the initial $^{143}\text{Nd}/^{144}\text{Nd}$ (I) for a sample of age T is presented as the deviation of I from $I_{\text{UR}}(T)$ in parts in 10^4 (ϵ_1^{UR}):

$$\epsilon_1^{\text{UR}}(T) = \left[\frac{I_{\text{sample}}}{I_{\text{UR}}(T)} - 1 \right] \times 10^4 \approx \epsilon_0^{\text{UR}} - f_R Q T, \quad (2b)$$

where f_R is the Sm/Nd enrichment in the rock relative to UR and $Q \equiv \frac{\lambda(^{147}\text{Sm}/^{144}\text{Nd})_{\text{UR}} \cdot 10^4}{I_{\text{UR}}(0)}$ is a constant. Thus a sam-

ple with a present value of ϵ_0^{UR} which was derived from UR T years ago would have $\epsilon_1^{\text{UR}}(T) = 0$. A value of $\epsilon_1^{\text{UR}}(T)$ different from zero indicates that the source region was fractionated relative to UR prior to T. The average fractionation factor for the source (f_S) over the time interval $T_c - T$ is related to ϵ_1^{UR} by:

$$\langle f_S \rangle (T_c - T) \equiv \frac{\epsilon_1^{\text{UR}}}{Q} (\equiv f^* T^*). \quad (1)$$

in terms of a generalized quantity $f^* T^*$, where T^* represents the amount of time necessary to produce the deviation ϵ_1^{UR} with an enrichment factor f^* . From $\langle f_S \rangle$ and the measured Sm/Nd fractionation of the sample relative to UR (f_R), one can calculate the Sm/Nd fractionation factor for the sample relative to the source (g) assuming a simple two-stage history:

$1 + g = 1 + f_R / 1 + \langle f_S \rangle$. A similar theoretical factor (g_{TH}) can be calculated using Sm and Nd mineral/melt distribution coefficients for an assumed source mineralogy and degree of melting. Consideration of both g_{TH} and g allows the construction of more rigidly constrained models for the history of the sample and source than would be possible by either concentration or isotopic studies alone.

The above discussion of fractionation in source regions could have been made in terms of model ages (*Wasserburg and Papamastassiou, 1975*), as is normally done for Rb-Sr. The model age

$$T_M = \frac{1}{\lambda} \ln \left[1 + \frac{(^{143}\text{Nd}/^{144}\text{Nd})_{\text{meas}} - 1}{(^{147}\text{Sm}/^{144}\text{Nd})_{\text{meas}}} \right]. \quad (3)$$

Model ages give a strict upper limit to the time of last major equilibration of a system, but are most powerful where parent-daughter fractionation is large. For small fractionations, $T_M \approx T_c$ and the usefulness of model ages may be diminished. Therefore, we have tended to emphasize here the divergence of secondary growth curves from a primary reference curve. However, iso-

Table 2: Nd evolutionary parameters

Sample	Age (AE)	$^{147}\text{Sm}/^{144}\text{Nd}$	ϵ_0^{CHUR}	ϵ_1^{CHUR}	$f^* T^*$ (10^8 yr)
113031 (MORB)	0	0.1163 \pm 3	+5.4 \pm 0.8	+5.4 \pm 0.8	2.2
111240 (MORB)	0	0.204 \pm 4	+10.3 \pm 0.4	+10.3 \pm 0.4	4.2
113152 (Alk.Ba.)	0	0.2109 \pm 6	+8.7 \pm 0.7	+8.7 \pm 0.7	3.5
BCR (Cont.Ba.)	0	0.14 ^b	+0.1 \pm 0.4	+0.1 \pm 0.4	0.0
Khibina Ap.	0.29 ^d	0.0950 \pm 3	+0.5 \pm 0.3	+3.7 \pm 0.3	1.5
NAS(Shale)	'0'	0.12 ^c	-14.4 \pm 0.5	-14.4 \pm 0.5	-5.8
RHO (Gt. Dyke)	2.53 ^e	0.145 \pm 1	-16.5 \pm 1.0	-0.6 \pm 2.0	-0.3
RN3 (Grd.)	2.65 ^f	0.0996 \pm 3	-31.2 \pm 0.6	+0.9 \pm 1.4	0.2
OGG (Amitsoq)	3.59 ^g	0.118 \pm 1	-35.4 \pm 0.6	-0.3 \pm 1.7	-0.3
NN1	—	—	-29.7 \pm 0.4	—	—
NN2	—	—	-13.8 \pm 0.3	—	—
CHUR ^a	all T	0.1936 ^h	0	0	0

^aCHUR \equiv Chondritic uniform reservoir; $^{143}\text{Nd}/^{144}\text{Nd}$ in CHUR today = 0.511836 (Lugmair, pers. comm.) ^bApproximate value from literature.

^cHaskin *et al.* (1966b), ^dGerasimovsky *et al.* (1974), ^eDavies *et al.* (1970).

^fSteiger and Wasserburg (1969), ^gBaadsgaard (1973), ^hLugmair (pers. comm.)

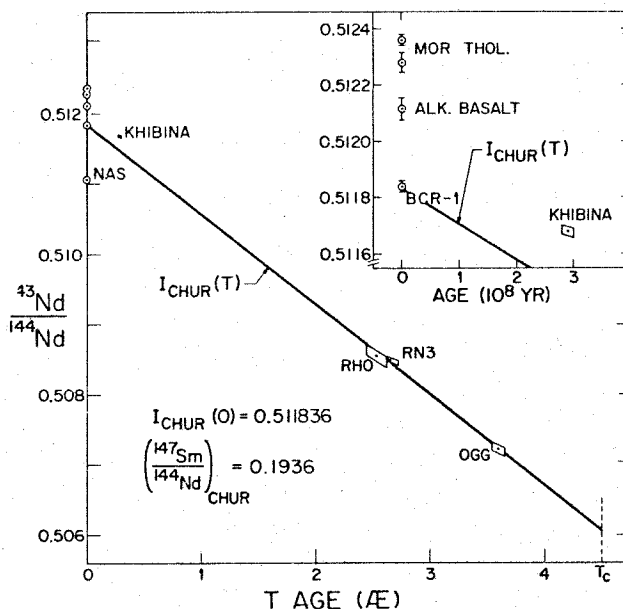


Fig. 2: Observed initial $^{143}\text{Nd}/^{144}\text{Nd}$ versus time. $I_{\text{CHUR}}(T)$ represents evolution of $^{143}\text{Nd}/^{144}\text{Nd}$ in a reservoir with chondritic Sm/Nd.

topic variations are small, so precise measurements and careful consideration will be necessary for their correct interpretation.

The data are given in Table 2 relative to a uniform reservoir whose characteristics are those of the Juvinas achondrite (*Lugmair*, 1974, pers. comm., and *Lugmair et al.*, 1975b). These characteristics were chosen because Juvinas has Sm/Nd very close to the average chondrite (0.308) (*Masuda*, 1973, c.f. *Lugmair*, 1975c) and therefore must approximate a chondritic uniform reservoir (CHUR), allowing direct comparison of terrestrial data to that expected in a chondritic earth. Since this paper was first submitted, we have been informed (*Lugmair*, pers. comm.) of a revised best estimate for $^{143}\text{Nd}/^{144}\text{Nd}$ in Juvinas, which differs significantly from that reported by *Lugmair* (1974). The revised value is used here, so that $I_{\text{CHUR}}(0) = 0.511836$ (normalized to $^{148}\text{Nd}/^{144}\text{Nd} = 0.243082$) and $(^{147}\text{Sm}/^{144}\text{Nd})_{\text{CHUR}} = 0.1936$. Model ages can be calculated relative to the initial value for Juvinas ($I_{\text{JUV}} = 0.50598 \pm 10$) (*Lugmair*, pers. comm.). The evolution of $^{143}\text{Nd}/^{144}\text{Nd}$ in CHUR and initial ratios for the samples are plotted in Fig. 2.

Results. The samples can be divided into two groups; zero age rocks and old rocks. The zero age suite consists of two mid-ocean ridge tholeiitic basalts of high Fe, Ti character (MOR Thol.; USNM113152, USNM111240), one oceanic alkalic basalt (USNM113031) dredged near St. Pauls Rocks (*Melson et al.*, 1967), and a continental basalt (BCR-1). Grouped with these are a sample of apatite ore from the Khibina nepheline syenite complex, USSR, and a composite of the North American shales (NAS) prepared by Paul W. Gast (cf. *Haskin et al.*, 1966b). The old samples include a diabase from the Great Dyke, Rhodesia (RHO), a sample of the granodioritic Preissac-Lacorne batholith in the Superior Province of Canada (RN3), and a granodiorite Amitsoq gneiss sample from West Greenland (OGG). These samples have been well dated by other methods.

The four basalts and the apatite ore have small positive values of ϵ_0^{CHUR} indicating that they were derived from regions whose time-integrated Sm/Nd is close to but somewhat higher than that of chondrites. The shale, however, has a large negative ϵ_0^{CHUR} which undoubtedly reflects the low Sm/Nd of average crustal rocks. The basalts, presumably derived from the mantle, indicate that a range of $^{143}\text{Nd}/^{144}\text{Nd}$ is now found there. The old samples all have low ϵ_0^{CHUR} values, representative of old lithic reservoirs with low Sm/Nd.

To evaluate $^{143}\text{Nd}/^{144}\text{Nd}$ in the mantle in the past a Great Dyke sample was chosen because its basaltic composition and mode of emplacement suggest derivation from the mantle. While it has $\epsilon_0^{\text{CHUR}} = -16.5$, its initial ratio lies within error on CHUR at 2.53 AE (see Figure 2), and is strong evidence that the CHUR curve is indeed relevant to mantle evolution. The other two ancient samples have large negative values of ϵ_0^{CHUR} . Although these rocks have no clear or direct relationship to the mantle, their initial ratios nonetheless also lie on CHUR within errors. For sample RN3, a two-point internal isochron (see tables) yields a Sm-Nd age of 2.64 ± 0.13 AE, in agreement with the U-Th-Pb result (Steiger and Wasserburg, 1969).

The positions of initial ratios relative to the CHUR curve can be seen clearly in Figure 3. In general the data demonstrate that the earth has a chondritic Sm/Nd to within $\sim 5\%$. The variation of ϵ_1^{CHUR} in young basalts indicates the existence of isotopic heterogeneities in their source regions, a phenomenon which was previously known from Pb and Sr isotope variations (Gast, *et al.*, 1964, Tatsumoto, 1966, Gast, 1968, and others). Oceanic tholeiite samples have the highest values of ϵ_1^{CHUR} and must be derived from sources with higher f_S than the other samples. The alkali basalt sample is clearly derived from a different reservoir than the tholeiites. BCR-1 has a much lower ϵ_1^{CHUR} than the oceanic samples, which may indicate gross differences between basalt source regions under continents and those under oceans. However BCR-1 could also have acquired a lower ϵ_1^{CHUR} through contamination from old crustal material. The range in f^*T^* values for the young basalts indicates that for differences of f in the sources of ~ 0.1 , these sources must have been isolated for times > 1 AE.

Basalt 113031 has a low Sm/Nd typical of alkali basalts, but its positive ϵ_1^{CHUR} is evidence that this oceanic alkali basalt is not derived from an ancient source region which is significantly enriched in LREE relative to chondrites. The Khibina apatite sample is from an alkalic complex strongly enriched in LREE (Balashov, 1963, cited in Haskin *et al.*, 1966a), yet ϵ_1^{CHUR} is also positive. Thus this data strongly suggest that the highly fractionated REE patterns in alkali basalts and alkalic intrusions are the result of short-duration magmatic processes rather than the result of derivation from ancient, low Sm/Nd source regions.

The fact that ϵ_1^{CHUR} of the ancient granitic rocks is zero means that these rocks were derived essentially directly from a chondritic Sm/Nd source. This implies derivation from mantle sources, since their ϵ_1^{CHUR} are identical with that of the Great Dyke sample. These data are not compatible with their derivation from much older, highly fractionated material. However, larger errors in ϵ_1^{CHUR} for these samples, resulting from a sum of errors in ϵ_0^{CHUR} , f_R , and the age, when coupled with the smaller time interval ($T_C - T$) place weaker constraints on their sources.

Inspection of Figure 3 shows that the range of ϵ_1^{CHUR} in young samples is larger than in the ancient samples. This may result simply from the fact that the difference in $^{143}\text{Nd}/^{144}\text{Nd}$ in reservoirs with different Sm/Nd grows with time. Alternative-

ly, it may be indicative of a real difference in the degree of heterogeneity in the Archean mantle as compared to the modern mantle.

Partial melting generally produces a liquid with lower Sm/Nd

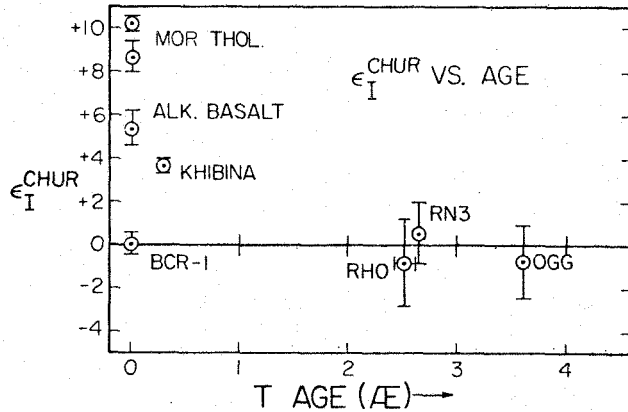


Fig. 3: Fractional deviations in parts in 10^4 of initial $^{143}\text{Nd}/^{144}\text{Nd}$ from evolution in a chondritic Sm/Nd reservoir (CHUR) vs. time.

and a residue with higher Sm/Nd than the starting material. This process tends to produce reservoirs with diverging $^{143}\text{Nd}/^{144}\text{Nd}$. The crust, since it represents the earth's low-melting fraction, must also contain the reservoirs of lowest $^{143}\text{Nd}/^{144}\text{Nd}$. If the Nd in the crust is a significant portion of that in the earth, then there must exist regions of the mantle with high $^{143}\text{Nd}/^{144}\text{Nd}$ corresponding to a high Sm/Nd residue. The source regions of oceanic tholeiites, by virtue of their high $^{143}\text{Nd}/^{144}\text{Nd}$ are the best candidates for this residue. This is clearly consistent with trace element (Gast, 1968, Kay and Gast, 1973) and other isotopic data (Peterman and Hedge, 1971) which indicate that these basalts are derivatives of a mantle which has been left as a residue from previous partial melting. In order to classify mantle source regions as having increased or decreased Sm/Nd on the basis of $^{143}\text{Nd}/^{144}\text{Nd}$, one needs precise knowledge of the bulk earth evolution curve. The CHUR curve appears to be a good first approximation.

The variation of ϵ_I^{CHUR} in the young basalts could be due to differences of Sm/Nd in source regions formed near the time of formation of the earth, or to differences formed by continuous large-scale differentiation and fractionation over a long time scale from some homogeneous initial reservoir, to form secondary reservoirs from which basalts are ultimately derived. The data presently provide no clear-cut indication of which is the case. For instance, tholeiite sample USNM113152 has a model age of 4.50 ± 0.07 AE. Using this datum, the model age of the source is $4.50 (1 + g_{TH})$ AE. If $g_{TH} = 0$, then one would conclude that the source region was formed during a very early terrestrial differentiation, essentially at the time of formation of the earth. But if $g_{TH} < 0$, then it is more likely that the source region for this basalt was generated in fractionation processes which occurred at least a few hundred million years after T_c .

If the isotopic composition and Sm/Nd of the shale are representative of average North American crust, then from f^*T^* we obtain $T^* = 1.5$ AE. This can be taken to be the "mean" age of this crustal material, i.e., the time it was fractionated from the CHUR evolution curve.

Conclusions. From the data presented we conclude that the Sm/Nd, and by inference the REE abundance pattern of the earth, is equal to the average of chondritic meteorites to within a few percent. Variations in $^{143}\text{Nd}/^{144}\text{Nd}$ in young basalts permits the identification of distinctive mantle sources and indicates the preservation of significant heterogeneities in the mantle for times of $\sim 1\text{-}4$ AE. The isotopic data also show that mantle source regions with Sm/Nd different by a factor of two from chondritic are not preserved for longer than a few hundred million years. Average continental crustal material has much lower $^{143}\text{Nd}/^{144}\text{Nd}$ than that found for the mantle, and reflects its low Sm/Nd, resulting from REE fractionation during formation of crust from the mantle.

Acknowledgments. We thank W. G. Melson, P. Vogt, G. Thompson, and L. A. Haskin for providing samples and K. Gschneider for providing high purity Nd metal (normal NN2). Technical assistance and advice from D. A. Papanastassiou, D. Curtis, and F. Tera were invaluable and are gratefully acknowledged. DJD would like to thank Arden Albee for steering him in the direction of this work. Precise Pb isotopic work by A. J. Gancarz (*Gancarz, Tera, and Wasserburg*, 1975) assured us of the antiquity of the Greenland sample collected by project Oldstone. This work represents a return to a problem first attempted using Rb-Sr by Paul W. Gast (*Gast*, 1955, 1960). This work was supported in part by NSF NPS 71-02670 AO5 and NASA NGL 05002188. An outline of these results was published in E&S (*DePaolo and Wasserburg*, 1976). Comments on our cryptography by cognizant colleagues, A. L. Albee, A. J. Gancarz, D. A. Papanastassiou and S. Jacobsen are hereby acknowledged. We appreciate the comments of G. Lugmair and his courtesy in making the revised Juvinas data available. This is contribution No. 2730 of the Div. of Geological and Planetary Sciences.

References

Baadsgaard, H., U-Th-Pb dates on zircons from the early precambrian Amitsoq Gneisses, Godthaab District, West Greenland, *Earth Planet. Sci. Lett.*, 19, 22-28, 1973.

Boynton, W.V., Fractionation in the solar nebula: condensation of yttrium and the rare earth elements, *Geochim. Cosmochim. Acta*, 39, 569-584, 1975.

Davies, R. D., H. L. Allsopp, A. J. Erlank, and W. I. Marston, Sr., isotopic studies on various layered mafic intrusions in southern Africa, *Spec. Publ. Geol. Soc. S. Africa* 1, 576, 1970.

DePaolo, D. J. and G. J. Wasserburg, Nd Isotopic variations and Petrogenetic Models (abs.) E&S 57, 351 (1976).

Eugster, O., F. Tera, D. S. Burnett and G. J. Wasserburg, The isotopic composition of Gadolinium and Neutron capture effects in some meteorites, *J. Geophys. Res.* 75, 2753-2768, 1970.

Gancarz, A. J., F. Tera and G. J. Wasserburg, 3.62AE Amitsoq gneiss from West Greenland and a 4.45AE "Age of the Earth" (abs.) *GSA Abs.* 7, 1081, 1975.

Gast, P. W., Abundance of Sr^{87} during geologic time, *Bull. Geol. Soc. Am.*, 69, 1369-1410, 1955.

Gast, P. W., Limitations on the Composition of the Upper Mantle, *J. Geophys. Res.*, 65, 1287-1297, 1960.

Gast, P. W., Trace element fractionation and the origin of tholeiitic and alkaline magma types, *Geochim. Cosmochim. Acta*, 32, 1057-1086, 1968.

Gast, P. W., G. R. Tilton, and C. Hedge, Isotopic Composition of Lead and Strontium from Ascension and Gough Islands, *Science*, 145, 1181-1185, 1964.

Gerasimovsky, V. I., V. P. Volkov, L. N. Kogarko, and A. I. Polyakov, Kola Peninsula, 206-21, in Sorenson, Ed., *The Alkaline Rocks*. John Wiley and Sons, New York, 62p., 1974.

Haskin, L. A., F. A. Frey, R. A. Schmitt, and R. H. Smith, Meteoritic, Solar and Terrestrial Rare-Earth Distributions, *Physics and Chemistry of the Earth*, 7, 167-321, 1966.

Haskin, L. A., T. R. Wilderman, F. A. Frey, K. A. Collins, C. R. Keedy, and M. A. Haskin, Rare Earths in Sediments, *J. of Geophys. Res.*, **71**, 6091-6105, 1966.

Kay, R. W., and P. W. Gast, The Rare Earth Content and Origin of Alkali-rich Basalts, *Jour. of Geol.*, **81**, 653-682, 1973.

Lugmair, G. W. Sm-Nd ages: a new dating method (abs.), *Meteoritics*, **9**, 369, 1974.

Lugmair, G. W., N. B. Scheinin, and K. Marti, Sm-Nd age of Apollo 17 basalt 75075: Two-stage igneous processes in mare basalt genesis (abs.), *Lunar Sci. VI*, Lunar Sci. Inst., Houston, 531-53, 1975a.

Lugmair, G. W., N. B. Scheinin, and K. Marti, Search for Extinct ^{146}Sm , 1. The isotopic abundance of ^{142}Nd in the Juvinas meteorite, *Earth. Plan. Sci. Lett.*, **27**, 79-84, 1975b.

Lugmair, G. W., N. B. Scheinin, and K. Marti, Sm-Nd Age and History of Apollo 17 Basalt 75075: Evidence for early differentiation of the lunar exterior, *Proc. Lunar. Sci. Conf. 6th*, 1419-1429, 1975c.

Lugmair, G. W., N. B. Scheinin, Sm-Nd Systematics of the Stannern Meteorite, *Meteoritics* **10**, 447-448, 1975.

Masuda, A., N. Nakamura, T. Tanaka, Fine structures of mutually normalized rare-earth patterns of chondrites, *Geochim. Cosmochim. Acta.*, **37**, 239-248, 1973.

Melson, W. G., E. Jarosewich, R. Cifelli, G. Thompson, Alkali Olivine Basalt dredged near St. Paul's Rock, Mid-Atlantic Ridge, *Nature*, **215**, 381-382, 1967.

Nier, A. O., A redetermination of the relative abundances of the isotopes of carbon, nitrogen, oxygen, argon, and potassium, *Phys. Rev.*, **77**, 789-793, 1950.

Peterman, Z. E. and C. E. Hedge, Related Strontium Isotopic and Chemical Variations in Oceanic Basalts, *G.S.A. Bull.*, **82**, 493-500, 1971.

Steiger, R. H. and G. J. Wasserburg, Comparative U-Th-Pb systematics in 2.7×10^9 yr plutons of different geologic histories, *Geochim. Cosmochim. Acta*, **33**, 1213-1232, 1969.

Tatsumoto, M., Isotopic composition of lead in volcanic rocks from Hawaii, Iwo Jima, and Japan, *J. Geophys. Res.*, **71**, 1721-173, 1966.

Wasserburg, G. J. D. A. Papanastassiou, E. V. Nenow, and C. A. Bauman, A Programmable Magnetic Field Mass Spectrometer with On-line Data Processing, *Rev. Sci. Instr.* **40**, 288-295, 1969.

Wasserburg, G. J. and D. A. Papanastassiou, Model Ages, *Nature*, **259**, 159, 1975.

APPENDIX 2

INFERENCES ABOUT MAGMA SOURCES AND

MANTLE STRUCTURE FROM VARIATIONS OF $^{143}\text{Nd}/^{144}\text{Nd}$

D. J. DePaolo and G. J. Wasserburg

The Lunatic Asylum of the Charles Arms Laboratory, Division of Geological and Planetary Sciences*,
California Institute of Technology, Pasadena, California 91125

Abstract: Continental flood basalts and mid-ocean ridge (MOR) tholeiitic basalts have distinctly different $^{143}\text{Nd}/^{144}\text{Nd}$ which may permit *a priori* distinction between "continental" and "oceanic" igneous rocks. Initial $^{143}\text{Nd}/^{144}\text{Nd}$ of continental igneous rocks through time fall on a Sm/Nd evolution curve with chondritic REE abundance ratio. These observations indicate that many continental igneous rocks are derived from a reservoir with chondritic REE pattern which may represent primary material remaining since the formation of the earth. Oceanic igneous rocks are derived from a different ancient reservoir which has Sm/Nd higher than chondritic. Initial $^{143}\text{Nd}/^{144}\text{Nd}$ and $^{87}\text{Sr}/^{86}\text{Sr}$ in young basalts from both oceans and continents show a strong correlation suggesting that Sm-Nd and Rb-Sr fractionation events in the mantle may be correlative and caused by the same process. From this correlation Rb/Sr for the earth is inferred to be 0.029.

This study was undertaken to determine if there exists a systematic difference in $^{143}\text{Nd}/^{144}\text{Nd}$ between young volcanic rocks from ocean basins and continental areas. It builds upon a small body of Nd isotopic data which suggested this contrast (DePaolo and Wasserburg, 1976, referred to as DPW). In the same study it was shown that continental igneous rocks of varying ages appear to be derived from a single uniform reservoir with chondritic relative REE abundances. Typical old continental crustal material was found to have $^{143}\text{Nd}/^{144}\text{Nd}$ today which is drastically different from that of young basalts suggesting that $^{143}\text{Nd}/^{144}\text{Nd}$ could be used to identify products of remelted ancient crust. This study tests with an extended data base the hypotheses that continental igneous rocks through time have been derived from a uniform reservoir with chondritic Sm/Nd (CHUR) and that oceanic igneous rocks are derived from a distinctly different reservoir. In addition it presents evidence that variations in initial $^{143}\text{Nd}/^{144}\text{Nd}$ and $^{87}\text{Sr}/^{86}\text{Sr}$ in young volcanic rocks are correlated.

To test these hypotheses $^{143}\text{Nd}/^{144}\text{Nd}$, $^{87}\text{Sr}/^{86}\text{Sr}$, Sm/Nd and Rb/Sr were measured in three groups of samples. 1) Mid-ocean ridge (MOR) tholeiitic basalts and continental flood basalts were measured to compare oceanic and continental magmas, since these represent the most voluminous lava types found in the two settings; 2) Samples of various volcanic lithologies from continents, including alkali basalt, rhyolite, and a carbonatite and basalts from oceanic islands were measured to further explore the variations found in young volcanic rocks; 3) Initial $^{143}\text{Nd}/^{144}\text{Nd}$ in five more Precambrian continental intrusive rocks of various ages were determined to further evaluate the uniform reservoir hypothesis for continental igneous rocks.

Analytical Procedure and Data: Chemical separation of Sm and Nd and mass spectrometry have been described by Eugster et al. (1970) and DPW. For all samples measured in this study, no corrections to Nd isotope ratios were necessary due to interferences from other species in the ion spectra or from chemistry blank. The intensity of the ^{144}NdO ion beam was between 3 and 6×10^{-11} A during data acquisition. All Nd isotopes were measured in every run. The measured values for the non-radiogenic Nd isotopes for all runs are shown in Figure 1. Strontium was separated using conventional ion exchange techniques. $^{87}\text{Sr}/^{86}\text{Sr}$ are normalized to $^{86}\text{Sr}/^{88}\text{Sr} = 0.1194$. Isotopic data, locations, and lithologic classifications for all samples are given in Table 1 and summarized in Figures 2, 3, and 4. Nd data are expressed using the notation of DPW.

Results. 1. *Continental Flood Basalt and MOR Tholeiites:* Nd isotopic data for these samples are shown in a histogram in Figure 2a. Included in this figure are data from DPW on two MOR tholeiites and BCR-1. BCR-1 was selected as representative of the chemically and (Sr) isotopically uniform Yakima basalts of the Columbia River province, the most voluminous lava type found in that province (McDougall, 1976). The Picture Gorge sample (PG16D) was selected for analysis because it is petrochemically distinct from BCR-1. Its $\epsilon_{\text{P}}^{\text{CHUR}}$ is much different than what appears to be the normal range for continental tholeiites, showing affinities to oceanic basalts. Sample PEA-3 was taken from an old collection and was assumed to be a Karroo basalt as it was labelled. Discussion of this sample must be deferred until it can be documented that its $\epsilon_{\text{P}}^{\text{CHUR}}$ is not a result of an incorrect age assignment. If the age is correct, this sample could be the product of massive crustal contamination or a derivative of a special mantle reservoir. As seen in the figure, the samples fall into two distinct groups. The MOR basalts have $\epsilon_{\text{P}}^{\text{CHUR}}$ averaging $\sim +10$ and ranging from $+7$ to $+12$ while continental flood basalts have $\epsilon_{\text{P}}^{\text{CHUR}}$ averaging ~ 0 and showing a range from -4 to $+2$. This striking data array confirms the existence of a profound difference in $^{143}\text{Nd}/^{144}\text{Nd}$ between major basalt provinces in continental and oceanic regions. It implies the existence of two distinctly different, widespread mantle magma sources. From the difference of f^*T^* values of $\sim 4 \times 10^8$ yr for the two groups of samples (Table 1), and assuming a difference of f_S of less than 0.4, we calculate that these two reservoirs must have been separate for at least 10^9 years. Thus MOR tholeiites and continental flood tholeiites appear to be derived from two ancient, profoundly different reservoirs in the earth's mantle. Differences in concentrations of certain minor and trace elements between these two lithologic types (Schilling, 1971; Haskin et al., 1966) thus are most likely a reflection of

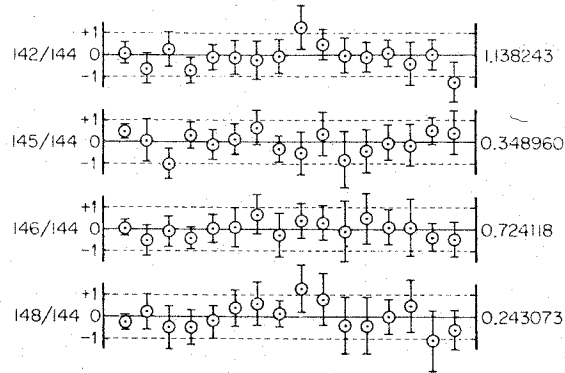


Fig. 1: Measured values of non-radiogenic Nd isotope ratios for each run plotted as fractional deviations in parts in 10^4 from the average of 16 runs given at right. Ratios are normalized to $^{140}\text{Nd}/^{142}\text{Nd} = 0.2096$; error bars are $2\sigma_{\text{mean}}$. These data demonstrate that reproducibility of measured ratios is ± 5 parts in 10^5 or better. Measurements of non-radiogenic isotopes are used in this laboratory as an indication of data quality.

ancient differences rather than a result of differentiation processes occurring at the time of magma generation as has been suggested (Schilling, 1971). The nominal value of $\epsilon_{\text{I}}^{\text{CHUR}} \approx 0$ for the continental flood basalts indicates they are derived from a reservoir which has maintained an unfractionated, chondritic Sm/Nd throughout the history of the earth. The MOR basalts, however, are derived from a reservoir which has had Sm/Nd at least 10% greater than chondritic.

II. *Other young volcanic rocks:* Nd isotopic data on these samples, plus an alkali basalt from the mid-Atlantic Ridge (OAB-1) (113031 of DPW) and three ocean island samples from Richard et al. (1976) are shown in Figure 2b. With the exception of two samples, the oceanic rocks have significantly higher $\epsilon_{\text{I}}^{\text{CHUR}}$ than the continental samples. For the most part ocean island basalts (both tholeiitic and alkalic) have $\epsilon_{\text{I}}^{\text{CHUR}}$ of +4 to +8, somewhat lower than those of the MOR tholeiites but definitely higher than the majority of continental basalts. The alkali basalts give no indication of being derived from an ancient light - REE enriched source, as has been suggested by Sun and Hanson (1975). Such a reservoir would yield basalts with $\epsilon_{\text{I}}^{\text{CHUR}} = -10$ to -30. Sample OLC-1 from a Na, Ca-carbonate lava flow represents an extreme rock type with highly fractionated REE pattern and high REE concentrations, but has $\epsilon_{\text{I}}^{\text{CHUR}}$ identical to the average continental flood basalt. This sample thus gives no evidence that carbonatites are derived from unique mantle reservoirs. The Hawaiian tholeiite has $\epsilon_{\text{I}}^{\text{CHUR}}$ similar to those of the continental flood basalts. A melilite nephelinite from the same island, however, has a drastically different $\epsilon_{\text{I}}^{\text{CHUR}}$, similar to those found in other ocean island basalts and in MOR tholeiites. Thus these two basalts are derived from different reservoirs despite their coincident location. These data again show that a single volcanic conduit system can access a variety of mantle reservoirs of distinctive chemistry and age. The tholeiite sample provides the only evidence that the reservoir represented by the continental flood basalts is present in oceanic areas. The Pisgah crater alkali basalt (PCB) differs markedly from the other continental basalts. Its $\epsilon_{\text{I}}^{\text{CHUR}}$ is similar to oceanic basalts and identical to that of the Picture Gorge sample. This basalt may be representative of the mantle underlying the Basin and Range province of the western United

Table 1: Nd evolutionary parameters and ${}^{87}\text{Sr}/{}^{86}\text{Sr}^a$

Sample	Age (AE)	$\frac{{}^{147}\text{Sm}}{{}^{144}\text{Nd}}$	ϵ_{CHUR}^0	ϵ_{CHUR}	$f^*\Gamma^*$ (10^8 yr)	$\left(\frac{{}^{87}\text{Sr}}{{}^{86}\text{Sr}}\right)_1$
I. Continental Flood Basalts						
PG-16D (Picture Gorge tholeiite, Columbia R. province)	0	nm	+6.6±0.5	+6.6±0.5	2.7	0.7034±6
DTB-8 (tholeiite, Mahabaleshwar plateau, Deccan, India)	0.05	0.1645	+1.5±0.7	+1.7±0.7	0.7	0.70413±12
SK-38 (tholeiite, Miki's Fjord, E. Greenland)	0.05	0.1329	-4.3±0.6	-3.9±0.6	-1.6	0.70540±11
SWB-1D (tholeiite, Stormberg series, Warmbad, S. Africa)	0.15	0.1691	-1.2±0.5	-0.7±0.5	-0.3	0.70630±6
PEA-3 (Karroo ? basalt, Mozambique)	0.15?	0.1170	-20.1±1.6	-18.6±1.6	-7.5	nm
PD-1 (Palisades diabase, 200' above base, Edgewater, N.J.)	0.20 ^b	0.1540	-1.2±0.7	-0.2±0.7	-0.1	0.70604±10
II. Mid-ocean Ridge tholeites						
VG295 (tholeiite, mid-Atlantic Ridge, 22.5N, 45W)	0	nm	+10.6±0.9	+10.6±0.9	4.3	0.70226±6
BD37-2 (tholeiite, mid-Atlantic R.; DSDP 37-332B-19-1)	0	0.1930	+11.0±3.0	+11.0±3.0	4.5	nm
BD17-1 (tholeiite, central Pacific; DSDP 17-164-28-6)	0.15 ^c	0.1988	+7.4±1.3	+7.4±1.3	3.0	nm
III. Other young volcanic rocks						
OLC-1 (carbonatite, Oldoinyo Lengai, Tanzania)	0	nm	+0.1±0.9	+0.1±0.9	0.0	nm
HN-1 (nephelinite, Oahu; USNM 113095-50)	0	0.1229	+7.3±0.6	+7.3±0.6	3.0	0.70320±8
HT-1 (tholeiite, Oahu; USNM 113095-60)	0	0.1590	+0.8±0.6	+0.8±0.6	0.3	0.70403±6
RGB-1 (alk. olivine basalt, Rio Grande Rift)	0	nm	+0.2±0.7	+0.2±0.7	0.1	0.70436±12
LAK-8D (tholeiite, Mt. Konocti, California)	0	0.112j	+1.3±0.8	+1.3±0.8	0.5	nm
GT-2 (tholeiite, Galapagos Is.; USNM 113180, F436)	0	0.1155	+6.2±0.8	+6.2±0.8	2.5	nm
PCB-1 (alk. basalt, Pisgah Crater, California)	0	0.1228	+6.2±0.8	+6.2±0.8	2.5	0.70346±6
IV. Precambrian intrusive rocks						
ZL-3D (Town Mtn. Granite, Llano, Texas)	1.01 ^d	0.1420	-4.4±0.7	+2.3±0.8	0.9	(0.706) ^d
DUL-4 (Anorthositic gabbro, Duluth complex, Minn.)	1.13 ^e	0.1036	-14.5±0.6	-1.7±0.7	-0.7	0.70655±7
MP22D (shonkinite, Mtn. Pass, California)	1.4-1.7 ^f	0.1053	-19.9±0.4	-3.0	-1.2-0	nm
WYWR-4D (Louis Lake granodiorite, Wind R. Mtns., Wyo.)	2.65 ^g	0.1095	-29.6±0.6	-0.9±1.0	-0.4	nm
WGA-210 (Fiskennasset anorthosite, West Greenland)	2.8 ^h	0.1146	-29.9±0.8	-1.1±1.7	-0.4	nm

Initial ${}^{87}\text{Sr}/{}^{86}\text{Sr}$ of OAB-1 (113031 of DPW) = 0.70287 ± 15 ; 111240 (DPW) = 0.70236 ± 11

^aNd data normalized as in DPW ^bErikson and Kulp (1961) ^cDSDP Inventory of Igneous Rock Recovery (1973) ^dZartman (1964)

^eSilver and Green (1972) ^fLamphere (1976); Black et al. (1973) ^gNaylor, et al. (1969) ^hGancarz (1976); Black et al. (1973) ⁱBowman, et al. (1973)

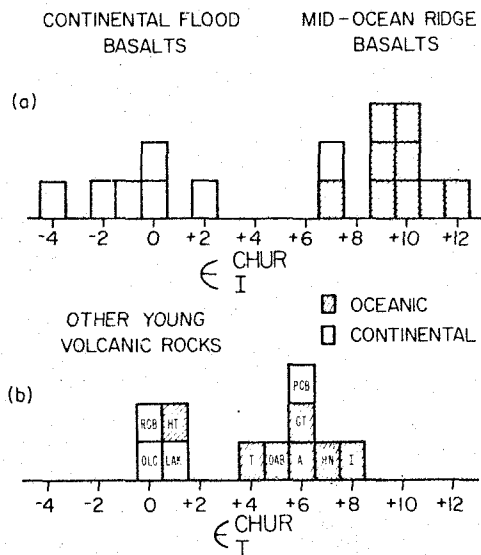


Fig. 2: Histograms of Nd isotopic results on young volcanic rocks and the Duluth gabbro, normalized as in DPW. In 2a) mid-ocean ridge samples include samples ARP74, PDIP, 111327, and AD3-3 of *Richard, et. al.* (1976). In 2b) samples T, A, and I are samples TF110, T4, and NAL27 of *Richard, et. al.* (1976).

States which resembles oceanic mantle in seismic structure and heat flow. $\epsilon_{\text{I}}^{\text{CHUR}}$ of the rhyolite sample is the same as that of the continental basalts, indicating that it appears to be derived from the same reservoir as the basalts.

III. Precambrian igneous rocks: All of the Precambrian samples analyzed, with the exception of the Mountain Pass sample, have been well-dated by other methods. The values of $\epsilon_{\text{I}}^{\text{CHUR}}$ as a function of age for all continental samples measured in this work and by DPW are shown in Figure 3. Of the samples analyzed in this work WYWR-4D and WGA210 fall within error on the CHUR evolution curve, and ZL-3D lies slightly above. The Duluth gabbro sample DUL-4, which represents an ancient continental basalt, lies slightly below the curve. MP22D is not plotted due to uncertainty in its age (Lanphere, 1964). However, the age of MP22D is bracketed between 1.4 and 1.7 AE so that its $\epsilon_{\text{I}}^{\text{CHUR}}$ must be between -3 and 0. Thus all of the Precambrian intrusive rocks, representing a wide variety of rock types, as well as the young continental volcanics appear to be derived from an *approximately* uniform, chondritic-Sm/Nd reservoir. Note in particular that four samples with ages of 2.5 to 2.8 AE from widely separated localities all lie within error on the curve and closely limit the position of the growth curve at 2.6 AE. Among the continental samples studied are gabbroic rocks which are taken to represent ancient continental flood basalts. All these data, when considered with the "zero" age continental samples, provide strong evidence that the CHUR curve describes Nd evolution in an important and widespread reservoir, most probably the mantle, and as such, can be taken as a representation of the bulk earth's evolution curve. As discussed by DPW, definition of the bulk earth evolution curve is necessary in order to infer what processes are responsible for variations of $\epsilon_{\text{I}}^{\text{CHUR}}$. The CHUR evolution curve given here was calculated from data of *Lugmair* (pers. comm.) on the

Juvinas achondrite which has Sm/Nd within 1% of the average of ordinary chondrites (0.309 atom ratio) as determined by *Masuda et. al.* (1973) and *Nakamura* (1974). Thus the earth appears to have Sm/Nd and presumably REE relative abundances essentially identical to chondritic meteorites.

Discussion: The data shown in Figure 3 clearly suggest that the source of magmas during the first 2 AE of Earth history was a uniform chondritic-Sm/Nd reservoir. *DPW*, however, suggested that this might only appear to be the case since the Sm/Nd heterogeneities of ~ 10% which can be inferred from Nd isotopic variations to exist today, may have produced only indiscernable isotopic differences 3 AE ago. However, as shown by *Lugmair* (1975) and *Lugmair, et. al.* (1976), data for the moon show no suggestion of a long-lived, uniform magma source with chondritic Sm/Nd. Lunar basalts with ages of 3.3-4.0 AE show a range of $\epsilon_{\text{I}}^{\text{CHUR}}$ from +7 to -2 which is much larger than the range shown by the terrestrial samples which were formed a billion years later. The lunar data clearly indicate that planetary differentiation processes exist which could have caused sufficient Sm/Nd fractionation to produce large variations in $\epsilon_{\text{I}}^{\text{CHUR}}$ in old terrestrial rocks. Thus the terrestrial data suggest that the earth, unlike the moon, did not undergo an early differentiation event which greatly fractionated the rare earth elements, or if it did, a mixing process operated during the subsequent AE to erase the variation of Sm/Nd produced in this event.

The data shown in Figure 3 also provide information on the origin of silicic rocks in the continental crust. As seen in Figure 3 all silicic rocks have $\epsilon_{\text{I}}^{\text{CHUR}} \sim 0$. Thus remelting of much older continental crust does not appear to be important in the formation of silicic igneous rocks. This surprising result strongly suggests that most continental igneous rocks are derived from ancient reservoirs, possibly original materials undifferentiated over all of geologic time.

The observation that the CHUR evolution curve is the locus of initial ratios of continental igneous rocks attaches age significance to the measured $^{143}\text{Nd}/^{144}\text{Nd}$ of these rocks. If the initial $^{143}\text{Nd}/^{144}\text{Nd}$ is given by the CHUR curve then measurement of $^{143}\text{Nd}/^{144}\text{Nd}$ and $^{147}\text{Sm}/^{144}\text{Nd}$ in any continental rock today gives a model age (T_{CHUR}):

$$T_{\text{CHUR}} = \frac{1}{\lambda} \ln \left[1 + \frac{^{143}\text{Nd}/^{144}\text{Nd}_{\text{meas}} - 1_{\text{CHUR}}(0)}{^{147}\text{Sm}/^{144}\text{Nd}_{\text{meas}} - (^{147}\text{Sm}/^{144}\text{Nd})_{\text{CHUR}}} \right]$$

T_{CHUR} may provide a real "crust-formation" age for a wide variety of rocks, since studies to date have shown that metamorphism does not significantly affect REE patterns (*Haskin et. al.*, 1968). T_{CHUR} ages may be a way to see past metamorphic events to the time when the sialic material differentiated from its source region.

The data reported here imply the existence of at least two distinct ancient magma sources, one which supplies the MOR

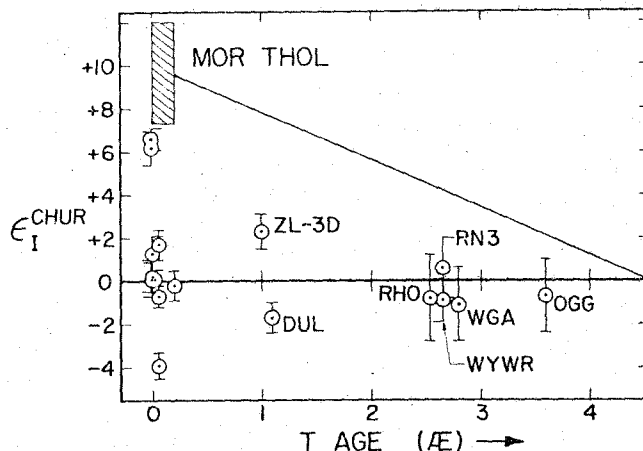


Fig. 3: ϵ_I^{CHUR} vs. Age with points plotted for all continental samples. Field of mid-ocean ridge (MOR) tholeiites is shown at upper left with simple growth curve diverging from CHUR at 4.5 AE.

basalts ($\epsilon_I^{\text{CHUR}} \approx +10$) and one which supplies continental rocks ($\epsilon_I^{\text{CHUR}} \approx 0$). The ocean island samples ($\epsilon_I^{\text{CHUR}} \approx +6$) may either represent a third magma source, or a blend of the other two. This grouping is not a detailed description of the data as evidenced by the sizeable dispersion within each group, but is used here to assess some elementary models. For simplicity, let us assume only two *sources* exist, that of the continental rocks (CHUR) and that of the MOR basalts (MORR). Any model given to explain the distribution of magmas derived from these sources must take into account the constraints that 1) CHUR supplies continental igneous rocks for all time and rarely supplies magmas in oceanic areas and 2) MORR supplies oceanic igneous rocks and rarely supplies magmas in continental areas. In addition, in the process of making continental crust with low Sm/Nd, residual matter (C*) from CHUR is left with increased Sm/Nd. This material may then evolve the Nd isotopic character of MORR after a time period of ~ 1 AE. Thus CHUR and MORR may be distinct entities dating from the formation of the earth (congenital sources), or MORR (=C*) may be derived from CHUR in the process of making continental crust (evolved sources).

One possible interpretation of the data might be that with the exception of a few anomalous areas, CHUR is found only under continents and MORR only under oceans. For stationary continents this model would be acceptable for the congenital case. For the case of evolved sources a mechanism for allowing the residual material C* from CHUR to migrate from under the continents to under the oceans over times of ~ 1 AE or more is necessary. For drifting continents it is necessary that CHUR is attached to the continents. This presents a problem in that the amount of mantle present in the attached lithosphere beneath the continents is at best barely sufficient to supply the Nd now present in the continents if primitive mantle has Nd equal to $\sim 2x$ chondrites and continental crust has $\sim 25x$ chondrites (Taylor, 1976).

Alternatively both sources could be present under both continents and oceans. MORR (shallow) supplies the MOR basalts but is essentially inactive under continents. CHUR (deep) is active under continents and oceans, but in oceanic regions its products are volumetrically insignificant in comparison to those of MORR. This configuration is much the same as hypotheses of mantle plumes (Morgan, 1971, Wilson, 1965) and may provide a reasonable explanation of the basalt data. That is, most continental basalts and some oceanic basalts are derived from diapirs originating from CHUR deep in the mantle. This would imply that continental granitic rocks are also derived from the same deep mantle sources.

A third possibility would be that MORR exists at shallow levels only under oceans and at deeper levels under both continents and oceans. At shallow levels beneath the continents a region with the isotopic character of CHUR is maintained in a

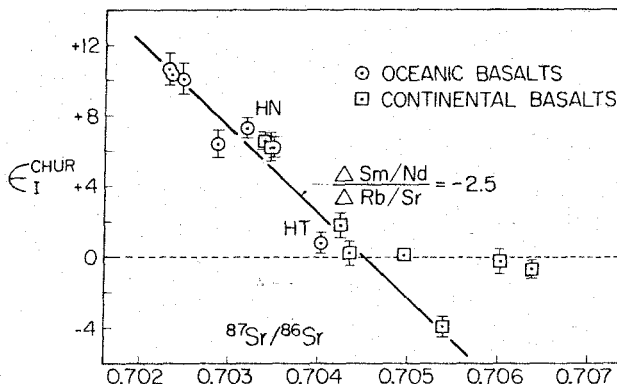


Fig. 4: ϵ_I^{CHUR} vs. initial $^{87}\text{Sr}/^{86}\text{Sr}$ for young basalts. Included are two samples from Richard, et. al. (1976) (PDIP, ARP74) and BCR-1 ($^{87}\text{Sr}/^{86}\text{Sr}$ for BCR-1 from Pankhurst and O'Nions, 1973). The solid line shows the inferred trend of the correlation and the relative magnitudes of correlated variations of Rb/Sr and Sm/Nd necessary to produce such a trend. The dashed line indicates the trend defined by four continental basalt samples which have $\epsilon_I^{\text{CHUR}} \approx 0$ but different $^{87}\text{Sr}/^{86}\text{Sr}$, all lying to the right of the main correlation line. This trend may result from contamination of magmas with crustal radiogenic Sr or indicate the existence of magma sources which have become enriched in Rb relative to Sr, but have retained unchanged Sm/Nd. Should new data populate the correlation line to values of ϵ_I^{CHUR} much less than zero, it would require serious revision of the simple two-reservoir model.

dynamic steady state. In this region Nd is continually transported to and stored in the crust in preference to Sm, but is continually replenished from MORR below or by transfer in subduction zones where material from MORR passes beneath the continent. This model requires a delicate balance but is consistent with drifting continents while still implying a fundamental chemical difference between suboceanic and subcontinental mantle.

Correlation of Sr and Nd: Data on samples for which both Nd and Sr isotopes were measured are shown in Figure 4 and show a correlation between initial Nd and Sr. The MOR basalts have the lowest $^{87}\text{Sr}/^{86}\text{Sr}$ and highest ϵ_I^{CHUR} while the continental basalts have highest $^{87}\text{Sr}/^{86}\text{Sr}$ and lowest ϵ_I^{CHUR} . Oceanic alkali basalts are intermediate but can be distinguished from the continental samples. This correlation suggests that Sm-Nd and Rb-Sr fractionation in the formation of magma

sources in the mantle are correlative. Samples PD-1 and SWB-1D may represent cases where significant Sr contamination occurred but the Nd isotopes were essentially unaffected. This possibility is plausible since reservoirs of extremely radiogenic Sr exist in the continental crust which could act as contaminants, whereas the existence of reservoirs of extreme Nd isotopic composition is unlikely due to the limited variation of Sm/Nd in nature. This suggests that Nd may provide a better tool for the study of sub-continental mantle magma sources than Sr. From Figure 4 it can be seen that a value of $\epsilon_{\text{CHUR}}^{\text{Nd}} = 0$ corresponds roughly to $^{87}\text{Sr}/^{86}\text{Sr} \sim 0.7045$. If $\epsilon_{\text{CHUR}}^{\text{Nd}} = 0$ represents an unfractionated reservoir then 0.7045 ± 5 might be taken as the present value of $^{87}\text{Sr}/^{86}\text{Sr}$ in unfractionated mantle. From this number and BABI we calculate Rb/Sr of unfractionated mantle material to be $0.029 \pm .003$. A $^{87}\text{Sr}/^{86}\text{Sr}$ growth curve calculated from this Rb/Sr may be more useful for interpretation of initial $^{87}\text{Sr}/^{86}\text{Sr}$ of ancient rocks than is one calculated from the present value of $^{87}\text{Sr}/^{86}\text{Sr}$ in MOR rocks (~ 0.7025).

Acknowledgements. We thank J. Gittins, T. Simkin, W. S. Baldridge, H. R. Bowman, W. G. Melson, G. Thompson, Tj. H. van Andel, V. Bowen, T. Bence, A. R. Mc Birney, A. J. Gancarz, L. T. Silver, and G. Goles for providing samples. This work was supported by NASA Grant NGL 05-002-188 and NSF Grant PHY 76-02724.

References

Black, L. P., S. Moorbath, R. J. Pankhurst, B. F. Windley, $^{207}\text{Pb}/^{206}\text{Pb}$ whole rock age of the Archaean granulite facies metamorphic event in West Greenland, *Nature*, 244, 50-53, 1973.

Bowman, H. R., F. Asaro and I. Perlman, On the uniformity of composition in obsidians and evidence for magmatic mixing, *J. Geol.*, 81, 312-327, 1973.

DePaolo, D. J. and G. J. Wasserburg, Nd isotopic variations and petrogenetic models, *GRL*, 3, 249-252, 1976.

Eriksen, G. P. and J. L. Kulp, Potassium-Argon measurements on the Palisades Sill, New Jersey, *Bull. G.S.A.*, 72, 649-652, 1961.

Eugster, O., F. Tera, D. S. Burnett, and G. J. Wasserburg, The isotopic composition of Gadolinium and neutron capture effects in some meteorites, *J. Geophys. Res.*, 75, 2753-2768, 1970.

Gancarz, A. J., I. Isotopic Systematics in Archean Rocks: West Greenland, unpublished Ph. D. thesis, California Inst. of Technology, 1976.

Haskin, L. A., M. A. Haskin, F. A. Frey, T. R. Wildeman, Relative and Absolute Terrestrial Abundances of the Rare Earths, in *Origin and Distribution of the Elements*, Ahrens, ed., Pergamon, 1178 pp, 1968.

Haskin, L. A., F. A. Frey, R. A. Schmitt, and R. H. Smith, Meteoritic, solar, and terrestrial rare-earth distributions, *Physics and Chemistry of the Earth*, 7, 167-321, 1966a.

Haskin, L. A., T. R. Wildeman, F. A. Frey, K. A. Collins, C. R. Keedy, and M. A. Haskin, Rare earths in sediments. *J. of Geophys. Res.*, 71, 6091-6105, 1966b.

Lanphere, M. A., Geochronologic studies in the eastern Mojave Desert, California, *J. Geol.*, 72, 381-399, 1964.

Lugmair, G. W., Sm-Nd systematics of some Apollo 17 basalts, in *Origins of Mare Basalts*, ISI, 205p, 1975.

Lugmair, G. W., K. Marti, J. P. Kurtz, N. B. Scheinin, History and Genesis of Lunar Troctolite 76535 or: How old is old? (in press) 1976.

Masuda, A., N. Nakamura, T. Tenaka, Fine structures of mutually normalized rare-earth patterns of chondrites, *Geochim. Cosmochim. Acta*, 37, 239-248, 1973.

McDougall, I., Geochemistry and origin of basalt of the Columbia River Group, Oregon and Washington, *G.S.A. Bull.*, 87, 777-792, 1976.

Morgan, W. J., Convection plumes in the lower mantle, *Nature*, 230, 42-43, 1971.

Nakamura, N., Determination of REE, Ba, Fe, Mg, Na and K in carbonaceous and ordinary chondrites, *Geochim. Cosmochim. Acta*, 38, 757-775, 1974.

Naylor, R. S., R. H. Steiger, and G. J. Wasserburg, U-Th-Pb and Rb-Sr systematics in 2700×10^6 -year old plutons from the southern Wind River Range, Wyoming, *Geochim. Cosmochim. Acta*, 34, 1133-1159, 1970.

Pankhurst, R. J., and R. K. O'Nions, Determination of Rb/Sr and $^{87}\text{Sr}/^{86}\text{Sr}$ ratios of some standard rocks and evaluation of X-ray fluorescence spectrometry in Rb-Sr geochemistry, *Chem. Geol.*, 12, 127-136, 1973.

Richard, P., N. Shimizu, and C. J. Allegre, $^{143}\text{Nd}/^{146}\text{Nd}$, a natural tracer: An application to oceanic basalts, *Earth Plan. Sci. Letters*, 31, 269-278, 1976.

Schilling, J. G., Sea-floor evolution: rare-earth evidence, *Phil. Trans. Roy. Soc. Lond. A*, 268, 663-706, 1971.

Silver, L. T. and J. C. Green, Time constants for Keweenawan igneous activity, *G.S.A. Abs.*, 4, 665, 1972.

Sun, S. S. and G. N. Hanson, Origin of Ross Island Basanitoids and limitations upon the heterogeneity of mantle sources for alkali basalts and nephelinites, *Cont. Min. Pet.*, 52, 77-106, 1975.

Taylor, S. R., Island arc models and the composition of the continental crust, Ewing Symposium, in press; 1976.

Wilson, J. T., Submarine fracture zones, aseismic ridges and the ICSU line: Proposed western margin of the East Pacific ridge, *Nature*, 207, 907-911, 1965.

Zartman, R. E., A geochronologic study of the Lone Grove Pluton from the Llano Uplift, Texas, *J. Petrol.*, 5, 359-408, 1964.

(Received September 30, 1976;
accepted November 4, 1976.)

APPENDIX 3

THE SOURCES OF ISLAND ARCS AS
INDICATED BY Nd AND Sr ISOTOPIC STUDIES

D. J. DePaolo and G. J. Wasserburg

The Lunatic Asylum, Div. of Geological and Planetary Sciences,

California Institute of Technology, Pasadena, California 91125

Abstract: Island arc lavas from New Britain and the Marianas have $^{143}\text{Nd}/^{144}\text{Nd}$ similar to other oceanic basalts and distinctly different from continental flood basalts and thus appear to be derived from a high Sm/Nd, light-REE-depleted reservoir. Consideration of both Nd and Sr isotopes suggests seawater involvement in the generation of some island arc lavas and thus indicates that they may be derived from altered subducted oceanic crust. Other island arc lavas show no evidence of seawater involvement and may be derived from mantle reservoirs with affinities to the sources of ocean island basalts. Andesite and rhyolite from an Andean volcano reflect assimilation of old continental crust. Nd and Sr in basaltic and ultrapotassic continental rocks indicate that some mafic magmas in continental regions may be derived from old low-Sm/Nd reservoirs or are heavily contaminated with old continental crustal material. Fish debris from the ocean floor provides an estimate of $^{143}\text{Nd}/^{144}\text{Nd}$ in seawater and indicates that light-REE in the marine environment are derived mainly from continents. Basalts erupted above sea level in oceanic and continental areas are isotopically distinct from those erupted on the ocean floor, suggesting a relationship between parental reservoirs and hydrostatic head.

This paper presents Nd and Sr isotopic data on lavas from oceanic island arcs which were obtained to (1) characterize the source of island arc magmas, (2) determine if these magmas are derived from mantle reservoirs which may be associated with either the sources of oceanic basalts or the sources of continental basalts, and (3) relate these observations to the role of island arcs in the growth of continental crust.

DePaolo and Wasserburg [1976a,b] (referred to as DPW, 1976a,b) showed that continental flood basalts are derived from reservoirs which have approximately chondritic Sm/Nd ratios. Mid-ocean ridge (MOR) tholeiitic basalts appear to be derived from ancient reservoirs (>1 AE old) which are distinct from those of the continental basalts and characterized by higher Sm/Nd [see also *Richard, Shimizu and Allegre*, 1976]. Basalts from oceanic islands have $^{143}\text{Nd}/^{144}\text{Nd}$ intermediate between MOR basalts and continental flood basalts and may represent a third type of reservoir from which basalts are derived. *O'Nions, Hamilton and Evensen* [1977] expanded the data on ocean island basalts and confirmed that they form a coherent group based on $^{143}\text{Nd}/^{144}\text{Nd}$. DPW [1976a,c] and *O'Nions et al.* [1977a] also showed that for young volcanic rocks with $^{87}\text{Sr}/^{86}\text{Sr}$ less than 0.705 there is a strong correlation between initial $^{143}\text{Nd}/^{144}\text{Nd}$ and $^{87}\text{Sr}/^{86}\text{Sr}$.

We have measured samples of basalt, andesite and dacite from two oceanic volcanic arcs to compare their Nd and Sr isotopic compositions with continental and other oceanic volcanic rocks. Nd isotope data provides a means of evaluating the sources of island arc magmas which is not sensitive to seawater contamination which has complicated interpretation of Sr isotope data [cf. *Meijer*, 1976]. We have concentrated primarily on rocks from volcanic arcs built upon oceanic crust

to avoid problems of crustal contamination. In particular, the Marianas Arc is far from possible interferences from continental material. New Britain is the only arc segment built upon oceanic crust which contains the entire range of magma compositions from basalt to rhyolite, and has been extensively studied by *Johnson* [1976]. Samples from a volcano in the Andes of South America, a province which has been associated with the addition of island arc materials to continents, have been included in order to compare possible arc materials in the continental margin environment. A sample of gabbro from a major linear batholith belt, which may have formed in a setting similar to an island arc, is also included. Fish bone detritus has been measured to estimate $^{143}\text{Nd}/^{144}\text{Nd}$ in present day ocean water. In addition analyses of continental basic lavas confirm the existence of samples with initial $^{143}\text{Nd}/^{144}\text{Nd}$ far displaced from the CHUR evolution curve.

Samples. Island arc samples analyzed are listed in Table 1. All of the island arc samples appear extremely fresh in thin section and show no evidence of having been affected by post-crystallization alteration. KAS-2 is a Karroo basalt from the Stormberg series in South Africa while PEA-3 is a Karroo basalt from Mozambique. PEA-3 was measured by DPW [1976b] but its age assignment was considered uncertain. A total K-Ar age on this sample of 103 m.y., obtained through the courtesy of S. P. Smith, confirms that it is a Karroo basalt.

Data Representation. Analytical procedures are described by DPW [1976a] and *Papanastassiou, DePaolo and Wasserburg* [1977]. Nd and Sr data are given in Table 1. Nd isotopic data are expressed using notation modified from DPW [1976a]. Initial $^{143}\text{Nd}/^{144}\text{Nd}$ are given as fractional deviations in parts 10^4 (ϵ_{Nd}) from the value in a Chondritic Uniform Reservoir (CHUR) and are given by:

$$\epsilon_{\text{Nd}}(T) \equiv \epsilon_{\text{I}_{\text{Nd}}}(T) \equiv [I_{\text{S}}(T)/I_{\text{CHUR}}(T) - 1] \times 10^4$$

For simplicity in notation we introduce ϵ_{Nd} to represent the deviations of initial Nd from the CHUR reference. $I_{\text{S}}(T)$ is the initial $^{143}\text{Nd}/^{144}\text{Nd}$ of a sample (S), T is the age of the sample, $I_{\text{CHUR}}(T) = I_{\text{CHUR}}(0) - (^{147}\text{Sm}/^{144}\text{Nd})_{\text{CHUR}}^0 [e^{\lambda_{\text{Sm}} T} - 1]$, $I_{\text{CHUR}}(0) = 0.511836$ is $^{143}\text{Nd}/^{144}\text{Nd}$ in CHUR today, $(^{147}\text{Sm}/^{144}\text{Nd})_{\text{CHUR}}^0 = 0.1936$, and $\lambda_{\text{Sm}} = 6.54 \times 10^{-12} \text{ yr}^{-1}$.

Initial $^{87}\text{Sr}/^{86}\text{Sr}$ are expressed as ϵ_{Sr} , defined in a manner analogous to ϵ_{Nd} . We define

$$\epsilon_{\text{Sr}}(T) \equiv \epsilon_{\text{I}_{\text{Sr}}}(T) \equiv [I_{\text{S}}(T)/I_{\text{UR}}(T) - 1] \times 10^4$$

$\epsilon_{\text{Sr}}(T)$ is the deviation of initial $^{87}\text{Sr}/^{86}\text{Sr}$ in a sample from the value in a standard uniform reservoir UR at time T. $I_{\text{S}}(T)$ is the initial $^{87}\text{Sr}/^{86}\text{Sr}$ of the sample, T is the sample's age, $I_{\text{UR}}(T) = I_{\text{UR}}(0) - (^{87}\text{Rb}/^{86}\text{Sr})_{\text{UR}}^0 [e^{\lambda_{\text{Rb}} T} - 1]$, $I_{\text{UR}}(0) = 0.7045$, $(^{87}\text{Rb}/^{86}\text{Sr})_{\text{UR}}^0 = 0.0839$ and $\lambda_{\text{Rb}} = 1.39 \times 10^{-11} \text{ yr}^{-1}$. We introduce this notation for Rb-Sr because it allows

comparison of Nd and Sr in a similar manner for rocks of arbitrary age and simplifies comparison of initial $^{87}\text{Sr}/^{86}\text{Sr}$ in rocks of greatly different ages by subtracting the effects of "normal" growth of $^{87}\text{Sr}/^{86}\text{Sr}$ with time.

I_{UR} (O) is taken to be 0.7045 so that the Nd-Sr correlation line of DPW [1976b] passes through the point $\epsilon_{\text{Nd}} = 0, \epsilon_{\text{Sr}} = 0$. The reference reservoirs proposed here for Nd and Sr are *thought* to be close approximations to bulk earth values [DPW, 1976b]. However, we are avoiding incorporating this inference into the notation because we presently prefer to regard the values in the bulk earth as still to be firmly established.

The isotopic data on young basalts which provide a basis for the interpretation of island arc data are shown in Figures 1 and 2. Figure 1 shows that ϵ_{Nd} values for young basalts fall into three fairly well-defined groups. Figure 2 shows data on basalts which have been analyzed for both $^{87}\text{Sr}/^{86}\text{Sr}$ and $^{143}\text{Nd}/^{144}\text{Nd}$. As first pointed out by DPW [1976c] and in more detail by DPW [1976b] and O'Nions *et al.* [1977] initial Nd and Sr in young basalts are strongly correlated for samples with ϵ_{Sr} less than $\sim +10$. The correlation holds for basalts from both oceanic and continental regions and appears to be a fundamental property of basalt magma sources.

Results: Island Arcs. Nd isotopic data on the island arc samples are shown in Figure 1. All samples have ϵ_{Nd} lying in the narrow range of +6.8 to +9.4. These values are distinct from the bulk of continental flood basalts but overlap the lower range of MOR basalts and the upper range of ocean island basalts. The data clearly show that these island arc rocks have not been derived from a CHUR reservoir ($\epsilon_{\text{Nd}} = 0$), but rather have been derived from a high-Sm/Nd (light-REE-depleted) reservoir with distinct affinities to the MOR basalts and ocean island basalts.

The Nd and Sr isotopic data for the island arc samples are shown in Figure 3. Of nine samples analyzed five basalts and basaltic andesites lie close to the correlation line. The dacite samples from New Britain and basalt from Guam lie slightly to the right of the correlation line and the dacite from Saipan lies far to the right. Thus, although ϵ_{Nd} for all samples is similar, there is a large range of ϵ_{Sr} . The samples which are most displaced from the correlation trend also have ϵ_{Nd} most similar to MOR basalts. Their positions on this graph strongly suggest the involvement of seawater.

The effects of seawater contamination on the Nd and Sr isotopic composition is shown in Figure 3. No change of $^{143}\text{Nd}/^{144}\text{Nd}$ will result due to the low abundance of Nd in ocean water while $^{87}\text{Sr}/^{86}\text{Sr}$ will increase in the rock. Isotopic equilibration of one gram of MOR tholeiite (100 ppm Sr, 10 ppm Nd) with 10 grams of seawater (6 ppm Sr, 3×10^{-5} ppm Nd) could change ϵ_{Sr} of the rock from -30 to +5 but change ϵ_{Nd} by only -0.0006. Thus if the higher ϵ_{Sr} values of island arc rocks are the result of their being melted from subducted

oceanic lithosphere which had ϵ_{Nd} and ϵ_{Sr} on the correlation line and then exchanged with seawater, then they should cover a region on Figure 3 extending to the right of the correlation line but with ϵ_{Nd} identical to that of the descending slab. Such a trend would be easily distinguishable from the correlation line and would be a clear indication of a special mode of origin for these rocks. If the island arc samples were to fall along the correlation line, which we infer to describe the isotopic compositions of normal mantle magma sources, then we would interpret this as indicating that they are derived from mantle reservoirs similar to those from which most basalts are derived. It is also possible that subducted lithosphere with chemical and isotopic characteristics similar to the mantle reservoirs could be the source of these lavas. The isotopic composition of uncontaminated subducted oceanic crust is probably similar to MOR basalts, but will depend on the proportions of ocean island basalt and sediment it contains. The island basalts generally have Nd concentrations about 5 to 10 times higher than MOR basalts. Therefore, if oceanic crust were comprised of 90% MOR basalt ($\epsilon_{\text{Nd}} = +10$) and 10% ocean island basalt ($\epsilon_{\text{Nd}} = +6$) it would have a bulk $\epsilon_{\text{Nd}} \approx +8$, lower than most MOR basalts, but still on the correlation trend. The effect of a sediment component in the subducted oceanic crust is more difficult to assess. A mixture of 1% sediment ($\epsilon_{\text{Nd}} = -10(?)$, 30 ppm Nd; $\epsilon_{\text{Sr}} = +200$, 150 ppm Sr) and 99% MOR basalt would have ϵ_{Nd} different from MOR basalt by -0.6 and ϵ_{Sr} different by +3. For small (2-5%) additions of sediment, the resulting isotopic composition of the subducted crust could still fall within the range of the basalt data which define the correlation trend. In addition, the composition of the oceanic crust could be displaced from that of MOR basalts even if sediments and ocean island basalts were volumetrically insignificant in the downgoing slab. For example, the oceanic crust being subducted beneath the Marianas is Jurassic in age. If the parent reservoir of the MOR basalts has a very high Sm/Nd (e.g., 40% higher than chondritic), then MOR basalts erupted in Jurassic times would have had $\epsilon_{\text{Nd}} \approx +8.5$ rather than +10 for the modern basalts. This value would be retained while the basalts moved from the ridge to the subduction zone since the MOR basalts have Sm/Nd approximately equal to chondritic.

Some scatter about the $\epsilon_{\text{Sr}} - \epsilon_{\text{Nd}}$ correlation line exists which is not presently understood. Therefore in addressing the problem of seawater contamination only samples which deviate substantially from this trend can be considered anomalous. Seawater contamination could conceivably occur in the island arc volcanic pile during magma ascent rather than in the oceanic crust prior to subduction. However, if this were the case, we might also expect it to occur in intraplate oceanic island volcanic piles and result in the production there of lavas with isotopic compositions displaced from the correlation line. Substantial evidence for this has not yet been found.

The samples which lie distinctly off the correlation trend, when projected back to the correlation line to remove the effects of seawater, fall well within the field of MOR basalts. This is consistent with their being derived in major part from subducted MOR basalts with (uncontaminated) isotopic compositions similar to modern ridge basalts. Those samples which lie near the correlation line have projected compositions which are somewhat displaced from the MOR basalts in the direction of the ocean island basalts. These lavas could be derived from subducted lithosphere only if it contains a significant amount of ocean island basalt or sediment or if it has an isotopic composition somewhat different from modern MOR basalt. Rather than call on the presence of sediment or ocean island basalt in the subducted slab to explain only the samples which show no evidence of seawater involvement, we consider it most likely that those samples with isotopic compositions on the correlation trend have been derived from mantle reservoirs with affinities to the sources of ocean island basalts and contain little or no slab-derived component.

In summary, our preferred interpretation of all the data is that island arc lavas are comprised of a component derived from a mantle reservoir similar in isotopic composition to ocean island basalts and a component derived from subducted MOR basalt. Silicic lavas may contain a larger slab-derived component than more mafic lavas. These conclusions are consistent with those outlined by *DePaolo and Wasserburg* [1977], and *O'Nions, Evensen, and Carter* [1977b].

Meijer [1976] measured Pb and Sr isotopes in rocks from the Mariana Island arc and concluded that island arc lavas were melted in part from altered subducted oceanic crust and not from mantle reservoirs similar to ocean island basalt sources. Although his data suggest melting of the slab, it is difficult to consider them as strong evidence against derivation from an ocean island type mantle reservoir, especially since the Pb data from Hawaii [*Tatsumoto*, 1966] are similar to island arc samples.

Continental Rocks. Nd data on continental rocks are shown in Figure 1. In contrast to the oceanic rocks, samples PER-1 and PER-2 have large negative ϵ_{Nd} , which suggest that they were formed by melting or assimilation of old continental crustal material with low Sm/Nd. This is not surprising since the central Andes are underlain by an extremely thick crust (up to 70 kilometers). These data provide the first strong indication that crustal anatexis may be an important process in some continental margin volcanic arcs. This interpretation is in disagreement with that of *Brooks, James and Hart* [1976] who suggested that these lavas were derived from special mantle reservoirs. Sample PEA-3, a Karroo lava, has a large negative ϵ_{Nd} and extremely high ϵ_{Sr} . These characteristics are expected in very old upper continental crustal material and suggest that this magma was massively contaminated with crustal Nd and Sr.

at shallow levels in the crust. Sample KAS-1 (Table 1) and SWB-1A [DPW, 1976b], however, indicate that this is not typical of the Karroo lavas, most of which have $\epsilon_{\text{Nd}} \approx 0$. Sample LH-1, a rare ultrapotassic lava has a large negative ϵ_{Nd} but in contra-distinction to PEA-3, it has ϵ_{Sr} near zero. This lava appears to be derived from a special reservoir which is old (>1 AE) and has low Sm/Nd and low Rb/Sr. Such a reservoir could possibly be found in the lower crust, which may be depleted in Rb and U [Heier, 1965; Zartman and Wasserburg, 1969], or in the mantle. Sample SMG-1 is from a major linear batholith belt and therefore could have originated in a tectonic setting similar to an island arc [c.f. Dickinson, 1970]. Its ϵ_{Nd} and ϵ_{Sr} fall within the field of ocean island basalts and very near the correlation line. This sample could be representative of a major addition of new crust which has ϵ_{Nd} different from zero.

Fish Debris — Seawater. Sample DOS-1 has $\epsilon_{\text{Nd}} = -9.2$ and thus lies far below the CHUR evolution curve (Figure 1). Fish debris is a scavenger of heavy metals in seawater during slow dissolution on the deep ocean floor [Arrhenius, Bramlette, and Picciotto, 1957] and may give an estimate of ϵ_{Nd} of seawater. The ϵ_{Nd} of this sample is similar to that of average North American shale [DPW, 1976a] which may be representative of REE in the continental crust [Haskin *et al.*, 1966] and is far displaced from the values found in oceanic volcanic rocks. If average crustal material has $\epsilon_{\text{Nd}} \approx -14$ and average oceanic volcanics have $\epsilon_{\text{Nd}} \approx +8$, then about 75% of the Nd in authigenic phases on the ocean floors is derived from continental sources and 25% is from oceanic regions.

Discussion: Continental growth. The bulk composition and REE abundances of island arcs and continental margin volcanics arcs closely approximate the composition of average continental crust [Taylor and White, 1965]. This observation together with the fact that island arcs are usually found at or near continental margins has lead to the hypothesis that they are the site of production of new continental crust. Continents thus may grow through time by accreting at their margins material produced in island arcs. If this is the case, then the measurements made in this study indicate that new continental material has a Nd isotopic composition similar to oceanic basalts and should *not* lie on the CHUR curve.

DPW [1976a,b] noted that if undifferentiated mantle had chondritic Sm/Nd, the ϵ_{Nd} of oceanic basalts were consistent with their being derived from mantle material which had been left as residue from ancient partial melting events. Trace element and Sr isotope ratios in MOR basalts had previously led to this hypotheses [Gast, 1968]. These ancient melting events could have contributed to building of the continental crust. Since island arc rocks have ϵ_{Nd} similar to the oceanic volcanics, they may also be derived from such residual material. Thus if island arcs represent the typical materials being added

to form new continental crust, then it must be concluded that continental crust is now being derived from depleted mantle reservoirs which were previously tapped to form continental crust in earlier epochs of crust-building. Since these reservoirs may be more depleted in "crustal components" today than in the past, new continental material derived from them may have a significantly different average composition than Archean crust. This problem is fundamentally related to the Sm/Nd and Rb/Sr values for the bulk earth.

Oceanic Topography and Magma Sources. Basalts erupted on the ocean floor have $\epsilon_{\text{Nd}} = +8$ to $+12$ and distinctive trace element chemistry while those erupted above sea level on continents, oceanic islands, and island arcs have $\epsilon_{\text{Nd}} < +8$. Such isotopic differences must be attributed to the lithic reservoirs in the mantle from which the magmas were melted. Thus there is a correlation between the isotopic characteristics of the lithic reservoir from which a magma is derived and the elevation at which that magma is erupted. From hydrostatic considerations the height of a volcano is proportional to the depth to the base of the magma column. This hydrostatic consideration and the isotopic data suggest a direct link between the depth of the chamber from which a magma is erupted and the associated mantle lithic reservoir from which the magma is derived. This suggests that ocean floor basalts could be derived from a layer close to the surface (Layer A; $\epsilon_{\text{Nd}} > +8$) whereas oceanic island basalts and continental basalts are derived from deeper levels (Layers B, C, etc; $\epsilon_{\text{Nd}} < +8$). Such a simple model would explain why basalts isotopically identical to MOR basalts are almost never found on continents or oceanic islands, and would imply that the major isotopic and chemical zonation in the mantle may be a planetary scale stratification. Layer A could be so shallow as to be nonexistent under continents, where its level would be occupied by the continental mass itself.

Acknowledgements: We are grateful to R. W. Johnson of the Australian Bureau of Mineral Resources for providing carefully selected samples from New Britain and comments on the manuscript. R. J. Stern and F. Barker kindly provided samples from the Marianas, some of which are currently under petrochemical study. We thank I. S. E. Carmichael for petrologic fireside chats and arousing our interest in alkaline lavas with funny names. W. G. Melson provided the Andean samples. We also thank G. Goles for samples of Karroo lavas. Special thanks go to G. Arrhenius who gave us his old teeth. This work has been supported by NSF Grant EAR 76-22494 and NASA Grant NGL 05-002188.

References

Arrhenius, G., M. N. Bramlette and E. Piccioto, Localization of radioactive and stable heavy nuclides in ocean sediments, *Nature* 180, 85-86, 1957.

Brooks, C., D. E. James and S. R. Hart, Ancient lithosphere: Its role in young continental volcanism, *Science* 193, 1086-1094, 1976.

Carmichael, I., The mineralogy and petrology of the volcanic rocks from the Leucite Hills, Wyoming, *Contr. Mineral. and Petrol.* 15 24-66, 1967.

DePaolo, D. J. and G. J. Wasserburg, Nd isotopic variations and petrogenetic models, *Geophys. Res. Lett.* 3, 249-252, 1976a.

DePaolo, D. J. and G. J. Wasserburg, Inferences about magma sources and mantle structure from variations of $^{143}\text{Nd}/^{144}\text{Nd}$, *Geophys. Res. Lett.* 3, 743-746, 1976b.

DePaolo, D. J. and G. J. Wasserburg, Variation of $^{143}\text{Nd}/^{144}\text{Nd}$ in continental and oceanic igneous rocks and chemical zonation of the mantle (abs.) *Geol. Soc. Am. Abs.* 8, 835, 1976c.

DePaolo, D. J. and G. J. Wasserburg, Nd in Island Arc and continental volcanic rocks (abs.), *EOS* 58, 1977.

Dickinson, W. R., Relations of andesites, granites and derivative sandstones to arc-trench tectonics, *Rev. Geophys. Space Phys.* 8, 813-860, 1970.

Gast, P. W., Trace element fractionation and the origin of tholeiitic and alkaline magma types, *Geochim. Cosmochim. Acta* 32, 1057-1086, 1968.

Haskin, L. A., T. R. Wildeman, F. A. Frey, K. A. Collins, C. R. Keedy and M. A. Haskin, Rare earths in sediments, *J. Geophys. Res.* 71, 6091-6105, 1966.

Heier, K. S., Metamorphism and the chemical differentiation of the crust, *Geol. Fören. Stockh. Förh.* 87, 249-256, 1965.

Johnson, R. W., Potassium variations across the New Britain volcanic arc, *Earth. Plan. Sci. Lett.* 31, 184-191, 1976.

Kay, R. W. and P. W. Gast, The rare-earth content and origin of alkali-rich basalts *J. Geol.*, 81, 653-682, 1973.

Meijer, A., Pb and Sr. isotopic data bearing on the origin of volcanic rocks from the Mariana island-arc system, *Geol. Soc. Am. Bull.* 87, 1358-1369, 1976.

O'Nions, R. K., P. J. Hamilton and N. M. Evensen, Variations in $^{143}\text{Nd}/^{144}\text{Nd}$ and $^{87}\text{Sr}/^{86}\text{Sr}$ ratios in oceanic basalts, *Earth Planet. Sci. Lett.* 34, 13-22, 1977a.

O'Nions, R. K., N. M. Evensen, P. J. Hamilton and S. R. Carter, Nd- and Sr- isotope compositions of altered oceanic crust and island arc tholeiites (abs.), *EOS* 58, 1977b.

Papanastassiou, D. A., D. J. DePaolo and G. J. Wasserburg, Rb-Sr and Sm-Nd chronology and genealogy of basalts from the Sea of Tranquility, *Proc. Lunar Sci. Conf. 8th* (in press), 1977.

Richard, P., N. Shimizu and C. J. Allegre, $^{143}\text{Nd}/^{146}\text{Nd}$, a natural tracer: An application to oceanic basalts, *Earth Planet. Sci. Lett.* 31, 269-278, 1976.

Tatsumoto, M., Isotopic composition of lead in volcanic rocks from Hawaii, Iwo Jima and Japan, *J. Geophys. Res.* 71, 1721-1723, 1966.

Taylor, S. R. and A. J. R. White, Geochemistry of andesites and the growth of continents, *Nature* 205, 271-273, 1965.

Zartman, R. E. and G. J. Wasserburg, The isotopic composition of lead in potassium feldspars from some 1.0 b.y. old North American igneous rocks, *Geochim. Cosmochim. Acta* 33, 901-942, 1969.

Table 1: Nd and Sr Evolutionary Parameters

	Age (AE)	Nd (ppm)	$^{147}\text{Sm}/^{144}\text{Nd}$	Sr (ppm)	$^{87}\text{Rb}/^{86}\text{Sr}$	ϵ_{Nd}	ϵ_{Sr}
I. Island Arcs: New Britain						^a	^a
BMR-1 (Bas. andesite, Sulu Range)	0	1.76	0.222	—	—	+7.7±0.4	-18.6±1.6
BMR-3 (Dacite, Welcker Volcano)	0	—	—	—	—	+7.8±0.5	-13.5±1.3
BMR-5 (Dacite, Garove Is.)	0	—	—	—	—	+8.3±0.5	-15.0±0.7
Marianas							
MAR-1 (Basalt, Agrigan Is.)	0	11.1	0.126	352	0.098	+7.9±0.6	-18.6±0.9
MAR-2 (Andesite, Sarigan Is.)	0	12.0	0.166	352	0.121	+6.8±0.5	-19.0±1.1
MAR-4 (Basalt, Agrigan Is.)	0	11.7	0.157	401	0.152	+7.2±0.5	-18.9±0.5
MAR-6 (Dacite, Saipan Is.)	0.05	5.01	0.128	94	0.099	+9.1±0.5	-1.5±1.0
GU-4 (Basalt, Guam Is.)	0.05	5.68	0.176	130	0.260	+9.4±0.5	-13.1±1.1
GU-7 (Basalt, Guam Is.)	0.05	—	—	—	—	+8.4±0.4	-21.0±1.1
II. Continental							
KAS-2 (Basalt, Karroo, S. Africa)	0.15	—	—	—	—	+0.3±0.6	+7.0±1.5
PEA-3 (Basalt, Karroo, Mozambique)	0.10	44.8	0.117	230	1.56	-18.6±1.6	+312.0±4.0
SMG-1 (San Marcos Gabbro, S. Cal.)	0.12	4.95	0.153	455	0.0274	+4.7±0.6	-14.7±0.7
LH-1 (Wyomingite, Leucite Hills, Wyo.)	0.05	130.8 ^b	0.076 ^b	2700 ^c	0.49 ^c	-13.5±1.0	+12.6±0.7
PER-1 (Andesite, El Misti, Peru)	0	28.1	0.098	1098	0.127	-8.9±0.5	—
PER-2 (Rhyolite, El Misti, Peru)	0	21.7	0.091	444	0.463	-12.7±0.1	+64.3±1.3
DOS-1 (Fish Debris, Pacific Ocean)	0	—	—	—	—	-9.2±0.7	—
CHUR	all T	—	0.1936	—	—	0	—
UR	all T	—	—	0.0839	—	0	—

^aInitial values; calculated from measured values and known ages; uncertainties 2σ . ^bKay and Gast (1973). ^cCarmichael (1967).

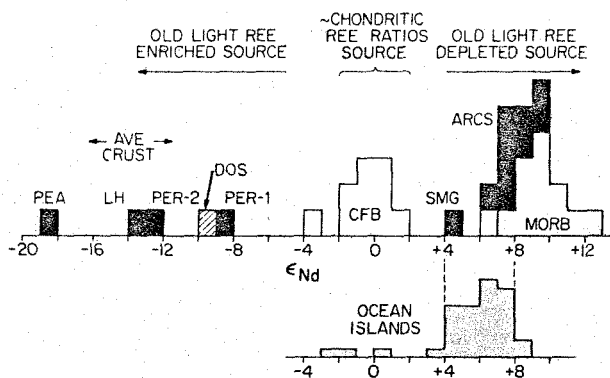


Fig. 1: Histogram of ϵ_{Nd} of three groups of young basalts (unshaded and lightly shaded) and in samples measured in this study (solid and ruled) with inferred REE pattern of parent reservoirs. Data on continental flood basalts (CFB) and mid-ocean ridge basalts (MORB) and ocean island basalts from DePaolo and Wasserburg [1976a,b], O'Nions *et al.*, [1977], and Richard *et al.* [1976].

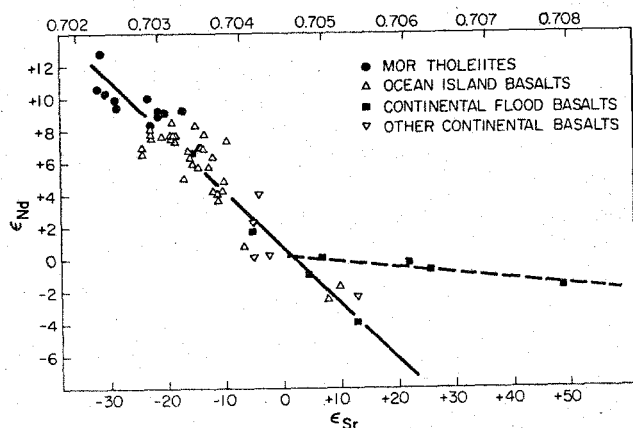


Fig. 2: ϵ_{Nd} versus ϵ_{Sr} for young oceanic and continental basalts showing strong correlation trend for samples with $\epsilon_{Sr} < 0$ and a trend of different slope defined by some continental flood basalts with $\epsilon_{Sr} > 0$. Data are from DePaolo and Wasserburg [1976a,b], O'Nions *et al.* [1977], Richard *et al.* [1976] and DePaolo and Wasserburg [unpublished].

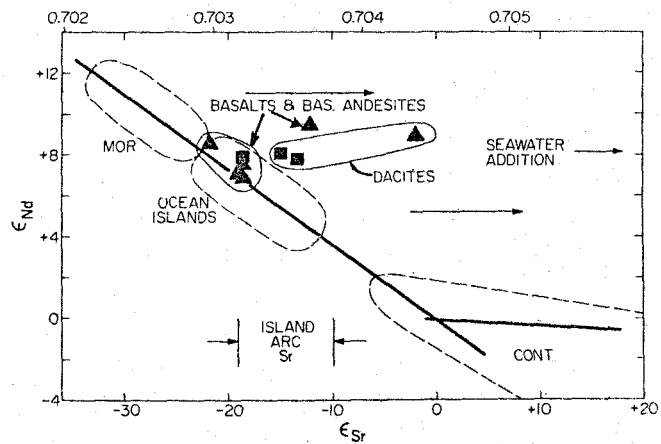


Fig. 3: ϵ_{Nd} and ϵ_{Sr} for island arc samples. Arrows indicate effect of seawater contamination. Approximate fields of MOR, ocean island and continental (CONT) basalts from Fig. 2 shown for comparison. Triangles represent Marianas samples and squares are New Britain samples. The typical range of ϵ_{Sr} for oceanic island arcs taken from the literature is also shown. $^{87}\text{Sr}/^{86}\text{Sr}$ ratios indicated at the top apply only at $T = 0$. Uncertainties are slightly larger than the symbols.

Rb-Sr and Sm-Nd chronology and genealogy of mare basalts from the Sea of Tranquility

D. A. PAPANASTASSIOU, D. J. DEPAOLO, and G. J. WASSERBURG

The Lunatic Asylum of the Charles Arms Laboratory, Division of Geological and Planetary Sciences, California Institute of Technology, Pasadena, California 91125

Abstract—Rb-Sr and Sm-Nd ages of two Apollo 11 mare basalts are 3.64 ± 0.05 and 3.57 ± 0.03 AE for high-K basalt 10072, and 4.01 ± 0.11 and 3.88 ± 0.06 AE for low-K basalt 10062. Rb-Sr, Sm-Nd, and ^{40}Ar - ^{39}Ar ages are in good agreement and show an extensive time interval for filling of the Sea of Tranquility, presumably by thin lava flows, in agreement with similar observations for the Ocean of Storms. The older ages indicate that mare filling may have started prior to the Imbrium event. Initial Sr and Nd isotopic compositions on Apollo 11 basalts identify at least two parent sources producing basalts. The low-K basalts may have been produced from a single reservoir over an extended time interval. The Sm-Nd isotopic data demonstrate that low-K and high-Ti basalts from Apollo 11 and 17 have been derived from totally distinct reservoirs while low-Ti Apollo 15 mare basalt sources have Sm/Nd similar to the sources of Apollo 11 basalts. It appears that groupings of mare basalt based on Ti content and on isotopic data do not coincide. Apollo 11 high-K basalts show no significant Sm/Nd fractionation near the time of crystallization in contrast to characteristically large Rb/Sr fractionation for these basalts.

INTRODUCTION

IN THIS REPORT we provide a review of the chronology of Apollo 11 mare basalts and present new Rb-Sr and the first Sm-Nd internal isochrons on two Apollo 11 mare basalts. The Sm-Nd work is an extension of the original development and application of Sm-Nd dating to problems of lunar chronology and petrogenesis by Lugmair and his colleagues (Lugmair, 1975; Lugmair, *et al.*, 1975). The aims of the present study are as follows:

- (a) Determination of more refined Rb-Sr ages and of the first Sm-Nd ages on A-11 samples and comparison of the chronologies defined by Rb-Sr, Sm-Nd, and ^{40}Ar - ^{39}Ar .
- (b) Determination based on age, initial Sr, and initial Nd compositions of how many distinct magma sources are required for the A-11 basalts.
- (c) Comparison of Rb-Sr and Sm-Nd chemical fractionation especially for the high-K A-11 basalts which are characterized by large Rb-Sr fractionation near the time of crystallization.
- (d) Comparison of Sm-Nd fractionation of A-11 and A-17 mare basalts. These basalts have similar major element compositions, including high-Ti contents. The A-17 basalts show the effects of large Sm-Nd fractionation (Lugmair *et al.*, 1975) near the time of formation of the moon. In contrast the data to be presented show that A-11 basalts underwent considerably less early Sm-Nd fractionation.

(e) Review of the time constraints for REE and Rb-Sr fractionation on the moon and of the constraints on petrogenetic models based on Rb-Sr, Sm-Nd, and on Eu fractionation.

We present data for a low-K and a high-K Apollo 11 basalt by both Rb-Sr and Sm-Nd. The choice of the samples was predicated on the need for crystallization ages on more low-K basalts to compare with the ^{40}Ar - ^{39}Ar gas retention ages, and on the importance of comparing Rb-Sr and Sm-Nd fractionation for A-11 high-K rocks which indicate significant Rb-Sr fractionation near the time of crystallization of these rocks.

Review

The great majority of reported Rb-Sr data on Apollo 11 rocks were based on the first sample allocation and examination seven years ago. Although some workers presented Rb-Sr whole-rock data on Apollo 11 samples, we shall restrict the discussion to the determinations of internal isochrons, since our purpose is to establish a precise chronology of crystallization at this site. Crystallization ages were reported by Papanastassiou *et al.* (1970), Gopalan *et al.* (1970), and Compston *et al.* (1970). Gopalan *et al.* (1970) reported ages on two high-K basalts which had relatively large uncertainties. Their report of an old age for 10024 was not confirmed (Papanastassiou and Wasserburg, 1971a). Compston *et al.* (1970) provided well-defined internal isochrons on two high-K basalts; the reported ages have been revised (De Laeter *et al.*, 1973) and are now in good agreement with the data presented by Papanastassiou *et al.* (1970). Papanastassiou *et al.* (1970) determined internal isochrons on four A-11 high-K rocks and on two low-K rocks. We have listed in Table 1 all precise determinations of Rb-Sr ages and initial $^{87}\text{Sr}/^{86}\text{Sr}$ on A-11 basalts. The first Rb-Sr data on Apollo 11 showed: (a) a uniform crystallization age for all samples, (b) two distinct rock groups based on initial $^{87}\text{Sr}/^{86}\text{Sr}$ indicating that the rocks were produced from at least two distinct magma reservoirs, (c) characteristically young whole-rock model ages for the high-K rocks indicating that, for these rocks, Rb/Sr was significantly increased at or very near the time of crystallization, and (d) low initial $^{87}\text{Sr}/^{86}\text{Sr}$ for all samples indicating that the source regions and presumably the moon formed with low Rb/Sr and with initial $^{87}\text{Sr}/^{86}\text{Sr}$ near BABI.

Extensive work on Apollo 11 samples by the ^{40}Ar - ^{39}Ar technique was reported by Turner (1970). This work established: (a) the existence of measured ages for low-K rocks as old as 3.92 AE, (b) that the high-K rocks had suffered significant ^{40}Ar loss so that an ^{40}Ar - ^{39}Ar apparent age plateau was not defined by whole rock data, and (c) that in a specific case of high-K basalt 10072 an apparently well-defined younger age was obtained. These data indicated that there existed differences in the ages of Apollo 11 basalts possibly as large as 4×10^8 yr. A report by the Lunatic Asylum (1970) showed that plagioclase was significantly more retentive for ^{40}Ar than whole rocks. Turner *et al.* (1971, 1972)

Table 1. Apollo 11 mare basalts.

Sample	K Content	$(^{87}\text{Sr}/^{86}\text{Sr})_I^a$	Rb-Sr ^a (AE)	$^{40}\text{Ar}-^{39}\text{Ar}^b$ (AE)	
10003	L	0.69909 ± 4	$3.84 \pm 0.08 (1)$	3.92 ± 0.07	TR;S (6)
				3.91 ± 0.03	P1;B (7)
10017	H	0.69932 ± 5	$3.59 \pm 0.05 (2)$	$> 3.23 \pm 0.06$	TR;S (6)
		0.69930 ± 10	$3.71 \pm 0.11 (3)$		
10020	L	—	—	(3.77 ± 0.03)	TR;B (8)
10022	H	—	—	3.59 ± 0.06	TR;S (6)
				(3.58 ± 0.04)	TR;B (8)
10024	H	0.69935 ± 8	$3.61 \pm 0.07 (4)$	$> 3.48 \pm 0.05$	TR;S (6)
10029	L	—	—	(3.89 ± 0.05)	TR;B (10)
10032	L	—	—	3.58 ± 0.05	TR;B (10)
10044	L	0.69909 ± 7	$3.71 \pm 0.11 (2)$	3.73 ± 0.05	TR;S (6)
				3.71 ± 0.03	TR;B (8)
10045	L	—	—	(3.75 ± 0.03)	TR;B (8)
10047	L	—	—	3.74 ± 0.03	TR;B (7)
10049	H	—	—	(3.45 ± 0.04)	TR;B (8)
10050	L	—	—	3.75 ± 0.03	P1;B (8)
10057	H	0.69939 ± 5	$3.63 \pm 0.04 (2)$	$> 3.39 \pm 0.04$	TR;S (6)
10058	L	0.69906 ± 5	$3.63 \pm 0.20 (2)$	(3.71 ± 0.03)	TR;B (8)
10062	L	0.69901 ± 4	$4.01 \pm 0.11 (5)$	3.82 ± 0.06	TR;S (6)
10069	H	0.69926 ± 8	$3.68 \pm 0.06 (2)$	$> 3.48 \pm 0.04$	TR;B (8)
10071	H	0.69923 ± 8	$3.68 \pm 0.02 (2)$	3.51 ± 0.06	P1;B (9)
10072	H	0.69926 ± 5	$3.64 \pm 0.05 (5)$	3.52 ± 0.05	TR;S (6)
		0.69940 ± 12	$3.71 \pm 0.11 (3)$	3.57 ± 0.04	TR;B (8)
				3.62 ± 0.04	P1;B (8)

^aUncertainties are 2σ ; initial $^{87}\text{Sr}/^{86}\text{Sr}$ from De Laeter *et al.* (1973) may be subject to inter-laboratory bias.

^bTR = Total rock sample; Pl = Plagioclase; ages in parentheses by the Berne group indicate intermediate temperature plateau only, and are considered by this group less reliable (Geiss *et al.*, 1977). S = Sheffield, B = Berne.

References: (1) Papanastassiou and Wasserburg (1975a). (2) Papanastassiou *et al.* (1970). (3) DeLaeter *et al.* (1973). (4) Papanastassiou and Wasserburg (1971a). (5) Present work. (6) Turner (1970). (7) Stettler *et al.* (1974). (8) Geiss *et al.* (1977). (9) Stettler *et al.* (1973). (10) Guggisberg *et al.* (1977).

and Podosek *et al.* (1972) have shown that plagioclase is the most retentive mineral. Podosek *et al.* (1972) have demonstrated differences in apparent $^{40}\text{Ar}/^{39}\text{Ar}$ between plagioclase and whole-rock plateau ages for a mare basalt even though both plateaus appeared well defined. There is good agreement between $^{40}\text{Ar}-^{39}\text{Ar}$ plateau ages defined by plagioclase and Rb-Sr internal isochron ages. Exceptions to the good agreement between $^{40}\text{Ar}-^{39}\text{Ar}$ plagioclase plateau ages and Rb-Sr ages exist for highland rocks with a more complex history (cf. Jessberger *et al.*, 1974). Some exceptions, e.g., for the troctolite 76535, are not well understood. We consider that the $^{40}\text{Ar}-^{39}\text{Ar}$ technique yields reliable ages for plagioclase from igneous rocks which exhibit little gas loss and high temperature plateau ages defined by a significant fraction of the ^{40}Ar

released in several steps. Subsequent to the work by Turner, the Berne group reexamined rock 10003 (Stettler *et al.*, 1974) and confirmed its old age. Furthermore this group has provided a large number of ^{40}Ar - ^{39}Ar analyses on Apollo 11 basalts (see Table 1 for references). The ^{40}Ar - ^{39}Ar ages on Apollo 11 mare basalts are shown in Table 1. The ages shown include: (a) whole-rock analyses and (b) analyses of plagioclase mineral separates. Some of the ages are based on "intermediate" temperature plateaus which are considered less reliable than ages defined by plagioclase high temperature plateaus (Geiss *et al.*, 1977). These details have been noted in Table 1. The data show a range in gas retention ages from 3.91 to 3.45 AE. Geiss *et al.* (1977) have proposed that the rocks may be subdivided in three to four age groups which coincide with petrologic types defined by Warner (1971). We note from Table 1 that there is in fact only a small number of ^{40}Ar - ^{39}Ar high temperature plateau ages obtained on plagioclase separates.

The chronology of A-11 basalts has so far been based only on Rb-Sr and ^{40}Ar - ^{39}Ar data. No crystallization ages have been reported yet by the U-Pb or Sm-Nd techniques for rocks of this mission. The data summarized above indicate the following major problems:

- (a) Rb-Sr data on only a limited number of A-11 low-K basalts exist and these data are not of sufficient precision to resolve some of the small age differences indicated by ^{40}Ar - ^{39}Ar ages. This problem is due to the rarity and difficulty of isolating high-Rb/Sr phases in low-K mare basalts.
- (b) The Rb-Sr data did not exhibit the wide spread in ages observed by ^{40}Ar - ^{39}Ar . This may be due to the limited Rb-Sr data on A-11 low-K rocks which have yielded old ^{40}Ar - ^{39}Ar ages. In addition some of the young ^{40}Ar - ^{39}Ar ages contributing to the wide spread were obtained on high-K basalts which exhibit significant gas loss and may not be reliable.

SAMPLING

High-K basalt 10072

This sample is the coarsest of the A-11 high-K rocks which are as a group fine-grained. Despite the coarser size of the pyroxene, interstitial, late crystallizing phases appear as small inclusions in all major phases and their exclusion from mineral separates of the major phases has required extreme care. A 4.2 g sample of the rock which included lunar exterior surfaces was received from the curator. These lunar exterior surfaces were removed using a tungsten chisel, and a sample of the total rock from totally interior material was obtained for Rb-Sr and Sm-Nd. Our aim was to obtain: (a) high purity plagioclase separates free of interstitial phases for both Rb-Sr and Sm-Nd, (b) high purity pyroxene especially for the Sm-Nd work, and (c) separates highly depleted in plagioclase and enriched in ilmenite which acts as a Sr-free carrier phase for the higher Rb/Sr interstitial phases.

Mineral separates were obtained from the debris produced during chiselling off of the exterior surfaces and separately from totally interior material. Two mineral separates were obtained from the chipping debris and are labelled CD in Table 2. Mineral separations involved: (a) only mechanical means (crushing, sieving) and magnetic separations (such separates are labelled M in the tables and figures), and (b) additional density separations using organic liquids ($\text{CH}_2\text{I}_2 + \text{CH}_3\text{COCH}_3$) followed by magnetic separations (labelled L).

In this study we found no evidence of differential leaching by the organic liquids in agreement with all our earlier work on mare basalts and in contrast to our work on the dunite 72417 (Papanastassiou and Wasserburg, 1975b). For Sm-Nd, improvement in the range in Sm/Nd for the plagioclase and pyroxene end members was obtained by first using density and magnetic separations for material crushed to less than 75 μm and then reprocessing samples highly enriched in plagioclase and in pyroxene after crushing to less than 44 μm . For Rb-Sr the small amount needed of highest purity plagioclase were obtained by handpicking.

Low-K basalt 10062

We received from the curator an 8.1 g sample which had been previously allocated for mineralogical investigations; the sample had been handled and exposed to terrestrial contamination. The sample also included exterior lunar surfaces. For this work most exterior surfaces were removed to produce essentially interior material. Complete removal of all exterior surfaces was not possible because of the concomitant decrease in the useful sample weight. Mineral separations were obtained by the techniques described above. The rock is fine-grained so that the production of mineral separates required extensive work. High purity mineral separates of pyroxene and plagioclase were obtained (better than 99% pure as shown by grain counts using the electron microprobe). These separates provided a sufficient spread for Sm/Nd. However, the mineral separations did not result in the identification of high-Rb/Sr materials. A survey by the electron microprobe of grain mounts of density separates, including separates enriched in cristobalite and in ilmenite, revealed no significant high-K concentration spots. Similarly, chemical analyses of small aliquots (0.1–1 mg) of mineral separates for K, Rb, and Sr showed no high Rb/Sr. The low abundance of mesostasis and the fine grain size (Carter and MacGregor, 1970) have prevented the separation of higher Rb/Sr phases. An ilmenite separate produced by magnetic separation showed a small enrichment of $^{87}\text{Sr}/^{86}\text{Sr}$ over the total rock. A second ilmenite separate produced by density separations did not show a significant improvement due to the presence of small amounts of plagioclase in binary grains. Rb-Sr concentrations in a small sample obtained by handpicking of clean ilmenite grains of size 75–44 μm under a binocular microscope showed that some improvement of Rb/Sr was possible. Therefore, two man-weeks were invested in handpicking clean ilmenite, free of plagioclase. The final separate shows an enrichment of $^{87}\text{Sr}/^{86}\text{Sr}$ over the plagioclase of 0.3%. It is clear from these results that it may be impossible to obtain sufficiently high-Rb/Sr phases in extremely low-K and fine-grained samples to provide Rb-Sr ages with an uncertainty lower than 0.1 AE. However, in these cases reasonable enrichments in Sm-Nd have been obtained which result in a precise age determination.

ANALYTICAL PROCEDURES

All samples were dissolved following standard procedures using HF and HClO_4 . Small (<1%) aliquots of each sample were used for establishing the concentrations of K, Rb, Sr, Ba, Sm, and Nd in a single mass spectrometer run. The major sample aliquots were then spiked in an optimal fashion. We have checked the cross-contamination between K, Rb, Sr, Sm, and Nd tracers. In all cases the cross-contamination is negligible except for Nd in the ^{41}K – ^{40}K spike solution. This effect has been reduced to negligible levels by adding less of the K spike, or eliminated for some samples by not spiking the Sm-Nd aliquot for K.

Rb-Sr

Rb and Sr blanks were monitored regularly and are 0.01–0.003 ng for Rb and 0.1–0.05 ng for Sr and are negligible for the data presented here. The concentrations in the tracer solutions were checked with four Rb and four Sr gravimetric solutions which were independently prepared using Johnson-Matthey spectrographically pure RbCl and SrCO_3 , and NBS SRM 987 SrCO_3 . The stoichiometry of the Johnson-Matthey salts has been confirmed in the past (Wasserburg *et al.*, 1962).

Using the four sets of Rb and Sr gravimetric solutions, the concentrations of the single ^{87}Rb tracer solution and two ^{84}Sr tracer solutions, in use, each agreed to 0.1%. A fifth gravimetric normal of SRM 987 gave results for both Sr tracer solutions 0.4% higher than the rest. We attribute this highly atypical result to unknown problems during the preparation of this gravimetric solution and have discarded this datum in view of the close agreement of the results of four other determinations using independently prepared gravimetric solutions. Sr mass spectrometric analyses were performed with new zone-refined Ta ribbon which shows no detectable ^{85}Rb signal during the Sr run (Wasserburg *et al.*, 1977). This has resulted in increased ease of analyzing Sr, as data collection is not restricted by waiting for the Rb signal to die.

Sm-Nd

Sm and Nd were isolated using chemical techniques described by Eugster *et al.* (1970) and DePaolo and Wasserburg (1976a). Rare earth elements were separated from major elements on a 1 cm diameter cation exchange column using HCl as elutriant. Sm and Nd were then separated on a second cation column using as elutriant 0.2M 2-methylallic acid with pH adjusted to approximately 4.7.

Samples were spiked with tracers enriched in ^{150}Nd and ^{147}Sm . Tracer concentrations were calibrated using gravimetric standard solutions which were made by dissolving ultra pure metal chunks of Sm and Nd obtained from Ames Laboratory, Iowa. The chunks of metal were analyzed for impurities and weighed at Ames prior to shipment in evacuated containers. Upon arrival at Caltech, the metal chunks were weighed and the weights agreed with those measured at Ames to better than 0.01%. Sm concentrations were calculated using the Sm isotopic composition reported by Russ *et al.* (1971) and Russ (1974). Nd concentrations were calculated using the isotopic composition of normal Nd reported by DePaolo and Wasserburg (1976a,c). $^{147}\text{Sm}/^{144}\text{Nd}$ ratios are precise to better than 0.1%, where this error represents the sum of errors resulting from weighing of spikes and uncertainties of isotope ratios of the spikes measured in the mass spectrometer.

Nd was measured in the mass spectrometer as NdO^+ and Sm was measured as SmO^+ . In this work, all Nd isotopic measurements were made on spiked samples. The ^{150}Nd tracer is approximately 96% ^{150}Nd . The small amounts of the other Nd isotopes in the tracer significantly change the measured isotope ratios and must be corrected. These corrections are made using the isotopic composition of the tracer measured by us. This measurement is quite precise, but additional uncertainty must be added to the measured ratios due to the inability to measure precisely the instrumental mass discrimination for the tracer. The uncertainty in mass discrimination is believed to be about 0.05% per mass unit. The net correction to $^{143}\text{Nd}/^{144}\text{Nd}$ under our spiking conditions (^{150}Nd -tracer added equal to twice ^{150}Nd in sample) is approximately $0.1500 \pm 0.0003\%$ where the uncertainty is due to uncertainty in the tracer composition. The added uncertainty to $^{143}\text{Nd}/^{144}\text{Nd}$ from this effect is negligible. Nd isotopic ratios were normalized to $^{146}\text{Nd}/^{142}\text{Nd} = 0.636155$ to remove the effects of instrumental isotope fractionation. This is equivalent to normalizing to $^{150}\text{Nd}/^{142}\text{Nd} = 0.2096$ for the unspiked samples (DePaolo and Wasserburg, 1976b) and is essentially the average value that is measured in the Lunatic I mass spectrometer (Wasserburg *et al.*, 1969) if no correction is made for mass fractionation.

In unspiked samples, $^{150}\text{Nd}/^{142}\text{Nd}$ is used for the determination of mass fractionation because the difference of 8 mass units for these isotopes minimizes the error in determining the fractionation factor per mass unit. Since we use a ^{150}Nd tracer, for spiked samples the $^{146}\text{Nd}/^{142}\text{Nd}$ ratio is used for the determination of fractionation. This ratio still provides a difference of 4 mass units, involves abundant Nd isotopes, and the contributions to ^{142}Nd and ^{146}Nd from the ^{150}Nd tracer are small.

In all Nd mass spectrometer runs made in our laboratory, all Nd isotope ratios are measured. Data for the non radiogenic isotopes for five samples from 10072 and five recently measured terrestrial samples are shown in Fig. 1. Measured values of $^{142}\text{Nd}/^{144}\text{Nd}$ and $^{145}\text{Nd}/^{144}\text{Nd}$, which can be measured with precision similar to $^{143}\text{Nd}/^{144}\text{Nd}$, agreed from run to run to $\pm 0.005\%$ or better. The isotopic composition of lunar Nd appears to be identical to that of terrestrial Nd to within the present limits of resolution of ~ 2 parts in 10^5 . Lugmair *et al.* (1975) first reported precise measurements of $^{143}\text{Nd}/^{144}\text{Nd}$ and $^{142}\text{Nd}/^{144}\text{Nd}$ in the Juvina achondrite and in reagent Nd. However, these numbers

were revised (Lugmair, pers. comm.). The revised value for $^{143}\text{Nd}/^{144}\text{Nd}$ measured in Juvinas by Lugmair was subsequently used by DePaolo and Wasserburg (1976a) and reported by Lugmair *et al.* (1976). High precision isotopic abundances of Nd for all isotopes were first reported by DePaolo and Wasserburg (1976a,c). The means of data shown in Fig. 1 agree with the means of measurements made by DePaolo and Wasserburg (1976a,b) to ± 2 parts in 10^5 for all nonradiogenic isotopes. Measurements made by Lugmair *et al.* (1976) on the troctolite 76535 and their reagent Nd standard agree reasonably well with our values (after renormalization) except for $^{145}\text{Nd}/^{144}\text{Nd}$, which they measure ~ 2 parts in 10^4 higher, and $^{142}\text{Nd}/^{144}\text{Nd}$, which shows substantial variation in their data (2 parts in 10^4). This difference is far outside analytical uncertainty and is not understood. Measurements made by Nakamura *et al.* (1976) also differ from ours by substantial amounts. Their measured $^{142}\text{Nd}/^{144}\text{Nd}$ is greater than ours by 2 parts in 10^4 and $^{145}\text{Nd}/^{144}\text{Nd}$ is less than ours by about 2 parts in 10^4 . Nakamura *et al.* (1976) made their measurements on Nd^{+} rather than on NdO^{+} as is done in this laboratory. We correct our data for the oxygen isotopic composition using the composition reported by Nier (1950). However, we measure the oxygen isotopic composition of NdO^{+} to be substantially different from Nier's values (see discussion below). If we were to correct our data using our measured oxygen composition, it would increase our calculated $^{142}\text{Nd}/^{144}\text{Nd}$ by 0.8 parts in 10^4 and decrease our $^{145}\text{Nd}/^{144}\text{Nd}$ by 0.4 parts in 10^4 . This change would bring our measured ratios closer to those measured by Nakamura *et al.* (1976) but would still leave a substantial discrepancy between the data from the two laboratories. The data on the nonradiogenic Nd isotopes provide an important indicator of data precision and a check on the absence of data artifacts which is not available for either Sr or Pb. In view of the high precision necessary for Nd isotopic work, collecting and reporting these data are necessary for an evaluation of the Nd data.

Total chemistry blank for Nd is ~ 70 – 100 pg and for Sm, although not measured, is presumed to be in the range 20–30 pg. No blank corrections were necessary to either Nd isotope ratios or Sm/Nd ratios. No corrections for neutron capture effects were applied to Nd isotope ratios. During a run, possible interfering species are monitored at masses 156($^{140}\text{Ce}^{16}\text{O}$), 157($^{141}\text{Pr}^{16}\text{O}$), and 170($^{154}\text{Sm}^{16}\text{O}$). We generally measure the ratios $156/160 \approx 10^{-5}$; $157/160 = 10^{-4}$ – 10^{-3} ; $170/160 \approx 5 \times 10^{-6}$ (mass 160 is $^{144}\text{Nd}^{16}\text{O}$) during a run, and no corrections to Nd isotope ratios are necessary. Only in one sample (10072, pyroxene-B) a correction of 0.006% was made to $^{143}\text{Nd}/^{144}\text{Nd}$ due to the contribution of $^{141}\text{Pr}^{18}\text{O}$.

Nd ISOTOPIC COMPOSITION

DEVIATIONS OF MEASURED ISOTOPE RATIOS FROM NORMAL IN PARTS IN 10^4

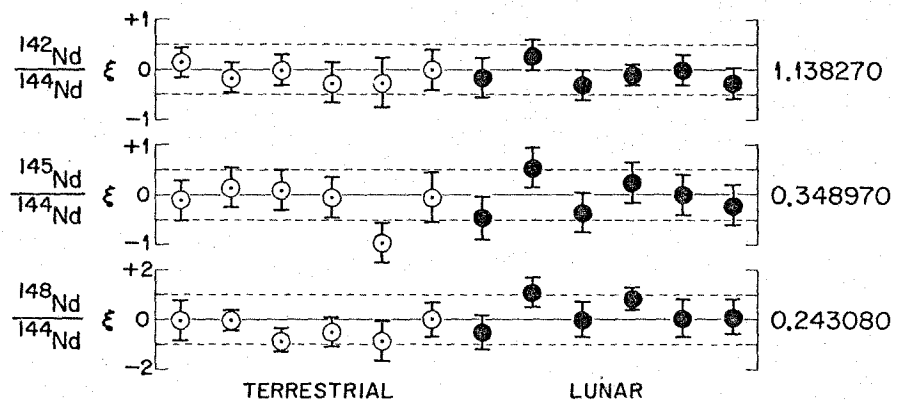


Fig. 1. Measured values of non-radiogenic Nd isotope ratios plotted as deviations (ξ) in parts in 10^4 from the mean values for these ratios as measured over the past year given at right. $\xi = ((R_i - R_i^{\text{GM}})/R_i^{\text{GM}}) \times 10^4$ (GM = grand mean). Data points represent terrestrial and lunar samples measured during this work; error bars are $2\sigma_{\text{mean}}$.

Oxygen isotopic abundance

Oxygen isotopic corrections to Nd isotope ratios were made assuming that the ratios $^{18}\text{O}/^{16}\text{O} = 0.002045$ and $^{17}\text{O}/^{16}\text{O} = 0.0003708$. These ratios are those measured by Nier (1950). Since a large variability of oxygen isotope ratios is found in nature, we have made preliminary measurements of $^{18}\text{O}/^{16}\text{O}$ and $^{17}\text{O}/^{16}\text{O}$ to check if the ratios given above are the same as those found in the Nd oxide ion beam. This was done by measuring the ratios $^{150}\text{Nd}^{18}\text{O}/^{150}\text{Nd}^{16}\text{O}$ and $^{150}\text{Nd}^{17}\text{O}/^{150}\text{Nd}^{16}\text{O}$ on a sample of our enriched ^{150}Nd tracer and on a spiked sample Nd run. The results obtained so far indicate $^{18}\text{O}/^{16}\text{O} = 0.00211-0.00213$ and $^{17}\text{O}/^{16}\text{O} = .000385-0.000392$. There is some variability in these ratios between runs as well as variation within a run. The measured $^{18}\text{O}/^{16}\text{O}$ is higher than the value given by Nier by about 4%. This difference could be the result of mass fractionation occurring: (a) in the mass spectrometer during evaporation of Nd_2O_3 from the filament as NdO^+ with concomitant loss of O atoms, (b) during oxidation of the Nd sample by heating in air, or (c) in Nier's spectrometer. It appears, however, that relative to the Nier values, our measured $^{17}\text{O}/^{16}\text{O}$ is higher than it should be relative to $^{18}\text{O}/^{16}\text{O}$ if the differences were only due to mass dependent fractionation. At present, the uncertainty in our $^{17}\text{O}/^{16}\text{O}$ is too large to evaluate critically this possibility. A more detailed description of this experiment will be given elsewhere. For our purposes here, it is only necessary to note that if our measured values were used to correct our Nd isotope ratios instead of the Nier values, the $^{143}\text{Nd}/^{144}\text{Nd}$ ratios reported here would be increased by 2 parts in 10^5 , which is approximately half the analytical uncertainty. Variation of O isotope composition between and during runs causes effects about one fourth this large, which are negligible. However the effects on Nd isotopic composition from correcting for the O isotope composition depend upon the type of sample being analyzed (e.g., spiked or unspiked) and on which pair of isotopes is used for the mass discrimination correction. The measured $^{143}\text{Nd}/^{144}\text{Nd}$ of Lugmair (1975) and Lugmair *et al.* (1975, 1976) would also be changed by +2 parts in 10^5 if our measured O ratios were the same as those found in the NdO^+ beam in their mass spectrometer. On our unspiked runs (DePaolo and Wasserburg, 1976a,b) a change of +4 parts in 10^5 would result.

Mass fractionation correction

Our normalization of the Nd isotopic data for instrumental mass fractionation is not identical to that used by Lugmair and his coworkers. A change in the normalization constant for any element changes the calculated relative proportions of the isotopes of that element and thus changes the atomic weight of the element. Relative to the normalization used by Lugmair and coworkers, our normalization causes us to calculate a 0.05% lower concentration of ^{144}Nd in a sample and 0.15% lower $^{143}\text{Nd}/^{144}\text{Nd}$. These differences cause us to calculate an isochron age which is lower by 0.2% than we would calculate if we used the other normalization. The shift in $^{143}\text{Nd}/^{144}\text{Nd}$ is large but uniform and can be

easily calculated. Our data can be made comparable to those of Lugmair by multiplying our $^{143}\text{Nd}/^{144}\text{Nd}$ by 1.001563 and our $^{147}\text{Sm}/^{144}\text{Nd}$ by 1.0005.

ANALYTICAL RESULTS

Rb-Sr

The Rb-Sr data are shown in Table 2 and in Figs. 2 and 3. Data have been obtained on seven samples of 10072. The data show a range in $^{87}\text{Sr}/^{86}\text{Sr}$ of 1.7% and permit a precise age determination. All data lie on a straight line with a best fit slope corresponding to an age of 3.64 ± 0.05 AE (2σ uncertainties; $\lambda(^{87}\text{Rb}) = 0.0139 \text{ AE}^{-1}$). The initial $^{87}\text{Sr}/^{86}\text{Sr}$ is 0.69928 ± 0.00006 ; samples of plagioclase with $^{87}\text{Sr}/^{86}\text{Sr}$ very near the initial value have been analyzed. The data show no evidence of differential leaching of Rb or Sr for the samples exposed to organic liquids. Similarly, samples obtained from the chipping debris (CD) which included lunar exterior surfaces are in agreement with data obtained from interior samples. The total rock has radiogenic $^{87}\text{Sr}/^{86}\text{Sr}$ and yields a well-defined model age $T_{\text{BAB1}} = 3.83 \pm 0.03$ AE. This model age is characteristic of all previously analyzed high-K A-11 samples. The age, initial Sr and model age are in total agreement with determinations on all other A-11 high-K basalts (Papanastassiou *et al.*, 1970).

Table 2. Rb-Sr analytical results.

Sample	Weight ^a (mg)	K (ppm)	Rb ^b (10^{-8} mole/g)	$^{88}\text{Sr}^b$	$^{87}\text{Rb}/^{86}\text{Sr}^c$ ($\times 10^2$)	$^{87}\text{Sr}/^{86}\text{Sr}^d$
10072						
Plag-M	2.0	3320	1.075	434.1	0.578	0.69958 ± 4
Plag-M (CD)	5.9	2544	4.021	400.9	2.340	0.70036 ± 10
Plag + Quint-L	4.2	3584	7.07	419.1	3.935	0.70138 ± 6
Pyroxene-L	42*	380	1.023	32.46	7.35	0.70307 ± 5
Total-M	116*	2752	7.33	165.6	10.32	0.70463 ± 5
Ilmenite-M (CD)	21	3046	8.66	139.3	14.50	0.70678 ± 4
Ilmenite-L	9.8	2204	6.80	68.98	23.00	0.71129 ± 9
10062						
Plag-M	2.4	—	0.175	325.9	0.126	0.69908 ± 6
Plag-L	19	445	0.238	374.8	0.148	0.69910 ± 5
Total-M	117*	607	0.950	181.2	1.223	0.69970 ± 6
Pyroxene-L	35*	142	0.2201	38.23	1.343	0.69976 ± 6
Ilmenite-M	19*	311	0.603	55.01	2.555	0.70048 ± 5
Ilmenite-L	23	352	0.731	43.60	3.910	0.70116 ± 9
				43.56	3.914	0.70128 ± 5

^aSamples marked by an asterisk were analyzed also for Sm-Nd.

^bConcentrations calculated using $^{85}\text{Rb}/^{87}\text{Rb} = 2.591$; $^{86}\text{Sr}/^{88}\text{Sr} = 0.1194$; and $^{84}\text{Sr}/^{88}\text{Sr} = 0.006748$.

^cUncertainties $\pm 0.4\%$.

^dUncertainties are $\pm 2\sigma$, in the last significant figures.

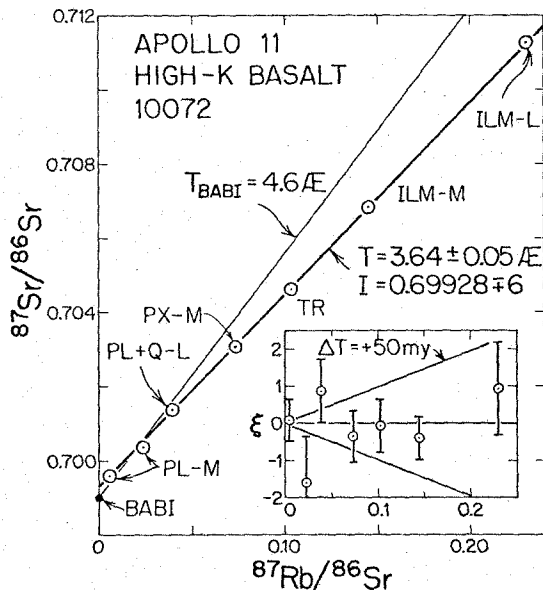


Fig. 2. Rb-Sr evolution diagram for high-K basalt 10072. Inset shows deviations (ξ) of the $^{87}\text{Sr}/^{86}\text{Sr}$ data off the best fit line in parts in 10^4 . T, I uncertainties are 2σ ; the range in measured $^{87}\text{Sr}/^{86}\text{Sr}$ is 1.7%.

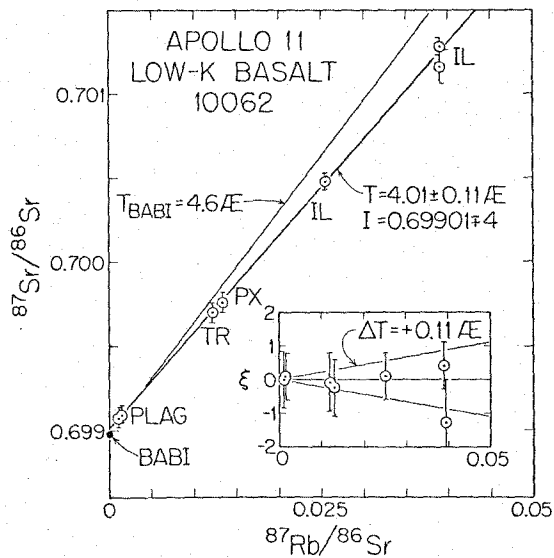


Fig. 3. Rb-Sr evolution diagram for low-K basalt 10062. Inset is explained in Fig. 2 caption. The range in measured $^{87}\text{Sr}/^{86}\text{Sr}$ is 0.3%.

Data have been obtained on six samples from 10062. The data show a range in $^{87}\text{Sr}/^{86}\text{Sr}$ of 0.3%. All data lie on a straight line on the Sr evolution diagram corresponding to $T = 4.01 \pm 0.11$ AE and $(^{87}\text{Sr}/^{86}\text{Sr})_i = 0.69901 \pm 0.00004$ (2σ). All data lie on the best fit line well within experimental uncertainties except for one duplicate, less precise analysis of an ilmenite sample. The $^{87}\text{Sr}/^{86}\text{Sr}$ measurements are of high quality and the lower precision in the age as compared to 10072 is primarily due to the low enrichment in $^{87}\text{Sr}/^{86}\text{Sr}$ for the mineral separates obtained. The initial $^{87}\text{Sr}/^{86}\text{Sr}$ is very close to the value of BABI; the total rock has a model age $T_{\text{BABI}} = 4.1 \pm 0.3$ AE.

Sm-Nd

The Sm-Nd data for six samples from high-K basalt 10072 and five samples from low-K basalt 10062 are given in Table 3. The range of $^{143}\text{Nd}/^{144}\text{Nd}$ obtained for both samples is about 50 parts in 10^4 and enables a precise age determination for both rocks. As seen in Fig. 4, the data points from 10072 all lie within 2 parts in 10^5 of a straight line and determine an excellent isochron corresponding to an age of 3.57 ± 0.03 AE (2σ uncertainties; $\lambda^{(147)\text{Sm}} = 0.00654 \text{ AE}^{-1}$). The 10062 data (Fig. 5) also all lie well within uncertainties (4 parts in 10^5) of the best fit line and yield an age of 3.88 ± 0.06 AE. The Sm-Nd age of 10072 is slightly lower than the Rb-Sr age of 3.64 ± 0.05 AE but is just within analytical errors. For 10062, the Sm-Nd age is in reasonable agreement with the less precise Rb-Sr age of 4.01 ± 0.11 AE. Comparison of the Sm-Nd and the Rb-Sr results shows that the age of 10072 is well resolved from that of 10062 for both techniques. This

Table 3. Sm-Nd analytical results.

Sample	Weight ^a (mg)	Sm ^b (10^{-8} mole/g)	$^{144}\text{Nd}^b$	$^{147}\text{Sm}/^{144}\text{Nd}^c$	$^{143}\text{Nd}/^{144}\text{Nd}^d$
10072					
Quint-L	3.5	34.975	26.716	0.1963	0.511998 ± 16
Plag-L	26	3.098	2.515	0.1847	0.511721 ± 18
Ilmenite-L	21	14.027	10.623	0.1980	0.512035 ± 21
Total-M	116*	14.681	10.680	0.2061	0.512238 ± 17
Pyroxene-A-L	42*	5.306	2.930	0.2715	0.513788 ± 15
Pyroxene-B-L	15	4.591	2.391	0.2879	0.514154 ± 17
10062					
Pyroxene-L	35*	4.705	2.499	0.2823	0.514258 ± 20
Pyroxene-M	20	4.985	2.791	0.2679	0.513847 ± 23
Total-M	117*	8.412	5.848	0.2157	0.512524 ± 19
Ilmenite-M	19*	3.852	2.693	0.2145	0.512487 ± 53
Plag-L	29	1.1518	0.9155	0.1887	0.511839 ± 20

^aSamples marked by an asterisk were analyzed for Rb-Sr also.

^bConcentrations calculated using $^{147}\text{Sm}/^{148}\text{Sm} = 1.33386$, $^{150}\text{Nd}/^{144}\text{Nd} = 0.238585$.

^cUncertainty $\pm 0.1\%$.

^dMeasured on spiked samples; normalized to $^{146}\text{Nd}/^{142}\text{Nd} = 0.636155$.

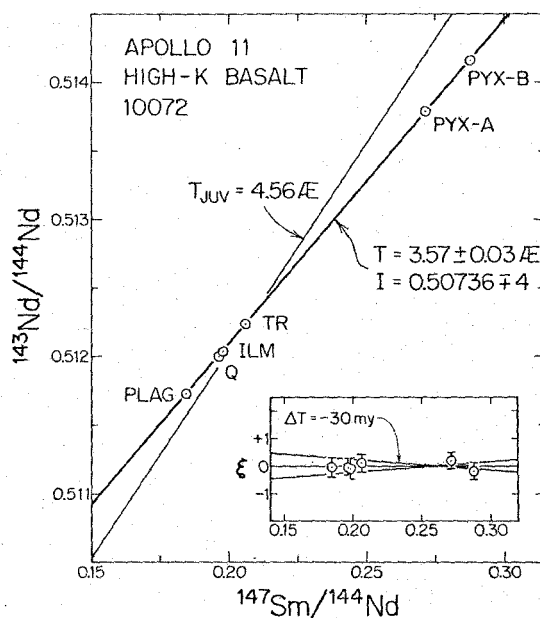


Fig. 4. Sm-Nd evolution diagram for high-K basalt 10072. The precise age and initial $^{143}\text{Nd}/^{144}\text{Nd}$ result from the large range of $^{143}\text{Nd}/^{144}\text{Nd}$ of 50 parts in 10^4 and the fact that all data lie within 0.2 parts in 10^4 of the isochron. Inset shows deviations of $^{143}\text{Nd}/^{144}\text{Nd}$ from the best fit line in parts in 10^4 . The Juvinas isochron is shown for comparison.

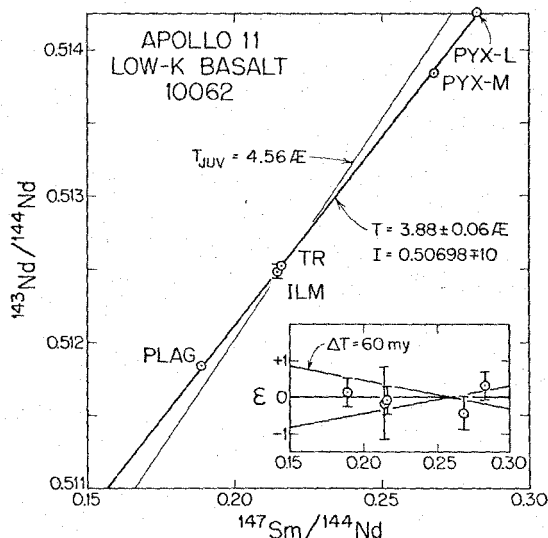


Fig. 5. Sm-Nd evolution diagram for low-K basalt 10062. The range in $^{143}\text{Nd}/^{144}\text{Nd}$ is 50 parts in 10^4 . The Juvinas isochron is shown for comparison.

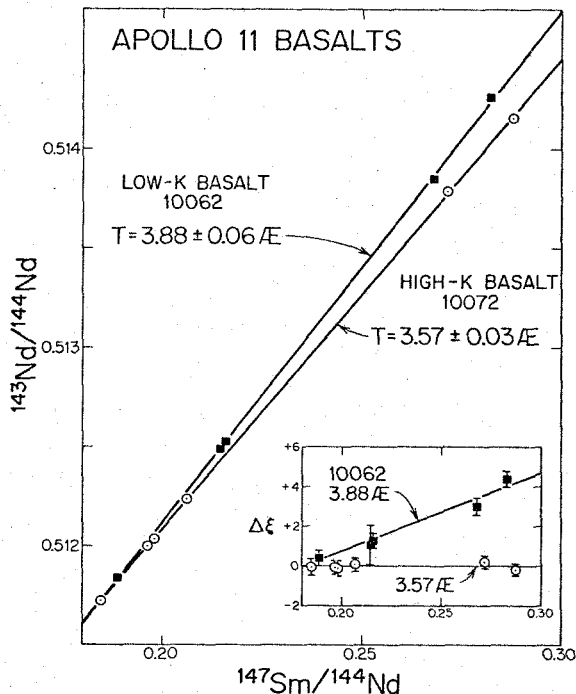


Fig. 6. Sm-Nd evolution diagram showing data for both low-K basalt 10062 and high-K basalt 10072. The data define two well-resolved linear arrays and indicate an unambiguous difference in ages for the two basalts. The inset shows the deviations in parts in 10^4 of the 10062 data points from the isochron defined by the 10072 data.

can be seen most clearly for the Sm-Nd results by inspection of Fig. 6 in which the age difference from the distinct slopes of the isochrons is readily apparent. Since the extremum points on the Sm-Nd isochrons are plagioclase and pyroxene, which are ubiquitous in lunar basalts, the Sm-Nd system could provide precise ages for most lunar basalts. In particular, precise Sm-Nd ages are obtainable on low-alkali basalts, which are difficult to date by Rb-Sr due to the rarity of high-Rb/Sr phases.

DISCUSSION

The Rb-Sr ages of all measured A-11 mare basalts are listed in Table 1; the ages for 10072 and 10062 for all dating schemes are given in Table 4. The Rb-Sr ages for all six high-K basalts are tightly clustered within 0.09 AE from 3.59 to 3.68 AE; sample 10072 falls well within this range. The A-11 high-K basalt data are consistent with crystallization at a single time or within a very narrow time interval. The Rb-Sr ages on four low-K mare basalts have larger uncertainties of $\sim \pm 0.1$ AE (except 10058, Table 1). The data yield a range in ages from

3.63 ± 0.20 AE to 4.01 ± 0.11 AE. The previously published Rb-Sr data (Papanastassiou and Wasserburg, 1975a) confirmed an older ^{40}Ar - ^{39}Ar age for 10003 (Turner, 1970; Stettler *et al.*, 1974); the data on 10062 confirm the existence of additional ancient basalts at the Apollo 11 site. The Rb-Sr data indicate that rocks 10058 and 10044 are indistinguishable in age, rock 10062 is distinctly older and rock 10003 is intermediate in age. Rb-Sr ages for these low-K basalts indicate the existence of three essentially distinct ages.

The Sm-Nd crystallization ages for 10072 and 10062 (Table 4) are clearly distinct and are in good agreement with the Rb-Sr ages. The precise Sm-Nd data on 10062 demonstrate that the Sm-Nd system can result in higher resolution measurements for these rocks than Rb-Sr. The Sm-Nd data clearly permit the identification of a 0.3 AE interval for volcanism at the A-11 site. Additional Sm-Nd data are required to resolve possible small time differences for some A-11 basalts.

The data presented here, which agree with ^{40}Ar - ^{39}Ar data (Turner, 1970; Geiss *et al.*, 1977), demonstrate that mare filling at the Sea of Tranquility occurred over an extended time interval of ~ 0.4 AE. This observation is consistent with the observation of extended intervals of mare filling for the Ocean of Storms of ~ 0.3 AE. Similarly for Taurus-Littrow, the younger age of the orange glass determined by U-Pb (3.48 AE; Tera and Wasserburg, 1976) and by ^{40}Ar - ^{39}Ar (3.54 ± 0.05 ; cf. Hunek *et al.*, 1973, also note discussion of trapped ^{40}Ar problems) provides strong evidence for extended volcanism at this valley. The sampling of rocks with distinct ages at locations on the moon which do not have significant contributions from large distant impacts, indicates that the filling of a single mare basin consisted of thin flows over relatively long time intervals ($2-4 \times 10^8$ yr). These flows must comprise a veneer over the older debris blanket contained in the basin. Both the flows and the older debris must contribute significantly to the local soil chemistry.

The observation of crystallization ages for mare basalts approaching 4.0 AE is of great importance in connection with the time of excavation of the large basins. Similarly the observation of mare basalt ages older than 4.0 AE would provide important constraints for the thermal evolution of the moon in the interval 4.4-4.0 AE. From the combined Rb-Sr and Sm-Nd data on 10062, an age for 10062 not less than 3.90 AE is obtained. Independent of uncertainties associated with the determination of absolute decay constants (see below), these data show that the age of a mare basalt is identical to or older than the inferred

Table 4. Age summary (AE).

	Rb-Sr	Sm-Nd	^{40}Ar - ^{39}Ar	I_{Sr}	I_{Nd}
10062	4.01 ± 0.11	3.88 ± 0.06	3.82 ± 0.06^a	0.69901 ± 4	0.50698 ± 10
10072	3.64 ± 0.05	3.57 ± 0.03	3.62 ± 0.04^b	0.69928 ± 6	0.50736 ± 4

^aTurner (1970) whole rock data.

^bGeiss *et al.* (1977) plagioclase data.

age of the Imbrium event (cf. Papanastassiou and Wasserburg, 1971b). If mare volcanism was triggered by large impacts, e.g., by weakening of the lunar crust and outer mantle, the data on 10062 indicate that an event slightly prior to the Imbrium impact may be responsible for the initial volcanism at the Sea of Tranquility. Alternatively the observation of mare basalt crystallization ages older than the terminal lunar cataclysm would indicate that mare volcanism occurred largely independently of the major impacts on the moon. Based on data on 10003 Geiss *et al.* (1977) have discussed the possibility that mare basalt lavas had begun to invade the Tranquillitatis Basin when the Imbrium impact occurred, so that the Tranquillitatis Basin may be filled with alternating layers of basalt and debris. The identification of mare volcanism at 4.0 AE and at possibly earlier times remains an important problem in lunar chronology and evolution. The data show a distinct overlap between "early" mare volcanism and major impact melting and metamorphism between 4.0 and 3.8 AE. An incisive analysis of the nature and sequence of events in this period has yet to be presented.

Age comparison and ^{87}Rb half-life

Rb-Sr and Sm-Nd crystallization ages have been reported on four mare basalts: 10062 and 10072 (this work); 75075 (Lugmair *et al.*, 1975; Murthy and Coscio, 1976); and 15065 (Papanastassiou and Wasserburg, 1973; Nakamura *et al.*, 1977). The data of 10072 are of sufficient precision to attempt to check on the ^{87}Rb half-life. The half-life of ^{147}Sm has been determined most recently by Gupta and MacFarlane (1970) as 106 ± 2 AE. This value is also essentially the mean of the most precise determinations (cf., Donhoffer, 1963). Much of the quoted uncertainty in the reported half-lives was the result of uncertainty in the isotopic composition of Sm (cf., Wright *et al.*, 1961), which has since been determined more precisely (Russ *et al.*, 1971). It thus appears that the best value for the ^{147}Sm half-life is 106 AE ($\lambda = 0.00654 \text{ AE}^{-1}$) and the uncertainty in this number is about $\pm 1\%$. The Rb-Sr and Sm-Nd data on 10072 show a difference in age of 0.07 AE. If this difference is due to the uncertainty in the half-life of ^{87}Rb , a downward revision in the ^{87}Rb half-life by 2% is indicated corresponding to a revised $\lambda(^{87}\text{Rb}) = 0.0142 \text{ AE}^{-1}$. This would be in close agreement to the revision of $\lambda(^{87}\text{Rb})$ required for concordance with the U-Pb system using the revised U decay constants (Jaffey *et al.*, 1971). We note that use of the less precise Sm-Nd data on 15065 and on 75075 would result in different conclusions about $\lambda(^{87}\text{Rb})$. Although arguments about half-lives based on high quality age determinations of good igneous rocks are of merit, we believe that Rb-Sr ages should still be reported using $\lambda = 0.0139 \text{ AE}^{-1}$, until the ^{87}Rb decay constant is in fact accurately determined by mass spectrometric methods or until more high quality age comparisons are made. In cases where detailed comparison is necessary for ages obtained by different techniques, it may be advisable to use the revised half-life for establishing agreement or disagreement between the different techniques.

From a comparison of reliable $^{40}\text{Ar}-^{39}\text{Ar}$ age determinations for samples subject to small gas loss and no serious trapped ^{40}Ar problems (cf. review by

Turner, 1977; Tera *et al.*, 1974; Stettler *et al.*, 1974; Kirsten and Horn, 1974) it appears that there is good agreement between Rb-Sr crystallization ages and $^{40}\text{Ar}-^{39}\text{Ar}$ gas retention ages. Therefore a revision of $\lambda(^{87}\text{Rb})$ by +2% would require an increase in $\lambda(^{40}\text{K})$ of 3% (for constant λ_e/λ) in order to avoid having $^{40}\text{Ar}-^{39}\text{Ar}$ ages systematically older than Rb-Sr ages. Additional absolute calibrations of the $^{40}\text{Ar}-^{39}\text{Ar}$ technique are desirable for a detailed comparison of ages.

For 10072, the results of all three methods are in close agreement when the plagioclase data for $^{40}\text{Ar}-^{39}\text{Ar}$ are considered (Geiss *et al.*, 1977). For 10062, the Rb-Sr and $^{40}\text{Ar}-^{39}\text{Ar}$ are barely in agreement; the Sm-Nd age has an intermediate value and is in agreement within uncertainties with both the Rb-Sr and $^{40}\text{Ar}-^{39}\text{Ar}$ ages. However, it is possible that the $^{40}\text{Ar}-^{39}\text{Ar}$ apparent age obtained on a total rock sample is slightly depressed due to ^{40}Ar loss. There is good agreement for all other Rb-Sr and $^{40}\text{Ar}-^{39}\text{Ar}$ ages for A-11 except for rock 10071 as pointed out by Geiss *et al.* (1977). The Rb-Sr data on 10071 should possibly be reexamined; similarly Rb-Sr data on 10049 would be useful for comparing with the much younger $^{40}\text{Ar}-^{39}\text{Ar}$ for this sample, although most probably the intermediate temperature $^{40}\text{Ar}-^{39}\text{Ar}$ plateau age on a total rock cannot be considered reliable (Geiss *et al.*, 1977). We note from the data in Table 1 that there is still only a limited number of $^{40}\text{Ar}-^{39}\text{Ar}$ high temperature plateaus on plagioclase.

Artifacts from mixing lines

In our work on Rb-Sr crystallization ages we have pointed out the possibility that the linear arrays obtained on Rb-Sr evolution diagrams may be the result of mixing of only two end members, plagioclase and late crystallizing interstitial phases. In such a case it is in principle possible to obtain an erroneous age if one of the end members has been an open system subsequent to the crystallization of the rock. We have expended a considerable effort in analyzing phases with distinct major element chemistry and K, Rb, Sr abundances (cristobalite, ilmenite, quintessence) for the purpose of establishing the presence in individual samples of more than two phases which are carriers of Rb and Sr. In many instances it has been possible to demonstrate by element correlations (Papanastassiou and Wasserburg, 1971a; Wasserburg and Papanastassiou, 1971b) that more than two phases were sampled and that therefore the data defined true isochrons. In contrast to the Rb-Sr system, where incompatible elements in the late crystallizing phases may be easily mobilized, the Sm-Nd age determinations depend primarily on Sm and Nd in major minerals (pyroxene and plagioclase) in which the REE would be expected to be much less mobile. The agreement of Sm-Nd and Rb-Sr crystallization ages demonstrates that for mare basalts the phases used for dating have not been disturbed since the time of crystallization. This conclusion is contrary to the discussion by Birck *et al.* (1975), who have again reexamined this problem and who believe that the possibility that the isochrons are the result of mixing lines may not permit reliable Rb-Sr age determinations.

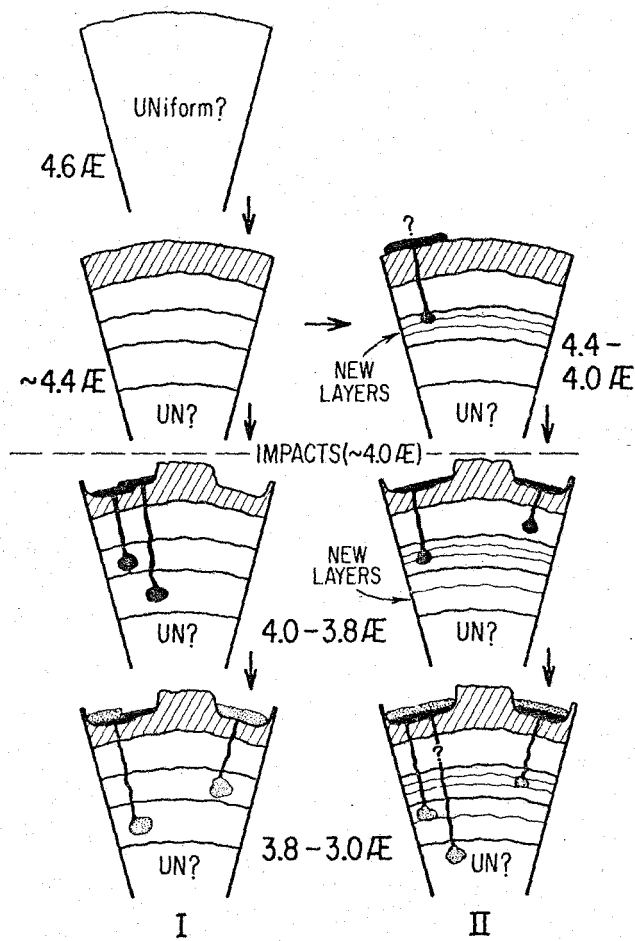


Fig. 7. Idealized representation of two possible versions for the formation of parent reservoirs for mare basalts. The coarse layering shown represents the chemically distinct reservoirs formed during the early lunar differentiation near 4.4 AE while the finer-scale layering represents reservoirs formed during the period 4.4–3.0 AE. The ruled layer represents the lunar crust. The solid and stippled blobs and layers represent mare basalt magmas generated by melting in the different layers and then erupted at the surface as lava flows filling the great lunar basins which were excavated by major impacts at ~4.0 AE. The solid blobs represent magmas formed before or near the time of impacts while the stippled blobs and flows represent the later stages of mare volcanism. UN represents possible undifferentiated material in the lunar interior from which some lunar rocks may be derived. In I, the differentiation of the lunar crust and mantle into a layered structure takes place during a single event at ~4.4 AE and volcanism is restricted to times more recent than the time of major impacts at ~4.0 AE. II depicts the possibility that volcanism and the production of new layers was an ongoing process which continued without interruption from 4.4 to 3.0 AE essentially independently of impacts at 4.0 AE.

Lunar differentiation and the formation of magma sources

Models for the evolution of the moon consider an early differentiation which resulted in a basically layered structure for the crust and "upper mantle" of the moon (cf. Taylor and Jakeš, 1974). The basalts produced in the interval 4.0–3.0 AE are therefore viewed as being crystallized from magmas which were produced from the earlier-formed layers and not as direct products from an undifferentiated moon. A highly schematic scenario for the early history of the moon is shown in Fig. 7 and will serve as a basis for subsequent discussion of the isotopic data. Two alternatives for an early lunar history are shown. In both cases, we assume the moon is formed as a compositionally uniform sphere ~4.6 AE ago. At about 4.4 AE the outer portion of the moon is differentiated and a sequence of distinct layers is formed corresponding to the crust and a layered upper mantle. Each of these layers is reasonably uniform within itself but distinct from other layers above and below it. In case I, depicted on the left half of the diagram, the layering in the moon is formed in a single distinct event at ~4.4 AE. The period ~4.4–4.0 AE is quiescent and there is only rare volcanism. Volcanism is triggered by impacts at ~4.0 AE and basaltic magmas are generated by melting in these layers in the time interval 4.0–3.0 AE. The magmas are envisioned volumetrically insignificant in comparison to the layers they were melted from, so the layers formed at 4.4 AE are undisturbed by the removal of magmas to the surface. The right half of Fig. 7 shows another possibility (II). In this case, the formation of layers or segregated pods in the older layers in the lunar interior is viewed as a continuing process which began at 4.4 AE. Under these conditions a substantial amount of basalt could have been extruded prior to 4.0 AE. For basalt magma formation between 4.4 to 3.0 AE, magmas are being melted from layers formed at 4.4 AE, and, in addition, from layers that were formed at times distinctly younger than 4.4 AE. During the time that the more ancient basalts were being produced, even more new layers were being formed in the lunar mantle. Basaltic magmas formed later are then derived from layers of a variety of ages. Some magmas are melted from 4.4 AE old layers, others are melted from layers formed 4.4–4.0 AE ago, and still others are derived from layers which were not formed until much more recently than 4.0 AE. New layers formed during the era of basaltic volcanism could have formed as a result of magma removal from pre-existing layers. For instance, a large amount of magma removed from one part of a layer could cause that part of the layer to be left with a different composition, thereby creating in effect a new sublayer. By very limited partial melting, it is also possible to obtain basaltic magmas from a single layer at successively younger times without significantly affecting the composition of the layer. In this case the same layer can provide similar basaltic melts over a prolonged interval. For our purposes different layers may have distinct major and trace element abundances. To the extent that different layers have a different Rb/Sr or Sm/Nd, they will be evolving different $^{87}\text{Sr}/^{86}\text{Sr}$ and $^{143}\text{Nd}/^{144}\text{Nd}$ from 4.4 AE onward. At any given time after 4.4 AE, each layer will have its own characteristic $^{87}\text{Sr}/^{86}\text{Sr}$ and $^{143}\text{Nd}/^{144}\text{Nd}$. If two batches of basaltic

magma were formed at ~ 3.9 AE in two different layers and were then erupted at the surface, we would observe a difference in initial Sr and Nd in the basalts which would indicate that they were derived from different "layers" or "parent reservoirs." The major issues are whether substantial differentiation of the old layered mantle took place after ~ 4.4 AE and whether there exists a significant volume of the moon which remained undifferentiated. In the ensuing discussion we will use the terms "layer" and "reservoir" or "parent reservoir" interchangeably. In each case these terms are used to describe regions of the lunar interior analogous to the layers described above from which basaltic magmas have been melted and erupted at the surface.

Figure 8 shows a schematic evolution of a radiogenic isotope in two reservoirs A and B. Basalts (A1 and B1) produced at the same time with different I values must have been melted from different reservoirs ("layers") with distinct (P/D) ratios. Basalts A1 and A2 produced at different ages were extracted from a single reservoir A without altering the P/D of the parent reservoir A. This simple evolution model, where basalt parent reservoirs are formed at one time T_0 (~ 4.4 AE), and the basalts are formed at later times is analogous to the lunar history scheme I of Fig. 7. For model II of Fig. 7, where parent reservoirs are being formed after T_0 , more complicated trajectories are possible in Fig. 8. For instance, it is possible to produce basalt A2 from a reservoir B' which at some time prior to T_2 (e.g., at T_1) was produced from B with a P/D sufficiently large to evolve from point B1 to point A2 in the available time $T_1 - T_2$. The extent to which a reservoir can reach A2 from B1 is only constrained by the size of fractionation in P/D.

We consider the evolution of the Sr and Nd isotopic composition prior to the time of crystallization of a basalt. The ^{87}Sr and ^{143}Nd evolution is constrained to

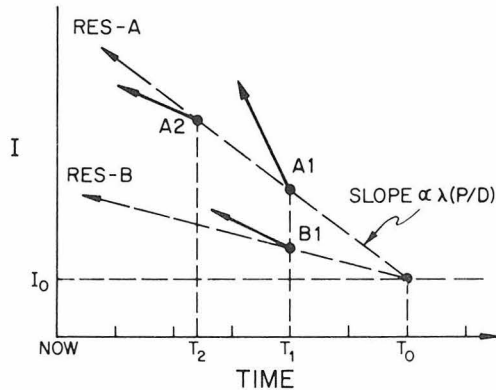


Fig. 8. Evolution of a radiogenic isotope in two distinct reservoirs as a function of time; the difference in slopes is proportional to the parent/daughter ratio (P/D) in the rock, the magma and the parent reservoir. Basalts A1 and B1 produced at the same time from distinct reservoirs will have distinct initial isotopic composition as determined from their isochrons. Basalt A2 is compatible with production from reservoir A; however, alternate, more complex or independent evolution paths are also possible.

yield the initial $^{87}\text{Sr}/^{86}\text{Sr}$ (I_{Sr}) and $^{143}\text{Nd}/^{144}\text{Nd}$ (I_{Nd}) determined by the isochrons at the time of crystallization. For Rb-Sr (Papanastassiou and Wasserburg, 1971a) and Sm-Nd we get similar equations:

$$I_{\text{Sr}} - I_{\text{Sr}}^0 = \lambda_{\text{Rb}}(^{87}\text{Rb}/^{86}\text{Sr})_1 \cdot \Delta T_1 + \lambda_{\text{Rb}}(^{87}\text{Rb}/^{86}\text{Sr})_2 \cdot \Delta T_2 + \dots$$

$$I_{\text{Nd}} - I_{\text{Nd}}^0 = \lambda_{\text{Sm}}(^{147}\text{Sm}/^{144}\text{Nd})_1 \cdot \Delta T_1 + \lambda_{\text{Sm}}(^{147}\text{Sm}/^{144}\text{Nd})_2 \cdot \Delta T_2 + \dots$$

If T_0 is the time of formation of the moon and T_x is the time of crystallization of a particular basalt then:

$$\Delta T_1 + \Delta T_2 + \Delta T_3 + \dots = T_0 - T_x$$

The ratios $(^{87}\text{Rb}/^{86}\text{Sr})_1/(^{87}\text{Rb}/^{86}\text{Sr})_2$ and $(^{147}\text{Sm}/^{144}\text{Nd})_1/(^{147}\text{Sm}/^{144}\text{Nd})_2$ are the fractionation factors for Rb-Sr and for Sm-Nd between stages 1 and 2. I_{Sr}^0 and I_{Nd}^0 are the initial ratios with which the moon formed. For two basalts with identical ages, a difference in the I values requires differences in the P/D ratios in parent sources lasting for some finite time intervals ΔT_i . The size of the differences in I_{Sr} and I_{Nd} depends on the degree of fractionation of P/D elements and on the length of the intervals ΔT_i for which particular $(P/D)_i$ values remain constant. Differences in I_{Sr} and in I_{Nd} provide distinct information about the parent reservoirs. One of the basic distinctions between Rb-Sr and Sm-Nd systematics is that the maximum magnitude of Sm-Nd fractionations is expected to be much smaller than possible Rb-Sr fractionations. Therefore, production of large differences in I_{Nd} requires relatively large time intervals ΔT_i .

Initial $^{87}\text{Sr}/^{86}\text{Sr}$ values of lunar rocks are presented and discussed in terms of a (T, I) diagram identical to Fig. 8. However, because Sm/Nd varies by a much smaller amount relative to the average Sm/Nd of most reservoirs than does Rb/Sr, we have represented the Nd isotopic data in a different way, as discussed at some length by DePaolo and Wasserburg (1976b). In this representation, the initial ratios are compared to the evolution of $^{143}\text{Nd}/^{144}\text{Nd}$ in a reference reservoir (CHUR) which has a chondritic Sm/Nd and initial Nd equal to that measured in Juvinas (Lugmair *et al.*, 1975; Lugmair *et al.*, 1976). Initial Nd for a rock which crystallized at T is given as the fractional deviation in parts in 10^4 of the initial $^{143}\text{Nd}/^{144}\text{Nd}$ from the $^{143}\text{Nd}/^{144}\text{Nd}$ in CHUR ($I_{\text{CHUR}}(T)$). This quantity is termed ϵ_I^{CHUR} and defined

$$\epsilon_I^{\text{CHUR}} = \frac{I_{\text{ROCK}} - I_{\text{CHUR}}(T)}{I_{\text{CHUR}}(T)} \times 10^4.$$

The initial $^{87}\text{Sr}/^{86}\text{Sr}$ data for Apollo 11 basalts are shown in Fig. 9, and the initial $^{143}\text{Nd}/^{144}\text{Nd}$ data for all mare basalts measured are shown in Fig. 10. For Sr a single straight line evolution curve can be drawn through all of the A-11 low-K basalts, which indicates that these basalts could all have been derived from the same reservoir at distinct times. Because of the very low Rb/Sr in the parent reservoirs of these basalts, departures from a single reservoir are difficult to detect. In contrast to this result, Beatty *et al.* (1977) have presented arguments for distinct groups of A-11 low-K basalts based on major element chemistry, and stated that the observed major element differences are neither the result of

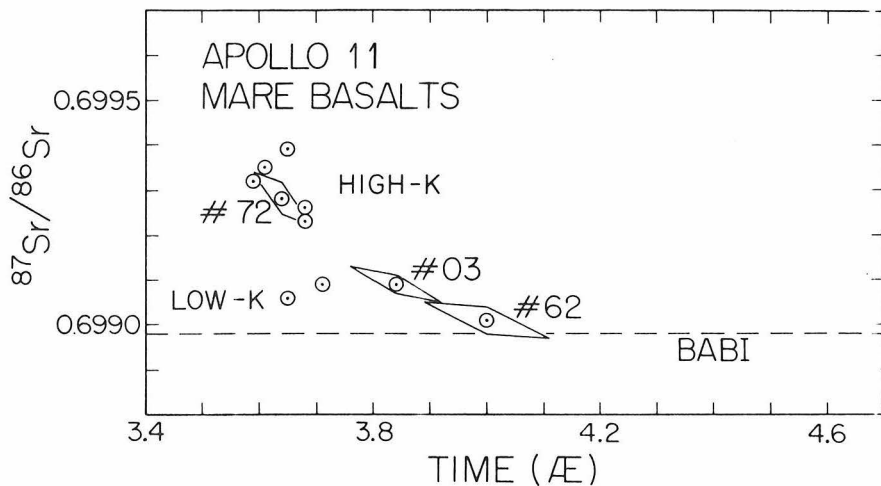


Fig. 9. Age (T), Initial $^{87}\text{Sr}/^{86}\text{Sr}$ (I) for Apollo 11 mare basalts. All high-K rocks (including 10072) are tightly grouped in both T and I . Low-K rocks show a distinct range in T and relatively lower I values. Unlabelled low-K rocks are 10044 and 10058.

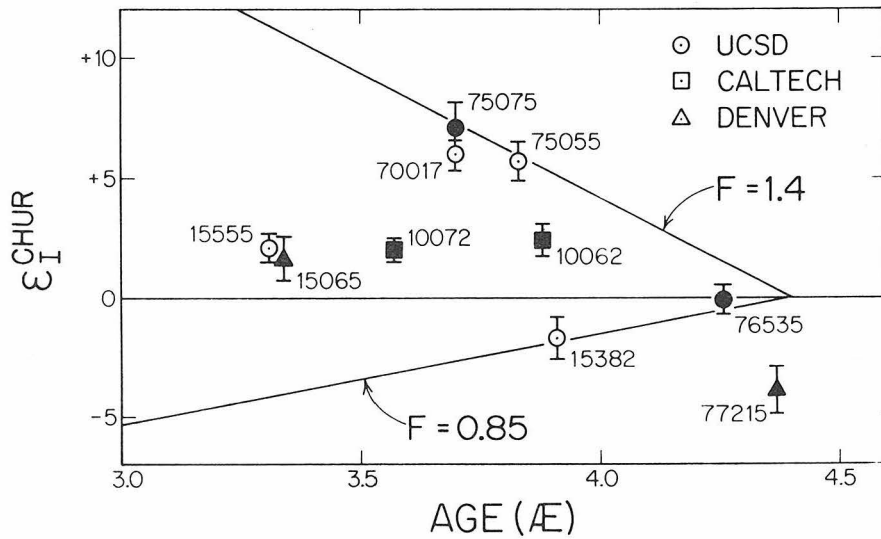


Fig. 10. Fractional deviations in parts in 10^4 of the initial $^{143}\text{Nd}/^{144}\text{Nd}$ of lunar rocks from the evolution of $^{143}\text{Nd}/^{144}\text{Nd}$ in a chondritic Sm/Nd reservoir (CHUR) plotted versus time. Solid lines diverging from CHUR at 4.4 AE represent Nd evolution in reservoirs fractionated from CHUR at that time with Sm/Nd 1.4 and 0.85 times chondritic. Filled points are samples for which Sm-Nd internal isochrons have been determined. Open points are calculated from whole rock Sm-Nd data of Lugmair (1975) and Rb-Sr internal isochron ages. CHUR line is calculated using modern $^{143}\text{Nd}/^{144}\text{Nd} = 0.511836$ and $^{147}\text{Sm}/^{144}\text{Nd} = 0.1936$ (De Paolo and Wasserburg, 1976a).

differences in the extent of partial melting in the source at different times nor of near surface crystal fractionation prior to crystallization. Thus, this must be the result of differences in parent reservoirs of the basalts which are not reflected in their isotopic compositions.

The A-11 high-K basalts could all be derived from a single reservoir at the same time; however, their parent reservoir must obviously have been different from that of the low-K basalts. This general conclusion (cf. Papanastassiou and Wasserburg, 1971a) and the inferences based on experimental petrologic studies (Walker *et al.*, 1975) are in accord. Based on Rb-Sr, the reservoir which produced the high-K basalts could have been formed early in lunar history with a relatively low Rb/Sr or as late as the time of extrusion of some of the low-K basalts (~ 3.9 AE) with a considerably higher Rb/Sr. If the high Rb/Sr of the high-K basalts was a characteristic of their *parent* reservoir, then that parent reservoir could not have been formed earlier than ~ 3.9 AE, the model age of these basalts (Papanastassiou *et al.*, 1970).

For Sm-Nd, rocks 10072 and 10062 were clearly produced at distinct times. From Fig. 10, ϵ_I^{CHUR} for 10072 is slightly below that for 10062, even though 10072 is the younger basalt. Therefore, it is not possible to derive 10072 from the same reservoir as 10062. This conclusion is in agreement with the Sr data. It can also be seen in Fig. 10 that Apollo 15 basalts 15555 and 15065 (Lugmair, 1975; Nakamura *et al.*, 1977) could be derived from a reservoir similar to that of 10072, a somewhat surprising result considering the striking chemical differences in major elements between Apollo 11 and 15 basalts (Table 5). This conclusion on A-15 basalts is in agreement with Rb-Sr data (Papanastassiou and Wasserburg, 1973). It can also be seen that Apollo 17 basalts must be derived from a different reservoir than the Apollo 11 basalts as discussed more fully below. We note in Fig. 10 that sample 77215 falls in a nearly inaccessible part of the diagram and this may be the result of experimental artifacts, or due to partial isotopic equilibrium achieved for this sample, which is a clast in a highland breccia (Nakamura *et al.*, 1976).

Sources of high-Ti mare basalts

Models of the early history of the moon depict the entire outer moon as being extensively melted very soon after the moon accreted (Taylor and Jakeš, 1974). In a model such as this, the layering of the outer moon represents crystal cumulates which formed as different minerals crystallized from this magma (Philpotts and Schnetzler, 1970). The isotopic data can be related to the mineralogy of these layers and thus are directly applicable to the problem of the characterization of magma sources and lunar interior structure. The relationship of Rb/Sr and Sm/Nd to mineralogy is summarized below. The major minerals which crystallized from the magma are believed to be olivine, orthopyroxene, clinopyroxene, plagioclase, and ilmenite or spinel (Hodges and Kushiro, 1974). Of these, olivine, orthopyroxene, and ilmenite would crystallize with very low concentrations of REE, Rb, and Sr, so crystallization of these minerals from the

magma will merely cause the concentrations of the trace elements in the residual liquid to be increased with *no* significant change of Rb/Sr or Sm/Nd. Clinopyroxene will crystallize with a higher Sm/Nd and lower Rb/Sr than the magma from which it crystallized (Shih *et al.*, 1975). Thus layers rich in clinopyroxene will have high Sm/Nd and low Rb/Sr, and the liquid left after clinopyroxene has crystallized will have a low Sm/Nd and slightly higher Rb/Sr. Plagioclase will crystallize with a low Sm/Nd and extremely low Rb/Sr (Drake and Weill, 1975), so layers rich in plagioclase will reflect these traits as well as have a high-Eu concentration. Residual liquids left after most of the magma is crystallized will have high concentrations of REE and Rb, high Rb/Sr and somewhat low Sm/Nd relative to the original magma. The consequences of layering in the lunar mantle for Rb-Sr and Sm-Nd systematics in second generation magmas would be directly dependent on the different proportions of clinopyroxene and plagioclase (or their high, *P*, *T* equivalents) and the presence of interstitial, trace-element rich material. In most models, plagioclase and residual liquids are expected to be more abundant in the upper part of the magma body; i.e., at relatively shallow depths in the lunar mantle. In addition, Ma *et al.* (1976) have emphasized the role of individual trace phases such as apatite in determining the trace element pattern in the layers. However, the following discussion will be limited to major phases.

It has been observed that the low-K, high-Ti basalts found on the Apollo 17 and 11 missions are similar in both major and trace element abundances (cf. Table 5) and that their compositions can be related by near surface removal of olivine (Walker *et al.*, 1975; Dymek *et al.*, 1975). It might be expected, then, that these magmas were formed by melting of the same mineralogical "layer" in the moon. The ages and initial $^{87}\text{Sr}/^{86}\text{Sr}$ of these basalts are very similar, so from Sr isotopes it could be concluded that these magmas originated in the same layer of the moon. Inspection of Fig. 10, however, shows that ϵ_i^{CHUR} of Apollo 17 basalts is +6 to +7, while for Apollo 11 low-K basalt it is about +2. This indicates that the A-17 basalts were derived from a layer which had a much higher Sm/Nd than did the source of the low-K A-11 basalts. If it is assumed that the moon formed 4.55 AE ago with $^{143}\text{Nd}/^{144}\text{Nd}$ equal to the initial ratio of the Juvinas achondrite (Lugmair *et al.*, 1975), then the layer from which the Apollo 17 basalts were derived must have had Sm/Nd at least 30% higher than chondritic. This represents a very high Sm/Nd and indicates that this layer must have been dominantly composed of clinopyroxene or possibly small amounts of garnet, the only major minerals which can have such high Sm/Nd. The layers from which the Apollo 11 basalts were derived, however, must have included higher proportions of plagioclase or residual liquid which have lower Sm/Nd. The initial $^{87}\text{Sr}/^{86}\text{Sr}$ of the low-K basalts indicate that the source layer of the A-11 basalts had Rb/Sr the same or lower than did the parent layer of the A-17 basalts. It is difficult for the A-11 *source* layer to be enough enriched in residual liquid to have a lower Sm/Nd and still have a low Rb/Sr. However, an increased amount of plagioclase in the A-11 (low-K) source layer would provide a low Rb/Sr and Sm/Nd. This conclusion is not in disagreement with experimental results on

Table 5. Chemical composition of mare basalts.

	10072 ^a	10062 ^b	75075 ^c	15555 ^d
SiO ₂	40.53	38.8	38.51	44.57
TiO ₂	11.74	10.3	13.33	2.10
Al ₂ O ₃	8.52	12.1	8.29	8.69
FeO	19.76	18.3	18.85	22.53
MnO	0.24	0.27	0.25	0.29
MgO	7.68	7.21	9.68	11.36
CaO	10.42	12.0	10.17	9.40
Na ₂ O	0.54	0.69	0.37	0.27
K ₂ O	0.27	0.07	0.11	0.04
P ₂ O ₅	0.14	<0.02	0.12	0.06
S	0.24	—	—	0.06
Cr ₂ O ₃	0.35	0.25	0.55	0.61
K	2752	607	435	230
Rb	6.26	0.81	0.46	0.54
Sr	176	192	165	74.1
Sm	22.1	12.6	7.22	3.87
Nd	64.8	35.5	17.0	11.8
Sm/Nd ^e	0.341	0.355	0.425	0.328
Sm/Eu ^e	8.7	6.6	4.7	4.4

^aMaxwell *et al.* (1970), trace elements from our data and Haskin *et al.* (1970).

^bRose *et al.* (1970), trace elements from our data and Gast *et al.* (1970).

^cRose *et al.* (1974), trace elements from Shih *et al.* (1975), Lugmair *et al.* (1975).

^dPapike *et al.* (1976), trace elements from Schnetzler *et al.* (1972), Lugmair *et al.* (1975).

^eSm/Eu in chondrites = 2.6; Sm/Nd in chondrites = 0.32.

Apollo 11 compositions (Walker *et al.*, 1975) which indicate that plagioclase was not a *residual* mineral in the source, since *all* of the plagioclase present in the source layer could have entered the melt. The higher initial ⁸⁷Sr/⁸⁶Sr and relatively low $\epsilon_{\text{I}}^{\text{CHUR}}$ of the Apollo 11 high-K basalts indicate that their source layer was slightly enriched in residual liquid component (and possibly also depleted in plagioclase) compared to the sources of the low-K basalts. The amounts of olivine, orthopyroxene, and ilmenite are not indicated by the isotopic data, since these minerals are essentially devoid of the trace elements considered here.

In summary, it appears that high-Ti mare basalts have been derived from a multiplicity of mineralogically distinct "layers" in the lunar mantle. The Apollo 17 basalts must be derived from a layer comprised dominantly of clinopyroxene or perhaps some garnet and devoid of trapped late-stage residual liquid. The Apollo 11 low-K basalts must be derived from a similar clinopyroxene-rich layer,

but containing significantly greater amounts of plagioclase. Apollo 11 high-K basalts parent sources could correspond to a clinopyroxene-rich layer which contains a small amount (1%) of trapped K, REE and Rb-rich liquid. In the simplest models (Taylor and Jakeš, 1974) this would place the source layer of the Apollo 17 basalts at the greatest depth, with the source layers of the Apollo 11 low-K basalts and Apollo 11 high-K basalts at successively shallower levels.

Sm-Nd fractionation during basalt formation and the time of the early lunar differentiation

We have reviewed recently the evidence for early lunar differentiation based on Rb-Sr and U-Pb (Papanastassiou and Wasserburg, 1976). We view as the strongest current evidence for early lunar differentiation the existence of two ancient rocks (a troctolite and a dunite) and of a polymict breccia (12013) highly enriched in KREEPUTh elements and with Rb-Sr systematics strongly indicating production of this material at ~ 4.5 AE. While the Rb-Sr and Sm-Nd data on troctolite 76535 indicate an ancient age, there exists a significant discrepancy. The distinct behavior of Sm-Nd and of Rb-Sr systematics for the troctolite (Lugmair *et al.*, 1976; Papanastassiou and Wasserburg, 1976) requires further investigation, although possible mechanisms for making the Rb-Sr and Sm-Nd data compatible have been presented which consider the Rb-Sr ancient age as the primary age. We have also reviewed extensively in the past the Rb-Sr model ages of soils and most breccias and mare basalts which indicate in a general way an early interval for lunar differentiation. More recently Nyquist *et al.* (1976) have presented more complex two-stage models to interpret the Apollo 17 mare basalt Rb-Sr data. These models require precursors to the parent sources of mare basalts from 4.6–4.4 AE with a significant range in Rb/Sr. Furthermore, the Rb/Sr in these early reservoirs are much higher than observed in basalts today. Whereas these models are constructed to assure that the Rb/Sr in the basalts are higher than in the parent reservoirs, these models do not provide a better definition of the chronology of early lunar differentiation processes. This is basically due to the small initial $^{87}\text{Sr}/^{86}\text{Sr}$ enrichments found for mare basalts which makes these calculations relatively insensitive. By contrast, U-Pb data on mare basalts and on highland samples yield a well-defined upper intersection with concordia at 4.42 AE (Tera and Wasserburg, 1974, 1976). Data on concordant whole rocks as well as isochrons for mare basalts of distinct ages define a unique intersection at 4.42 AE. Although this time is model dependent, it implies a precise time at which mare basalt reservoirs were produced. We review now the evidence for early lunar differentiation based on Sm-Nd.

The first Sm-Nd data bearing on early lunar differentiation were obtained by Lugmair *et al.* (1975) and Lugmair (1975). Their data on mare basalt 75075 showed that the fractionated rare earth element pattern relative to chondrites of Apollo 17 basalts was a characteristic of the parent reservoir of these rocks. To estimate the time at which the parent reservoirs acquired their fractionated Sm/Nd, Lugmair *et al.* (1975) calculated two types of model ages, which are

illustrated in Fig. 12. T_{CHUR} ages (also called T_{ICE} by Lugmair *et al.*, 1976) are based on the intersection of a basalt evolution line with the chondritic evolution line. The chondritic evolution line is calculated from data on the Juvinas achondrite. Sm-Nd *model* ages can also be defined which are analogous to T_{BAB1} Rb-Sr model ages by extrapolation of the evolution of mare basalts to the initial $^{143}\text{Nd}/^{144}\text{Nd}$ of Juvinas. Lugmair *et al.* (1975) found that T_{CHUR} of 75075 was close to 4.4 AE and noted that this number was similar to the 4.42 AE event indicated by U-Pb. They noted that this T_{CHUR} age could be explained if the parent reservoir for this basalt had formed at 4.4 AE with the Sm/Nd measured in 75075 from a pre-existing chondritic Sm/Nd reservoir. If T_{CHUR} ages of additional mare basalts were to cluster very near 4.4 AE, then this would provide substantial evidence for the time of early differentiation on the moon. In addition, this would imply that the Sm/Nd of each mare basalt was the same as the Sm/Nd of its parent reservoir and would therefore represent a strong constraint on the petrogenesis of mare basalts. To further investigate this possibility Lugmair (1975) obtained Sm-Nd data on three additional mare basalts. He found that 75075, 75055, and 15555 whole rocks defined an isochron indicating an age of 4.40 ± 0.06 AE and having initial $^{143}\text{Nd}/^{144}\text{Nd}$ equal to the value expected in a chondritic reservoir at 4.40 AE. This is equivalent to saying that the three basalts have T_{CHUR} ages which are all equal to 4.40 AE. These data thus provided support for the simple model for 75075 and were entirely consistent with a model for lunar differentiation in which the moon was formed with a chondritic Sm/Nd and then differentiated at 4.4 AE to form the different parent reservoirs of the mare basalts, and the basalts were formed from 4.0–3.0 AE with Sm/Nd unchanged from that of their respective parent reservoirs. One additional basalt, 70017, did not lie on the isochron defined by the other three rocks, but could be made consistent with the early differentiation at 4.4 AE if a change of Sm/Nd in the basalt of 2% relative to the parent reservoir had occurred during genesis of 70017 at ~ 3.7 AE. Thus, all the data suggested that less than about 2% change of Sm/Nd occurred during melting, extrusion and crystallization of the basalts. However, the T_{CHUR} ages of Lugmair *et al.* (1975) and Lugmair (1975) were calculated relative to the $^{143}\text{Nd}/^{144}\text{Nd}$ of Juvinas prior to its revision. The revision of the Juvinas data causes the T_{CHUR} ages of those basalts to be increased by amounts greater than or equal to 100 m.y. depending upon the Sm/Nd of the basalt. This change makes the whole rock isochron of Lugmair (1975) more difficult to interpret. If, for instance, the 4.4 AE isochron age is taken as the age of the basalt parent reservoirs, then the initial $^{143}\text{Nd}/^{144}\text{Nd}$ from this isochron is not consistent with chondritic evolution prior to 4.4 AE. Assuming that the three point total rock isochron defines a true age, the distinct T_{CHUR} ages of the basalts indicate that the Sm/Nd of the basalts is substantially different ($\sim 4\text{--}6\%$) from their parent reservoirs. This situation represents a substantially different Nd evolution model than the simple two-stage model suggested by Lugmair (1975). Alternatively, it can be considered that the isochron is an accident and has no real time meaning. In any case, the revision of the Juvinas data has necessitated some major changes in interpretation of the Sm-Nd isotope, which have not been explored in the literature to date. However, it should be made clear that the conclusions from model age

calculations discussed here and by Lugmair are very sensitive to the choice of parameters. As in the case of Sr evolution, it is not evident that a definite assignment for primary source ages is possible if multi-stage models must be invoked. Certainly, the Sm-Nd data show evidence of early lunar differentiation but do not precisely define the time of that event.

The revision of the Juvinas data and the acquisition of a substantial amount of new data necessitate reevaluation of the Sm-Nd evidence bearing on the time of early lunar differentiation and the behavior of rare earth elements at the time of formation of the basalts. The two are intimately related so we have chosen to discuss them in terms of a diagram (Fig. 11) which shows the relationship between the time of formation of the source reservoirs of mare basalts and the inferred Sm/Nd fractionation during genesis and crystallization of the basalts.

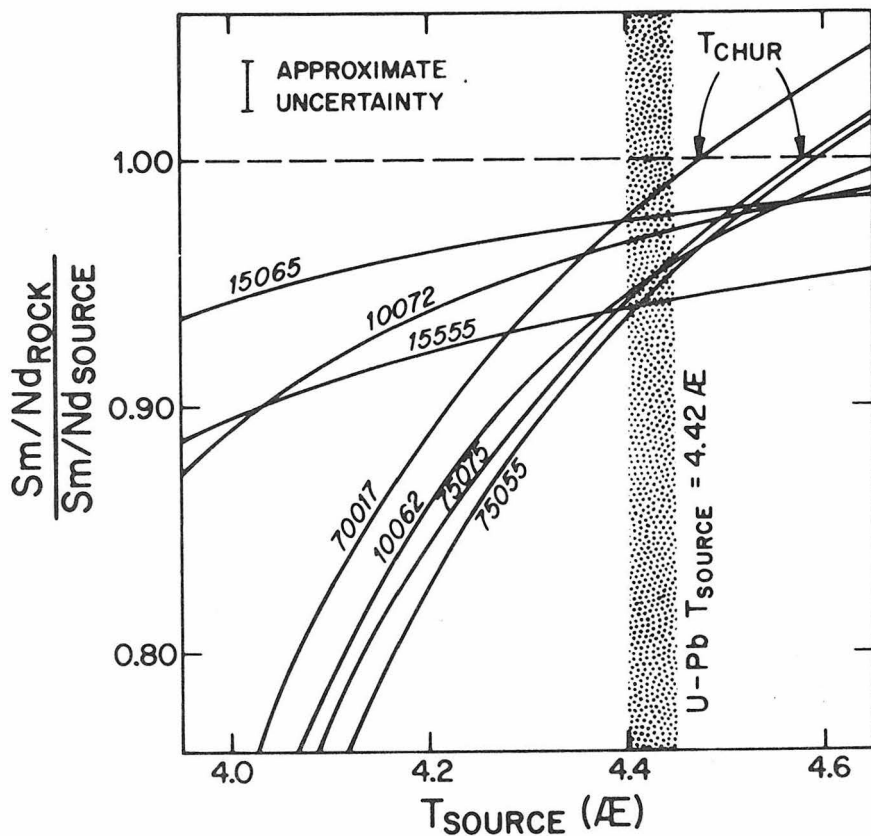


Fig. 11. Sm/Nd fractionation at the time of crystallization of mare basalts as a function of the time of formation of the source. We assume a single-stage evolution of the source and that the source was derived from a chondritic Sm/Nd reservoir. For a source age of 4.429 AE Sm/Nd fractionation range of 0.94–0.98 is obtained. For a fractionation of unity the T_{CHUR} ages are obtained (see Fig. 12). Note bunched intersections of curves in the interval 4.4–4.6 AE which, however, do not precisely define a unique T_{source} . Rock 70017 appears unique.

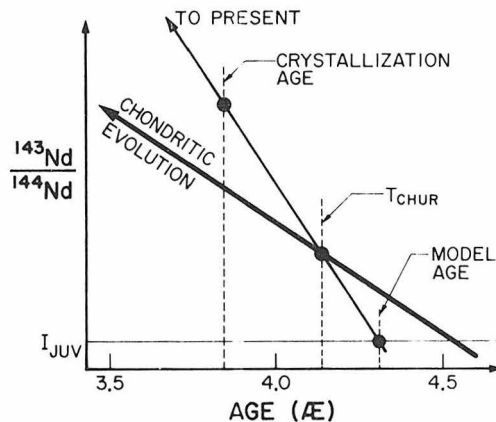


Fig. 12. Comparison of the evolution of $^{143}\text{Nd}/^{144}\text{Nd}$ in a sample and a reservoir with a chondritic Sm/Nd. The initial $^{143}\text{Nd}/^{144}\text{Nd}$ and the crystallization age are determined from an internal isochron. Extrapolation of the evolution line of $^{143}\text{Nd}/^{144}\text{Nd}$ in the sample to earlier times yields the T_{CHUR} age where it intersects the chondritic curve and the model age (equivalent to T_{BABI} for Rb-Sr) where it intersects the initial $^{143}\text{Nd}/^{144}\text{Nd}$ of Juvina (I_{JUV}).

This diagram is calculated assuming a homogeneous moon originated with Sm/Nd and $^{143}\text{Nd}/^{144}\text{Nd}$ equal to that in the Juvina achondrite (revised data, Lugmair *et al.*, 1976) and that at some later time, T_{source} , the source reservoir for each basalt formed with a fixed Sm/Nd ratio such that it could evolve to the initial $^{143}\text{Nd}/^{144}\text{Nd}$ of that basalt at the time of crystallization. The curves shown on this diagram are calculated from the following equation:

$$f = \frac{(\text{Sm/Nd})_{\text{rock}}}{(\text{Sm/Nd})_{\text{source}}} = \frac{\lambda (^{147}\text{Sm}/^{144}\text{Nd})_{\text{rock}} (T_s - T_x)}{[\epsilon_I^{\text{CHUR}}(T_x) \cdot I^{\text{CHUR}}(T_x)] \cdot 10^{-4} + \lambda (^{147}\text{Sm}/^{144}\text{Nd})_{\text{CHUR}} (T_s - T_x)}$$

where $T = 0$ refers to the present; $I^{\text{CHUR}}(0) = 0.511836$; $\lambda = 0.00654 \text{ AE}^{-1}$; $(^{147}\text{Sm}/^{144}\text{Nd})_{\text{CHUR}} = 0.1936$; T_x is the crystallization age of the basalt; and $T_s = T_{\text{source}}$, the time at which the parent reservoir of the basalt was fractionated from a chondritic reservoir. In addition, $I^{\text{CHUR}}(T) = I^{\text{CHUR}}(0) - \lambda T (^{147}\text{Sm}/^{144}\text{Nd})$. For convenience we have chosen a chondritic Sm/Nd evolution prior to T_{source} . However, these calculations can also be performed with Sm/Nd values distinct from the chondritic value for the stage prior to T_{source} . At this time it is not in fact known whether the moon formed with chondritic Sm/Nd.

Referring to Fig. 11, if the source reservoir of 70017 was formed at 4.4 AE ago, then the Nd isotopic data indicate that the Sm/Nd of 70017 is 0.97 of Sm/Nd in its source reservoir, or that a 3% Sm/Nd fractionation occurred during the genesis of 70017 near the time of its crystallization at 3.7 AE. However, if the source reservoir of 70017 was formed at 4.2 AE, the data indicate that approximately 11% Sm/Nd fractionation occurred at 3.7 AE. The curves on this diagram intersect the dashed line corresponding to $(\text{Sm/Nd})_{\text{rock}}/(\text{Sm/Nd})_{\text{source}} = 1.0$, at a time T_{source} which is equal to the T_{CHUR} age of the basalt. Thus $T_{\text{CHUR}} = 4.47 \text{ AE}$.

for 70017. If the curves for two basalts intersect on this diagram, then T_{source} of the intersection is equal to the age of an isochron drawn for the total rock data for the two basalts. As can be seen in this figure, if the source regions for the mare basalts were formed from an original chondritic reservoir at about 4.4 AE ago, then the inferred Sm/Nd fractionation factors for the basalts show a narrow range of about 0.94–0.98. If the source regions were formed at younger times, for instance 4.3 or 4.2 AE ago, then, especially for Apollo 17 basalts, the inferred Sm/Nd fractionation at the time of crystallization would change to values of 0.9 or less. This would constitute quite significant Sm/Nd fractionation. It should be noted (Fig. 11) that essentially regardless of the age of the source of the mare basalts, some Sm-Nd fractionation, about 2–6%, must be inferred at the time of crystallization of the basalts. Also, it can be seen that T_{CHUR} ages show quite a large spread, some being much greater than 4.6 AE, and therefore do not provide a precise estimate of the time of the early lunar differentiation. Nevertheless, the data in Fig. 10 show that large fractionations of Sm/Nd occurred in the formation of the parent reservoirs of mare basalts at times significantly older than the time of mare volcanism (Lugmair *et al.*, 1975). The data base is still small, but the range of ϵ_I^{CHUR} values seen in Fig. 10 indicates that, if the moon started out with chondritic Sm/Nd, then Sm/Nd fractionations which occurred *early* in lunar history range from 0.85 to a maximum of about 1.4. In contrast to this large Sm-Nd fractionation, the Sm-Nd fractionation which occurred at the time of mare basalt crystallization is probably on the order of 5%. Thus it can be concluded that the Sm-Nd data clearly indicate the existence of an early lunar differentiation, but presently do not precisely define the age of that event.

Lunar Sm/Nd

Interpretation of much of the Nd isotopic data is dependent on the Sm/Nd and initial $^{143}\text{Nd}/^{144}\text{Nd}$ of the moon. To evaluate the problem of lunar Sm/Nd it is instructive to compare lunar and terrestrial isotopic data. DePaolo and Wasserburg (1976a,b) have determined ϵ_I^{CHUR} for a variety of terrestrial igneous rocks of ages ranging from 0 to 3.6 AE. Most of these samples have ϵ_I^{CHUR} approximately equal to zero. These results indicate the existence of major magma sources with chondritic Sm/Nd over at least 4/5 of the earth's history. These authors consider this to be strong evidence that the earth has chondritic Sm/Nd to within a few percent. The most aberrant samples are mid-ocean ridge basalts, but even these samples are derived from a reservoir which has had an average Sm/Nd only about 10% higher than chondritic. Thus, a reasonable case can be made for a chondritic Sm/Nd for the earth.

In contrast to the apparent uniformity of Sm/Nd in the earth, lunar samples (Fig. 10) have ϵ_I^{CHUR} which deviate greatly from 0 and have a range comparable to that observed in young terrestrial basalts. This range exists despite the fact that the lunar samples are very old. Thus, large variations of ϵ_I^{CHUR} were able to evolve in the moon over a time interval of only 1 AE, whereas similar variations on the earth took 4.5 AE to develop. The lunar data indicate a range of Sm/Nd of

some 40–50% in magma sources on the moon compared to the ~10% on the earth. Of the ten data shown in Fig. 10, only one has $\epsilon_{\text{I}}^{\text{CHUR}} = 0$. Lugmair and Marti (1977) have interpreted their data on green glass balls as indicating that some magmas were differentiated from a deep chondritic lunar source. However, there is a general lack of evidence for the existence of a long-lived chondritic Sm/Nd reservoir in the moon as found in the earth. The variability of Sm/Nd in the moon makes it impossible to deduce with confidence the bulk lunar Sm/Nd.

The contrast between the lunar and terrestrial Nd isotope data may imply a grossly different early differentiation history for these two planets. The lunar data indicate that reservoirs with greatly different Sm/Nd were formed very early in lunar history and preserved over at least 1.5 AE until the end of mare volcanism. Rare earth element abundance and Rb–Sr data also suggest early lunar differentiation in order to account for the Eu anomaly. The Sm/Nd and Eu fractionations probably resulted from the same lunar differentiation event, although it is possible that they are the result of different processes. The earth seems to have remained a fairly uniform Sm/Nd reservoir over most of its early history. A possible explanation for this difference between the earth and the moon is that a profound differentiation event, such as affected the moon, never occurred in the earth. However, this would be surprising since the gravitational energy possibly available for the moon is much smaller than for the earth. Alternatively, the differentiation began in both planets early but it was “frozen in” on the moon at an early stage due to the limited energy available. In this case, the lunar reservoirs which formed early with variable Sm/Nd remained subsequently largely undisturbed and were able to evolve their widely varying $^{143}\text{Nd}/^{144}\text{Nd}$. On the earth, however, sufficient energy may have been available so that mixing processes, e.g., convection, competed with differentiation and prevented reservoirs from being isolated long enough to evolve isotopic differences. In any case, this contrast appears to represent a first-order difference in planetary evolution and must be closely related to the early thermal histories of the two planets.

Petrogenesis of Apollo 11 high-K basalts

Most lunar basalts have Rb–Sr model ages of approximately 4.5 AE (cf. Papanastassiou and Wasserburg, 1971a). This indicates that Rb–Sr fractionation at the time of basalt crystallization was small (less than a factor of two). The Apollo 11 high-K basalts are an exception to this rule. Their model ages are approximately 3.8–3.9 AE, very close to the age of their crystallization at 3.65 AE. These low model ages correspond to about a factor of five enrichment in Rb/Sr at the time of crystallization. Thus these basalts have apparently been affected by some process during their formation which makes them unique among lunar mare basalts. Nyquist *et al.* (1976) showed that some Apollo 17 basalts also show a smaller but significant Rb/Sr fractionation. The Sm–Nd isotopic investigation of two Apollo 11 basalts presented in this paper was undertaken to determine if the apparent uniqueness of these basalts based on

Rb-Sr fractionation also applies to REE fractionation. As can be seen in Fig. 11, if the age of the source of all the basalts is the *same* and is approximately 4.4–4.5 AE then the Sm-Nd fractionation factor for the Apollo 11 high-K basalts is essentially identical to the fractionation factors found in low-K Apollo 11 basalts and in most other mare basalts. Thus there is no evidence for a unique fractionation history of the Apollo 11 basalts based on Sm-Nd isotopic systematics.

Any hypothesis to explain the formation of high-K basalts must account for the following: (1) Rb/Sr fractionation factor of about five, (2) lack of large Sm/Nd fractionation, (3) major element compositional similarity to low-K and high-Ti basalts and similarity in Sr concentrations, (4) high concentrations of KREEPUTh elements, (5) large negative Eu anomaly, and (6) absence of plagioclase as a near-liquidus phase at any pressure. Shih *et al.* (1975) have suggested that the high REE concentrations, relatively flat REE pattern, and fractionated Rb/Sr could be explained if the high-K basalts were derived by a very small degree (~1%) of partial melting of a source rock with clinopyroxene as the dominant residual phase. The Nd isotopic data indicate that if the source reservoir of high-K basalt 10072 was formed at 4.4 to 4.6 AE, then its Sm/Nd is only 2–5% lower than that of its source (Fig. 11). In contrast, the model of Shih *et al.* (1975) predicts that high-K magmas have Sm/Nd ~20–30% lower than their source. As can be deduced from Fig. 11, such large Sm/Nd fractionation during generation of high-K basalts could only be the case if the parent reservoir for these basalts was formed at ~3.8 AE rather than in an early lunar differentiation at 4.4–4.5 AE.

The basic contrast of large Rb/Sr and small Sm/Nd fractionation at the time of crystallization of the Apollo 11 high-K rocks significantly complicates petrogenetic models for these rocks. Significant change in Rb/Sr with moderate fractionation in Sm-Nd can be obtained by removal of plagioclase, but for these high-K basalts, plagioclase is neither a residual phase at the time of magma removal nor a liquidus phase at any time during transit of the magma to the surface. It only begins to crystallize during the later stages of crystallization after extrusion. Thus if plagioclase crystallization is responsible for the unique trace element characteristics of high-K basalts, then these characteristics must have been generated during the crystallization of the magma after extrusion. A conceivable way in which this could happen is by redistribution within a single lava flow of the last remaining 1–2% of liquid after the flow is mostly crystalline and a large amount of plagioclase has crystallized. Simplified calculations indicate that these residual liquids could have extremely high Rb/Sr but Sm/Nd only slightly different from the original magma. Preferential concentration of this late liquid in certain parts of a lava flow could result in segments of the flow being enriched in trace elements and having high Rb/Sr and thus resembling the Apollo 11 high-K basalts. In this manner these basalts could be derived from lavas which originally had lower Rb/Sr and lower trace element concentrations more typical of other mare basalts. However, the existence of a mechanism by which the late-stage liquid could be extracted from a major volume of a mostly crystalline lava flow and concentrated in a different portion of the flow is not clear, especially in thin lava flows. A petrogenetic mode for the origin of high-K basalts remains as a perplexing problem.

Acknowledgment—Through the offices of The Curator of Lunar Samples, well documented materials from all the Apollo missions have been made available for use. The continuing accessibility of lunar samples as well as their careful preservation and preparation is gratefully acknowledged. This research was supported by NASA grant No. NGL 05-002-188. This work is contribution No. 2909 of the Division of Geological and Planetary Sciences, California Institute of Technology.

REFERENCES

Beaty D. W., Dymek R. F., and Albee A. L. (1977) Petrographic investigation of sample 10003, the oldest mare basalt (abstract). In *Lunar Science VIII*, p. 79–81. The Lunar Science Institute, Houston.

Birck J.-L., Fourcade S., and Allegre C. J. (1975) $^{87}\text{Rb}/^{86}\text{Sr}$ age of rocks from the Apollo 15 landing site and significance of internal isochrons. *Earth Planet. Sci. Lett.* **26**, 29–35.

Carter J. L. and MacGregor I. D. (1970) Mineralogy, petrology and surface features of some Apollo 11 samples. *Proc. Apollo 11 Lunar Sci. Conf.*, p. 247–265.

Compston W., Chappell B. W., Arriens P. A., and Vernon M. J. (1970) The chemistry and age of Apollo 11 lunar material. *Proc. Apollo 11 Lunar Sci. Conf.*, p. 1007–1028.

DeLaeter J. R., Vernon M. J., and Compston W. (1973) Revision of lunar Rb–Sr ages. *Geochim. Cosmochim. Acta* **37**, 700–702.

DePaolo D. J. and Wasserburg G. J. (1976a) Nd isotopic variations and petrogenetic models. *Geophys. Res. Lett.* **3**, 249–252.

DePaolo D. J. and Wasserburg G. J. (1976b) Inferences about magma sources and mantle structure from variations of $^{143}\text{Nd}/^{144}\text{Nd}$. *Geophys. Res. Lett.* **3**, 743–746.

DePaolo D. J. and Wasserburg G. J. (1976c) Nd isotopic variations and petrogenetic models (abstract). *EOS (Trans. Amer. Geophys. Union)* **57**, 351.

Donhoffer D. (1963) Determination of the half-lives of radioactive nuclides ^{147}Sm and ^{176}Lu occurring in nature by means of liquid scintillators. *Nucl. Phys.* **50**, 489–496.

Drake M. J. and Weill D. F. (1975) The partition of Sr, Ba, Ca, Y, Eu, and other REE between plagioclase feldspar and magmatic liquid: An experimental study. *Geochim. Cosmochim. Acta* **39**, 689–712.

Dymek R. F., Albee A. L., and Chodos A. A. (1975) Comparative mineralogy and petrology of Apollo 17 mare basalts: Samples 70215, 71055, 74255, and 75055. *Proc. Lunar Sci. Conf. 6th*, p. 49–77.

Eugster O., Tera F., Burnett D. S., and Wasserburg G. J. (1970) The isotopic composition of Gadolinium and neutron capture effects in some meteorites. *J. Geophys. Res.* **75**, 2753–2768.

Gast P. W., Hubbard N. J., and Wiesmann H. (1970) Chemical composition and petrogenesis of basalts from Tranquility Base. *Proc. Apollo 11 Lunar Sci. Conf.*, p. 1143–1163.

Geiss J., Eberhardt P., Grögler N., Guggisberg S., Maurer P., and Stettler A. (1977) Absolute time scale of lunar mare formation and filling. *Phil. Trans. Roy. Soc. Lond.* **285A**, 151–158.

Gopalan K., Kaushal S., Lee-Hu C., and Wetherill G. W. (1970) Rb–Sr and U–Th–Pb ages of lunar materials. *Proc. Apollo 11 Lunar Sci. Conf.*, p. 1195–1206.

Guggisberg S., Eberhardt P., Geiss J., Grögler N., and Stettler A. (1977) Youngest and oldest mare basalts: The temporal extent of mare filling (abstract). In *Lunar Science VIII*, p. 386–388. The Lunar Science Institute, Houston.

Gupta M. C. and MacFarlane R. D. (1970) The natural alpha radioactivity of Samarium. *J. Inorg. Nucl. Chem.* **32**, 3425–3432.

Haskin L. A., Allen R. O., Helmke P. A., Paster T. P., Anderson M. R., Korotev R. L., and Zweifel K. A. (1970) Rare earths and other trace elements in Apollo 11 lunar samples. *Proc. Apollo 11 Lunar Sci. Conf.*, p. 1213–1231.

Hodges F. M. and Kushiro I. (1974) Apollo 17 petrology and experimental determination of differentiation sequences in model moon compositions. *Proc. Lunar Sci. Conf. 5th*, p. 505–520.

Huneke J. C., Jessberger E. K., Podosek F. A., and Wasserburg G. J. (1973) ^{40}Ar – ^{39}Ar measurements in Apollo 16 and 17 samples and the chronology of metamorphic and volcanic activity in the Taurus-Littrow region. *Proc. Lunar Sci. Conf. 4th*, p. 1725–1756.

Jaffey A. H., Flynn K. F., Glendenin L. E., Bentley W. C., and Essling A. M. (1971) Precision measurements of half-lives and specific activities of ^{235}U and ^{238}U . *Phys. Rev. C4*, 1889–1906.

Jessberger E. K., Hunke J. C., and Wasserburg G. J. (1974) Evidence for a ~ 4.5 AE age of plagioclase clasts in a lunar highland breccia. *Nature* **248**, 199–202.

Kirsten T. and Horn P. (1974) Chronology of the Taurus-Littrow region III: Ages of mare basalts and highland breccias and some remarks about the interpretation of lunar highland rock ages. *Proc. Lunar Sci. Conf. 5th*, p. 1451–1475.

Lugmair G. W. (1975) Sm-Nd systematics of some Apollo 17 basalts (abstract). In *Papers presented to the Conference on Origins of Mare Basalts and their Implications for Lunar Evolution*, p. 107–110. The Lunar Science Institute, Houston.

Lugmair G. W. and Marti K. (1977) Evolution of the lunar interior: Sm-Nd systematics of A15 green glass and the question of the lunar initial $^{143}\text{Nd}/^{144}\text{Nd}$ (abstract). In *Lunar Science VIII*, p. 597–599. The Lunar Science Institute, Houston.

Lugmair G. W., Marti K., Kurtz J. P., and Scheinin N. B. (1976) History and genesis of lunar troctolite 76535 or: How old is old? *Proc. Lunar Sci. Conf. 7th*, p. 2009–2033.

Lugmair G. W., Scheinin N. B., and Marti K. (1975) Sm-Nd age and history of Apollo 17 basalt 75075: Evidence for early differentiation of the lunar exterior. *Proc. Lunar Sci. Conf. 6th*, p. 1419–1429.

Lunatic Asylum (1970) Ages, irradiation history, and chemical composition of lunar rocks from the Sea of Tranquility. *Science* **167**, 463–466.

Ma M.-S., Murali A. V., and Schmitt R. A. (1976) Chemical constraints for mare basalt genesis. *Proc. Lunar Sci. Conf. 7th*, p. 1673–1695.

Maxwell J. A., Peck L. C., and Wiik H. B. (1970) Chemical composition of Apollo 11 lunar samples 10017, 10020, 10072 and 10084. *Proc. Apollo 11 Lunar Sci. Conf.* p. 1369–1374.

Murthy V. R. and Coscio M. R., Jr. (1976) Rb-Sr ages and isotopic systematics of some Serenitatis mare basalts. *Proc. Lunar Sci. Conf. 7th*, p. 1529–1544.

Nakamura N., Tatsumoto M., Nunes P. D., Unruh D. M., Schwab A. P., and Wildeman T. R. (1976) 4.4 b.y. old clast in Boulder 7, Apollo 17: A comprehensive chronological study by U-Pb, Rb-Sr and Sm-Nd methods. *Proc. Lunar Sci. Conf. 7th*, p. 2309–2333.

Nakamura N., Unruh D. M., Gensho R., and Tatsumoto M. (1977) Evolution history of lunar mare basalts: Apollo 15 samples revisited (abstract). In *Lunar Science VIII*, p. 712–714. The Lunar Science Institute, Houston.

Nier A. O. (1950) A redetermination of the relative abundances of the isotopes of carbon, nitrogen, oxygen, argon and potassium. *Phys. Rev.* **77**, 789–793.

Nyquist L. E., Bansal B. M., and Wiesmann H. (1976) Sr isotopic constraints on the petrogenesis of Apollo 17 mare basalts. *Proc. Lunar Sci. Conf. 7th*, p. 1507–1528.

Papanastassiou D. A. and Wasserburg G. J. (1971a) Lunar chronology and evolution from Rb-Sr studies of Apollo 11 and 12 samples. *Earth Planet. Sci. Lett.* **11**, 37–62.

Papanastassiou D. A. and Wasserburg G. J. (1971b) Rb-Sr ages of igneous rocks from the Apollo 14 mission and the age of the Fra Mauro formation. *Earth Planet. Sci. Lett.* **12**, 36–48.

Papanastassiou D. A. and Wasserburg G. J. (1973) Rb-Sr ages and initial Sr in basalts from Apollo 15. *Earth Planet. Sci. Lett.* **17**, 324–337.

Papanastassiou D. A. and Wasserburg G. J. (1975a) A Rb-Sr study of Apollo 17 Boulder 3: Dunite clast, microclasts, and matrix (abstract). In *Lunar Science VI*, p. 631–633. The Lunar Science Institute, Houston.

Papanastassiou D. A. and Wasserburg G. J. (1975b) Rb-Sr study of a lunar dunite and evidence for early lunar differentiates. *Proc. Lunar Sci. Conf. 6th*, p. 1467–1489.

Papanastassiou D. A. and Wasserburg G. J. (1976) Rb-Sr age of troctolite 76535. *Proc. Lunar Sci. Conf. 7th*, p. 2035–2054.

Papanastassiou D. A., Wasserburg G. J., and Burnett D. S. (1970) Rb-Sr ages of lunar rocks from the Sea of Tranquility. *Earth Planet. Sci. Lett.* **8**, 1–19.

Papike J. J., Hodges F. N., Bence A. E., Cameron M., and Rhodes J. M. (1976) Mare basalts: crystal chemistry, mineralogy and petrology. *Rev. Geophys. Space Sci.* **14**, 475–540.

Philpotts J. A. and Schnetzler C. C. (1970) Apollo 11 lunar samples: K, Rb, Sr, Ba and rare-earth

concentrations in some rocks and separated phases. *Proc. Apollo 11 Lunar Sci. Conf.*, p. 1471–1486.

Podosek F. A., Huneke J. C., and Wasserburg G. J. (1972) Gas retention and cosmic-ray exposure ages of lunar rock 15555. *Science* **175**, 423–425.

Rose H. J., Cuttitta F., Dwornik E. J., Carron M. K., Christian R. P., Lindsay J. R., Ligon D. T., and Larson R. R. (1970) Semimicro X-ray fluorescence analysis of lunar samples. *Proc. Apollo 11 Lunar Sci. Conf.*, p. 1493–1497.

Rose H. J., Jr., Cuttitta F., Berman S., Brown F. W., Carron M. K., Christian R. P., Dwornik E. J., and Greenland L. P. (1974) Chemical composition of rocks and soils at Taurus-Littrow. *Proc. Lunar Sci. Conf. 5th*, p. 1119–1133.

Russ G. P., III (1974) Neutron stratigraphy in the lunar regolith. PhD. thesis, California Institute of Technology, Pasadena.

Russ G. P., Burnett D. S., Lingenfelter R. E., and Wasserburg G. J. (1971) Neutron capture on ^{149}Sm in lunar samples. *Earth Planet. Sci. Lett.* **13**, 53–60.

Schnetzler C. C., Philpotts J. A., Nava D. F., Schuhmann S., and Thomas H. H. (1972) Geochemistry of Apollo 15 basalt 15555 and soil 15531. *Science* **175**, 426–428.

Shih C., Haskin L. A., Wiesmann H., Bansal B. M., and Brannon J. C. (1975) On the origin of high-Ti mare basalts. *Proc. Lunar Sci. Conf. 6th*, p. 1255–1285.

Stettler A., Eberhardt P., Geiss J., Grögler N., and Maurer P. (1973) ^{39}Ar – ^{40}Ar ages and ^{37}Ar – ^{38}Ar exposure ages of lunar rocks. *Proc. Lunar Sci. Conf. 4th*, p. 1865–1888.

Stettler A., Eberhardt P., Geiss J., Grögler N., and Maurer P. (1974) On the duration of lava flow activity in Mare Tranquillitatis. *Proc. Lunar Sci. Conf. 5th*, p. 1557–1570.

Taylor S. R. and Jakeš P. (1974) The geochemical evolution of the moon. *Proc. Lunar Sci. Conf. 5th*, p. 1287–1305.

Tera F., Papanastassiou D. A. and Wasserburg G. J. (1974) Isotopic evidence for a terminal lunar cataclysm. *Earth Planet. Sci. Lett.* **22**, 1–21.

Tera F. and Wasserburg G. J. (1974) U–Th–Pb systematics on lunar rocks and inferences about lunar evolution and the age of the moon. *Proc. Lunar Sci. Conf. 5th*, p. 1571–1599.

Tera F. and Wasserburg G. J. (1976) Lunar ball games and other sports (abstract). In *Lunar Science VII*, p. 858–860. The Lunar Science Institute, Houston.

Turner G. (1970) Argon-40/Argon-39 dating of lunar rock samples. *Proc. Apollo 11 Lunar Sci. Conf.*, p. 1665–1684.

Turner G. (1977) Potassium–argon chronology of the moon. *Phys. Chem. Earth* **10**, 145–195.

Turner G., Huneke J. C., Podosek F. A., and Wasserburg G. J. (1971) ^{40}Ar – ^{39}Ar ages and cosmic ray exposure ages of Apollo 14 samples. *Earth Planet. Sci. Lett.* **12**, 19–35.

Turner G., Huneke J. C., Podosek F. A., and Wasserburg G. J. (1972) ^{40}Ar – ^{39}Ar systematics in rocks and separated minerals from Apollo 14. *Proc. Lunar Sci. Conf. 2nd*, p. 1589–1612.

Walker D., Longhi J., Stolper E. M., Grove T. L., and Hays J. F. (1975) Origin of titaniferous lunar basalts. *Geochim. Cosmochim. Acta* **39**, 1219–1236.

Warner J. L. (1971) Lunar crystalline rocks: Petrology and geology. *Proc. Lunar Sci. Conf. 2nd*, p. 469–480.

Wasserburg G. J. and Papanastassiou D. A. (1971) Age of an Apollo 15 mare basalt; lunar crust and mantle evolution. *Earth Planet. Sci. Lett.* **13**, 97–104.

Wasserburg G. J., Papanastassiou D. A., Nenow E. V., and Bauman C. A. (1969) A programmable magnetic field mass spectrometer with on-line data processing. *Rev. Sci. Inst.* **40**, 288–295.

Wasserburg G. J., Tera F., Papanastassiou D. A., and Huneke J. C. (1977) Isotopic and chemical investigations on Angra dos Reis. *Earth Planet. Sci. Lett.* **35**, 294–316.

Wasserburg G. J., Wetherill G. W., Silver L. T., and Flawn P. T. (1962) A study of the ages of the precambrian of Texas. *J. Geophys. Res.* **67**, 4021–4047.

Wright P. M., Steinberg E. P., and Glendenin L. E. (1961) Half-life of Samarium-147. *Phys. Rev.* **123**, 205–208.

APPENDIX 5: ANALYTICAL PROCEDURESA5.1 Chemistry

Chemical separation of Sm and Nd was accomplished using a procedure modified somewhat from that described by Eugster et al. (1970) for Gd separation. A detailed description of this procedure is given by Russ (1974). The following description of the procedures used for Sm and Nd is in part a duplication of the discussion by Russ (1974), but the procedures are sufficiently different that they are here described in full to avoid confusion. The discussion by Russ (1974), however, is valuable because it is explicit and complete and should be read in conjunction with the following by anyone wishing to duplicate the procedure.

A. Crushing

For most of the terrestrial samples measured, especially the geologically young samples, the primary aim was to obtain the isotopic composition of Nd, which should be uniform throughout a given rock sample. For this reason sample size was generally not strongly considered in preparing the sample. The rock samples, obtained by collecting or from other sources, varied greatly in mass ranging from a few grams to several kilograms. For the larger samples a fresh piece of ~20-200 g was usually obtained by breaking up the larger sample. This size sample was found to be optimum for handling under reasonably clean conditions. The sample was placed in a ~2 quart stainless steel pan (~4" deep) which was covered tightly with plastic wrap. A chisel was poked through the plastic wrap and all chiseling

was done inside the covered pan to prevent particles from flying out onto the work surface. Normally a one to 10 gram interior piece was chiseled from the sample. The sample was then examined under a low-power binocular microscope to check the mineralogy, texture and any alteration effects. The interior piece was then placed in a clean electropolished stainless steel mortar and pestle and crushed to approximately -20 or -40 mesh. The crushed material was then poured out onto weighing paper. In most cases the sample was crudely split by pouring it onto overlapping pieces of weighing paper and then spreading it out and separating the pieces of weighing paper. This was done until a split of approximately 0.5 g was obtained. This was then poured into a plastic 3-1/2 dram vial with a snap-on top to be taken into the laboratory. The plastic vials were not cleaned prior to use except for a cursory wiping of the exterior with a kimwipe. However, caution was taken not to touch the outside of the vial with either hand or plastic glove which had been exposed to the sample in any way. This precaution is extremely important to avoid getting rock powder on the balance pan in the laboratory during weighing.

For several samples, powders of rock which had been previously analyzed for other elements were obtained. In these cases the procedure used to crush the sample was verbally verified to be clean enough that contamination was expected to be negligible. About 500 mg of the powders were then poured into plastic vials and thereafter treated in a manner identical to that used for those which were crushed at Caltech.

For samples of Precambrian age much larger samples were crushed to attempt to avoid problems caused by element redistribution at times

more recent than the crystallization age. For these samples the amount crushed range from ~25 g for finer-grained samples to more than 2 kg for the coarse-grained granite sample ZL-3D. ZL-3D was crushed using a jaw crusher and pulverizer and then split to obtain a sample of about 1-2 g for dissolution.

B. Dissolution

The samples contained in the clean plastic vials were then taken into the chemistry lab for dissolution. The full vials were weighed and then the contents were poured into a clean teflon breaker containing a few grams of 4N HCl and sitting in a teflon-coated stainless steel collar. The HCl and the collar tend to reduce static and thus prevent small particles from flying out of the breaker. Some of the sample powder tends to stick to the side of the beaker; this is rinsed down with more 4N HCl from a squeeze bottle until the entire sample is sitting in about 3-4 grams of HCl. The empty vial is then weighed and the difference is taken as the weight of the sample.

A one-to-one mixture of concentrated HF and concentrated HClO_4 is then added to the sample; usually in the amount of about 1 ml per 100 mg of sample. The mixture is then vigorously swirled to prevent the sample from forming a cake, which will be difficult to dissolve because the inside is not exposed to the acids. The sample beaker is then covered with parafilm, labelled and set aside. The samples are kept in or close to a hood to prevent the HF fumes from being circulated through the lab. The sample is allowed to sit in the HF- HClO_4 mixture at least overnight and sometimes for 2 to 3 days.

It is swirled vigorously as often as possible during this time to speed the dissolution process. When the sample has turned completely to a white fluff and there are few or no remaining unreacted particles it is then cooked down on a hotplate. The sample beaker is placed in a teflon-coated aluminum or stainless-steel base and covered with a teflon pot through which high purity dry nitrogen is passed. The sample is first heated at about 120-140°C. At this temperature most of the HF and HCl will evaporate after 2 to 3 hours. If the sample is heated hotter than this while there is still a significant amount of HCl left, the HCl will boil and the bursting bubbles will splatter the sample out of the beaker. After most of the HCl has evaporated the temperature can be increased to about 180°C. The nitrogen flow is reduced somewhat at this stage. High nitrogen flow tends to cool the pot lid and sometimes causes the HClO_4 evaporating from the beaker to recondense on the lid. This should be avoided since the HClO_4 can leach metals out of the teflon and then drip back into the sample beaker. When the sample is essentially dry the nitrogen flow is turned off and the sample is heated slightly hotter to evaporate the remaining fluorides. After about one hour of this intense heating the sample is removed from the heat and allowed to cool. When cooled it is taken up in 1.5 N HCl. Generally the volume of the solution should be about 3-4 ml for each 100 mg of original sample. The sample is then usually left for several hours until the solution is clear. Again, swirling the solution will hasten the process. If the solution does not clear it is then heated gently under a heat lamp, which will usually clear it. If it does not the sample is allowed to sit and the

supernate is decanted off into another clean beaker. If the residue is very fine it may be necessary to centrifuge the solution to separate out the residue. The residue can then be treated with some additional HF-HClO₄, cooked to dryness, brought into solution in 1.5N HCl and then recombined with the rest of the sample.

C. Aliquanting and Spiking

When the sample is completely dissolved it is then ready to be passed through the ion exchange columns to separate the desired elements. The capacity of the ion exchange columns used is equivalent to approximately 50 mg of a typical silicate sample. Since this amount of an average sample contains sufficient Nd for several analyses, 50 mg is the amount of sample normally passed through the chemical procedure. An aliquant corresponding to ~50 mg is poured from the sample solution and the weight of the total sample solution and the aliquant are determined. Before pouring off the aliquant, the sample solution is poured back and forth between two teflon beakers about 20 to 30 times to ensure that the solution is well-mixed and homogeneous. For samples for which only the Nd isotopic composition is desired, the aliquant can then be loaded directly on the first ion exchange column.

For samples for which both a precise Nd isotopic composition and precise Sm and Nd concentrations are necessary, at this point solutions of ¹⁴⁷Sm and ¹⁵⁰Nd tracers are added to the sample aliquant. These tracer solutions are kept in tightly capped polyethylene bottles and their concentrations are verified periodically as described below.

The desired amount of ¹⁵⁰Nd tracer is poured into a clean teflon beaker

and carefully weighed, correcting for evaporative loss between the time the solution is poured and the time the weight is obtained. The evaporation correction is done by reading the weight about 3 times at one or two minute intervals and then extrapolating back to the time the solution was poured. The solution is then carefully poured into the sample aliquant so as not to cause any splashing. The empty beaker which contained the tracer can then be tared to determine the mass of the tracer solution which has been added. The ^{147}Sm tracer is weighed out in a similar fashion. After both tracers have been added to the sample solution, the solution is poured back and forth between two beakers 20 to 30 times to mix the sample and tracers. The mixture is then dried down by placing the beaker into a teflon base, covering it with a teflon pot which has a quartz lid, and putting this under a heat lamp. High purity dry nitrogen is passed through the pot while the solution is evaporating. When the sample is almost dry it can be taken up in 2 ml of 1.5N HCl.

D. Ion exchange elution chromatography

The separation of Sm and Nd involves two ion exchange columns. The first column is made of quartz glass and is 1 cm in inside diameter and filled to a height of about 17 cm with Dowex 50-8x, 100-200 mesh, cation exchange resin. This resin has a capacity of about 1.4 milliequivalents/ml so the column has a total capacity of about 19 milliequivalents. For good separation the sample should be limited to less than 2 milliequivalents (10% of the total column capacity) and

preferably less than one milliequivalent. A 50 mg sample comprised of 50% Diopside ($\text{Ca Mg Si}_2\text{O}_6$) and 50% anorthite ($\text{Ca Al}_2\text{Si}_2\text{O}_6$) represents about 1.18 meq of sample (Si is removed as Si F_4 during dissolution). Before an elution the resin is first prepared by passing through it 300 ml of high purity 4N HCl in 3-100 ml batches. This is followed by 10 ml of 1.5N HCl. The 1.5N treatment is to increase the pH on the upper part of the column so the sample will be strongly partitioned onto the resin and will therefore be held on the top of the column. The addition of the 1.5N HCl causes the resin to expand by about 10% in volume. The sample solution is then centrifuged in a glass tube and loaded onto the resin with a disposable Pyrex pipette. The sample solution is expelled from the pipette as close to the top of the resin as possible to avoid getting sample smeared on the reservoir at the top of the column. The sample solution is allowed to pass through the column under its own weight until no liquid remains above the resin. Next, 2 ml of 1.5N HCl are poured onto the column and allowed to pass through. This 2 ml rinses down onto the resin any sample which is remaining on the walls of the column above the resin. At this point the elution of the sample from the column is begun. A typical elution curve is shown in Figure A5-1. As shown in Figure A5-1, this elution procedure with HCl results in some separation of rare-earth elements from each other. In order to be certain that all of the Nd is recovered, a large fraction is collected which contains most of the heavy REE (terbium) as well as barium. Strontium is also recovered as

Figure A5-1: Typical elution curves for Sr, REE, and Ba from first cation exchange column.

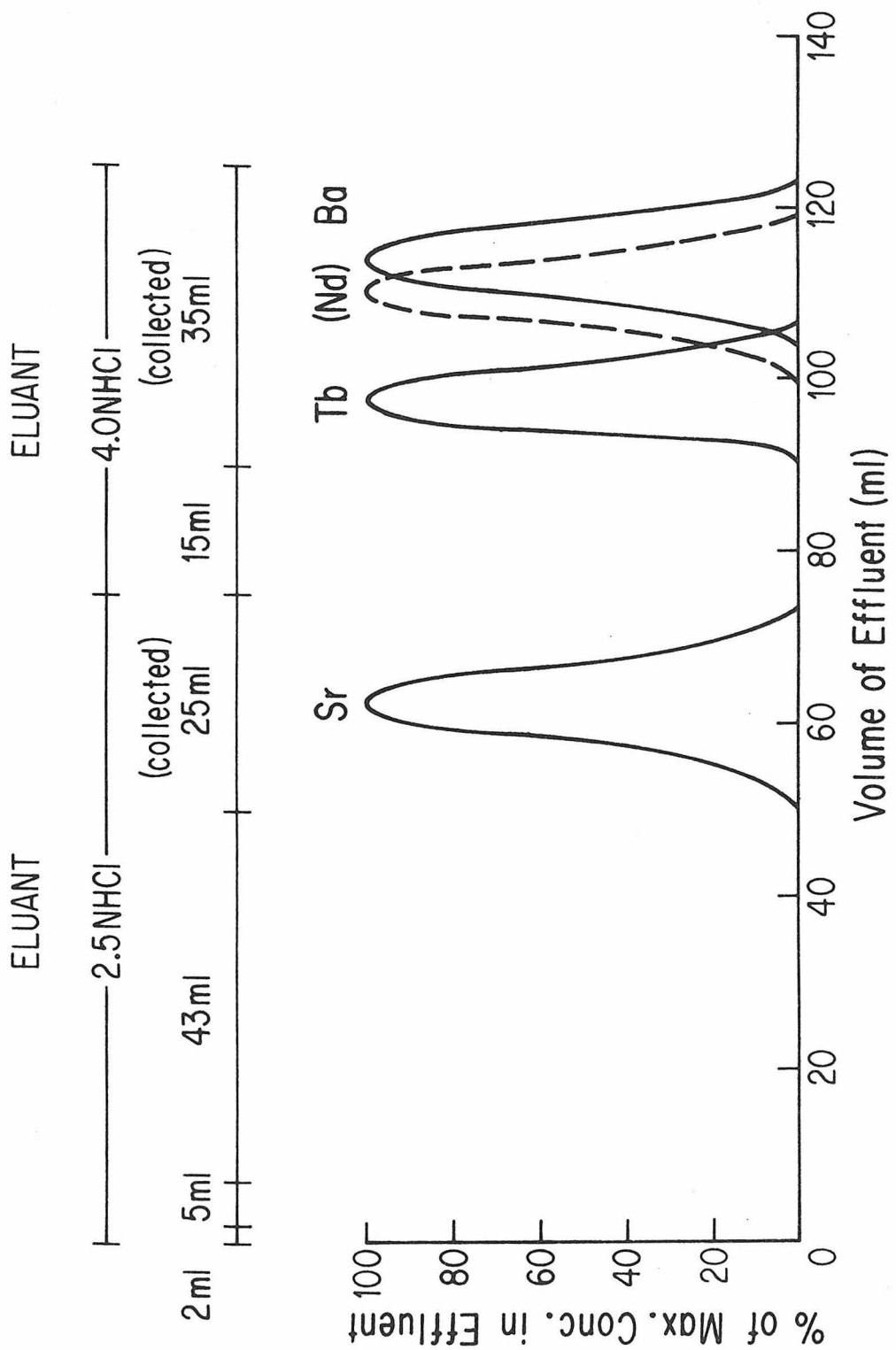


Fig. A5-1

shown, and the solution containing the Sr can be evaporated to dryness under a heat lamp and loaded directly on a filament for the mass spectrometer run. The solution containing the REE and Ba is also dried down and is then ready to be loaded on the second ion exchange column where Ba will be eliminated and Sm and Nd are cleanly separated both from each other and from the other rare-earths.

The second ion exchange column is made of thick-walled Pyrex tubing, is 33 cm long with a 0.2 cm inside diameter, and is capped by a reservoir of about 8 ml volume. The column is filled with Dowex 50W-X4 cation exchange resin to a height of 30 cm. The decreased amount of cross-linking (4% rather than 8% for the first column) is thought to facilitate more rapid ion exchange and therefore decreases kinetic effects which tend to widen the elution bands (F. Tera, personal communication). The total capacity of this column is about 1.3 meq. A typical 50 mg basalt sample contains about 4×10^{-4} meq of REE and Ba, so the amount of sample typically loaded onto this column is negligible compared to the column capacity. The resin is held in the column by a piece of filter paper which covers the bottom of the column and is held in place by a machined teflon nipple which fits over the end of the column. The resin is discarded after each elution and the column is then filled with new resin for the next sample. The top of the column is connected via a ground glass ball joint to a Tygon tube. This Tygon tube is in turn attached to two 2 liter bottles half-filled with water which are connected by about 3m of Tygon tubing and suspended one about 2.5m above the other to provide air pressure to the top of the column to

increase the rate at which the eluant passes through the column. The amount of effluent leaving the column during an elution is monitored with a photoelectric drop counter. The drop counter can also control a fraction collector so that individual drops can be collected in separate vials for column calibrations.

Resin for this column is prepared in batches large enough for about 40 or 50 elutions. The resin is first placed in a 30 cm long column with 2 cm inside diameter which is capped by a reservoir of 500 ml volume. The column is usually filled with resin up to the bottom of the reservoir. The resin is first rinsed by passing 1 liter of distilled water through it. Next 1 liter of 4N HCl is passed through, followed by another liter of water. This is followed by 1 liter of 0.4M 2-methyllactic acid with pH adjusted to 4.7 and finally by another liter of water. The top 1/3 of the resin is discarded (c.f. Russ, 1974). The resin is then stored in a polyethylene bottle under water.

The 2-methyllactic acid is prepared by simply weighing out 0.4 moles of the acid which is obtained in solid form and dissolving it in one liter of H_2O . The pH of this solution is then adjusted to 4.7 by adding concentrated NH_4OH . The NH_4OH solution is prepared by bubbling NH_4 gas through high purity distilled water. This solution acts as a buffer so the pH is stable over long periods.

Samples are eluted from the second ion-exchange column with 0.2M 2-methyllactic acid with pH adjusted to about 4.6. Before a sample is passed through the column the column is first calibrated by eluting a mixture of radioactive tracers (^{152}Eu , ^{154}Eu , ^{151}Sm , and ^{147}Nd) in the

same manner as a sample would be eluted. ^{147}Nd ($\tau_{1/2} = 11$ days) must be ordered specially from a radiochemical supplier; the Eu and Sm species are stock items. ^{147}Nd can be obtained inexpensively from Oak Ridge National Laboratory, but only immediately following a reactor run. A typical elution curve using these tracers is shown in Figure A5-2. Two or three calibrations are done before the resin and eluant are used for samples, to make sure the elution curve is reproducible.

As is shown in Figure 2 the separation of individual rare-earths by this method is extremely efficient. The Nd fraction can be better than 99.95% pure as determined from mass spectra. The main impurities are La (0.01-0.02%) and Sm (0.002 - 0.01%). More than 95% of the Nd can be recovered. The purity of the Nd separate obtained by this method is much better than is required for measurement of isotopic ratios to 2-3 parts in 10^5 . It would be entirely adequate even if the precision of the measurements was improved by a factor of 10. With this separation method the purity of the Nd separate is mostly dependent on the way in which the sample is loaded onto the column to begin the elution (discussed below).

The procedure used for the second ion exchange column is as follows. The resin used for the previous sample is first removed from the column and discarded. This is done with a 40 cm long, 1.5 mm outside diameter capillary tube connected to a 5 or 10 ml disposable syringe. The resin is sucked out of the column and into the syringe and then expelled into a waste beaker. After the resin has

Figure A5-2: Typical elution curves for Eu, Sm, and Nd from second cation exchange column. Note the excellent separation of Nd from Sm.

ELUANT: 0.2 M 2-METHYLLACTIC ACID (pH = 4.60)

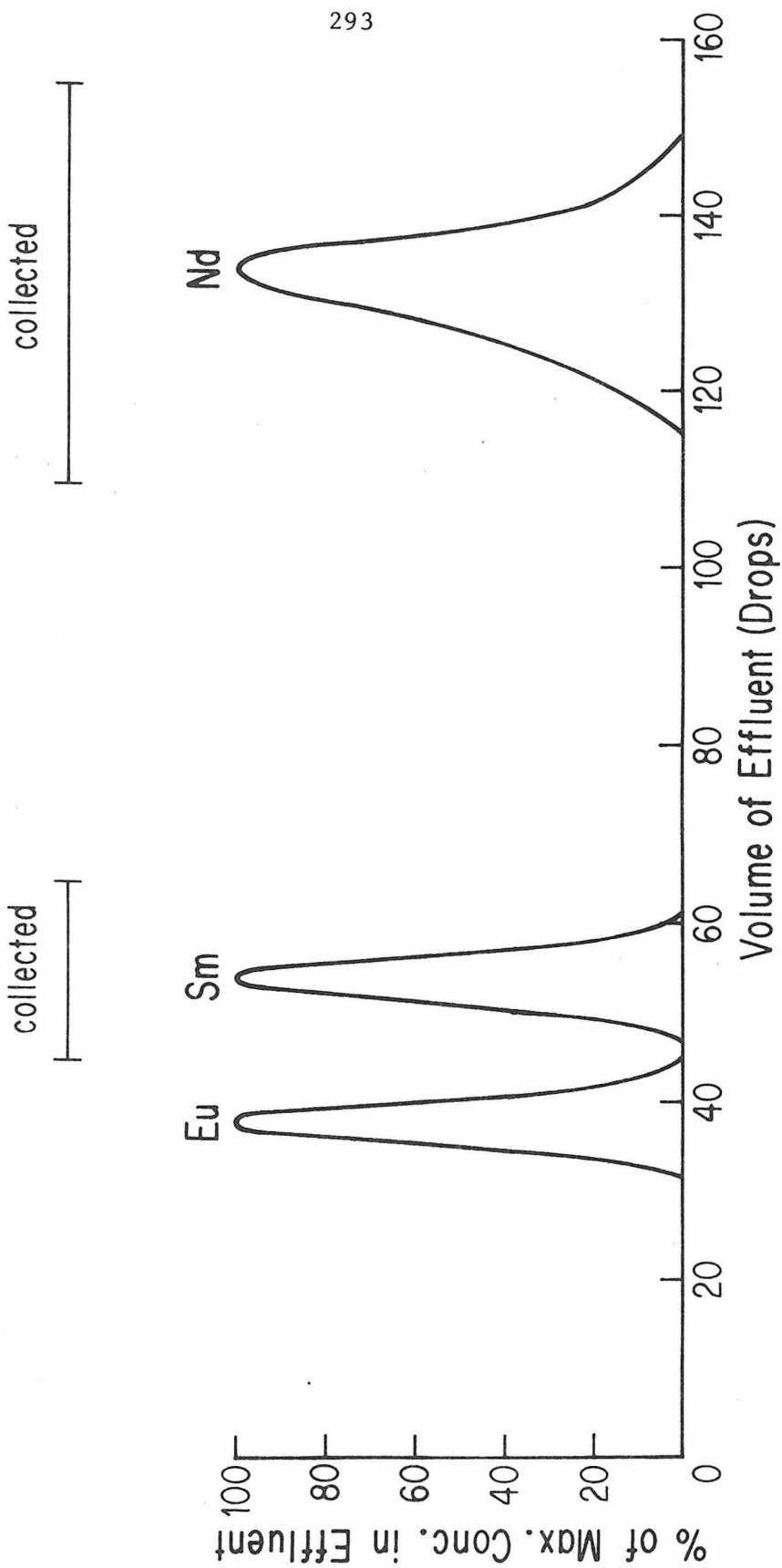


Fig. A5-2

been removed, the reservoir atop the column is filled with H_2O four or five times and this is sucked out through the capillary. The tip of the capillary should be held as close as possible to the bottom of the column so that the water circulates through and rinses the column. Care must be taken not to damage the filter paper with the tip of the capillary. At some time during this process the capillary should be held very close to the filter paper and the water sucked hard enough to actually draw air up through the filter paper. This serves to blow out the filter paper which tends to get clogged up with fine resin particles resulting in slower flow rates through the column. About 2 ml of H_2O is left in the column and reservoir after the last rinse. At this point new resin is put into the column. The bottle containing the stored resin is thoroughly shaken. Then, a clean disposable pyrex pipette is used to suck up resin from the bottom of the bottle and then expell it into the reservoir at the top of the column. Care is taken not to touch the pipette to the sides of the column if possible. Enough resin to fill the capillary part of the column and about 3 or 4mm of the reservoir is added all at once. The resin settles in the column so that the finest resin particles will be concentrated at the top and can be removed so they will not clog the filter paper during the elution of the sample. When the resin has completely settled (about 2 hours) the pipette can be used to remove the topmost resin down to the top of the capillary and then to draw off the excess water. Then the reservoir is filled with 0.2M 2-Methyllactic acid with pH adjusted to 4.6. This can then be left to drip through the column overnight or

it can be passed through under air pressure to save time. At least 100 drops are normally passed through before continuing. After this the disposable pipette is used to remove extra resin until the height of the resin is 30 cm and then to remove and discard the extra eluant. The column is then filled to the top of the capillary with H_2O and this is passed through under air pressure. Care must be taken to remove the air pressure just as the last water is reaching the top of the resin. If this is not done the air will force all the liquid out of the resin, causing the resin to dry out and crack, and then the resin will have to be removed and the process started over.

At this point the sample is loaded on the column. In loading the sample, the aim is to get the entire sample down onto the top of the resin before beginning the elution. This is critical for a good separation. The sample is first dissolved in two drops of 0.75N HCl from a squeeze bottle. It is then loaded onto the column using a clean disposable pipette. The pipette used to load the resin should not be used for this purpose. This is because the inside of that pipette is usually coated with resin. The sample, when drawn up into the pipette will be partitioned onto that resin, and may not come back out when the sample solution is expelled from the pipette. The sample solution is put onto the column by touching the tip of the pipette to the bottom of the column reservoir immediately adjacent to the top of the capillary. If the sample is slowly expelled from the pipette it will run down the side of the capillary to the resin and gradually fill the capillary. This liquid can then be left to pass into the resin or it can be pushed through under pressure. Extreme care must be taken

not to touch the tip of the pipette to any other surface of the reservoir. If sample gets onto the side of the reservoir, then when the reservoir is filled with eluant for the elution, the eluant will dissolve the sample and become a REE solution and heavy rare earths will be found in every fraction of effluent collected. An additional two drops of 0.75N HCl are then put into the sample beaker to assure that the entire sample is recovered from the beaker. This is then loaded onto the column in the pipette by touching the pipette to the same spot on the bottom of the reservoir and slowly expelling the sample. This liquid is then also allowed to pass into the column or is passed through under pressure. At this point most of the sample is absorbed on the top of the resin in a thin disk. However, some sample still remains on the sides of the capillary above the resin as well as on the bottom of the reservoir.

At this point, about 7 or 8 ml of eluant is poured out into a clean teflon beaker. A clean disposable pipette is used to draw up about 0.5 ml of eluant from this beaker. The column is then filled to the top of the capillary with eluant. This is done again by touching the tip of the pipette to the bottom of the reservoir and expelling the liquid slowly. This eluant should be used to rinse the sample down onto the resin from the bottom of the reservoir. Retain the remaining eluant in the pipette. The drop counter should be turned on and set to zero and the eluant passed through the column under air pressure. Again care must be taken to remove the air pressure before the eluant

runs out. Then the capillary is again filled with eluant while rinsing down the bottom of the reservoir and the liquid is passed through under pressure. Finally, the capillary is filled a third time, the remaining eluant in the beaker is poured into the reservoir, and the air pressure is applied. The flow rate through the column used for this work is normally about 30 drops per hour and can be kept constant to about $\pm 10\%$. At no time should the pipette be returned to the eluant remaining in the beaker after the pipette has been touched to the column.

The effluent fractions containing the Sm and Nd are collected in a clean teflon beaker. The solution is then dried down under a heat lamp. Aluminum or stainless steel bases are normally used for this evaporation because their use ensures that the beaker will get hot enough to completely evaporate the methyl lactate, which is rather involatile. The sample should be completely dry before removing it from the heat. There is no worry about not being able to find the sample if it is dried completely because a brown residue always remains. Radioactive Eu is normally added to a sample every few runs to check if there is any shift in the elution curves. The Eu tracer used has been cleaned by passing it through the column and collecting the Eu fraction. It can be added to the sample prior to loading the sample on the first column or it can be added to the effluent from the first column before it is evaporated. The primary cause of shifting elution peaks is variability in the volume of 0.75N HCl used to load the sample onto the column. The HCl converts 1/8 of the resin from the NH_4^+ form to the H^+ form and lowers the pH at the top of the resin and

thus has a rather large effect on the behavior of the column. If the volume of HCl is regulated to $\pm 5\%$, there will probably be no effect.

E. Blanks

Total chemistry blank was measured several times during the course of the work. Because the blank levels have been entirely negligible for the samples processed to date, the contributions to the blank from each step in the chemistry have not been determined. The blank has gradually decreased during the time from December, 1975, to October, 1977, as the water produced from the M40 still has improved. The Nd blank was 120 picograms in December 1975, 75 picograms in February, 1976, and was down to 22 picograms in October 1977. Sm blanks are about 20% of the Nd blank, the approximate crustal proportion of Sm. A typical sample contains about 1 μg of Nd, so the blanks are negligible.

F. Preparation of tracers and gravimetric standards

The determination of ages of rocks by the Sm-Nd method requires precise determination of the concentrations of Sm and Nd. To do this by the isotope dilution method requires tracer solutions (in this case ^{147}Sm and ^{150}Nd) whose concentrations are known both precisely and accurately. Determination of the concentration of, for example ^{150}Nd tracer solution, is done by mixing a measured mass of the solution with a measured mass of a solution containing "normal" Nd in known concentration and then measuring the change in the isotopic composition of the tracer solution by the addition of the normal Nd.

Nd gravimetric solutions were prepared from two different starting materials: Nd_2O_3 salt and Nd metal. Specpure Nd_2O_3 was obtained from Johnson-Mathey Company. When exposed to air Nd_2O_3 absorbs CO_2 and H_2O and thus must be dried at high temperature to insure stoichiometry. The procedure used is as follows. Approximately 250 mg of specpure Nd_2O_3 powder was poured out of the vial received from Johnson-Mathey onto glassine paper. The powder was then poured into a quartz glass vial which has a quartz cover and the vial was carefully weighed. The vial was then placed into a quartz glass canister. The vial was left uncovered with the cap lying beside it. The canister was covered with 2 nested quartz covers and placed on a Pyrex petri dish. This entire assembly was then placed inside a dessicator. The quartz canister was removed from the dessicator and placed in a furnace at 800°C and left overnight, about 18 hours. The next morning the temperature in the oven was decreased to 400°C . After the furnace had cooled to this temperature, the canister was removed from the oven and placed in the dessicator while still hot and the dessicator covered. About 30 minutes later the excess pressure built up in the dessicator was bled off and the canister allowed to cool to room temperature. When cooled the canister was removed from the dessicator, uncovered, and the vial containing the powder was weighed and then returned to the dessicator. To check whether the powder was rehydrating the vial was weighed again about six hours later. This heating procedure was repeated until the change in weight between two successive weighings was less than 0.05% of the total weight of the powder. Prior to putting the Nd_2O_3 powder in the quartz vial, the empty vial was passed through this heating-

weighing procedure three times to determine if the vial was losing mass as a result of the intense heating, which it was not. The total weight loss of the Nd_2O_3 powder was about 15%. The powder was dissolved and removed from the quartz vial by first placing the vial into a 100 ml teflon beaker and then immersing it in 4.0N HCl. When all of the powder was apparently dissolved, the liquid was poured off into a 2 liter polyethylene bottle filled with about 1.5 l of H_2O . The 100 ml beaker was then refilled with 4.0N HCl and then decanted again; and this procedure was repeated an additional three times. The empty quartz vial was then dried and weighed to check that no change in the vial weight had occurred during the process. The liquid in the polyethylene bottle was brought up to about 2l volume by addition of more H_2O and the bottle was then tightly capped. Prior to this the 2l bottle containing teflon-coated Alnico stir bar had been washed and carefully tared. The full bottle was weighed, shaken vigorously and then left on a stirring plate overnight. The concentration of Nd in this solution was expected to be correct to $\pm 0.1\%$.

A similar procedure was used to prepare the ^{150}Nd tracer. The weight loss for the ^{150}Nd powder was also about 15%. Since only 10.5 mg of this powder were weighed, the concentration of the tracer solution was considered to be correct to about 0.4%.

Aliquots of both the normal Nd solution and the tracer solution were taken and diluted to the concentrations desired. Aliquots of these more dilute solutions were taken, dried down, loaded onto a filament, and individually run in the mass spectrometer to determine their isotopic compositions. The isotopic composition of the normal

Nd was calculated assuming that the ratio $^{150}\text{Nd}/^{142}\text{Nd} = 0.2096$ and using this value to correct for mass discrimination in the mass spectrometer. (This is discussed more fully in a later section.) For the tracer solution, which has an isotopic composition much different from normal, this mass discrimination correction cannot be made. Thus, when the tracer Nd was measured, a procedure was used which was identical to that used for the measurement of the normal Nd; the same amount of Nd was loaded onto the filament and data were taken at the same beam intensity and filament temperature. In this way the mass discrimination could be estimated within about $\pm 0.02\%$ to $\pm 0.03\%$ per mass unit. This estimate is sufficient for the tracer because it contains only small amounts of the isotopes other than ^{150}Nd .

Measured amounts of the normal and tracer solutions were then mixed and the isotopic composition of the mixture was measured. The concentration of ^{150}Nd in the tracer solution $[^{150}\text{Nd}]_t$ can be calculated from an isotope ratio measured in the mixture (e.g., $(^{144}\text{Nd}/^{150}\text{Nd})_m$) and the concentration of Nd in the normal solution $([^{144}\text{Nd}]_N)$. Thus:

$$\left[^{150}\text{Nd}\right]_t = \frac{1 - (^{144}\text{Nd}/^{150}\text{Nd})_m \cdot (^{150}\text{Nd}/^{144}\text{Nd})_N}{(^{144}\text{Nd}/^{150}\text{Nd})_m - (^{144}\text{Nd}/^{150}\text{Nd})_t} \cdot \left[^{144}\text{Nd}\right]_N \cdot \frac{M_N}{M_t}$$

where $(^{150}\text{Nd}/^{144}\text{Nd})_N$ is the value measured in the normal, $(^{144}\text{Nd}/^{150}\text{Nd})_t$ is that measured in the tracer, M_N and M_t are the masses of the normal and tracer solutions respectively which were added to the mixture, and concentrations are given in moles/gram. When this was done it was found that $[^{150}\text{Nd}]_t$ calculated was lower by 0.5% than that determined

by gravimetry. This was considered to be outside of analytical uncertainty and thus not acceptable as a confirmation of the concentration of the tracer.

A second gravimetric standard was made by dissolving an ultra-pure chunk of Nd metal obtained from Ames Laboratory, Ames, Iowa. The metal was analyzed for both cation and anion impurities at Ames and was weighed just prior to shipment. It was shipped here in evacuated-glass tubes. The metal was removed from the container upon arrival at Caltech and weighed. The weight agreed with that measured at Ames to within 0.01%. The metal was then dropped into a 2 ℓ polyethylene bottle and dissolved in 2.5N HCl. No stir bar was put in this solution; it was shaken vigorously to homogenize it. An aliquant of this solution was then poured into a second polyethylene bottle (1 ℓ) and diluted. This solution was then used to determine $[^{150}\text{Nd}]_t$ as described above. The calculated concentration in this case agreed with the gravimetric result to within 0.2% and a repeat determination agreed with the first determination to 0.08%. Because the Nd metal standard required essentially no handling, the value of $[^{150}\text{Nd}]_t$ determined from it was assumed to be the correct value. The source of the discrepancy between this value and the value determined with Nd_2O_3 remains unidentified.

The ^{147}Sm tracer was prepared from an oxide powder in the same way that the ^{150}Nd tracer solution was prepared. $[^{147}\text{Sm}]_t$ was determined from a calibration using a Sm normal standard solution prepared by dissolving a chunk of ultra-pure Sm metal in the same way as the Nd metal normal was prepared. $[^{147}\text{Sm}]_t$ calculated from the

tracer-normal mixture agreed with that determined by gravimetry to within 0.2% which was considered to be good agreement.

The Nd and Sm standard solutions are kept tightly capped and weighed about every six months to monitor evaporation. The tracer solutions are calibrated against the standards at similar intervals.

A5.2 Mass Spectrometry

A. Loading and analysis

Nd samples are loaded onto flat Re filaments for isotopic analysis. Polyethylene tubing (0.023" I.D.) connected to a syringe is used to transfer the sample to the filament. The tubing is first cleaned by drawing 4N HCl up into it and then expelling it 3 or 4 times. The outside of the tubing should also be rinsed down with 4N HCl from a squeeze bottle. Then approximately 5 to 10 μ l of 1.5N HCl are drawn up into the tubing, and this is expelled onto the sample and the solution is allowed to stand for a few minutes. Then the tubing is used to scrape the sample up from the bottom of the beaker and to mix up the solution. When the sample is completely dissolved the solution should have a pale brown color. At this point the entire solution is drawn up into the tubing and its volume is determined by measuring the length of the solution in the tubing. The solution is then expelled and an amount equivalent to about 200 nanograms of Nd is drawn up. This is then loaded onto the center 1/4 of the filament in several very small drops. Each drop is evaporated by passing a current of 0.5A through the filament. If after the entire solution has been placed on the filament and evaporated the sample is distributed unevenly, the tip of the tubing

can be used to gently spread the sample around and even it out. Care must be taken to make sure the filament is cold when the tubing is touched to it, otherwise the tubing will melt on the filament and cause deposits which can affect the beam stability. When the sample is satisfactorily loaded on the filament the current is increased gradually up to about 1.8-2.0A in order to oxidize the Nd to Nd_2O_3 . As the current is increased the organic residue burns away; the sample appears white or bluish-white when completely oxidized. During this process the Re filament may also become somewhat oxidized and some recrystallization may be evident.

After the filament has been loaded into the mass spectrometer source, it is heated up to a temperature of about 1250°C over a period of a few hours. It can be heated quickly up to 1000°C over about 10 minutes, but should then be heated more slowly up to the running temperature. At some point during the heating the signal may begin to grow by itself, without further increasing the filament temperature. However, usually the signal will not continue to grow throughout the run.

The efficiency of formation of Nd^+ ions from the Nd_2O_3 is remarkably high, so that a sample of about 30 ng will provide a $^{144}\text{Nd}^{16}\text{O}^+$ beam of $8 \times 10^{-12}\text{A}$ for a period of several hours. Generally, the ratio of Nd^+ ions appearing at the collector to Nd atoms originally loaded onto the filament is about 0.05. Usually about 100 ng of Nd is loaded onto the filament and the intensity of the $^{144}\text{Nd}^+$ beam is kept between 7 and $9.5 \times 10^{-12}\text{A}$ during data acquisition. This intensity is chosen so that all the isotopes can be measured on the same range of the digital voltmeter (DVM) to avoid scale corrections.

For the $10^{11}\Omega$ feedback resistor this results in voltages ranging in intensity from $\sim 0.2V$ for $^{148}\text{Nd O}^+$ and $^{150}\text{Nd O}^+$ up to $1.0V$ for $^{142}\text{Nd O}^+$. For samples containing high enough concentrations of Nd, about 500-700 ng of Nd can be loaded and the ion beam intensity increased by a factor of 10. In this case the $10^{10}\Omega$ feedback resistor can be used resulting in the same voltages.

A typical Nd O^+ mass spectrum is shown in Figure A5-3. For a source slit width of $0.010''$ and collector slit width of $0.025''$ the peak tops are flat to 1 part in 10^5 of the peak intensity for ± 1.5 gauss from the peak center (equivalent to about ± 0.07 mass units). Background (zeros) are measured at ± 8.5 gauss from the peak centers (0.36 mass units). The background at ± 0.36 m.u. is offset by 0.005% to 0.007% of the peak intensity from the value measured with the beam off. This proportional offset is approximately equal for all isotopes and thus cancels out in the measurement of isotope abundance ratios. Possible spectral interferences are monitored at mass 156 ($^{140}\text{Ce O}^+$), mass 157 ($^{141}\text{Pr O}^+$) and mass 170 ($^{154}\text{Sm O}^+$). Normally the peaks at these masses are $< 10^{-5}$, 10^{-5} to 10^{-3} , and 5×10^{-6} to 10^{-4} respectively of the $^{144}\text{Nd O}^+$ peak, and no corrections to the Nd isotope ratios due to interfering species are necessary. Corrections are made for interference from Sm if the peak at mass 170 is greater than 5×10^{-5} of the $^{144}\text{Nd O}^+$ peak, however, this correction does not affect the measured $^{143}\text{Nd}/^{144}\text{Nd}$. La O^+ (mass 155) and sometimes Ba $^+$ (mass 138) are also detected in the spectrum at intensities of about 10^{-3} to 10^{-4} of $^{144}\text{Nd O}^+$ but do not interfere.

Figure A5-3: (a) Strip chart recording of a magnetic field scan of the Nd mass region taken during a run. $^{154}\text{SmO}^+$ can barely be detected at mass 170; in this run the peak at mass 170 is about 0.2mV compared to 8.5 volts for $^{144}\text{NdO}^+$, a ratio of $\sim 2.4 \times 10^{-5}$. The oxygen isotope spectrum can be seen clearly at mass 166, 167, and 168. The apparent longer beam tails on the high mass side of all the peaks are due to the fairly long time necessary for the decay of the peak current in the feedback resistor; scan is from right to left (low to high mass). Note that there is no detectable PrO^+ or CeO^+ in the spectrum; LaO^+ does not interfere.

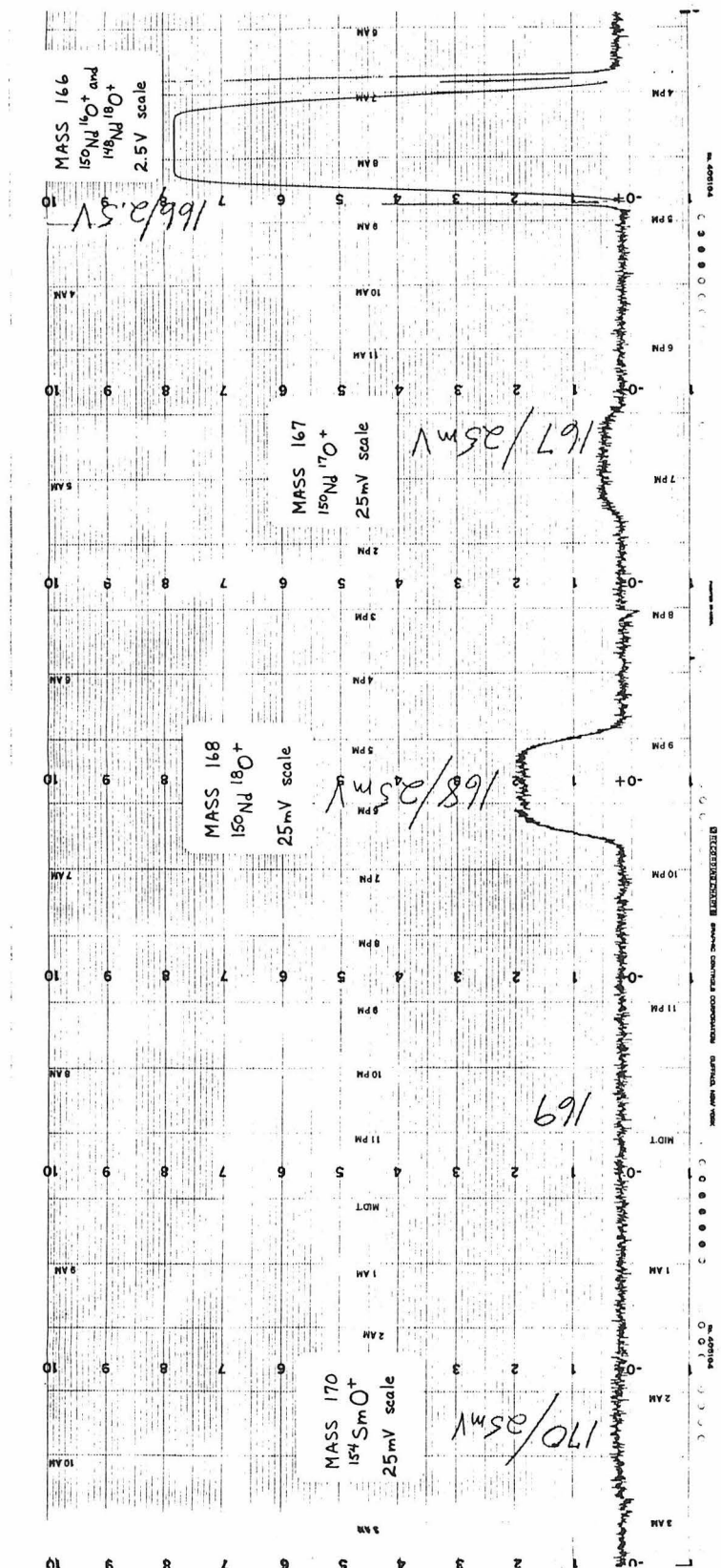


Fig. A5-3a

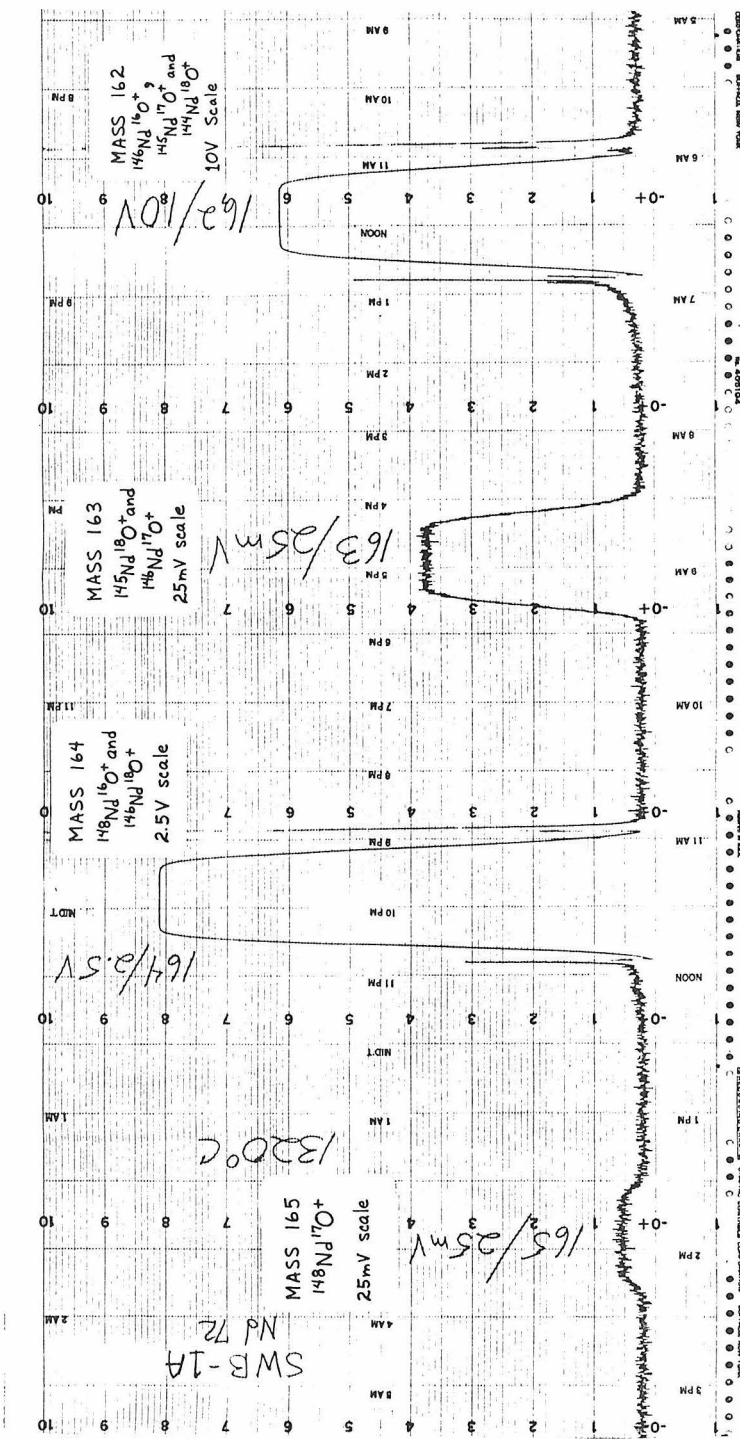


Fig. A5-3a

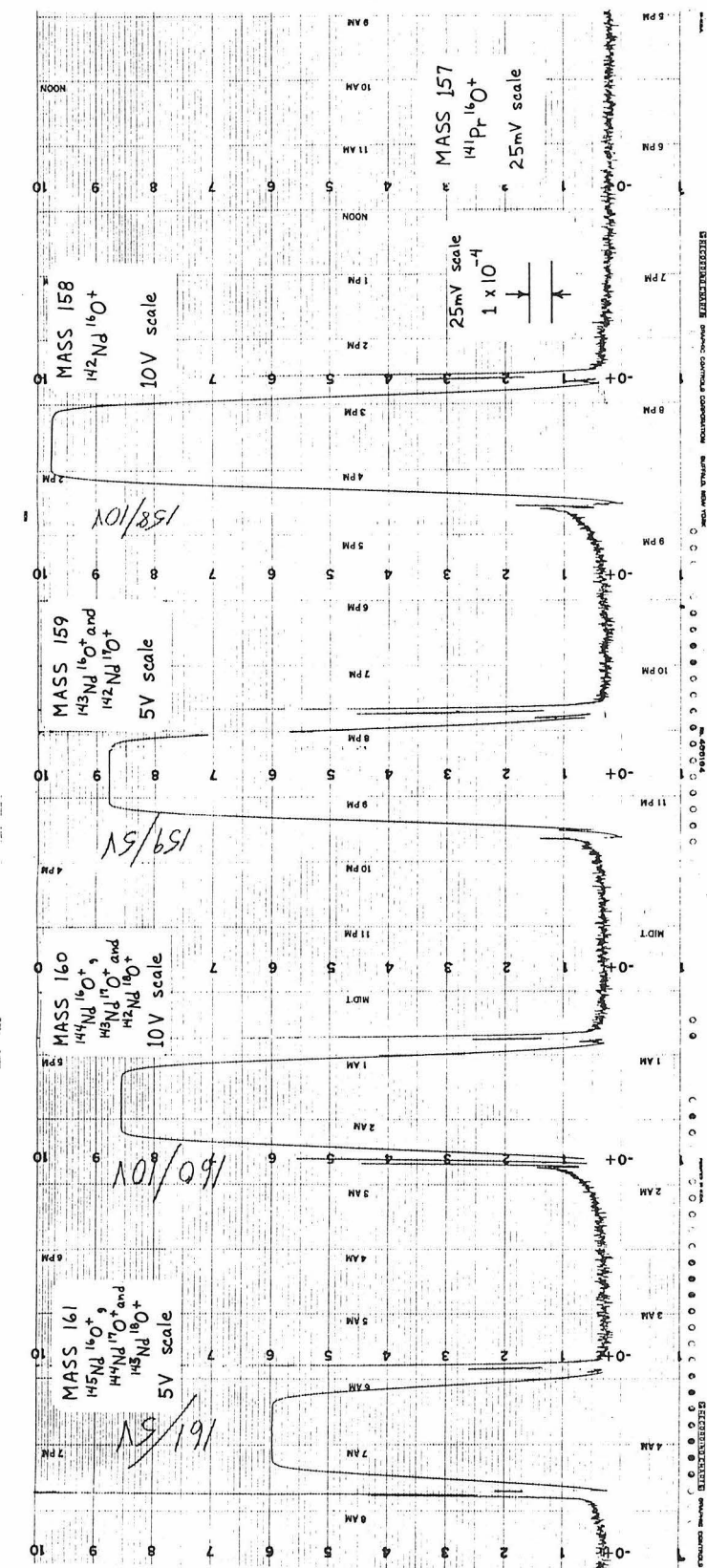


Fig. A5-3a

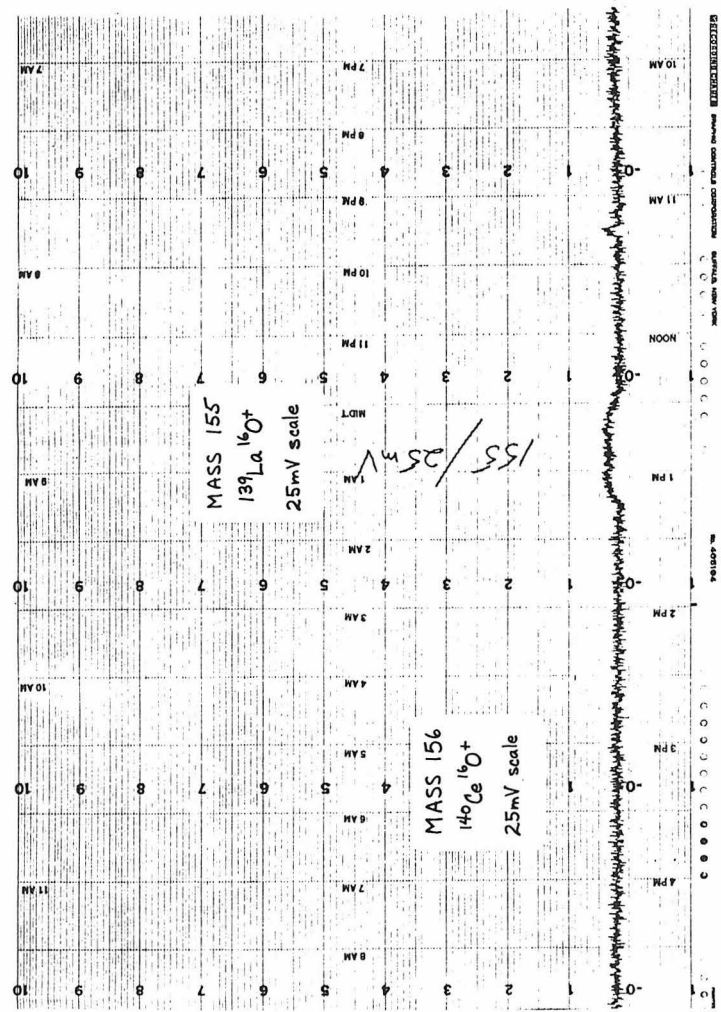


Fig. A5-3a

Figure A5-3: (b) Digital peak profile of $^{144}\text{Nd}^{16}\text{O}^+$ peak taken during a run. The source slit was set at 0.010 inches wide and the collector slit was 0.025 inches wide. Overall peak width at 99% of full intensity is 4 gauss, and over a 2.5 gauss interval the peak top is flat to one part in 10^5 . The magnetic field can be controlled to ± 0.1 gauss, and thus the peak intensity can be easily measured well within the flat section of peak top on each mass scan.

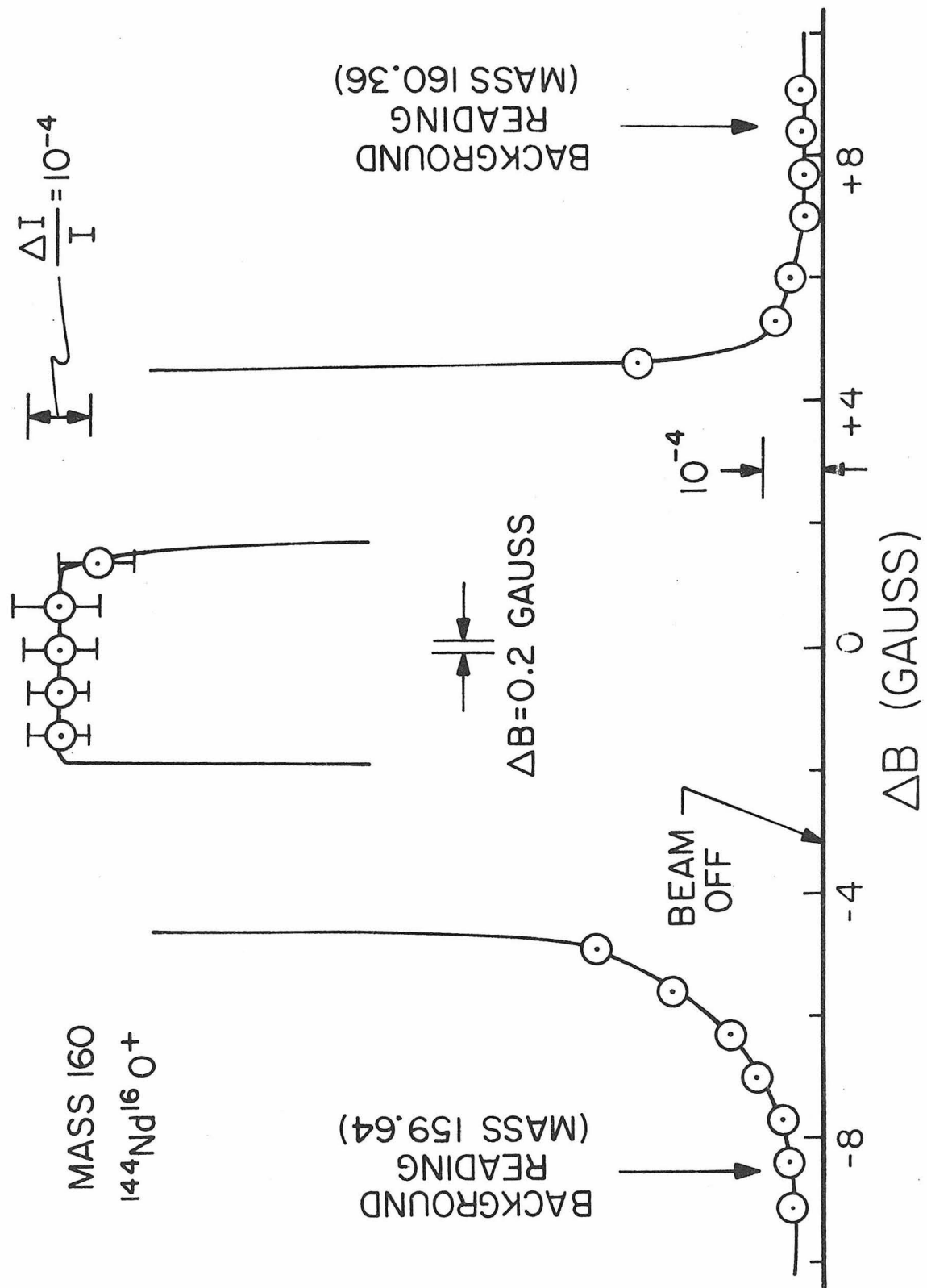


Fig. A5-3b

Figure A5-3: (c) Magnetic field scan of masses 167-173 taken during a run using an electron multiplier with a gain of ~ 7000 to enhance the ion currents. One large division on the chart scale is equal to 10mV for masses 169 to 173, 1.0 volts for mass 168 and 0.1 volt for mass 167. As shown, the intensity of the $\text{Sm}0^+$ beam is 10^{-5} that of $\text{Nd}0^+$, and the intensity of the $\text{Gd}0^+$ beam is 5×10^{-7} that of $\text{Nd}0^+$. The electron multiplier is used to precisely determine the amount of any interfering species in the spectrum. This can be done even when the interferences are very small and reduces uncertainties in the Nd isotopic data due to these interferences to essentially nil.

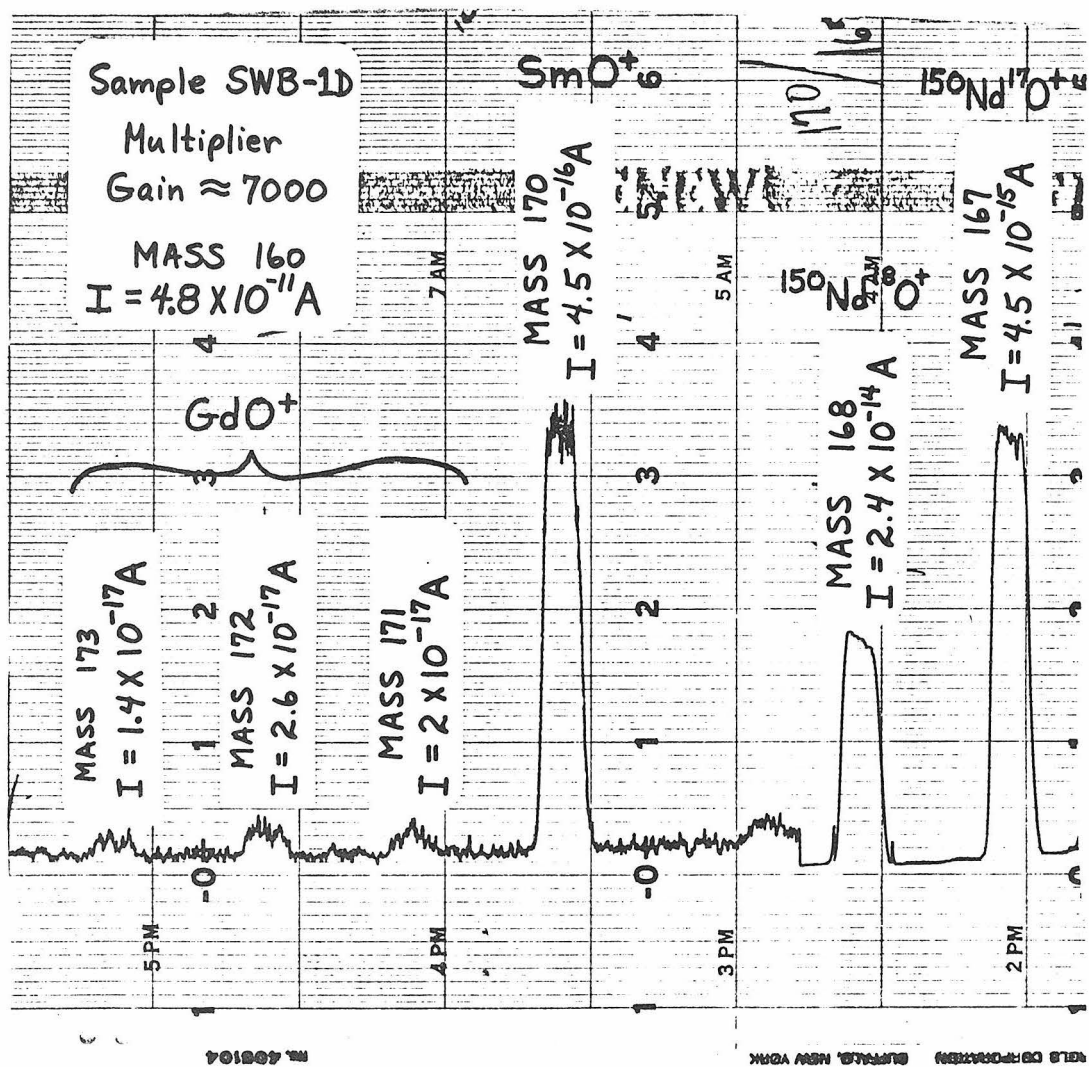


Fig. A5-3c

Nd ion beam intensity ratios are calculated relative to $^{144}\text{Nd } 0^+$. At each mass the peak intensity and the background on each side of the peak are measured. At each position the signal is integrated for 1 second. The amount of time between the start of the DVM integration at the first zero position and the start of the DVM integration at the peak position, and between the peak and the second zero integration at each mass is kept constant at 2.94 seconds. The peak intensities are measured in the sequence $^{144}\text{Nd } 0^+$, $^{143}\text{Nd } 0^+$, $^{142}\text{Nd } 0^+$, $^{150}\text{Nd } 0^+$, $^{148}\text{Nd } 0^+$, $^{146}\text{Nd } 0^+$, $^{145}\text{Nd } 0^+$ which corresponds to masses 160, 159, 158, 166, 164, 162, and 161. Data are taken in sets of 10 mass scans, averaged, corrected for oxygen isotope composition, and then corrected for mass discrimination. Oxygen isotope corrections were made using the composition given by Nier (1950). The procedure used for making the oxygen corrections is outlined in Table A5-1. Mass discrimination corrections were made by normalizing to $^{150}\text{Nd}/^{142}\text{Nd} = 0.2096$, which is the average value measured in the Lunatic I mass spectrometer (Wasserburg *et al.*, 1969). This value for $^{150}\text{Nd}/^{142}\text{Nd}$ is somewhat higher than that measured by other laboratories (c.f. Lugmair *et al.*, 1975; O'Nions *et al.*, 1977a; Tatsumoto *et al.*, 1976). However, due to the better performance characteristics of the Lunatic mass spectrometer this value will be retained until such time as a precise determination of the absolute abundances of the Nd isotopes is made. The ratio $^{150}\text{Nd}/^{142}\text{Nd}$ is used for the determination of mass fractionation because the difference of 8 mass units for these isotopes minimizes the error in determining the fractionation factor per mass unit. The fractionation factor per mass unit α is calculated from:

Table A5-1: Oxygen isotope corrections to measured NdO^+ isotope ratios.*

A. $143^* = (159/160)_m - (158/160)_m R_{17}$
 $144^* = 1 - (158/160)_m R_{18} - 143^* R_{17}$
 $145^* = (161/160)_m - 143^* R_{18} - 144^* R_{17}$
 $146^* = (162/160)_m - 144^* R_{18} - 145^* R_{17}$
 $148^* = (164/160)_m - 146^* R_{18}$
 $150^* = (166/160)_m - 148^* R_{18}$

B. $142/144 = (158/160)_m / 144^*$
 $143/144 = 143^* / 144^*$
 $145/144 = 145^* / 144^*$
 $145/144 = 146^* / 144^*$
 $148/144 = 148^* / 144^*$
 $150/144 = 150^* / 144^*$

where: $R_{17} \equiv {}^{17}\text{O}/{}^{16}\text{O}$; $R_{18} \equiv {}^{18}\text{O}/{}^{16}\text{O}$; m denotes measured (oxide)

mass abundance ratio.

*Numbers refer to the masses of the Nd isotopes and the masses of the NdO^+ isotopic species. Thus $142/144$ is equivalent to $^{142}\text{Nd}/^{144}\text{Nd}$ and $158/160$ is equivalent to $^{142}\text{NdO}/^{144}\text{NdO}$.

$$\alpha = \frac{1}{8} \left[\frac{(^{150}\text{Nd}/^{142}\text{Nd})_{\text{meas}}}{0.2096} - 1 \right]$$

Each measured isotope ratio $(^{i}\text{Nd}/^{144}\text{Nd})_{\text{meas}}$ is then corrected for mass fractionation using the formula:

$$(^{i}\text{Nd}/^{144}\text{Nd})_{\text{corr}} = (^{i}\text{Nd}/^{144}\text{Nd}) / [1 + \alpha(i-144)]$$

In many cases Nd isotopic measurements are made on samples to which ^{150}Nd tracer has been added. The ^{150}Nd tracer is approximately 95% ^{150}Nd . The small amounts of the other Nd isotopes in the tracer significantly change the measured isotope ratios so that corrections must be made. These corrections are made using the measured isotopic composition of the tracer. As noted previously this measurement is quite precise, but additional uncertainty must be added to the measured ratios due to the inability to precisely measure the instrumental mass discrimination during the measurement of the tracer. As an example of the magnitude of corrections due to the tracer composition the net correction to $^{143}\text{Nd}/^{144}\text{Nd}$ under normal spiking conditions (^{150}Nd -tracer added equal to twice ^{150}Nd in sample) is approximately $(0.15 \pm 0.0003)\%$ where the uncertainty is due to uncertainty in the tracer composition. The added uncertainty to $^{143}\text{Nd}/^{144}\text{Nd}$ from this effect is therefore negligible. Due to the presence of the ^{150}Nd tracer, $^{150}\text{Nd}/^{142}\text{Nd}$ cannot be used to correct for instrumental mass discrimination. Therefore, in these runs Nd isotopic ratios were normalized to $^{146}\text{Nd}/^{142}\text{Nd} = 0.636155$. This is equivalent to normalizing to $^{150}\text{Nd}/^{142}\text{Nd} = 0.2096$ for the

unspiked samples (DePaolo and Wasserburg, 1976b) and is essentially the average value that is measured in the Lunatic I mass spectrometer (Wasserburg *et al.*, 1969) if no correction is made for mass fractionation. The $^{146}\text{Nd}/^{142}\text{Nd}$ ratio is used for the determination of fractionation because this ratio still provides a difference of 4 mass units, involves abundant Nd isotopes, and the contributions to ^{142}Nd and ^{146}Nd from the ^{150}Nd tracer are small.

B. Oxygen Isotopic Abundance

Oxygen isotopic corrections to Nd isotope ratios were made assuming that $^{18}\text{O}/^{16}\text{O} = 0.002045$ and $^{17}\text{O}/^{16}\text{O} = 0.0003708$ (Nier, 1950). However, since a large variability of oxygen isotope ratios is found in nature, preliminary measurements of $^{18}\text{O}/^{16}\text{O}$ and $^{17}\text{O}/^{16}\text{O}$ in the Nd O^+ ion beam have been made to determine if the ratios given above are actually the same as those found in the ion beam. This was done by measuring the ratios $^{150}\text{Nd}^{18}\text{O}/^{150}\text{Nd}^{16}\text{O}$ and $^{150}\text{Nd}^{17}\text{O}/^{150}\text{Nd}^{16}\text{O}$ on a sample of the ^{150}Nd tracer, a spiked sample and on an unspiked sample. The isotope ^{150}Nd was chosen for this measurement because it is the heaviest Nd isotope so that the peaks due to $^{150}\text{Nd}^{17}\text{O}^+$ and $^{150}\text{Nd}^{18}\text{O}^+$ are not interfered with by other Nd O^+ ions. An analogue spectrum of masses 166, 167 and 168 is shown in Figure A5-3. Under normal operating conditions for measuring Nd isotope ratios (i.e., collector slit width = 0.025"), the tail of the 166 peaks creates a sloping background at mass 167. To minimize this effect, when measurements of oxygen ratios were made the collector slit width was narrowed to 0.020". Under these conditions the peak tops are still flat

to $\leq 1 \times 10^{-4}$ for about ± 1.2 gauss from the peak magnetic field setting. When measuring a small ion current such as at mass 167 (^{17}O) after measuring a much larger current (mass 166, ^{16}O), ample time must be allowed for the current to decay from the circuit before the next measurement is made. To accomplish this, the current at mass 167 was measured twice (zeros and peak) during each mass scan, and the first measurement was discarded. Measurements were made with an ion current at mass 166 of about 7×10^{-11} A, four times greater than shown in Figure A5-3. The current at mass 168 was then $\sim 1.5 \times 10^{-13}$ A and that at mass 167 was $\sim 2.8 \times 10^{-14}$ A. At these intensities, $^{18}\text{O}/^{16}\text{O}$ can be measured with a precision of $\sim 0.1\%$ and $^{17}\text{O}/^{16}\text{O}$ can be measured with a precision of $\sim 0.4\%$. Interfering Sm ions at mass 168 ($^{152}\text{Sm}^{16}\text{O}^+$) are corrected for by monitoring $^{154}\text{Sm}^{16}\text{O}^+$ during the run. A small peak was also sometimes detected at mass 169 (0.002% of peak at 167). This peak is probably due to $^{153}\text{Eu}^{16}\text{O}^+$ or possibly $^{169}\text{Tm}^+$. It was assumed that the peak was $^{153}\text{Eu}^{16}\text{O}^+$ and a correction for $^{151}\text{Eu}^{16}\text{O}^+$ was made to the measured 167/166 ratio. Both the 167/166 and 168/166 ratios were corrected where necessary for the contribution of $^{148}\text{Nd}^{18}\text{O}^+$ to mass 166.

As shown in Figure A5-4 the measurements by Nier (1950) show a narrow range of $^{18}\text{O}/^{16}\text{O}$ but there is one value of $^{17}\text{O}/^{16}\text{O}$ measured on air that does not agree with the other three values. It is this discrepant composition which was selected to be used for the oxygen corrections to Nd ratios, mainly because it was the most precise

Figure A5-4: A comparison of the determinations of oxygen isotope abundances done in this work with those of Nier (1950). T represents a measurement made using a ^{150}Nd tracer solution and T+N is a measurement made on a mixture of ^{150}Nd tracer and normal reagent Nd. The two measurements made in this work and three of Nier's measurements lie close to the same mass discrimination line. One of Nier's measurements appears to be anomalous.

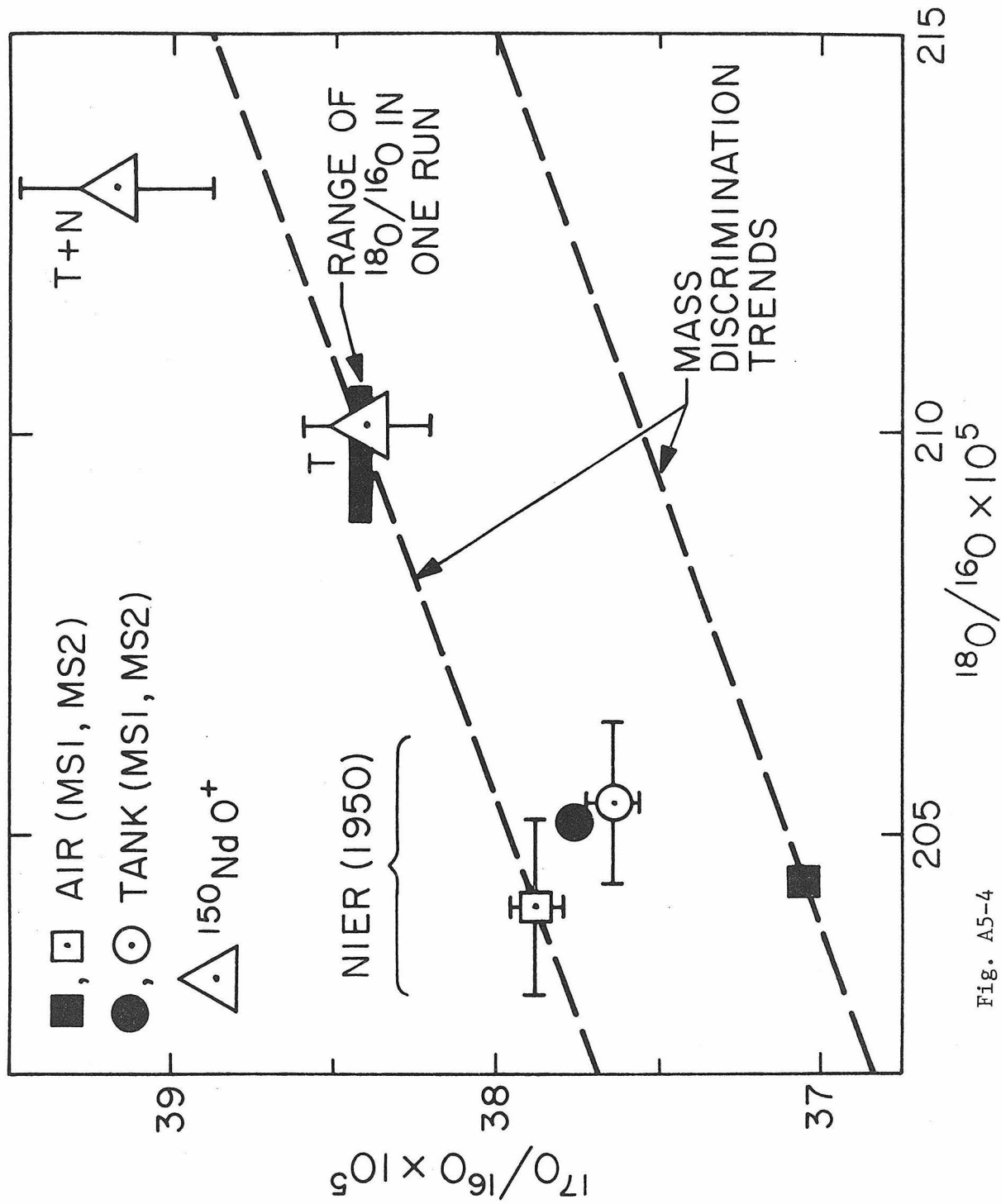
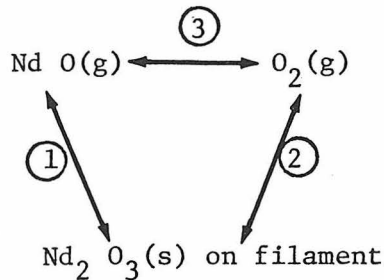


Fig. A5-4

determination and was the value listed by Lederer *et al.* (1967). The oxygen isotopic composition measured on $^{150}\text{Nd O}^+$ for the ^{150}Nd tracer (T) and the tracer-normal Nd mixture (T+N) show much higher $^{18}\text{O}/^{16}\text{O}$ ratios than the Nier measurements. The $^{150}\text{Nd O}^+$ measurements are reasonably consistent with this difference being attributed solely to mass-dependent fractionation if the Nier measurements with the higher $^{17}\text{O}/^{16}\text{O}$ are accepted as correct. They are not consistent with simple fractionation relative to the Nier composition with the lower $^{17}\text{O}/^{16}\text{O}$. The difference in the isotopic composition measured by Nier and the current measurements of $^{150}\text{Nd O}^+$ could be due to mass fractionation which occurs 1) in Nier's mass spectrometer 2) in the Lunatic mass spectrometer during evaporation and ionization of $\text{Nd}_2\text{O}_3(s)$ to form $\text{Nd O}^+(g) + \text{O}_2(g)$ or 3) during the process of oxidizing the Nd on the Re filament by heating in air. At present the cause is undetermined. However, the new results suggest that the low $^{17}\text{O}/^{16}\text{O}$ point of Nier's is indeed discrepant, and that a consistent set of oxygen isotope ratios would be approximately $^{17}\text{O}/^{16}\text{O} = 0.00038$ and $^{18}\text{O}/^{16}\text{O} = 0.00205$. However, the question of what is the absolute composition of average terrestrial oxygen is raised by the new data. Although Nier took precautions to monitor mass discrimination in his mass spectrometers, it is well known that mass-dependent effects at low mass can be very large, of the order of several percent. Because the measurement of $^{150}\text{Nd O}^+$ involves high mass species, it was thought that it might give a closer approximation to the true oxygen isotopic composition. However, the evaporation and ionization of Nd O^+ from a Re filament may

be a complicated process, and this assumption may not be true. The evaporation-process could be diagrammed as follows:



We are interested in the isotopic composition of the Nd O(g) relative to the Nd₂ O₃(s) on the filament. If the oxygen isotope compositions of these species are governed primarily by an "equilibrium" such as

(1) in the diagram, we would expect the Nd O units to behave as fractionating species of mass ~ 160 and thus we would expect little oxygen isotope fractionation between Nd O(g) and Nd₂ O₃(s). However, if the oxygen isotopic composition of these species are controlled by "equilibria" such as (2) and (3), then there could be large differences of $^{18}\text{O}/^{16}\text{O}$ and $^{17}\text{O}/^{16}\text{O}$ between the species involved and oxygen isotopic composition during a run could change at a rate which is much faster than the fractionation-produced changes of Nd isotopic composition.

In order to make the right oxygen isotopic corrections to the Nd O⁺ isotope ratios, it is necessary to know the correct oxygen isotopic composition in the Nd O⁺ ion beam. To this end it is necessary to know 1) the average O isotopic composition in the ion beam 2) the variability of this composition from run to run 3) the variability of this composition during a single run and 4) whether or not the O composition can be determined during a Nd run. To begin with

the last question, the $^{18}\text{O}/^{16}\text{O}$ ratio can be determined quite accurately on a sample during a run if the $^{144}\text{Nd O}^+$ beam intensity is $5 \times 10^{-11}\text{A}$ or higher during a run. For many samples such high beam intensities are impossible because the sample is too small. As shown in Figure A5-5, $^{18}\text{O}/^{16}\text{O}$ can vary by at least 1.5% between two runs and in one run a variation of 0.8% was observed. In addition to the two runs shown in Figure A5-5, $^{18}\text{O}/^{16}\text{O}$ was measured in two other runs, and fell between 0.00210 and 0.00213. Thus, the average value measured on Nd O^+ appears to be about 0.00211 or 0.00212.

The effect of varying O isotopic composition on the Nd element ratios which are calculated from a given set of Nd O^+ ratios is shown in Table A5-2. One set of Nd isotope ratios was calculated assuming $^{18}\text{O}/^{16}\text{O} = 0.002050$ and $^{17}\text{O}/^{16}\text{O} = 0.000380$ and the other set was calculated assuming $^{18}\text{O}/^{16}\text{O} = 0.00215$ and $^{17}\text{O}/^{16}\text{O} = 0.000389$. The first O isotopic composition is close to that measured by Nier and the second is fractionated from that composition along the line shown in Figure A5-5. As can be seen from Table A5-2, the change in the calculated Nd isotope ratios is quite significant for such a change in the O isotope composition. Thus if the O isotope composition used to calculate the corrections were different from that in the ion beam by this amount ($\sim 5\%$ in $^{18}\text{O}/^{16}\text{O}$), the calculated $^{143}\text{Nd}/^{144}\text{Nd}$ would be in error by almost 1×10^{-4} , much larger than the attainable precision of 3×10^{-5} . These effects would be important in comparing Nd ratios measured on Nd O^+ with those measured on Nd^+ in other laboratories.

Table A5-2:

	$\frac{142_{\text{Nd}}}{144_{\text{Nd}}}$	$\frac{143_{\text{Nd}}}{144_{\text{Nd}}}$	$\frac{145_{\text{Nd}}}{144_{\text{Nd}}}$	$\frac{146_{\text{Nd}}}{144_{\text{Nd}}}$	$\frac{148_{\text{Nd}}}{144_{\text{Nd}}}$	$\frac{150_{\text{Nd}}}{144_{\text{Nd}}}$
Oxide Ratios	1.135411	.510971	.349506	.724456	.243949	.238478
A) Corrected w/	1.138280	.511831	.348963	.724106	.253086	.238584
$^{17}\text{O}/^{16}\text{O} = 0.00038$						
$^{18}\text{O}/^{16}\text{O} = 0.00205$						
B) Corrected w/	1.138393	.511876	.348949	.724111	.243052	.238607
$^{17}\text{O}/^{16}\text{O} = 0.000389$						
$^{18}\text{O}/^{16}\text{O} = 0.00215$						
$\varepsilon_{\text{B-A}} (10^{-4})$	+0.99	+0.88	-0.40	+0.07	-1.40	+0.99
Fractional Change per 1% change in $^{18}\text{O}/^{16}\text{O}$	+0.21	+0.18	-0.08	+0.01	-0.29	+0.21

In order to limit the uncertainty in $^{143}\text{Nd}/^{144}\text{Nd}$ due to uncertainty in O isotope composition to 1×10^{-5} it is necessary to know $^{18}\text{O}/^{16}\text{O}$ to 0.5%.

$^{142}\text{Nd}/^{144}\text{Nd}$ is the isotope ratio which can be measured most precisely relative to the changes expected due to shifts in O isotope composition. Shifts in the measured $^{142}\text{Nd}/^{144}\text{Nd}$ larger than experimental precision have been noted which may be the result of shifts in O isotope composition. Furthermore, it has been found that the measured value of $^{142}\text{Nd}/^{144}\text{Nd}$ tends to be correlated with the Nd discrimination from run to run. Figure A5-6 shows a plot of the measured $^{142}\text{Nd}/^{144}\text{Nd}$ versus the average Nd discrimination for several mass spectrometer runs where the precision was good. Although the error bars are large compared to the total variation, there appears to be a strikingly good correlation. This correlation could result from variations of O isotope composition from run to run only if $^{18}\text{O}/^{16}\text{O}$ were correlated with the Nd discrimination. From the dashed line shown in Figure A5-6 describing the approximate trend and the data in Table A5-2 it can be calculated that a total range of $^{18}\text{O}/^{16}\text{O}$ of ~5% is necessary to explain the range in $^{142}\text{Nd}/^{144}\text{Nd}$. In view of the fact that in the two runs shown in Figure A5-4 $^{18}\text{O}/^{16}\text{O}$ differed by 1.5%, such a range seems plausible.

At present there are not enough data to know the correct values of $^{18}\text{O}/^{16}\text{O}$ and $^{17}\text{O}/^{16}\text{O}$ to use for the corrections. However, it appears that an empirical relationship between $^{18}\text{O}/^{16}\text{O}$ and $^{17}\text{O}/^{16}\text{O}$ could be deduced. As a step in this direction, $^{18}\text{O}/^{16}\text{O}$ was measured in a basalt sample Nd run where $^{142}\text{Nd}/^{144}\text{Nd}$ and the discrimination were well known. For this run the Nd discrimination = 1.00055, $^{142}\text{Nd}/^{144}\text{Nd}$ =

Figure A5-5: Graph showing a correlation between the measured mean $^{142}\text{Nd}/^{144}\text{Nd}$ for a run and the average Nd mass discrimination for a run. Several mass spectrometer runs are shown. This effect is believed to be caused by variations of the oxygen isotope composition in the NdO^+ beam which are correlated with the Nd discrimination. Corrections for the O isotope composition which are applied to the NdO^+ measured ratios are done assuming constant values for $^{18}\text{O}/^{16}\text{O}$ and $^{17}\text{O}/^{16}\text{O}$. Thus if the oxygen ratios are different from run to run, the (corrected) Nd isotope ratios will change, as appears to be the case.

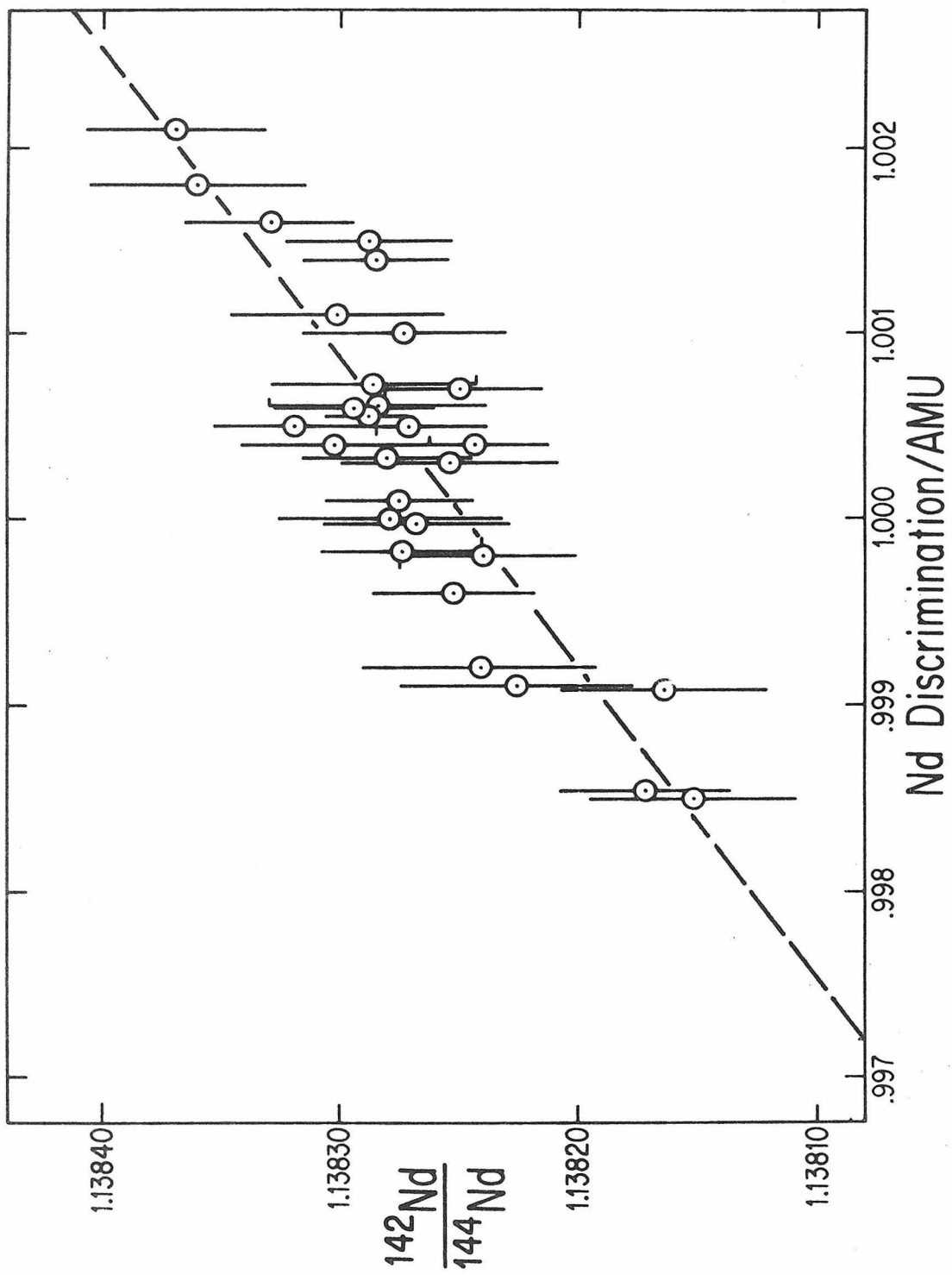


Fig. A5-5

1.138291 ± 27 and $^{18}\text{O}/^{16}\text{O} = 0.002117 \pm 7$. The discrimination and $^{142}\text{Nd}/^{144}\text{Nd}$ lie almost exactly on the dashed line in Figure A5-6. From these data we can calculate a tentative relationship between $^{18}\text{O}/^{16}\text{O}$ and α , the Nd discrimination factor defined in a previous section:

$$^{18}\text{O}/^{16}\text{O} = 0.002092 + 0.045\alpha$$

$^{17}\text{O}/^{16}\text{O}$ can then be calculated from $^{18}\text{O}/^{16}\text{O}$ provided one pair of self-consistent $^{18}\text{O}/^{16}\text{O} - ^{17}\text{O}/^{16}\text{O}$ ratios is known. This relationship implies that the variation of O isotopic composition observed in the mass spectrometer is due to processes occurring in the mass spectrometer during the evaporation and ionization of Nd_2O_3 . If this relationship or one similar to it can be shown to be approximately correct, it would be possible to easily determine the $^{18}\text{O}/^{16}\text{O}$ to the required accuracy to make the appropriate corrections to the Nd ratios by an iterative procedure. The wide variation of $^{18}\text{O}/^{16}\text{O}$ necessary to explain the $^{142}\text{Nd}/^{144}\text{Nd}$ effects suggests that the escaping O_2 gas during the evaporation of Nd_2O_3 from the filament may be playing an important role in determining the behavior of O isotopes in the process.

C. Data Quality:

For mass spectrometer data taken when the $^{144}\text{Nd}^+$ signal is $\sim 9 \times 10^{-12}$ A, the standard deviation of the mean of 10 measurements of $^{143}\text{NdO}/^{144}\text{NdO}$ averages about 0.008%-0.009%. Each measurement of $^{143}\text{NdO}/^{144}\text{NdO}$ involves one integration of the $^{143}\text{NdO}^+$ beam (4.5×10^{-12} A which is equivalent to 2.8×10^7 ions) and two integrations of the $^{144}\text{NdO}^+$ beam ($2 \cdot 9.0 \times 10^{-12}$ A or 11.2×10^7 ions). Thus from counting

statistics alone the standard deviation of the mean for 10 measurements of $^{143}\text{NdO}/^{144}\text{NdO}$ should be about 0.008% (including uncertainty introduced by the mass discrimination correction). Thus at the ion beam intensity given above, the uncertainty in the measured isotope ratios comes essentially entirely from counting statistics and is not limited by beam stability or electronic noise. For 250 measurements, the $2\sigma_{\text{mean}}$ (95% confidence level) uncertainty in $^{143}\text{Nd}/^{144}\text{Nd}$ is about 0.003% to 0.004%. At 10 times higher beam intensities ($^{144}\text{NdO}^+ = 9 \times 10^{-11} \text{ A}$), which can be obtained with larger samples, the error due to counting can be decreased by a factor of $\sqrt{10}$. If the measurement of $^{143}\text{Nd}/^{144}\text{Nd}$ were still limited by statistics at these higher intensities, $1\sigma_{\text{mean}}$ for ten ratios would be expected to be 0.0025%. Two samples were measured at these higher beam intensities and the $2\sigma_{\text{mean}}$ for runs of 170 ratios and 140 ratios were 0.0014% and 0.0017% respectively, very close to the expected counting errors of 0.0013% and 0.0014%. In these two runs all measured isotope ratios agreed within error with the previously determined grand mean values for those ratios.

The Nd isotopic measurements described here represent the most stringent tests to date of the precision and reproducibility attainable with the Lunatic mass spectrometers. The results indicate that even at a level of 1×10^{-5} , inherent limitations in precision due to instabilities in filament current and filament temperature, electronic background noise, nonlinearities in the electrometer and DVM, instabilities in magnetic field and accelerating potential, and possible non-uniform peak shape are still small compared to ion counting

statistics. Thus isotopic ratio measurements to a precision of $\pm 1 \times 10^{-5}$ or perhaps $\pm 5 \times 10^{-6}$ are apparently attainable with current instrumentation.

The excellent ionization efficiency of Nd combined with its stable emission characteristics suggest that it may become a useful tool for mass spectrometer calibration and intercalibration. Because Nd has seven isotopes with isotope ratios ranging from 0.2 to 0.9, all of which can be precisely measured, it is probable that linearity and scale factors for a given instrument can be worked out with confidence by performing the correct experiments and carefully considering the data.

D. Isotopic Composition of Neodymium

The first high-precision measurements of Nd isotopic abundances were made in this study. In all Nd mass spectrometer runs all seven Nd isotopes were measured. This was done as a means of monitoring the precision and reproducibility of the measurements. The use of Nd in geochemistry requires the routine measurement of $^{143}\text{Nd}/^{144}\text{Nd}$ to a precision of 5 parts in 10^5 or better. Before this study, it was not clear that such precision and reproducibility over long periods could be attained with the present instrumentation. Measurement of all isotopes provides a built-in check to determine if isotope ratios that do not vary in nature can be reproducibly measured to very high precision. It also provides a check against possible artifacts introduced by the chemical separation procedures.

TABLE A5-3: Nd ISOTOPE MEASUREMENTS^a

Run #	Sample	$\frac{142_{\text{Nd}}}{144_{\text{Nd}}}$	$\frac{143_{\text{Nd}}}{144_{\text{Nd}}}$	$\frac{145_{\text{Nd}}}{144_{\text{Nd}}}$	$\frac{146_{\text{Nd}}}{144_{\text{Nd}}}$	$\frac{148_{\text{Nd}}}{144_{\text{Nd}}}$	$\frac{\text{DISC}^c}{144_{\text{Nd}}}$	$\frac{\text{I}_{160}^d}{\text{I}_{160}}$	
29	Khibina Ap.	1.138270 ± 36	.511862 ± 17	.348970 ± 19	.724116 ± 30	.243082 ± 20		.85	*
31	BCR-1	1.138273 ± 44	.511839 ± 22	.348977 ± 19	.724088 ± 36	.243070 ± 19		3.7	*
32	113152	1.138227 ± 60	.512280 ± 35	.348950 ± 42	b	.243112 ± 43	1.00005	.60	
33	113031	1.138211 ± 49	.512115 ± 40	.348952 ± 32	b	.243066 ± 22	.9993	2.0/.85	
35	RN3 Ap.	1.138250 ± 47	.511342 ± 23	.348965 ± 27	b	.243084 ± 28	.9995	.90	
36	111240	1.138279 ± 47	.512361 ± 22	.348975 ± 18	.724113 ± 26	.243091 ± 26	1.00000	.92	*
37	RN3-TR (TSP)	1.138214 ± 88	.510234 ± 37	.348913 ± 46	b	.243065 ± 58	1.0003	.55	
38	OGG128.10	1.138255 ± 71	.510034 ± 36	.348959 ± 20	.724118 ± 49	.243079 ± 24	.9988	5.0/.8	
39	RN3-TR	1.138303 ± 83	.510245 ± 31	.348977 ± 42	.724139 ± 58	.243072 ± 38	.9998	.90	
41	RHO-1D	1.138185 ± 151	.510994 ± 48	.348943 ± 48	.724079 ± 113	.243089 ± 34	1.00000	.90	

TABLE A5-3: Nd ISOTOPE MEASUREMENTS (CONTINUED)

Run #	Sample	$\frac{142_{\text{Nd}}}{144_{\text{Nd}}}$	$\frac{143_{\text{Nd}}}{144_{\text{Nd}}}$	$\frac{145_{\text{Nd}}}{144_{\text{Nd}}}$	$\frac{146_{\text{Nd}}}{144_{\text{Nd}}}$	$\frac{148_{\text{Nd}}}{144_{\text{Nd}}}$	<u>DISC</u>	<u>I_{160}</u>
42	NAS-216D	1.138229 ± 42	.511101 ± 27	.348968 ± 38	.724086 ± 54	.243110 ± 29	1.0003	.94
44	MP-22D	1.138254 ± 46	.510819 ± 20	.348977 ± 9	.724121 ± 29	.243067 ± 29	1.0003	4.5 *
47	ZL-3D		.511611 ± 34				1.0004	8.0
48	OGG210	1.138104 ± 89	.510306 ± 43	.348976 ± 34	.724084 ± 56	.243059 ± 22	.9991	3.2
49	WYWR-4	1.138243 ± 74	.510319 ± 32	.348979 ± 20	b	.243039 ± 28	.9985	6.0
51	OLC-1	1.138179 ± 76	.511840 ± 46	.348964 ± 33	.724072 ± 53	.243079 ± 21	.9970	.92
54	HN-D1	1.138272 ± 85	.512212 ± 30	.348926 ± 24	.724110 ± 48	.243061 ± 25	1.0002	.8/2.6/4.3
57	HT-D1	1.138180 ± 55	.511879 ± 32	.348973 ± 23	.724087 ± 38	.243060 ± 20	.9982	.8/4.4
58	RGB-1	1.138234 ± 66	.511852 ± 38	.348956 ± 26	.724121 ± 45	.243068 ± 18	.9992	.9/3.5
59	LAK-8D	1.138233 ± 82	.511903 ± 30	.348965 ± 26	.724127 ± 65	.243082 ± 21	1.0002	.85/4.5

TABLE A5-3: Nd ISOTOPE MEASUREMENTS (CONTINUED)

Run #	Sample	$\frac{142_{\text{Nd}}}{144_{\text{Nd}}}$	$\frac{143_{\text{Nd}}}{144_{\text{Nd}}}$	$\frac{145_{\text{Nd}}}{144_{\text{Nd}}}$	$\frac{146_{\text{Nd}}}{144_{\text{Nd}}}$	$\frac{148_{\text{Nd}}}{144_{\text{Nd}}}$	<u>DISC</u>	<u>I₁₆₀</u>
60	VG295	1.138220 ±97	.512378 ±47	.348984 ±26	.724166 ±65	.243088 ±25	.9991	5.4
61	GT-D2	1.138239 ±84	.512152 ±39	.348949 ±22	.724099 ±71	.243077 ±15	.9998	.90
63	BD17-1	1.138198 ±112	.512217 ±68	.348955 ±33	.724125 ±98	.243086 ±30	.9995	3.5/.9
65	DOS-1	1.138177 ±117	.511367 ±47	.348923 ±51	.724084 ±101	.243072 ±38	1.0010	2.5
67	PCB-1	1.138382 ±111	.512153 ±43	.348942 ±43	.724149 ±60	.243106 ±26	1.0000	.8/3.5
68	PD-1	1.138298 ±73	.511773 ±35	.348974 ±36	.724139 ±54	.243092 ±28	.9999	.70
69	DTB-1	1.138238 ±87	.511914 ±36	.348933 ±45	.724111 ±99	.243064 ±32	.9994	.9/2.0
70	PEA-3	1.138265 ±193	.510819 ±78	.348960 ±51	.724118 ±101	.243083 ±50	1.0004	.70
72	SWB-1A	1.138234 ±74	.511777 ±28	.348947 ±34	.724157 ±84	.243064 ±33	.9995	6.0
73	SK-38	1.138252 ±65	.511618 ±30	.348967 ±22	.724128 ±60	.243073 ±19	.85/2.4	

TABLE A5-3: Nd ISOTOPE MEASUREMENTS (CONTINUED)

Run #	Sample	$\frac{142_{\text{Nd}}}{144_{\text{Nd}}}$	$\frac{143_{\text{Nd}}}{144_{\text{Nd}}}$	$\frac{145_{\text{Nd}}}{144_{\text{Nd}}}$	$\frac{146_{\text{Nd}}}{144_{\text{Nd}}}$	$\frac{148_{\text{Nd}}}{144_{\text{Nd}}}$	DISC	I_{160}
74 DUL-4	1.138258	.511093 ±71	.348997 ±31	.724133 ±59	.243049 ±28	1.0020	5.0	
81 PG-16D	1.138294	.512172 ±34	.348966 ±25	.724113 ±23	.243076 ±15	1.0006	.87	*
82 CHA-2	1.138252	.512038 ±34	.348975 ±17	.724120 ±13	.243081 ±20	.9996	.89	*
83 V-9	1.138271	.511955 ±33	.348974 ±15	.724149 ±21	.243059 ±10	1.0005	3.5	*
84 DU111	1.138240	.511718 ±39	.348968 ±20	.724124 ±15	.243070 ±29	.9998	.95/3.0	*
85 BD17-1	1.138241	.512245 ±49	.348936 ±31	.724101 ±12	.243059 ±44	.9992	.70	*
86 Ar-g1	1.138273	.511734 ±43	.348968 ±22	.724106 ±19	.243081 ±29	1.0010	.77	*
87 10072,127 TR	1.138254	.512238 ±44	.348954 ±17	b ±15	.243067 ±16	1.0005	.85	
88 10072,127 Pyx-A	1.138302	.513788 ±32	.348990 ±15	b ±14	.243107 ±13	1.0017	.90	
89 10072,127 I1m	1.138237	.512035 ±32	.348957 ±21	b ±14	.243080 ±17	1.0005	.80	

TABLE A5-3: Nd ISOTOPE MEASUREMENTS (CONTINUED)

Run #	Sample	$\frac{142_{\text{Nd}}}{144_{\text{Nd}}}$	$\frac{143_{\text{Nd}}}{144_{\text{Nd}}}$	$\frac{145_{\text{Nd}}}{144_{\text{Nd}}}$	$\frac{146_{\text{Nd}}}{144_{\text{Nd}}}$	$\frac{148_{\text{Nd}}}{144_{\text{Nd}}}$	DISC	I ₁₆₀
90	10072,127 3.3 f1.	1.138260 ± 20	.511998 ± 16	.348979 ± 16	b	.243101 ± 10	1.0010	.85
91	10072,127 Pyx-B	1.138269 ± 34	.514154 ± 17	.348969 ± 14	b	.243081 ± 18	1.0005	.85
93	10072,127 Flag	1.138239 ± 32	.511721 ± 18	.348962 ± 16	b	.243082 ± 16	1.0002	.80
94	BMR-1	1.138288 ± 35	.512230 ± 19	.348966 ± 14	.724079 ± 29	.243079 ± 19	1.0015	.85
95	BMR-3	1.138250 ± 35	.512218 ± 21	.348981 ± 14	.724089 ± 30	.243076 ± 19	1.0007	.88 *
96	BMR-5	1.138276 ± 57	.512271 ± 22	.348970 ± 17	.724088 ± 24	.243072 ± 15	1.0008	.85 *
97	10062,33 TR	1.138255 ± 52	.512524 ± 19	.348981 ± 19	b	.243096 ± 29	1.0004	.85
98	10062,33 Pyx (M)	1.138278 ± 44	.513847 ± 23	.348966 ± 19	b	.243094 ± 23	1.0002	.80
100	PAR-1	1.138275 ± 31	.511688 ± 20	.348981 ± 18	.724098 ± 26	.243086 ± 17	1.0001	.85 *
102	10062,33 I1m	1.138214 ± 43	.512487 ± 53	.348992 ± 44	b	.243064 ± 42	.9986	.75

TABLE A5-3: Nd ISOTOPE MEASUREMENTS (CONTINUED)

Run #	Sample	$\frac{142_{\text{Nd}}}{144_{\text{Nd}}}$	$\frac{143_{\text{Nd}}}{144_{\text{Nd}}}$	$\frac{145_{\text{Nd}}}{144_{\text{Nd}}}$	$\frac{146_{\text{Nd}}}{144_{\text{Nd}}}$	$\frac{148_{\text{Nd}}}{144_{\text{Nd}}}$	DISC	I_{160}
103	10062,33 Pyx (L)	1.138301 ^{±47}	.514258 ^{±20}	.348966 ^{±13}	b	.243082 ^{±12}	1.0006	.88
104	10062,33 Plag	1.138265 ^{±26}	.511839 ^{±20}	.348939 ^{±18}		.243096 ^{±15}	1.0010	.70
105	SMG-1	1.138264 ^{±46}	.512045 ^{±30}	.348976 ^{±21}	.724138 ^{±35}	.243076 ^{±17}	1.0015	.65
106	WBK-1	1.138226 ^{±49}	.512091 ^{±19}	.348987 ^{±13}	.724135 ^{±30}	.243106 ^{±15}	.9991	.90 *
107	KAS-2	1.138280 ^{±36}	.511798 ^{±19}	.348979 ^{±20}	.724127 ^{±34}	.243089 ^{±18}	1.0003	.88 *
108	MAR-1	1.138314 ^{±66}	.512240 ^{±30}	.348986 ^{±23}	.724108 ^{±48}	.243091 ^{±30}	1.0005	.80
109	MAR-2	1.138279 ^{±57}	.512183 ^{±26}	.348946 ^{±25}	.724070 ^{±38}	.243075 ^{±19}	1.0009	.90 *
110	MAR-4	1.138286 ^{±43}	.512203 ^{±23}	.348977 ^{±14}	.724060 ^{±32}	.243072 ^{±26}	1.0007	.72 *
111	PER-2	1.138288 ^{±18}	.511185 ^{±7}	.348961 ^{±6}	.724108 ^{±11}	.243082 ^{±6}	1.0006	7.5 *
112	MAR-6	1.138285 ^{±31}	.512283 ^{±27}	.348982 ^{±16}	.724081 ^{±28}	.243078 ^{±21}	1.0014	.80

TABLE A5-3: Nd ISOTOPE MEASUREMENTS (CONTINUED)

Run #	Sample	$\frac{142_{\text{Nd}}}{144_{\text{Nd}}}$	$\frac{143_{\text{Nd}}}{144_{\text{Nd}}}$	$\frac{145_{\text{Nd}}}{144_{\text{Nd}}}$	$\frac{146_{\text{Nd}}}{144_{\text{Nd}}}$	$\frac{148_{\text{Nd}}}{144_{\text{Nd}}}$	DISC	I ₁₆₀
113	PER-1	1.138360 ±45	.511382 ±26	.348958 ±18	.724078 ±57	.243076 ±21	1.0018	.87
115	GU-4	1.138369 ±38	.512309 ±30	.348963 ±21	.724086 ±25	.243088 ±12	1.0021	.85
116	WMG-1	1.138286 ±73	.511977 ±27	.348968 ±24	.724091 ±32	.243128 ±15	.9997	.70 *
117	PAR-2	1.138152 ±43	.511577 ±26	.348966 ±16	.724089 ±28	.243085 ±18	.9985	.70
118	CSQ-3	1.138284 ±51	.512177 ±28	.348969 ±19	.724105 ±27	.243095 ±15	1.0000	.70 *
119	GU-7	1.138274 ±34	.512256 ±20	.348966 ±16	.724124 ±22	.243099 ±14	.9998	.87 *
120	SPP-1	1.138329 ±35	.512138 ±26	.348954 ±19	.724092 ±24	.243083 ±20	1.0016	.85
121	CAS-1	1.138247 ±56	.512069 ±18	.348950 ±17	.724124 ±41	.243091 ±20	1.0005	4/.9 *
122	ANB2102Q	1.138319 ±34	.512067 ±15	.348950 ±16	.724109 ±25	.243087 ±17	1.0005	6.0 *
123	ADT-2	1.138269 ±63	.511543 ±20	.348952 ±19	.724060 ±32	.243084 ±16	1.0004	5.5 *

TABLE A5-3: Nd ISOTOPE MEASUREMENTS (CONTINUED)

Run #	Sample	$\frac{142_{\text{Nd}}}{144_{\text{Nd}}}$	$\frac{143_{\text{Nd}}}{144_{\text{Nd}}}$	$\frac{145_{\text{Nd}}}{144_{\text{Nd}}}$	$\frac{146_{\text{Nd}}}{144_{\text{Nd}}}$	$\frac{148_{\text{Nd}}}{144_{\text{Nd}}}$	$\frac{\text{DISC}}{144_{\text{Nd}}}$	Γ_{160}
124	RL-1	1.138243 ± 32	.511868 ± 24	.348968 ± 18	.724094 ± 28	.243078 ± 19	1.0004	.87 *
125	AF-133	1.138164 ± 43	.512085 ± 28	.348978 ± 17	.724111 ± 31	.243078 ± 15	.9991	.75 *
126	ANB2128	1.138291 ± 27	.512040 ± 9	.348973 ± 9	.724115 ± 22	.243085 ± 9	1.0005	8.0 *
127	BMR-6	1.138274 ± 41	.512211 ± 26	.348974 ± 22	.724124 ± 37	.243105 ± 18	1.0006	.80 *
128	BMR-4	1.138301 ± 45	.512238 ± 26	.348970 ± 17	.724109 ± 36	.243095 ± 20	1.0011	.80
MAR-6 (repeat)		1.138268 ± 39	.512264 ± 16	.348985 ± 15	.724112 ± 41	.243078 ± 30	1.0000	.55 *
129	ANB2128	1.138302 ± 40	.512042 ± 18	.348977 ± 13	.724106 ± 25	.243081 ± 13	1.0004	7.0 *

^aNormalized to $^{150}_{\text{Nd}}/^{142}_{\text{Nd}} = 0.2096$ to correct for mass discrimination. $^{180}_{\text{Nd}}/^{160}$ and $^{170}_{\text{Nd}}/^{160}$ in the Nd0+ ion beam assumed to be 0.002045 and 0.0003708 respectively.

^bSample spiked with $^{150}_{\text{Nd}}$ tracer and ratios normalized to $^{146}_{\text{Nd}}/^{142}_{\text{Nd}} = 0.636155$.

^cApproximate average discrimination for the mass spectrometer run.

^dIntensity of ion beam at mass 160 ($^{144}_{\text{Nd}}{^{160}_{\text{O}}^+}$) in units of 10^{-11} A. For samples where more than one intensity is given, data were taken at different intensities in the same run.

Table A5-4: Isotopic Composition of Neodymium*

	$\frac{142_{\text{Nd}}}{144_{\text{Nd}}}$	$\frac{145_{\text{Nd}}}{144_{\text{Nd}}}$	$\frac{146_{\text{Nd}}}{144_{\text{Nd}}}$	$\frac{148_{\text{Nd}}}{144_{\text{Nd}}}$
A.	1.138268 ±10	0.348969 ±4	0.724107 ±7	0.243083 ±5
B.	1.138331 ±10	0.348954 ±4	0.724108 ±7	0.243067 ±5

*Normalized to $^{150}_{\text{Nd}}/^{142}_{\text{Nd}} = 0.2096$.

A. NdO^+ measured ratios corrected for oxygen isotopes using

$^{18}_{\text{O}}/^{16}_{\text{O}} = 0.002045$ and $^{17}_{\text{O}}/^{16}_{\text{O}} = 0.0003708$.

Chondritic $^{143}_{\text{Nd}}/^{144}_{\text{Nd}} = 0.511836$.

B. NdO^+ measured ratios corrected for oxygen isotopes using

$^{18}_{\text{O}}/^{16}_{\text{O}} = 0.00210$ and $^{17}_{\text{O}}/^{16}_{\text{O}} = 0.000384$; current best

estimate of Nd isotope ratios. Chondritic $^{143}_{\text{Nd}}/^{144}_{\text{Nd}} =$

0.511852.

The measured Nd isotope ratios for all runs are given in Table A5-3. These data represent NdO^+ ratios which were corrected for oxygen using $^{17}\text{O}/^{16}\text{O} = 0.0003708$ and $^{18}\text{O}/^{16}\text{O} = 0.002045$.

Grand mean values and 2σ uncertainties for all the isotope ratios have been computed and are given in Table A5-4. These numbers were computed by averaging only those unspiked runs which were most precise and where the absolute value of the Nd fractionation factor α was less than 0.001. The latter stipulation was to minimize the possible effects of varying O isotope composition on the calculated Nd ratios. The criterion for the precision of a run to be selected for the grand mean averaging was that all isotope ratios (except $^{148}\text{Nd}/^{144}\text{Nd}$) have a $2\sigma_{\text{mean}}$ uncertainty for the run of 5 parts in 10^5 . A total of thirty runs on Nd extracted from rocks were averaged. These 30 runs are marked by asterisks in Table A5-3. The grand means represent the current best estimate of the isotopic composition of terrestrial Nd. Measurements by Papanastassiou *et al.* (1977) show that lunar Nd is isotopically identical to terrestrial Nd for all isotopes except ^{143}Nd . Also given in Table A5-4 are the grand mean values recalculated using $^{18}\text{O}/^{16}\text{O} = 0.00210$ and $^{17}\text{O}/^{16}\text{O} = 0.00038$, the current best estimate of the mean O isotope composition of the NdO^+ ion beams. The second set of Nd ratios should be considered the current best values of the Nd isotope ratios.

E. Isotopic composition of Sm and λ^{147}

The isotopic composition assumed for terrestrial Sm is that given by Russ (1974) with $^{144}\text{Sm}/^{154}\text{Sm} = 0.13510$, $^{148}\text{Sm}/^{154}\text{Sm} = 0.49419$,

$^{149}\text{Sm}/^{154}\text{Sm} = 0.60750$, $^{150}\text{Sm}/^{154}\text{Sm} = 0.32440$, and $^{152}\text{Sm}/^{154}\text{Sm} = 1.17537$ when normalized to $^{147}\text{Sm}/^{154}\text{Sm} = 0.65918$. A value of λ (^{147}Sm) = 0.00654 AE^{-1} was used for all calculations. This value is that adopted by Lugmair (1974) and is the weighted mean of recent experimental determinations by Donhoffer (1963), Gupta and McFarlane (1970), and Wright et al. (1961).

Selection of ^{150}Nd and ^{147}Sm Tracers

There are several factors which were taken into consideration in selecting the isotopes to be used as tracers for the isotope dilution determination of Sm and Nd concentrations in rocks and minerals. ^{150}Nd was selected because 1) ^{150}Nd is a low-abundance isotope in nature, 2) the ^{150}Nd tracer contained very small amounts of ^{143}Nd and ^{144}Nd , and 3) $^{143}\text{Nd}/^{144}\text{Nd}$ in the ^{150}Nd tracer is close to the values found in nature. Thus a precise determination of Nd concentration can be obtained by adding only a small amount of ^{150}Nd tracer to the sample, and the small amounts of the other isotopes present in the tracer cause only small changes in the relative abundances of the other Nd isotopes for which precise corrections can be made. Because of this, a precise determination of $^{143}\text{Nd}/^{144}\text{Nd}$ can be made on a spiked sample, and involves only a small correction to the measured $^{143}\text{Nd}/^{144}\text{Nd}$.

For Sm, ^{144}Sm is the least abundant isotope, but was not chosen as a tracer because of the possible problems with interference on ^{144}Nd if chemical separation of Sm and Nd is not perfect. ^{149}Sm and ^{150}Sm were not chosen because their abundances are variable in lunar samples due to neutron capture effects. Since ^{152}Sm and ^{154}Sm are the

most abundant Sm isotopes, this leaves ^{147}Sm and ^{148}Sm as possible candidates for tracers. ^{147}Sm was chosen because it is not isobaric with any Nd isotope. Using the ^{147}Sm tracer, $^{148}\text{Sm}/^{154}\text{Sm}$ can be used to provide a precise estimate of mass discrimination, and in addition to the Sm concentration determination $^{149}\text{Sm}/^{154}\text{Sm}$ and $^{150}\text{Sm}/^{154}\text{Sm}$ in the sample can be measured to monitor neutron fluence if desired. However problems arise in the measurement of ^{150}Sm and could be due to interference from the ^{150}Nd tracer. ^{152}Sm may also be affected by neutrons in some lunar materials.

APPENDIX 6: SAMPLE DESCRIPTIONS

Old Mafic Rocks

<u>Sample</u>	<u>Previous #</u>	<u>Description</u>
DUL-4	Dul-gb #4	Anorthositic gabbro; Duluth Complex, obtained from L. T. Silver.
*AR	Ar-Gi-RC db #1	Diabase, Sierra Ancha sill; Arizona; described by Smith and Silver (1975).
RHO-1	RHO-1	Diabase, Great Dyke, Rhodesia; sample from Western Minerals collection.
WGA-210	OGG210	Anorthosite, Fiskenaesset, West Greenland; U-Th-Pb studied by Gancarz and Wasserburg (1977).
MP22D	MP-22	Shonkinite, Mountain Pass, California, c.f. Lanphere (1964)

Old Granitic Rocks

ZL-3D	ZL-3	Town Mountain Granite, Petrick Quarry, Lone Grove Pluton, Llano, Texas; Rb-Sr study by Zartman (1964).
WYWR-4D	WYWR-4	Granodiorite, Louis Lake batholith, Wind River Range, Wyoming; Rb-Sr and U-Th-Pb studied by Naylor et al. (1970).
RN-3	RN-3	Granodiorite, Preissac-Lacorne batholith, Southwest Quebec. Described by Dawson and Whitten (1962); Rb-Sr and U-Th-Pb by Steiger and Wasserburg (1969).
OGG128,10	OGG128,10	Granodiorite, Amîtsoq Gneiss, West Greenland; U-Th-Pb studied by Gancarz and Wasserburg (1977).

*Asterisk indicates that the major element chemistry of the sample is given in Appendix 7.

Mid-Ocean Ridge Basalts

<u>Sample</u>	<u>Previous #</u>	<u>Description</u>
111240	USNM111240/195	Fresh basaltic glass from the Juan de Fuca Ridge. Somewhat enriched in Fe and Ti (44°40'N, 130°20'W, 2195-2220 m depth)
*113152	USNM113152.D121, VGA11	Fe- and Ti-rich basalt, Galapagos Ridge (00°42.3'N, 85°30.0'W, 1360 fathoms depth)
*VG295	VG295	Tholeiite, Mid-Atlantic Ridge (22.52°N, 45.05°W, 2495m depth) Dredge 14, <u>R/V Thomas Washington</u> .
*BD37-2	DSDP37-332B-19-1 (107-110)	Olivine tholeiite, adjacent to Mid-Atlantic Ridge; described by Bence and Taylor (1976) and Hodges and Papike (1975).
*BD17-1	DSDP17-164-28-6 (71-73)	Tholeiite, Central Pacific Ocean Age: Barremian (overlying sediments)
*113031 (OAB-1)	USNM113031/43-53	Alkali basalt, dredged near St. Paul's Rocks, equatorial Atlantic; described by Nelson <u>et al.</u> (1967b), REE analyzed by Frey (1970). (04°N, 29°24'W, 2990-1975m depth).

Oceanic Island Basalts

**HN-1	USNM113095-50 (OA-1)	Mellilite Nephelinite, Honolulu Series, Moliili Quarry, Honolulu, Oahu. Described by Cross (1915), REE analyzed by Schilling and Winchester (1969), Pb isotopes analyzed by Tatsumoto (1966, his sample #HMc-2).
HT-1	USNM113095-56 (OA-7)	Tholeiite, dike in roadcut near Makapuu Point, Oahu; described by Kuno <u>et al.</u> (1957), analyzed for Pb isotopes by Tatsumoto (1966, his sample #HMc-1).

Oceanic Island Basalts (Continued)

<u>Sample</u>	<u>Previous #</u>	<u>Description</u>
GT-2	USNM113180, F436	Volcan Fernandina, Galapagos Islands, caldera lava flow of December, 1973.

Continental Flood Basalts

BCR-1	BCR-1	Quartz tholeiite, Yakima section, Columbia River Basalts; chemistry given by Flanagan (1973), general chemistry of Yakima basalts given by Waters (1961), McDougall (1976) Nathan and Fruchter (1974), and Wright <u>et al.</u> (1973).
*PG16D	PG16	Tholeiite, Picture Gorge, Oregon; Columbia River basalt; trace elements measured by Goles (1969), major elements of adjacent flows analyzed by McDougall (1976)
SK-38	SK-38	Basalt, Miki's Fjord, East Greenland. Eocene flood basalt, obtained from A. McBirney.
SWB-1D	SWB-1A	Tholeiite, Stormberg Series, Karroo basalts, Warmbad, South Africa, obtained from G. Goles
KAS-2	16/12/74-1	Tholeiite, 600m above base of Stormberg Series near Barkeley East, Karroo basalts, South Africa; obtained from G. Goles.
PEA-3	PEA-3	Basalt, Karroo series, Mozambique; about 1 mi. N.W. of Canxixe Village, SW of Zambezi River, c.f. Mennell (1922, 1929).

Continental Flood Basalts (Continued)

<u>Sample</u>	<u>Previous #</u>	<u>Description</u>
PD-1	PD-1	Palisades diabase, 120' above base, Edgewater, New Jersey; chemistry of Palisades diabase described by Walker (1940).
PAR-1	SPK-0048	Parana basalt; from base of lava flow plateau at vertical fault scarp, Serra de Aparados-Turvo-Bom. Jesus road, elevation 300m, Santa Catarina ($49^{\circ}55'W$, $28^{\circ}46'S$). K-Ar age given by Amaral <u>et al.</u> (1966). 1.30% K, 121.2my.
PAR-2	SPK-0050	Parana basalt; from middle part of lava plateau, same profile as SPK-0048, elevation 750m. K-Ar age given by Amaral <u>et al.</u> (1966) 0.855% K, 119.0 my. Chemistry of Parana basalts given by Cordani and Vandoros (1967) and Compston <u>et al.</u> (1966).
*ADT-2	M210	Red Hill diabase, Tasmania, Quartz dolerite Sr isotopes measured by Compston and McDougall (1965).
AF-133	133-1(75)	Afar flood basalt, Ethiopia; obtained from J. Aronson.

Island Arcs

*BMR-1	51NG0217F	Andesite, Sulu Range, New Britain, Bismark Volcanic Arc; obtained from R.W. Johnson.
*BMR-2	53NG1051	Dacite, Lolobau Island, North of New Britain, Bismarck Volcanic Arc; obtained from R.W. Johnson

Island Arcs (Continued)

<u>Sample</u>	<u>Previous #</u>	<u>Description</u>
*BMR-3	5ING3064	Dacite, Welcker Volcano, Talasea Peninsula, New Britain, Bismarck Volcanic Arc; obtained from R.W. Johnson
*BMR-4	51NG0259	Andesite, Dakataua Volcano, New Britain, Bismarck Volcanic Arc; obtained from R. W. Johnson.
*BMR-5	48NG0549	Dacite, Garove Island, North of New Britain, Bismarck Volcanic Arc; obtained from R. W. Johnson.
*BMR-6	48NG0038A	Basalt, Undaka Island, North of New Britain, Bismarck Volcanic Arc; obtained from R. W. Johnson.
*BMR-7	5ING0271	Rhyolite, Talasea Harbour, New Britain, Bismarck Volcanic Arc; obtained from R. W. Johnson.
MAR-1	AG-1-3	Basalt, Agrigan Islands, Marianas; collected by R. J. Stern.
MAR-2	SRGN-5	Andesite, Sarigan Island, Marianas; collected by R. J. Stern.
MAR-4	AG-10-1	Basalt, Agrigan Island, Marianas; collected by R. J. Stern.
MAR-6	SAI-3	Dacite, Saipan Island, Marianas; collected by R. J. Stern.
GU-4	GU-4	Basalt (?), Alutom Formation, near Piti, Guam; obtained from F. Barker.
GU-7	GU-7	Basalt (?), Alutom Formation, near Piti, Guam; obtained from F. Barker.

Continental Margin Magmatic Arcs

<u>Sample</u>	<u>Previous #</u>	<u>Description</u>
*PER-1	USNM113642 (B19 121.30m)	Andesite, (Pleistocene or Recent) El Misti Volcano, Arequipa Volcanics, Peru.
*PER-2	USNM113641	Rhyolite, El Misti Volcano, Arequipa Volcanics, Peru. From Pleistocene or recent dome (Volcan Cilla) on N slope of El Misti.
*CAS-1	242	Olivine basalt, cinder cone, Mt. Shasta, N. California. Chemistry given by Smith and Carmichael (1968) and Peterman and Carmichael (1970).
MEX-1	USNM113637	Basaltic andesite, Arenal Volcano, Costa Rica, erupted August- September, 1976.
WMG-1	-	Woodson Mtn. Granodiorite, Average chemistry given by Larsen (1948).
SMG-1	-	San Marcos Gabbro, Peninsular Ranges batholith, Southern California (Pala), average chemistry given by Larsen (1948).
RL-1	Cal-SCB-36 MRLgr #2	Rubidoux Leucogranite, Peninsular Ranges batholith, S. California; described by Larsen (1948).
LAK-8D	LAK-8	Rhyolite, Mt. Konocti, California. Chemistry given by Bowman <u>et al.</u> (1973).

Continental Alkali Basalts

*CSQ-3	CSQ-3	Basanite, San Quintin, Baja California; described by Bacon and Carmichael (1973).
--------	-------	---

Continental Alkali Basalts (Continued)

<u>Sample</u>	<u>Previous #</u>	<u>Description</u>
PCB-1	-	Trachy basalt, Pisgah Crater, Mojave Desert, S. California; described by Smith and Carmichael (1969).
*ANB2128	2128	Nepheline Basanite, Mt. Porndon, Newer basalts, Victoria, Australia; described by Irving and Green (1976), Stuckless and Irving (1976).
*ANB2102Q	2102Q	Nepheline Mugearite, the Anakies, Newer basalts province, Victoria, Australia; described by Irving and Green (1976), Stuckless and Irving (1976).
*RGB-1	74-005-JM-WSB	Alkali olivine basalt, Rio Grande Rift, New Mexico; described by Baldridge (1978).
WBK-1	WBK-1	Miocene alkali basalt, Tiberios, Golan Heights, Israel.
CHA-2	CHA-2	Quaternary basalt, Patagonia (Southern Argentian) $50^{\circ}11.5'S$, $71^{\circ}07'W$ $K_2O=1.91\%$.
V-9	V-9	Quaternary basalt, Patagonia (Southern Argentina) $49^{\circ}28'S$, $72^{\circ}25'W$ $K_2O=0.79\%$.
Khibina	-	Apatite from Khibina nepheline syenite intrusion, Kola Peninsula, U.S.S.R., described by Gerasimovsky <u>et al.</u> (1974).

Lavas of Extreme Composition

*OLC-1	October 1960 Na, Ca-carbonate lava flow, Oldoinyo Lengai Volcano, Tanzania; described by Dawson (1962, 1964); obtained from J. Gittins.
--------	---

Lavas of Extreme Composition (Continued)

<u>Sample</u>	<u>Previous #</u>	<u>Description</u>
*LH-1	LH-1	Wyomingite, Leucite Hills, Wyoming; described by Carmichael (1967).
DULL1	DU-111	Ugandite, Uganda; obtained from I. Carmichael.

Ultramafic Rocks

*SPP-1	NE-4	Spinel peridotite mylonite, St. Paul's Rocks, equatorial Atlantic; described by Melson <i>et al.</i> (1972); REE analyzed by Frey (1970).
--------	------	---

Other Samples

NAS-216D	NAS-216	North American shale composite prepared by P.W. Gast; REE given by Haskin <i>et al.</i> (1966).
DOS-1	-	Fish debris (apatite), Pacific Ocean floor, described by Arrhenius <i>et al.</i> (1957).

APPENDIX 7: MAJOR ELEMENT CHEMISTRY OF ANALYZED SAMPLES

APPENDIX 7 (cont.)

	BCR-1	ADT-2	BMR-1	BMR-2	BMR-3	BMR-4	BMR-5	BMR-6
SiO ₂	54.5	53.93	53.1	69.2	68.5	53.5	63.4	49.2
TiO ₂	2.20	0.80	0.30	0.74	0.54	0.71	1.29	1.15
Al ₂ O ₃	13.61	18.88	14.7	13.7	14.6	15.8	15.0	14.4
Fe ₂ O ₃	3.68	1.38	1.91	0.99	1.80	3.55	1.80	1.40
FeO	8.80	7.31	6.90	4.20	2.15	5.80	5.30	8.10
MnO	0.18	0.17	0.16	0.14	0.09	0.18	0.17	0.18
MgO	3.46	3.09	9.20	1.10	1.27	6.05	1.79	10.8
CaO	6.92	10.32	10.9	3.80	3.60	10.8	4.40	11.4
Na ₂ O	3.27	2.09	1.58	4.15	3.75	2.40	4.95	2.15
K ₂ O	1.70	0.95	0.28	1.28	2.80	0.51	1.29	0.19
P ₂ O ₅	0.36	0.16	0.03	0.24	0.16	0.14	0.39	0.11
H ₂ O+	0.77	1.21	0.30	0.46	0.07	0.34	0.13	0.28
H ₂ O-	0.80	0.20	0.22	0.04	0.19	0.17	0.21	0.20
CO ₂	0.03	0.04	<0.05	<0.05	0.16	0.02	0.05	0.05

50

BaO

S10

五

APPENDIX 7 (cont.)

	BMR-7	PER-1	PER-2	CAS-1	RGB-1	CSQ-3
SiO ₂	75.6	61.20	71.34	52.03	49.01	46.58
TiO ₂	0.27	0.70	0.22	0.66	1.48	2.41
Al ₂ O ₃	12.8	17.80	15.76	16.51	15.90	15.08
Fe ₂ O ₃	0.33	3.10	1.27	3.41		2.09
FeO	0.84	2.23	0.44	4.51	10.48*	8.60
MnO	0.07		0.06	0.14		0.19
MgO	0.26	2.60	0.36	9.59	8.63	9.42
CaO	1.22	5.46	2.32	9.48	9.06	8.86
Na ₂ O	3.95	4.29	4.25	2.97	3.65	3.42
K ₂ O	3.85	2.21	3.05	0.41	0.89	1.51
P ₂ O ₅	0.03		0.09	0.12	0.28	0.52
H ₂ O ⁺	0.56	0.09	0.40	0.30		0.35
H ₂ O ⁻	0.02	0.06	0.36	0.09		0.04
CO ₂		0.05				
SO ₃						
C1						
BaO						
SrO						
F						

APPENDIX 7 (cont)

	ANB2102 Q	ANB2128	OLC-1	LH-1	SPP-1
SiO_2	48.88	46.21	tr	50.23	44.38
TiO_2	2.19	2.51	0.10	2.30	0.08
Al_2O_3	15.41	12.38	0.08	10.15	2.36
Fe_2O_3	3.45	2.00	0.26	3.65	0.98
FeO	6.90	9.98		1.21	7.18
MnO	0.16	0.18	0.04	0.09	0.22
MgO	7.20	11.71	0.49	7.48	41.66
CaO	6.52	8.56	12.74	6.12	1.01
Na_2O	5.74	3.54	29.53	1.29	0.14
K_2O	2.87	2.01	7.58	10.48	0.04
P_2O_5	0.68	0.90	0.83	1.81	<0.05
H_2O^+	(0.08	0.33	(8.59	2.34	1.08
H_2O^-		0.09		1.09	0.09
CO_2	0.04	0.13	31.75	0.08	
SO_3			2.00	0.35	0.11
Cl			3.86		
BaO			0.95		
SrO			1.24		
F			2.69		

APPENDIX 7: REFERENCES

<u>Sample</u>	<u>Reference</u>
AR	Smith and Silver (1975)
113152	W.G. Melson, written communication
113031	W.G. Melson, written communication
VG295	W.G. Melson, written communication
BD37-2	Bence and Taylor (1975)
BD17-1	A.E. Bence, written communication
HN-1	Cross (1915)
HT-1	Kuno <u>et al.</u> (1957)
BCR-1	Flanagan (1973)
ADT-2	McDougall (1962)
BMR-1	R.W. Johnson, written communication
BMR-2	R.W. Johnson, written communication
BMR-3	R.W. Johnson, written communication
BMR-4	R.W. Johnson, written communication
BMR-5	R.W. Johnson, written communication
BMR-6	R.W. Johnson, written communication
BMR-7	R.W. Johnson, written communication
PER-1	W.G. Melson, written communication
PER-2	W.G. Melson, written communication
CAS-1	Smith and Carmichael (1968)
RGB-1	Baldridge, personal communication
CSQ-3	Bacon and Carmichael (1973)
ANB2102Q	Irving and Green (1975)
ANB2128	Irving and Green (1975)
OLC-1	Dawson (1962)
LH-1	Carmichael (1967)
SPP-1	Melson <u>et al.</u> (1972)

APPENDIX 8: TRACE ELEMENT CONCENTRATIONS

Sample	K(%)	Rb	Sr	Ba	Sm	Nd	Rb/Sr	Sm/Nd	K/Rb	Sr/Nd	Ba/Nd
DUL-4	0.248	2.25	371	140.0	0.40	2.35	0.0061	0.170	1102.0	158	59.6
AR	0.294	4.48	596	134.0	1.78	6.90	0.0075	0.258	656.0	86.4	19.4
RHO-1	-	-	-	-	0.578	2.405	-	0.244	-	-	-
WGA210	-	-	-	-	0.938	4.95	-	0.189	-	-	-
MP22D	-	-	-	-	42	240	-	0.175	-	-	-
ZL-3D	-	-	-	-	17.21	73.3	-	0.235	-	-	-
WYWR-4D	-	-	-	-	8.135	44.95	-	0.181	-	-	-
RN-3	-	-	-	-	10.74	65.2	-	0.165	-	-	-
OGG128,10	-	-	-	-	14.66	75.0	-	0.195	-	-	-
111240	0.178	1.84	117	6.37	3.67	10.88	0.0157	0.337	967.0	10.8	0.585
113152	-	-	-	-	9.376	26.89	-	0.349	-	-	-
BD37-2	-	-	-	-	17.1	1.69	5.32	-	0.318	-	3.21
BD17-1	-	-	-	-	3.30	10.02	-	0.329	-	-	-
113031	1.29	32.7	644	-	7.51	39.09	0.0508	0.192	394.0	16.5	-
HN-1	1.46	38.0	1497	424.0	12.5	61.9	0.0254	0.202	384.0	24.2	6.85
HT-1	0.483	8.10	428	133.0	5.74	21.8	0.0189	0.263	596.0	19.6	6.10

APPENDIX 8: TRACE ELEMENT CONCENTRATIONS (CONTINUED)

Sample	K(%)	Rb	Sr	Ba	Sm	Nd	Rb/Sr	Sm/Nd	K/Rb	Sr/Nd	Ba/Nd
GT-2	—	—	—	—	5.55	21.6	—	0.257	—	—	—
PG16D	0.381	3.89	257	283.0	—	—	0.0151	—	979.0	—	—
DTB-1	0.330	10.86	222	113.0	6.41	23.6	0.0489	0.272	304.0	9.41	4.79
SK-38	0.377	7.89	417	212.0	6.19	28.2	0.0189	0.219	478.0	14.8	7.52
SWB-1D	0.292	3.08	178	139	4.37	15.63	0.0173	0.280	948.0	11.4	8.89
KAS-2	0.216	1.71	98	99	1.94	6.96	0.0174	0.279	1263.0	14.1	14.2
PEA-3	1.186	124.0	230	798.0	8.65	44.8	0.539	0.193	95.6	5.13	17.8
PD-1	0.362	13.2	134	120.0	2.20	8.64	0.0985	0.255	274.0	15.5	13.9
PAR-1	1.52	36.4	679	277.0	7.82	46.1	0.0536	0.170	418.0	14.7	6.01
PAR-2	0.88	23.3	353	317.0	6.13	27.7	0.0660	0.221	378.0	12.7	11.4
BMR-1	0.23	2.6	167	30	0.65	1.76	0.016	0.369	880	95	17
BMR-2	1.06	21.0	255	320	3.4	12	0.082	0.28	505	21	27
BMR-3	2.32	41.0	406	390	2.5	12	0.101	0.21	570	34	33

APPENDIX 8 : TRACE ELEMENT CONCENTRATIONS (CONTINUED)

Sample	K(%)	Rb	Sr	Ba	S _m	Nd	Rb/Sr	S _m /Nd	K/Rb	Sr/Nd	Ba/Nd
BMR-4	0.42	5.2	446	100.0	1.7	6.4	0.012	0.27	808.0	70.0	15.6
BMR-5	1.07	16.0	184	150.0	7.6	28.0	0.087	0.27	670.0	6.6	5.4
BMR-6	0.16	24.0	187	30.0	2.4	8.9	0.013	0.27	670.0	21.0	3.4
BMR-7	3.20	54.5	206	480.0	2.4	13.0	0.265	0.18	590.0	15.8	37.0
MAR-1	0.76	11.9	352	152.0	2.32	11.1	0.0338	0.209	639.0	31.7	13.7
MAR-2	0.84	14.7	352	363.0	3.43	12.0	0.0418	0.286	571.0	29.3	30.3
MAR-4	0.79	21.1	401	171.0	3.04	11.7	0.0526	0.260	374.0	34.3	14.6
MAR-6	1.13	3.23	94	46.0	1.06	5.01	0.0344	0.212	3500.0	18.8	9.18
GU-4	0.585	11.7	130	60.7	1.65	5.68	0.0900	0.290	500.0	22.9	10.7
GU-7	0.08	2.23	148	—	1.63	5.10	0.0151	0.320	359.0	29.0	—
PER-1	1.96	48.2	1098	1081.0	4.55	28.1	0.0439	0.162	407.0	39.1	38.5
PER-2	2.54	71.0	444	1166.0	3.30	21.7	0.160	0.152	358.0	20.5	53.7
CAS-1	—	6.6	366	—	—	—	0.018	—	—	—	—
WMG-1	2.19	65.7	158	992.0	1.70	7.18	0.416	0.237	333.0	22.0	138.0

APPENDIX 8 : TRACE ELEMENT CONCENTRATIONS (CONTINUED)

Sample	K(%)	Rb	Sr	Ba	Sm	Nd	Rb/Sr	Sm/Nd	K/Rb	Sr/Nd	Ba/Nd
SMG-1	0.23	4.10	451	121.0	1.25	4.95	0.0091	0.253	561.0	91.1	24.4
RL-1	4.54	223.0	104	1180.0	2.84	11.5	2.14	0.247	204.0	9.0	103.0
LAK-8D	4.4	221.0	—	636.0	5.31	28.7	—	0.185	199.0	—	22.0
PCB-1	—	—	—	—	11.79	58.1	—	0.203	—	—	—
RGB-1	0.69	13.2	354	385.0	—	—	0.0373	—	523.0	—	—
CHA-2	1.77	45.2	491	490.0	—	—	0.0921	—	392.0	—	—
V-9	0.73	21.0	477	—	—	—	0.440	—	348.0	—	—